Investigation on the Autonomic Structural Self-Healing of FRPC using Microencapsulated 5E2N/Grubbs Catalyst System for Low Temperature Applications

Mohammad Asgar Khan

A Thesis
In the Department
of
Mechanical and Industrial Engineering

Presented in Partial Fulfillment of the Requirements
For the Degree of
Doctor of Philosophy (Mechanical Engineering) at
Concordia University
Montreal, Quebec, Canada

September 2016

Signature page

Examining committee:

Dr. Tarek Zayed, Chair
Dr. Suong Van Hoa, Supervisor
Dr. John Oh
Dr. Martin Pugh
Dr. Mehdi Hojjati

External Examiner:

Dr. Zhibin Ye

ABSTRACT

Investigation on the autonomic structural self-healing of FRPC using microencapsulated 5E2N/Grubbs catalyst system for low temperature applications

Mohammad Asgar Khan, Ph.D.
Concordia University, 2016

Structural self-healing of Fiber Reinforced Polymer Composites (FRPC) using microencapsulated 5E2N/Grubbs catalyst system is investigated in this work for low temperature applications. Microcapsule containing liquid 5E2N monomer in poly melamine urea formaldehyde (PMUF) shells have been synthesized following the in-situ polymerization technique. The effects of stirring speed and concentration of surfactant on the quality of microcapsules in terms of their average sizes, size distribution, surface morphology and shell thickness are investigated. An optimum combination of stirring speed-SLS concentration is established through numerous synthesis trials of microcapsules. The feasibility of self-healing with the current materials system is first demonstrated by visually observing the healing of crack network that is created on unreinforced epoxy samples impacted with high velocity projectiles. Different strength-based approaches like impact-heal-flexure, flexure-heal-flexure are examined to evaluate the self-healing performance of FRPC in the preliminary investigations. A fracture based approach based on the mode II delamination of FRPC which deals with determining material properties independent of geometry of samples is found to be a better choice for the evaluation of healing performance of FRPC. In the new proposed protocol, healing performance is evaluated by measuring and comparing the mode II fracture toughness of regular neat (not incorporated with healing agents) and modified (incorporated with healing agents) FRPC samples during the Non pre-cracked (NPC) and Pre-cracked (PC) test post healing without any manual intervention for achieving healing. Healing performance index, instead of healing efficiency, is defined by comparing the fracture toughness of regular and modified samples taking into account the possible toughening or weakening effect of incorporating healing agents into the composites. Healing performance index is shown to be a better and realistic indicator of actual healing performance than conventional healing efficiency definition. Effects of average size and

concentration of microcapsules on the self-healing performance of FRP composites are investigated at room temperature using the proposed protocol. Finally, the effect of low temperature on self-healing performance of FRP composites is evaluated.

Acknowledgements

I like to express my sincere gratitude to my supervisor, Dr. Suong Van Hoa, for his support in guiding me towards achieving my dream Ph.D. degree in mechanical engineering at Concordia University. His passion for excellence enlightened and energized me to love my work and overcome the difficulties of research works through tireless efforts. His suggestions, valuable discussions and continuous guidance stimulated critical thinking and showed me the right directions in fulfilling the objectives of my Ph.D. research works.

I would like to remember and be grateful to late Dr. Ming Xie who helped me feel at home as a member of CONCOM (Concordia Centre for Composite Materials) research group. He and subsequently, Dr. Daniel Rosca, helped me a lot in providing technical supports to carry out my research works. I would also like to acknowledge the supports of the technical and administrative support staff of the department and all my colleagues for their support and cooperation.

I appreciate the support of my wife, Hasna Hena Zamal, and our child, Warsi Azam Khan, who sacrificed a lot and made this challenging journey enjoyable for me. I also like to thank all my family members who were always a source of inspiration for me. I would like to dedicate my work to my late father, Golam Mohiuddin Khan, who transferred his passion for knowledge to me.

Finally, the financial support from NSERC (Natural Sciences and Engineering Research Council of Canada) and CSA (Canadian Space Agency) in carrying out this study is gratefully acknowledged.

Table of Contents

List of figures

List of tables

CHAPTER 1

Framework and Scope of the Work

1.1 Introduction

Use of structures and parts made of Fiber Reinforced Polymer Composites (FRPC) in various engineering applications, especially, in space and aerospace field, is a very attractive option due to their high strength to weight ratio. Structures and parts made of FRPC are often subjected to low temperature in service. For example, external key structures and parts like the fuselage, wings and rotor blades of modern air planes and helicopters made of FRPC are subjected to cold temperatures (-40^{o}C to -60^{o}C) at cruising altitudes during in-flight operations. These air vehicles also often stay in mild cold temperatures in runways and tarmacs for a considerable time in colder regions on earth where the environment temperature remains as low as -40^{o}C and less, especially, during the winter seasons. Further, after the inflight operations at high altitude, the air vehicles land in warmer environments thus might be subjected to thermal cycling. Further, damages in composite parts in aerospace structures can be caused by a simple drop weight impact or bending situations caused by artificial or environmental factors. Most of the modern satellites launched into earth orbit, and even some manned spacecraft are also constructed with specially designed composite panels as their primary load bearing elements [1]. They also serve as the protection systems for the internal critical parts like fuel tank, precision devices and sensitive equipment like optical sensors, mirrors etc. [2]. Modern satellites and their components made of FRPC are also exposed to extreme cold (down to -150^{o}C) conditions and again return to extreme hot (up to +150^{o}C) conditions during their orbiting in space. Further, the composite parts in the satellites or spacecraft structures are susceptible to damage caused by the impact of micrometeoroids and space debris with a wide range of sizes and velocities. These damages in aerospace and space structures can vary from very severe (where holes are punctured through the structure) to minor damages (where small dents are made into the structure). In-service manual repair of the damaged composite parts may be carried out but with a great cost and complexities. The concept of self-healing of structural polymeric materials using microencapsulated healing agents, first introduced and demonstrated by research group of White et al. [3], can be a potential

alternative to difficult manual repair of composites. Most of the studies of self-healing of polymer composites, however, involve different types of monomer and resin systems which are not suitable for low temperature applications. It is thus interesting to investigate the effect of low temperatures as well as effect of thermal cycling on self-healing of composites. The current work thus examines the effect of thermal cycling on self-healing of unreinforced epoxy samples and investigates in detail the effect of mild low temperature (-40ºC) on the self-healing of Fiber Reinforced Polymer (FRP) composites.

The damage behavior of FRPC is complex, especially, under realistic loading conditions like impact or bending. Even the apparently minor dents on the surface due to impact can actually result in internal subsurface critical damage. Unlike metals, FRPC consists of many types and patterns of damages as shown in figure 1.1.

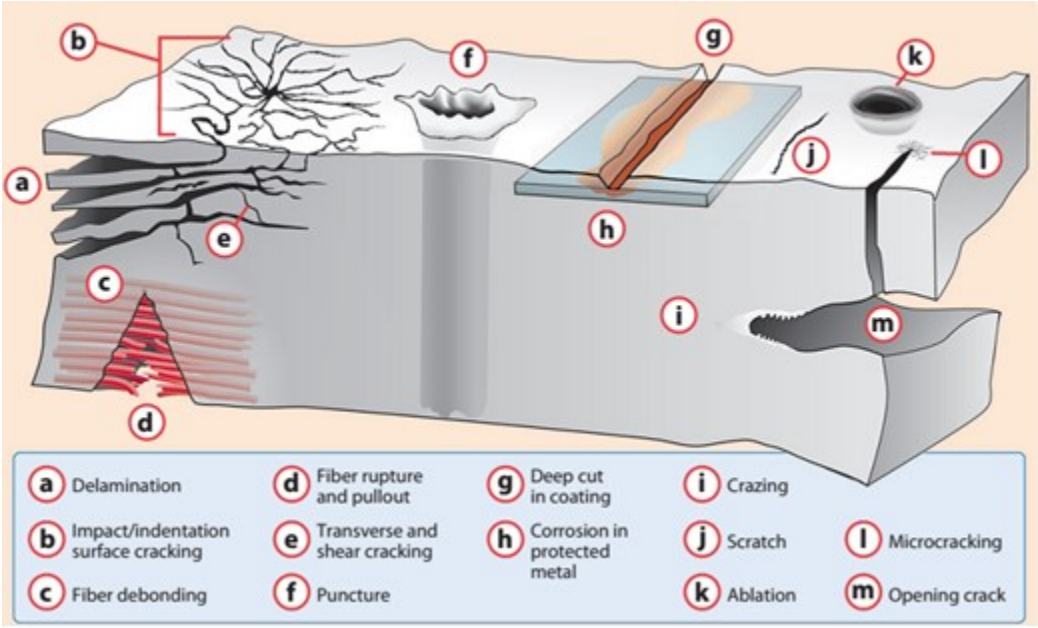

Figure 1.1 Damage modes in polymer composites. Indentation, impact, corrosive environments, ballistic punctures, surface scratching, and fatigue can lead to various damage modes in polymer composites, as shown here: The type of composite system, the nature of the polymer matrix, and the extent and rate of loading all influence the type and extent of damage modes [2]

Study of damage mechanism of FRPC [4] reveals that the damage usually starts at the matrix as tiny micro cracks, which, depending upon the loading condition, may make branches, coalesce, grow and propagate finally causing severe damages or failure. Thus, if the damage can

be repaired at its very early stage, its development to severe damage can be retarded or even stopped ensuring reliable service of the component for longer lifetime. The primary limitation of this early repair idea is that it is extremely difficult to reliably detect the very initiation of damage which might be created at the subsurface locations of the FRPC. Even if the subsurface damage can be detected using the available damage detection techniques like dye penetrants, fiber optical sensor, ultrasonic, infrared thermography, X-ray tomography and electrical resistance measurements [5], its repair by external manual intervention can be impossible due to the lack of human access to the damage site. Even, if it is possible to do so, in-service manual repair may be carried out but with a great cost and complexities. An alternative and more recent concept in this regard is to impart a healing functionality to the matrix of the FRPC composites which upon the occurrence of a damage event can be stimulated immediately to repair by itself.

Healing is a process by which a material can undergo the repair and restoration of the original functionality at a damage event by using only the materials that are inherently available to them [6]. The concept of autonomic self-healing in FRPC actually came from natural biological systems where the injuries/cut is healed by regeneration of cells at the site of injury. In fact, healing functionality can be observed or engineered to impart to any synthetic materials (ceramic, concrete and polymers). However, it was in the last two decades that the process of self-healing was seriously considered as a desirable function for man-made materials [7]. Research in autonomic self-healing of structural polymeric materials has gained momentum after White et al. [3] introduced and experimentally verified a microcapsule based healing concept (figure 1.2) and reported successful healing of cracks in structural polymer matrix.

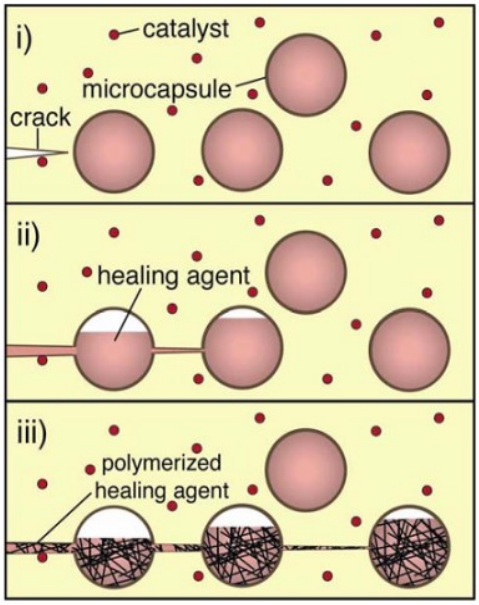

Figure 1.2 The autonomic healing concept. A microencapsulated healing agent is embedded in a structural composite matrix containing a) catalyst capable of polymerizing the healing agent. i) Cracks form in the matrix wherever damage occurs; ii) the crack ruptures the microcapsules, releasing the healing agent into the crack plane through capillary action; iii) the healing agent contacts the catalyst, triggering polymerization that bonds the crack faces closed. [3]

Among the various healing approaches (e.g. microcapsules, hollow fiber, hollow channel, microvascular network) discussed in the literature review section, the microcapsule based healing system has gained much attention because of its relative simplicity. Several microcapsules based healing systems involving different chemistries have been studied by several groups of researchers. Among these, Dicyclopentadiene (DCPD)/Grubbs catalyst based microencapsulated healing system has been studied more extensively. In fact, the quality of healing (capability of recovering mechanical properties under a damage event) directly depends on a number of physical and chemical properties of the chosen healing agent [8]. DCPD/Grubbs system although showed good potentials for some specific applications, it is not suitable for low temperature applications.

In the current work, 5-ethylidene-2-norbornene (5E2N) which remains functional in a wider range of temperatures and possesses faster cure kinetics than DCPD, is selected for investigating the microcapsule based autonomic structural self-healing of Carbon Fiber Reinforced Polymer (CFRP) composites for low temperature applications.

1.2 Motivation

Self-healing of polymers and their composites using microencapsulated DCPD monomer/Grubbs catalyst system have been widely investigated in literature. 5-Ethylidene-2-Norbornene (5E2N) monomer, on the other hand, has several advantages over DCPD including much lower freezing point and higher reactivity with Grubbs catalyst making it an attractive candidate for self-healing, especially, for low temperature applications. However, 5E2N monomer is relatively unexplored as a healing agent for self-healing of polymer composites. The current work, thus, investigates the self-healing of microencapsulated 5E2N/Grubbs catalyst system for self-healing of composites both at room and cold temperatures. In order to study the effect of low temperature on the self-healing of FRPC, it is first necessary to understand the room temperature capability of the self-healing system. Thus, a variety of experiments involving resin only (without fibers) and fiber reinforced composite samples are intended to demonstrate the feasibility and effectiveness of the self-healing system at room temperature. A survey on the literature in this field reveals that there is also scope of improving the process of evaluating the healing performance of a self-healing system. Healing performance is widely evaluated by calculating the healing efficiency using a protocol based on measuring the mode I fracture toughness of unreinforced resin sample and FRPC sample. The protocol, however, involves some sort of manual intervention in the form of pressing the fractured surfaces together to achieve and influence healing. This condition influencing the self-healing might not be maintained in a real component in-service. Further, the healing efficiency in this protocol is determined by comparing the fracture toughness of samples already incorporated with healing agents. The healing efficiency value as determined by this protocol does not reflect the very likely toughening (or weakening) effect due to the incorporation of healing agents in to the neat sample (without any healing agents) as no comparison is made with it in the healing efficiency

definition. A simple scenario analysis of the existing protocol of determining healing efficiency reveals that it might provide unreliable indication in many likely situations. Furthermore, the process of determining the healing performance does not involve realistic loading conditions like impact or bending which the composites parts and structures are commonly subjected to, during its service and operations, especially, in space and aerospace environment. Thus, in order to evaluate the healing performance of a self-healing system a suitable protocol under a realistic loading condition and free from any manual intervention is searched for. Methods and processes are also intended to establish for producing quality microcapsules of intended average size, its dispersion into epoxy resin and manufacturing FRPC. Finally, the effect of average size of microcapsules, its concentration and cold temperature on the self-healing performance of CFRP is evaluated. The investigation is, thus believed to contribute to the advancement of knowledge in the field of microcapsule based structural self-healing of FRPC, especially, for low temperature applications.

1.3 Objectives of the work

The objectives of the work can be categorized into two types. One is the global objectives and the other is the local objectives. Local objectives are required to fulfil the global objectives. These are to:

1) Offer a complete package of procedures for producing FRPC with optimal healing performance starting from the raw materials (i.e. fiber, resin, monomer, catalyst, encapsulating reagents etc.).

The local objectives to achieve this are to

a) Produce microcapsules and investigate the effect of processing parameters on the quality of microcapsules

b) Establish procedures for manufacturing FRPC incorporating the healing agents (microcapsules and catalyst)

c) Investigate the effect of size and concentration of microcapsules on self-healing performance of FRPC

2) Propose a suitable protocol for evaluating self-healing performance of FRPC under realistic loading conditions and without any requirement for assisting healing by manual interventions

3) Investigate the effect of low temperature on self-healing performance of FRPC

1.4 Scope of the Current Work

Different strategies for the self-healing of structural polymer composites exist in literature. All these strategies commonly involve a storage system of reactive monomer assimilated into the matrix of the composite. These storage vessels are capable of delivering the reactive monomer into the damage site by breaking itself during a damage event triggering polymerization reaction to heal the damage. According to the type of storage vessels, the healing strategies are named which include hollow fiber, hollow channel, microvascular network and microcapsule based self-healing system. Among the various existing strategies, the microcapsule based self-healing system is relatively simple, easy to assimilate into the composites and possesses significant potential for real applications. Thus, microcapsule based self-healing system is selected for the current work.

Similar to the different self-healing strategies, several healing chemistry involving different reactive materials/monomers and catalyst capable of undergoing polymerization/crosslinking reaction to heal a damage is also present in the literature. These include DCPD/Grubbs, epoxy/ hardener, glycidyl methacrylate, styrene/initiator and monomer/solvent self-healing systems. Among these healing strategies, DCPD/Grubbs system capable of undergoing Ring Opening Metathesis Polymerization (ROMP) reaction is most widely investigated in the literature. One of the limitations of all of the above self-healing systems is that, none of them is really suitable for low temperature applications where the healing agents must remain sufficiently fluid at the low temperatures. For example, DCPD, the most widely investigated monomer, has a melting point of around 10^{o}C, which means that the healing mechanism proposed may not work by freezing of the healing agent below the temperature. Development of suitable healing agent with low temperature freezing point is thus essential [9]. 5E2N, on the other hand, has a freezing point around -80^{o}C and capable of undergoing ROMP reaction with Grubbs catalyst at a much faster

rate than DCPD. Microencapsulated 5E2N/Grubbs catalyst system is thus suitable for self-healing at low temperature applications and thus is investigated in the current work.

In order to understand the low temperature effect on the self-healing of 5E2N/Grubbs catalyst system, it is first necessary to investigate the effect of room temperature on self-healing. Thus the investigation is first carried out thoroughly at room temperature and later extended to the low temperature case.

1.5 Construction of the thesis

The thesis is organized by introducing the problem descriptions and the concept of microencapsulated self-healing followed by motivations behind the work. The objectives of the work are then enumerated. The scope of this research work is then discussed in the following subsections and the construction of the thesis is outlined. This constitutes the first introductory chapter of the thesis. A detailed review of the relevant literature is presented in chapter 2. The effects of the processing parameters on the quality characteristics of microcapsules are presented in chapter 3. The preliminary experiments carried out to demonstrate self-healing and the issues of the strength-based protocols followed to evaluate healing performance of FRP composites are discussed in chapter 4. In chapter 5, a mode II fracture based protocol for evaluating healing performance of FRP composites is proposed and compared with existing mode I fracture based protocol by theoretical scenario analysis. The relative features and advantages of the new protocol is summarized at the end of this chapter. Investigation of self-healing of FRP composites at room temperature is presented in chapter 6. The effects of average size and concentration of microcapsules on the self-healing performance of FRP composites evaluated based on the proposed mode II based protocol are presented in this chapter. Investigation of self-healing of FRP composites at low temperature is presented in chapter 7. The rational for choosing the value of low temperature and choosing the alternate catalyst (Hoveyda-Grubbs catalyst instead of Grubbs catalyst) for investigation in light of the ROMP reaction mechanism is also discussed in this chapter. The experimental set up for the low temperature tests and the self-healing performance of the selected types of composite samples are evaluated based on the proposed mode II fracture protocol. Finally, the results are compared with the room temperature results in this chapter to extract the effects of low temperature. The last chapter constitutes the overall conclusion, contribution and recommendations for future works.

CHAPTER 2

Literature Review

2.1 Introduction

Every material and structure is subjected to degradation and damage during its operation. Traditionally materials and structures when damaged are either repaired manually or replaced completely. Repair is attempted to ensure its safe intended operation and prolong its lifespan. Different established manual methods of repair are available for different classes of materials. Depending on various criteria including the quality, sophistication and precision requirement and the cost, the appropriate repair methods are selected.

Metallic structures and components can simply be repaired by mechanical fastening (e.g. bolting, riveting), or by various forms of fusion bonding (e.g. welding, brazing, soldering) and adhesive bonding techniques. These repair methods for metallic components are well established and most of these techniques possess the required sophistication and reliability for advanced level applications. Further, the mode and mechanism of damage initiation and accumulation in metals are relatively simple and predictable compared to ceramics, polymers and their composites.

A number of manual repair methods are also available for ceramic materials and their composites. Like metallic components and structures, they also include several forms of diffusion bonding (e.g. ceramic welding), adhesive bonding (e.g. high temperature curing of adhesives) and mechanical fastening techniques. Structural concretes are repaired by polymer injection, pre-stressing, geomembranes and polymer wraps [1]. However, the available manual repair technologies for ceramics are relatively new and less mature than metals.

Similarly, the polymers and their composites are conventionally repaired by various forms of diffusion bonding, adhesive bonding (e.g. patching, scarfing, resin infusion) and mechanical fastening (e.g. bolting) methods. However, the complex nature of damages in FRPC made the manual repair much complex, time consuming and expensive. It often involves rigorous surface preparation and requires strong technical skill to perform the repair. Further, the reliability of these repair methods of FRPC for advanced applications is not well established. The choice

between the conventional bolted and bonded repair methods of primary airplane composite structures is still an important issue of debate among the certification authorities like Federal Aviation Administration (FAA) and European Aviation Safety Agency (EASA) [10]. Further, the available manual repair methods of FRPC are applicable to relatively severe damages only. While these conventional repair methods are applied to relatively severe damages of FRPC structures, efforts are ongoing to search methods for repairing the minor damages at their very early stage of development.

The primary limitation of this early repair idea is that it is extremely difficult to reliably detect the very initiation of damage which might be created at the subsurface locations of the FRPC. Even when the subsurface damage can be detected using the available damage detection techniques [5] its in-service repair by external manual intervention can be impossible due to the lack of human access to the damage site, let alone in the space environment. Even when it is possible to do so, in-service manual repair may be carried out but with a great cost and complexities. Self-healing can be a potential simple solution to this complex problem.

2.2 Category of healing concepts

Theoretically, any synthetic material (metal, ceramic, polymers and their composites) can heal itself to some extent or can be engineered to do so. The phenomenon of autogenous (natural autonomous) healing in concrete water-retaining structures, culverts and pipes has been known for many years and according to Hearn [11], is first detected by French Academy of Science in 1836. It has been observed that some cracks in old concrete structures are lined with white crystalline material suggesting the ability of concrete to self-seal the cracks with chemical products by itself, perhaps with the aid of rainwater and carbon dioxide in air [12]. According to Breugel [13], a systematic analysis of healing phenomenon in concrete, executed by Glanville, dates back to 1926. Already at that time a distinction was made between healing and sealing [13].

The modern concepts of healing in synthetic materials can be broadly categorized into semi-autonomous and autonomous systems. Semi-autonomous healing system requires a minimal manual intervention often in the form of setting off some external stimulus like heating. Autonomous systems, on the other hand, can self-heal, i.e., requires no manual intervention at all. For the self-healing system, the damage event itself serves as the effective stimulus for

healing. Thus a healing system to be qualified for the self-healing category must be necessarily free from any kind of external manual intervention after the damage event occurs. This requirement has very important implications in terms of practical applications where the requirement of a seemingly casual manual intervention might not be feasible to ensure or maintain. For example, if a healing system requires some external pressure after the damage occurs, it should not be termed self-healing because it is not autonomous. For real applications, it might not be possible to maintain this required pressure whenever a damage event occurs. Many works reported in the literature in this field did not precisely differentiate between the semi-autonomous and autonomous healing and confusingly termed both as self-healing. In the current work, it is essentially ensured that no manual intervention is carried out in order to trigger or influence healing after a damage event occurs. Thus, the current work can be categorized as truly autonomous self-healing of composites.

The approach of healing might be divided into intrinsic and extrinsic approach. In intrinsic healing, the host material itself can close/heal the damage. No foreign healing agent is required to incorporate into the host material. In the case of intrinsic healing of polymers, the polymer matrix structure is modified in molecular level in order to include chemical groups that bond reversibly or dynamically [14]. In the extrinsic healing systems, on the other hand, foreign materials, solids or liquids as healing agent, is incorporated inside the host materials either physically or via microcapsules or tubes. The current work involves a microcapsule based extrinsic healing approach of FRPC.

The available repair methods and the key conceptual healing strategies for advanced FRPC are summarized in figure 2.1.

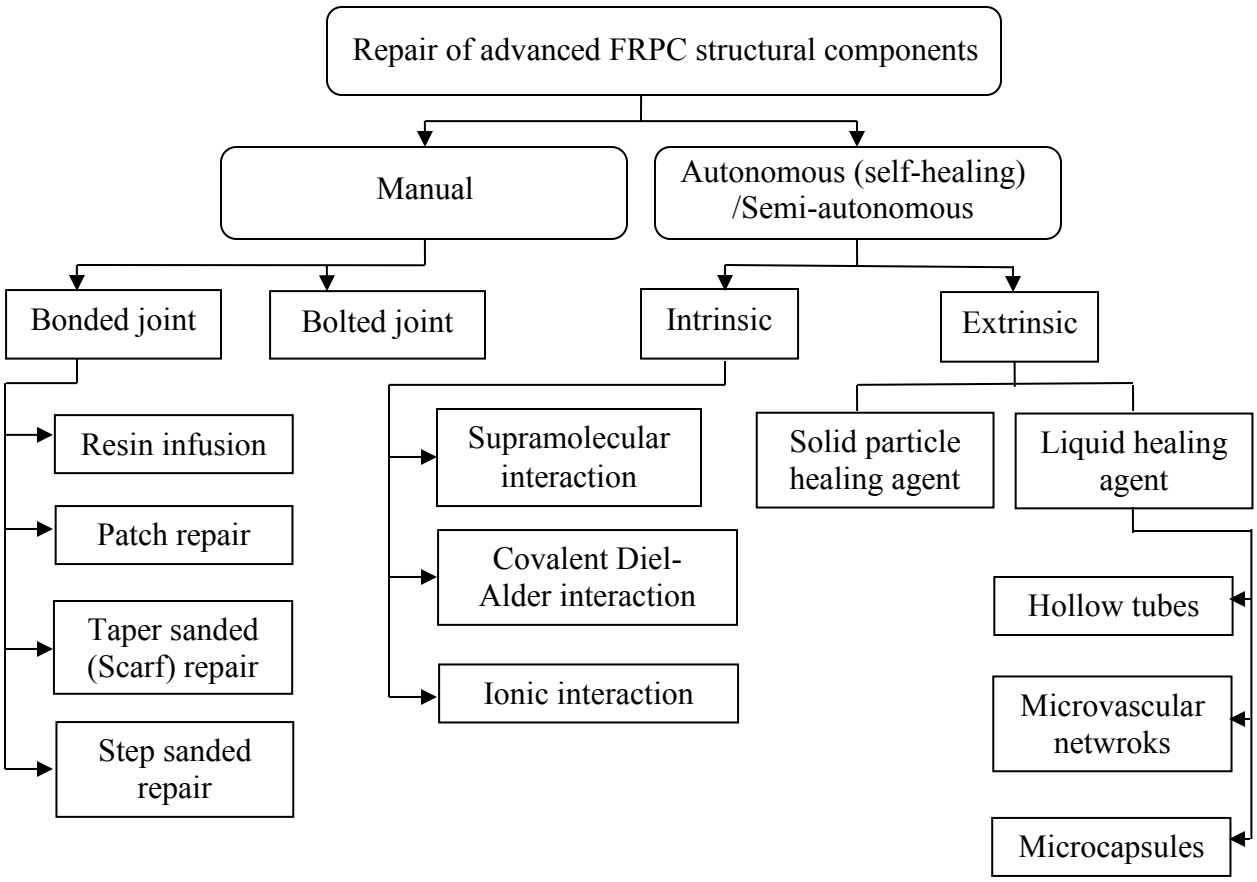

Figure 2.1 Common existing and conceptual repair methods for advanced FRPC structures

Healing can also be classified into structural and non-structural healing depending on their intended applications. Healing that can significantly restore the mechanical properties and structural integrity of materials after damage can be termed as structural healing. On the other hand, healing which can only restore other intended functionality (like filling, sealing, electrical conductivity, optical properties etc.) of the material other than its structural integrity can be termed as non-structural healing. While non-structural healing might be very important in some applications (e.g. maintaining containment of a sustaining atmosphere in space vessels and air planes through crack sealing, resisting corrosion of vehicles through paint healing), it is the structural healing which deserves the most attention considering its huge potential in ensuring the safety, reliability and prolonging the effective lifetime of a wide range of mobile structures and their critical components. The current work thus focuses on investigating the structural self-healing of FRPC.

Most of the healing techniques are still in their early stage of development and requires continuous and dedicated efforts to make them feasible for many practical applications. Ongoing efforts are being made by the dedicated material scientists and researchers to impart the healing capability to synthetic materials including ceramics, polymers and their composites. The efforts generate, so far, some very promising concepts and techniques with successful demonstration of healing capability for some class of materials system. Among them, the studies of healing in polymers and fiber reinforced composites are relatively more mature in comparison with efforts in ceramics, metals and other materials [6]. However, most of the efforts found in literature investigate the healing phenomenon at either room temperature or higher. Very few works are found dedicated to investigating self-healing at low temperatures.

A detailed review of the research works dedicated to investigating the extrinsic healing strategies is discussed in the following sections because of their relevance to the current work.

2.2.1 Hollow fiber approach

Dry [15] developed a design in which hollow porous fibers containing crack closing chemicals are embedded into cementitious materials. The chemicals are released from the fiber when degraded by chemicals or broken by structural loading repairing the crack (figure 2.2). She also proposed a vacuum assisted external delivery system which replenishes the healing agent once it is exhausted during operation.

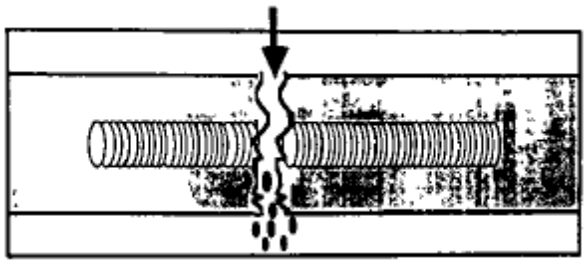

Figure 2.2 Fiber breaks due to loading; chemical is released at break [19]

Dry and coworkers [[16], [17], [18]] explored this extrinsic healing concept in concrete specimens. They embedded methyl methacrylate (MMA) inside hollow porous polypropylene fibers within concrete. Bleeding of MMA from these fibers was shown to reduce concrete permeability. In their earlier works they used cyanoacrylate as the healing agents to repair cracks

in concrete. Li et al. [19], argued that, the proposed self-healing mechanism cannot work in normal concrete, cement or even fiber reinforced concrete. This is because the width of the tensile cracks in such materials cannot be easily tuned. Localized fracture leads to continued increases in crack width under decreasing tensile load, and rapidly exhausts the amount of chemical available for crack sealing and composite re-healing. Thus, for the proposed self-healing concept to work, it is critical that the tensile crack width be controlled, and it must be limited to within tens of micrometers. Otherwise, very large hollow glass tubes will be needed, which in turn negatively modify the mechanical properties of the composite [19]. Further, according to Wu [20]. the requirement of external healing agent delivery system makes the casting of concrete difficult and can pose a severe problem if large amount of concrete needs to be cast on the construction site.

Li et al. [19], however, independently investigated and confirmed the feasibility of this approach using ethyl cyanoacrylate as healing agent inside hollow glass fibers within Engineered Cementitous Composite (ECC), a class of specially designed ductile cementitous composites having improved properties and crack width control than normal concrete, without using any external healing agent delivery system. The effectiveness of this extrinsic approach of self-healing was confirmed by measurement of the elastic modulus of the ECC. The elastic modulus was found to regain its original value in a repeat loading subsequent to damage in a first load cycle [13]. Several other groups of researchers [[21], [22], [23], [24], [25], [26]] explored this hollow fiber approach of self-healing in cementitious materials. Nishiwaki et al. [[24], [25]], for example, proposed and investigated an improved modification of hollow fiber approach of self-healing of concrete (figure 2.3). They embedded a pipe made of heat-plasticity organic film containing repair agent and a heating device in the concrete specimen. The specimen, termed as self-diagnosis composite, was made with fiber reinforced composites and electro-conductive material. Partial strain caused by the crack generated in the concrete cause the partial increase in electrical resistance. This, in turn, provided the selective heating around the cracks which can melt the film to allow the repair agent to fill up the crack and harden the repair agent in the crack. The effect of incorporating those organic film pipe and heating device on the host material is however, not investigated in the work.

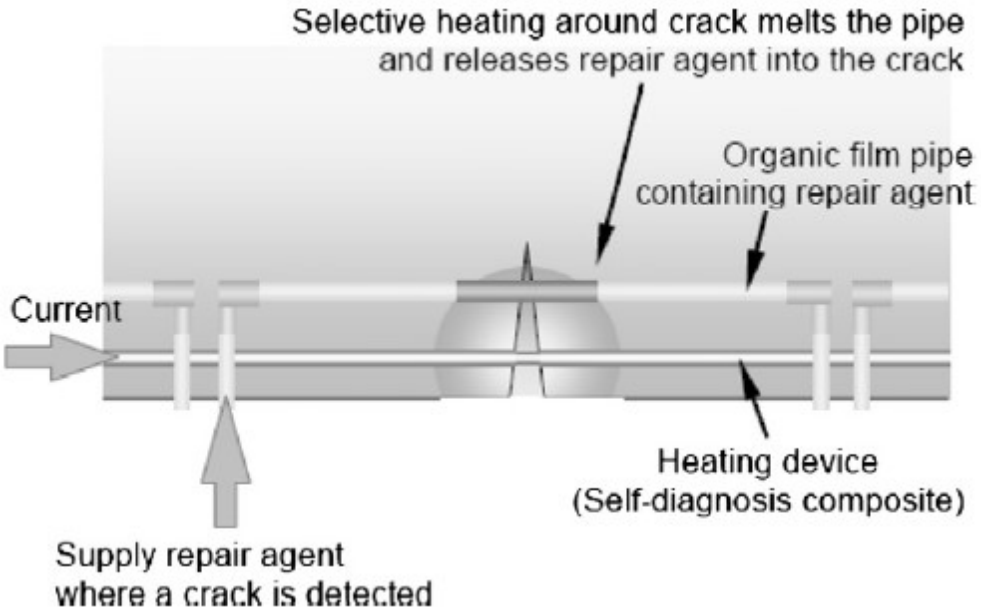

Figure 2.3 Self-healing system proposed and investigated by Nishiwaki et al. [24]

Dry [27] also expanded this healing approach to polymeric matrix using hollow glass tubes containing single part cyanoacrylate resin and two part epoxy adhesives as healing agents. The healing agent was infiltrated into glass pipette tube using vacuum. The tubes were then incorporated into epoxy resin during molding. Controlled cracking of a single repair fiber and subsequent release of repair chemical into matrix cracks was verified using optical microscopy. Impact tests demonstrated the ability of repair adhesives to migrate along and heal the cracked matrix. Quantified impact tests demonstrated that internally delayed release of adhesive restores the impact strength and ability to deflect while carrying a load. Quantified bend tests verified that release of adhesive from fibers does repair cracks, create crack reopening resistance and impede or stop crack propagation. Cyanoacrylate containing tubes incorporated epoxy specimens under second (three point bend) loading created new crack instead of reopening the crack that occurred during the first loading which indicates a good repair. However, the allowed healing time was very long (8-12 months) for most of the tests. The initial feasibility of this healing approach was verified in this work. However, the issues like the effect of incorporating external tubes on the properties of host matrix, method of filling tubes for large scale applications and the quality of

healing were not discussed in this work. Further the requirement for a very long healing time for the healing agent is not suitable for real applications in space environment.

Following her [27] work, Motuku et al. [28], Belay et al. [29], Kousourakis and Mouritz [30] and group of Bond and coworkers [[31], [32], [33]] explored this concept and extended it to the healing of FRPC. Motuku et al. [28] studied the parameters that influence the low velocity (drop weight) impact response of resin filled hollow fibers incorporated GFRP composites fabricated by Vacuum Assisted Resin transfer Molding (VARTM). The material, number, type, diameter and spatial distribution of the repairing tubes, specimen thickness, matrix material and the impact energy level were found to influence the mechanical properties and healing behavior of the composites in the investigations [[24], [26], and [29]]. Among the borosilicate glass micro-capillary pipets, flint glass pasteur pipets, copper tubing and aluminum tubing materials investigated in [28] work, the borosilicate glass micro-capillary pipets were found to be most suitable for the release of repairing solution to the damage site under impact loading. Higher number of repair tubes (more than 3), smaller spacing (less than 5 mm) among them and the higher outside diameter (1.5-1.6 mm) of the tubes were found to be reasons of non-uniform wetting of fibers adjacent to the tubes leading to formation of voids in the laminate during its fabrication by VARTM. An increased distance between the storage tubes and use of smaller diameter tubes eliminated the void problem. Repeatability of data improved with increased specimen thickness due to less micro-flaw sensitivity and the damage increased with impact energy as expected. Dry [27] and Motuku et al. [28] used large diameter (mm scale) repair tubes which might act as initiation sites for composite failure as pointed out by Belay et al. [29]. The work of Motuku et al. [28] thus confirms the fact that, modifying the host matrix by incorporating foreign materials and architecture in it might compromise the quality of the composites.

Belay et al. [29], on the contrary, utilized hollow glass fibers (μm scale) both as reinforcements and containers for the healing agents. They introduced three variations of the approach as shown in figure 2.4.

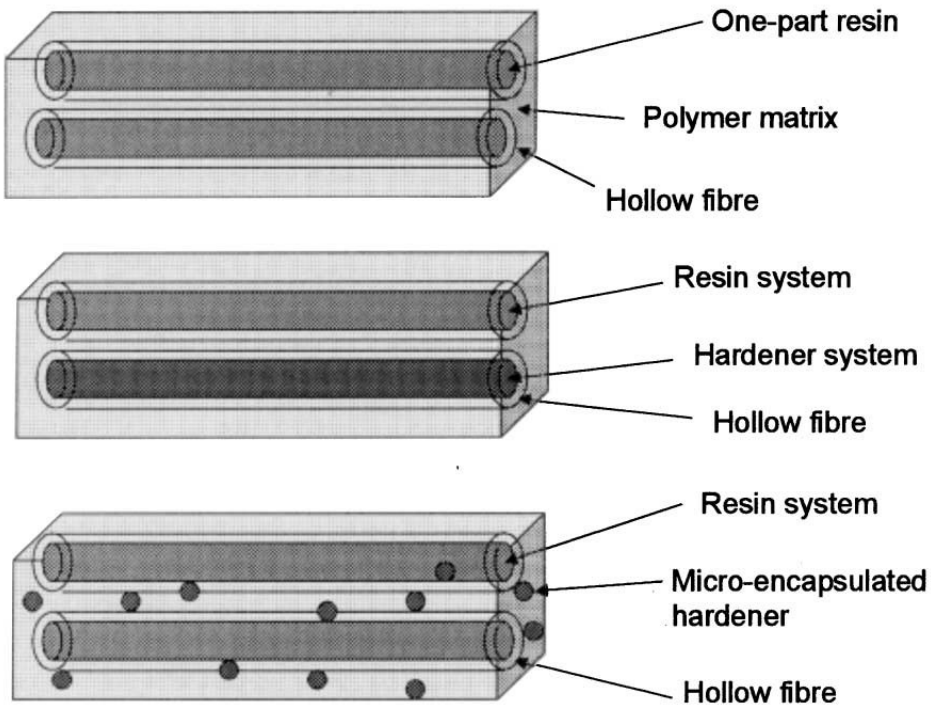

Figure 2.4 Variations of healing strategy using the hollow fiber approach [29]

In first case, all fibers are filled with one part curing resin. In the second variation, a two part system is adapted where the resin is filled into some fibers and the hardener is filled into other fibers. In the last variation, one component is filled in hollow fibers and the other component is encapsulated and dispersed into the matrix. The authors investigated the first two cases in this work. They also introduced a method by which the repair resins were reported to be successfully infiltrated into the microscale hollow fibers in the composite. The filling method consisted of a rotary vacuum pump sealed along one edge of the composite panel with the other end resting in the reservoir of the filling agent as shown in figure 2.5.

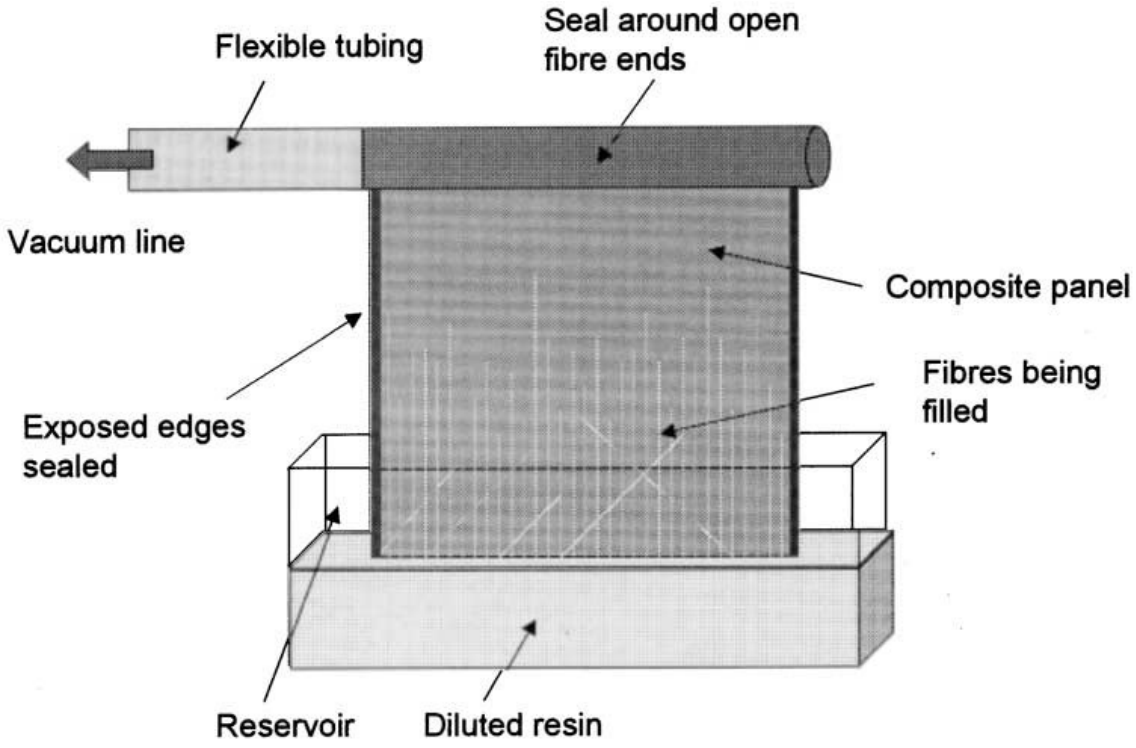

Figure 2.5 Schematic diagram of the vacuum assisted capillary action filling technique [29]

The vacuum assisted in pulling the resin up through the fibers of the composite panel by capillary action. Complete filling of the fibers was reported by this method. The authors [29] recommended the use of solvent for quicker filling of finer tubes.

Use of cyanoacrylate as the one part healing agent was unsuccessful as it cured quickly on contact with the mouth of the capillary tubes sealing the tubes. This material was thus not recommended as repair resin for small diameter hollow fiber systems. For the two part epoxy system, heating (60^{o}C) and vacuum treatment was required after the impact damage of the specimen to draw the resin and hardener out of the fibers in order to achieve healing. The healing is thus not autonomic. Even then, only 10% improvement in the compression strength after impact was achieved compared to the impacted control specimens (no healing agents filled). Further, the healed strength was much less in relation to the strength of the undamaged composites. This work, although, showed the potential and feasibility of this approach, the

quality of healing achieved was poor. Further, the healing agent (cyanoacrylates and epoxy/hardener) used in these works may not be suitable for low temperature space applications.

Pang and Bond [31] employed the second variation of Belay's work [29] in the cross ply GFRP composites. They achieved only 10% recovery of flexural strength in their flexure after impact (FAI) tests due to healing (room temperature, 24 hour) compared with the control (having hollow fiber layers without healing agent) specimens. The same group in another work [32] achieved 87% recovery of strength compared to undamaged control specimens as determined by four point bending tests when the healing treatment was carried out at 100C for 2 hours. 16% reduction of original flexural strength due to the inclusion of hollow glass fiber (60 μm dia) layers was also observed in their work. Placing individual hollow fibers with spacing distances 70 μm and 200 μm between the layers of CFRP laminates reduced the original strength by 8% and 2% respectively. They also found evidence, as they mentioned, to suggest that if crack faces separate by more than 30 μm, capillary forces may be insufficient, or there may be inadequate resin volume released to fully infiltrate the damage. This work, thus confirms a quantitative weakening effect of incorporating foreign materials/architecture into the host matrix. This weakening effect, however, is not considered in the calculation of recovery of strength. Further, the achievement of significant healing in this work was not autonomic as they needed to heat up the specimens.

Kousourakis and Mouritz [30] and Williams et al. [33] also studied the effect of hollow fibres on the mechanical properties of FRP composites. Williams et al. [33] found less than 10% loss in flexural strength to carbon/epoxy composites due to the incorporation of hollow fibers (60 μm dia). The studies of [33] showed that hollow fibres located along the mid-thickness plane of the composite material cause no change or a small loss (less than a few per cent) to the in-plane elastic modulus. The tension and compression strengths were not changed significantly when hollow fibres were aligned parallel to the loading direction. However, the strength properties were reduced when the fibres were normal to the load. The strength loss was caused by changes to the composite microstructure (e.g. increased ply waviness) [33]. Diameter of the hollow fibers, their orientation, fiber spacing and the percentage of the load-bearing area occupied by the hollow fibres were found to influence the mechanical properties of the composites significantly in these works. These weakening effects of incorporating foreign materials/architectures into the modified host matrix should always be considered in determining the healing efficiency of a self-

healing system. Otherwise, an unreliable likely high value of healing efficiency might give a wrong perception about the healing performance.

In recent years, studies of the hollow fiber approach tend to be shifted towards hollow channels and microvascular network approach of healing which is discussed in the following section.

2.2.2 Hollow channel/microvascular network approach

Therriault et al., the group of White and coworkers [34], demonstrated the fabrication of three-dimensional (3D) microvascular networks through direct-write assembly of a fugitive organic ink. This approach yielded a pervasive network of smooth cylindrical channels (~10–300 μm) with defined connectivity. Recent advances in soft lithographic and direct write assembly methods have enabled the creation of materials with complex embedded microvascular networks [35]. Toohey et al. [35] first demonstrated the healing of damage of a coating-substrate architecture having embedded microvascular networks as shown in figure 2.6.

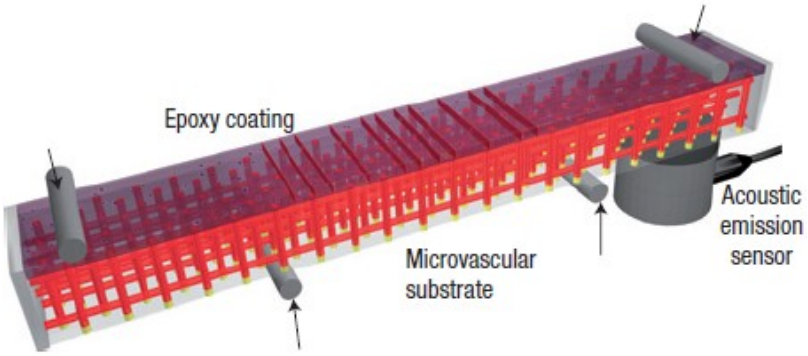

Figure 2.6 Schematic diagram of the self-healing structure composed of a microvascular substrate and a brittle epoxy coating containing embedded catalyst in a four-point bending configuration monitored with an acoustic-emission sensor [35]

An epoxy coating was deposited on a more ductile substrate that contained the three-dimensional (3D) microvascular network. The fabrication and healing characterization process as described in [35] is given here in detail for greater understanding of the work.

Direct-write assembly was used to embed fully interconnected 3D microchannel network(s) in an epoxy matrix. First a 3D scaffolds were fabricated with a fugitive organic ink using a

robotic deposition apparatus in a layer wise scheme. After deposition, the ink scaffold was infiltrated with uncured EnviroTex Lite epoxy (ETI) and allowed to cure. After curing, beam substrates were cut to size and polished. The fugitive ink was then removed by heating the substrate to 75°C and applying a light vacuum. A more brittle epoxy coating (approximately 700 μm thick) containing Grubbs' catalyst particles was applied to the top surface of the microvascular substrate. The coated microvascular substrates were then filled with DCPD healing agent. Finally, the bottom and sides of the substrate were sealed by selectively polymerizing a photopolymer in the channels using a mercury source. A rectangular network design was chosen in which the vertical channels deliver monomer to the cracks in the coating, whereas the horizontal channels enable the network to be filled from the side. The chosen channel diameter was 200 μm to balance the requirement of minimizing the total pore volume, ease of fabrication and network operation [35].

The coating–substrate beams were loaded in four-point bending placing the coating under tension to initiate a single crack in the coating without damaging the underlying microvascular substrate. With each loading cycle, the same crack reopened and was subsequently healed repeatedly. An acoustic-emission sensor was placed on the beam to detect the crack opening events during testing. The time at which the critical acoustic-emission event occurred was used to determine the loads of crack formation and reopening in the virgin and healed specimen tests. Quantitative healing tests were limited to a single crack by stopping the loading process after the first acoustic-emission signal was detected. After testing, the coating was healed at room temperature (approximately 25°C) for 12 h. The network was then replenished with monomer before carrying out the next bend test. This cycle was repeated until the crack could no longer heal. Healing efficiency was calculated for each healing cycle on the basis of the ratio of the critical loads for crack opening, $\eta = P^{\text{Healed}}/P^{\text{Virgin}}$, where P is the applied critical load when the crack occurs [35]. The healing efficiency at different catalyst concentrations and various healing cycles are shown in figure 2.7.

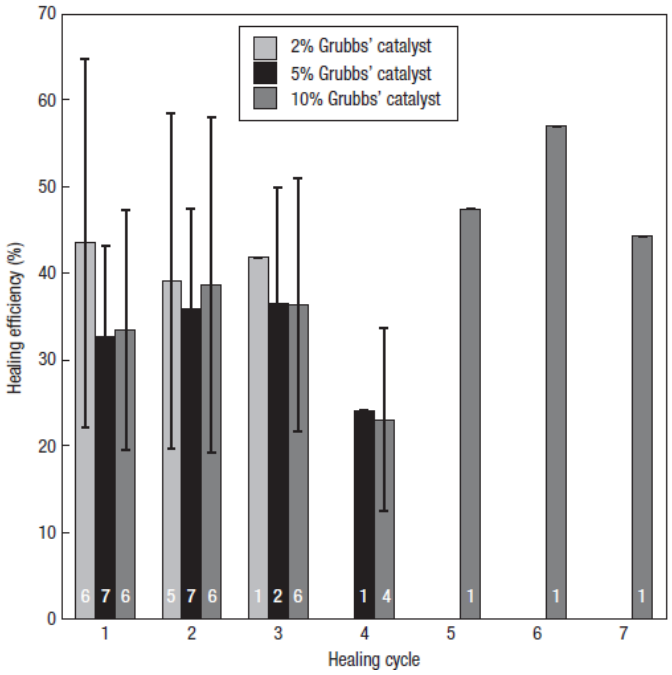

Figure 2.7 Healing efficiency for specimens with 2 wt%, 5 wt% and 10 wt% catalyst in the coating that exhibited healing. The white numbers at the bottom of each column denote the number of successfully healed specimens in the average and the error bars are one standard deviation [35]

Toohey et al. [36] pointed to another drawback of this design which is the restricted availability of the solid-phase catalyst that eventually became depleted upon repeated healing of the same crack [36]. They [36] overcame this difficulty by introducing a multi-network architecture for delivery of a two-part epoxy-based healing chemistry. Epoxy resin and amine-based curing agents were transported to the crack plane through two sets of independent vascular networks embedded within a ductile polymer substrate beneath the coating. Two separate independent vascular networks were created by first creating a continuous, interconnected microvascular network using the direct-write (DW) method. Multiple networks were then isolated by infilling the network with a photo curable resin and selectively photo-polymerizing thin parallel sections of these resin-filled micro channels. Through this approach, isolated microvascular networks were produced that can independently house different healing agents within the substrate until a crack forms in the coating. Both healing components were wicked by capillary forces into the crack plane where they reacted and bonded the crack faces closed. Same test protocol as in [35] was followed in this work and healing efficiencies of over 60% were

achieved for up to 16 intermittent healing cycles of a single crack. According to [36], the specimens were required to be subjected to cyclic loading to enhance fluid flow into the crack and promote mixing of the components. Polymerized layer of materials formed in the crack during the initial healing cycles inhibit the ability of resin and curing agent to flow further and adequately mix for subsequent healing. Thus, multiple healing of crack could not be achieved in an autonomous way using the microvascular network approach in this work.

Hansen et al. [[37], [38]] extended the capabilities of Direct Ink Writing (DIW) technique to include dual ink writing to separate neighboring networks and vertical ink writing to provide fluid access from the underlying networks to the surface damage region. They used epoxy resins and its hardener as the healing agents in these two separate networks. The specimens were subjected to cyclic flexure loading (50 cycles at 100mm displacement; external intervention) to enhance mixing of the fluids in the crack plane prior to healing at 30C for 48 h. Up to 30 cycles of healing (recovery of fracture toughness as measured by the ratio of critical loads during four-point bending) was achieved in this system. Clearly, the healing is not autonomic in this case.

In another work, Hansen et al. [39] reported the assembly and characterization of self-healing materials with embedded ternary interpenetrating microvascular networks in an epoxy coating/substrate architecture (figure 2.8). The networks were fabricated by direct-write assembly of two fugitive inks, in which one ink defines the three microvascular networks and the other ink functions solely as a spacer to isolate each network. Two of the microvascular networks were devoted to supplying the epoxy resin and hardener healing agents, while the third network circulates a thermally regulated fluid. The diameter of the microchannel networks for healing agent was 330 μm and the diameter of thermal fluid network was 200 μm. Each network had a single input and output connected to a macroscale reservoir that supplies the healing or thermal fluids, respectively. Heated water (30-70C) was circulated within the third network at a flow rate of 5 mL min^{-1}. Same test protocol as in [35] was followed to characterize healing. Healing times were reported to be reduced by over an order of magnitude by the localized heating in the damaged regions enabled by circulating temperature-controlled fluid through embedded microvasculature. Total healing times of 40, 4, and 1.5 hours were required for samples held at 30, 50 and 70 °C, respectively, to achieve comparable original fracture stress [39].

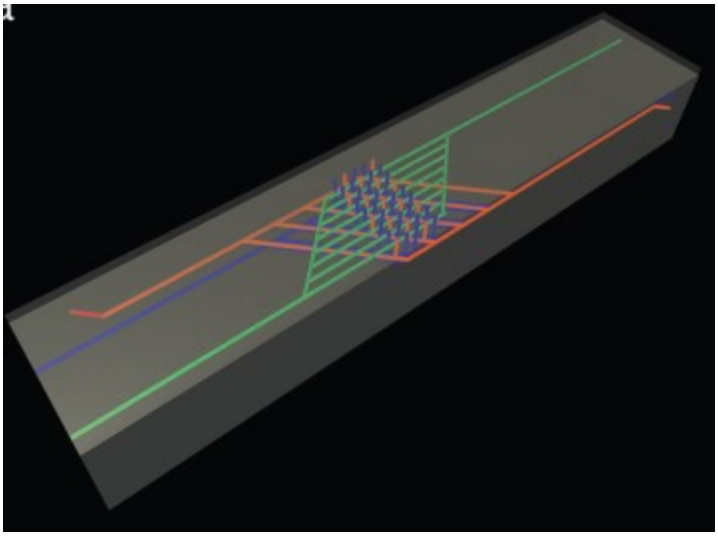

Figure 2.8 Schematic view of epoxy coating/substrate architecture with embedded interpenetrating microvascular networks. Two of these networks house epoxy resin (blue) and hardener (red), while the third network provides thermal control (green) to accelerate healing kinetics after damage occurs [39]

Critically, several limitations of the process of evaluating healing performance can be deduced from the above works. Firstly, the repeated healing events are not autonomic. The microvascular network was replenished with monomer after each healing cycle. In real applications, it might not be feasible to replenish monomer at each damage event. Secondly, it might be difficult to precisely select the critical acoustic signal (when the quasi-static loading needed to be stopped immediately). The uncertainty might significantly affect the value of the critical loading of the virgin and healed specimen which is the basis of the healing efficiency measurement. Finally, the effect of embedded microvascular network architecture on the mechanical properties of the matrix is not discussed in these works [[37], [38], [39]]. The above limitations necessitate the establishment of a suitable protocol for evaluating healing performance. Further, the above investigations were carried out for non-structural applications (coating-substrate assembly). The current work, on the contrary, deals with structural self-healing for low temperature applications. The healing agents (epoxy/hardener) investigated in the above works are also not suitable for low temperature applications.

Bond and coworkers [[40], [41]] incorporated vasculature into FRP composites using solder wire preforms. The solder wire was either laid between plies (fabrication route A) or nested in

pre-cut recesses within the plies (fabrication route B) during the stacking sequence. The solder was then removed for post-cure under the application of heat and vacuum in a 'lost-wax' type process. Based on the experimental results, they [[40], [41]] observed that fabrication route B offers the better potential for vascule-damage interactions, a pre-requisite for efficient healing [42]. Vascule orientation, diameter and location in the ply stack as well as the fabrication technique were found to be key factors in ensuring the integrity of the fiber architecture and maintaining the original mechanical properties of the laminate [[40], [41]]. These issues have also received significant attention from research groups studying the incorporation of Fibre Optic Sensors (FOS) into composite structures [41]. A compression after impact (CAI) test protocol was followed, with specimens tested in the undamaged, damaged (post 10J impact), and healed states. In the work of [40], syringes fitted with suitable gauge hypodermic needles were used to manually inject healing agent [100 pph DGEBA :EPON 828 as resin, 25 pph Ethyl Phenylacetate (EPA) as diluents to reduce resin viscosity and 12pph Diethylenetriamine (DETA) as curing agent for the resin] into the vascules located within the damaged region only. More than 97% of the post impact compression strength was recovered due to healing when the samples were kept at room temperature for 7 days. The healing process, however, is not autonomic as the healing agents were manually injected into the damage sites. The effect of vasculature on the original mechanical properties of the laminate was not discussed in the work of [30]. Norris et al. [41] pointed out that in the case of vascular networks, the knockdown in mechanical performance has been negligible due to the host materials ability to form around the networks. However, orientation of the vascules off-axis led to significant fiber waviness and resin pocket regions for fabrication route A and terminated fibers with fabrication route B (shown in figure 2.9), both of which significantly reduced the subsequent load bearing ability of the FRP composite specimens [41]. Norris et al. [43] also anticipated that the inclusion of the vascules will result in a slight decrease in laminate stiffness.

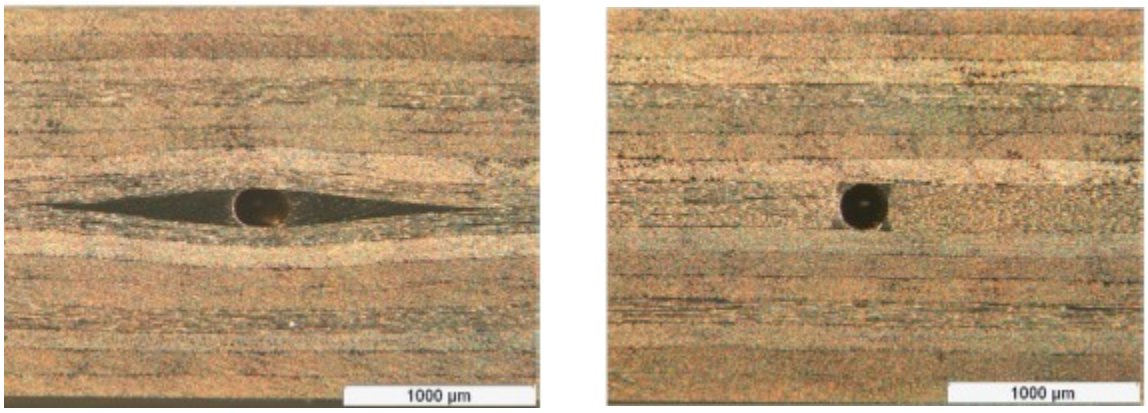

Figure 2.9 Transverse vascule fabricated via a) route A and b) route B [41]

These approaches, offer the potential for connection to an external reservoir that could pump large volumes of a pressurized, mobile liquid phase (healing agents) to the regions of damage [41].

Hamilton et al., the group of White [44] also investigated pressurized vascular systems for healing quasi-static and fatigue cracks. They overcame some limitations of capillary force induced delivery of healing agent to the crack site via micro channels by incorporating a pressurized healing agent delivery system. In this system, two micro channels having a diameter of 280 µm inside the sample matrix were filled separately with liquid resin and hardener as shown in figure 2.10. The micro channels were connected to pressurized reservoirs (case I- with static pressure head; case II- with computer controlled pumps) of healing agents via tubing and syringe tips inserted 1-2 mm into each microchannel. Healing efficiency as high as 100%, as measured by quasi-static fracture tests of the Double Cleavage Drilled Compression (DCDC) specimens, were reported even after 15 repeated healing cycles using dynamic pumping protocol. The specimens were kept clamped for certain period at the interval between the loadings to achieve healing. The increased degree of mixing resulting from the dynamic pumping protocols was attributed to the higher healing efficiencies as compared with the samples pumped using constant pressure or samples without pressurized vascular systems, in which capillary forces drove healing agent flow [44].

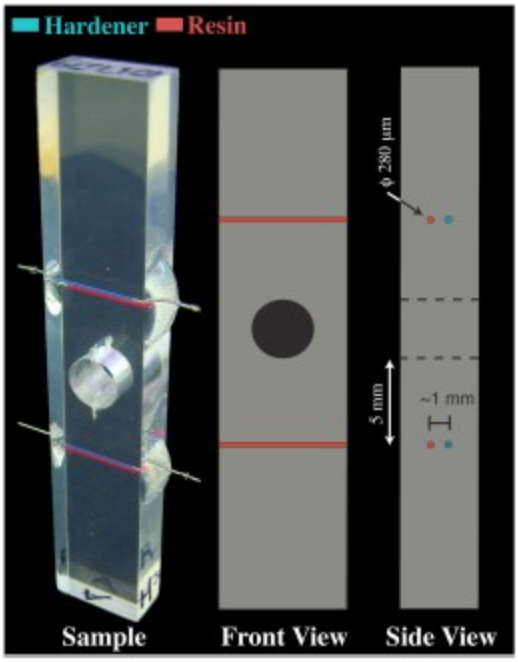

Figure 2.10 Image of the fracture sample and schematic detailing microchannel position and content [44]

Fatigue test of the same geometry specimen using two part epoxy adhesive components in the micro channels showed decrease in the rate of crack propagation using pressurized delivery system. They achieved better healing performance using pressurized vascular system that occupy only 0.1% specimen volume compared with a volume fraction of 1.3% in unpressurized system. As a concept, the healing system is interesting. However, the suitability of this healing approach in real applications is questionable as it requires a separate reservoir of healing agents and a delivery systems involving tubes, syringe tips and pumps. The healing process was also not autonomic as clamping of specimen was necessary to achieve significant healing.

According to [[45], [46]], neither of the approaches of healing, namely, hollow fiber approach or microvascular network via the direct ink writing of a fugitive ink, are suitable for rapid, large-scale production of fiber-reinforced composites with complex vasculatures due to either incompatibility with existing composites manufacturing methods and materials or lack of scalability and vascular complexity of the fabrication approach.

Group of White and Sottos [[45], [46], [47], [48]] demonstrated other interesting approaches in integrating the microvascular networks in commercial composite materials. In the epoxy matrix they embedded sacrificial polymer fibers which depolymerizes when heated,

resulting in a vaporization of fiber material. Vacuum removal of the depolymerized gaseous monomer produces hollow channels as inverse replica of the fiber diameter in the matrix as shown in figure 2.11.

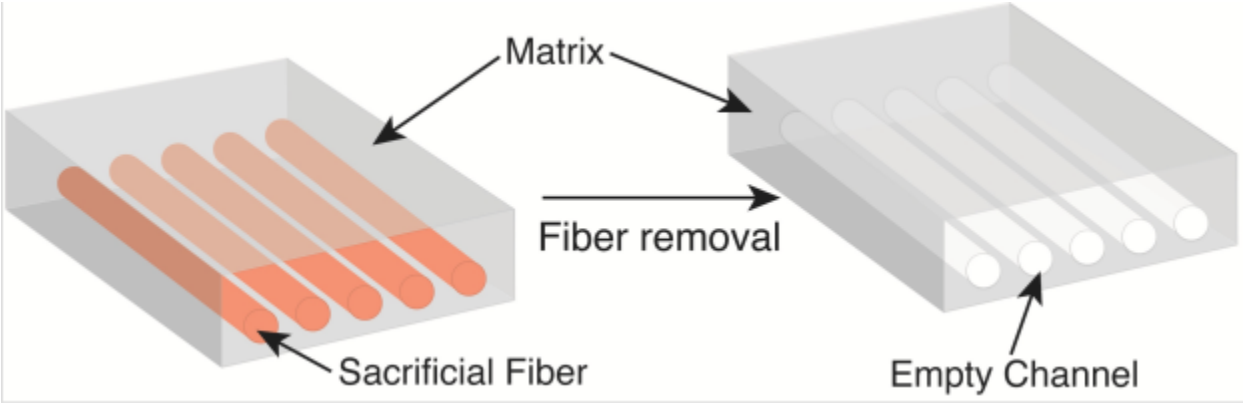

Figure 2.11 Schematic images of sacrificial fibers embedded in a matrix and subsequential fiber removal resulting in microvascular networks in the matrix [47]

Inside epoxy matrix, they embedded catalyst treated commercial poly lactic acid (PLA) fibers which can convert into gas at temperatures above 180ºC. Removal of the gas produced micro vascularized matrix. However, infiltration of commercial PLA fibers into the matrix poses a serious problem caused by incomplete removal of sacrificial fibers introducing imperfections (plugs, necks, etc.) that block the micro channels. In order to overcome this problem they introduced an alternative fiber manufacturing method which combines the preparation of viscous PLA solution mixed with metal catalysts and the traditional dry fiber spinning technique. In [46] they followed this approach and fabricated microvascular fiber-reinforced composites with channels over one meter in length that can be subsequently filled with a variety of liquids including aqueous solutions, organic solvents, and liquid metals , as shown in figure 2.12, for applications such as self-healing and thermal management [48].

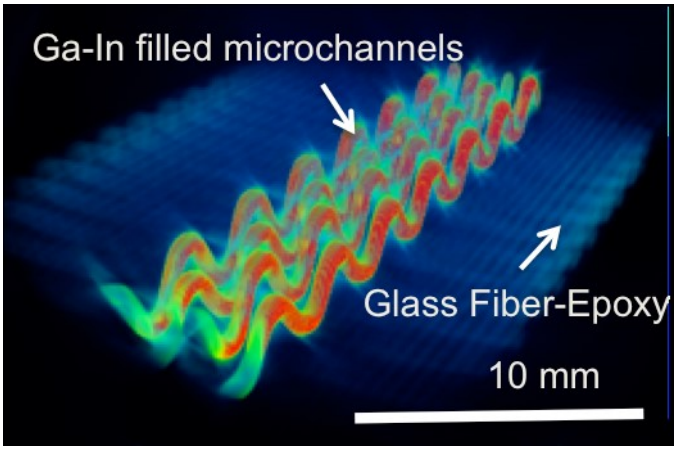

Figure 2.12 Micro CT image of glass/epoxy composite embedded with Ga-In filled 3D microvascular network [45]

Clearly, the hollow channel/microvascular network approach holds great promise for healing of polymer composites. However, the issues related to the fabrication of fiber reinforced composites with embedded microvascular networks, autonomic refilling of the network with liquid healing agents, their effect on the properties of the host material and the achievement of healing in an autonomic manner during a damage event need to be investigated elaborately to make this approach suitable for commercial applications. This is to be reminded here that none of the healing agents investigated in the above works were suitable for low temperature applications. Especially, the issues like the self-healing at low temperatures and evaluation of self-healing performance of FRPC are not settled. These issues are thus investigated in the current work.

As the current work deals with the microcapsule based autonomic structural self-healing of polymer composite materials, the available literatures associated are reviewed in greater details in the following sections.

2.2.3 Microencapsulation approach

a) Dicylopentadiene (DCPD)/Grubbs catalyst system

Numerous works have been carried out by the research groups of White and Sottos [3] to investigate the microcapsule based DCPD/Grubbs healing system. Keller and Sottos [49], Brown et al. [[50], [51]] and Rule et al. [52] investigated the effect of microcapsule properties on the modified (healing agent incorporated) epoxy specimen. They found that microcapsules if

adequately bonded to the matrix can actually improve its fracture toughness contrary to the presence of voids or other poorly bonded particles which tend to reduce the same. Keller and Sottos [49] found that geometry and fill content of microcapsules also influences the toughening mechanism of the matrix. However, they found a continuous reduction in strength of the epoxy specimen with increasing wt% of microcapsules. They pointed out that good adhesion of the microcapsules with the matrix is essential for encounter of microcapsules and its subsequent rupture by the approaching matrix crack triggering self-healing. The work of [51] revealed that the catalysts size and concentration has also significant effect on the properties of the matrix. Further, they suggested choosing the mixing order of the healing agents such that the amine curing agent does not come in direct contact with the Grubbs catalyst to prevent its degradation. To avoid degradation of catalyst, Rule et al. [52] incorporated wax protected catalyst into modified epoxy.

The research group of White and coworkers [[3], [49], [50], [51], [52], [53], [54]] employed the fracture-heal-fracture approach in fracture testing protocol with Tapered Double Cantilever Beam (TDCB) geometry, developed by Mostovoy et al. [55], to determine the healing efficiency of epoxy specimen. Brown et al. in [50] achieved over 70% healing efficiency with 5 wt% 180 μm (average diameter) microcapsules and 20 wt% 50 μm capsules with 2.5 wt% catalyst for both cases. Brown et al. in other work [51] achieved up to 90% healing efficiency of epoxy specimen with 5 wt% 180 μm capsules and 2.5 wt% catalyst after 10 hours of healing. Rule et al. [52] observed that the healing performance was maximized when sufficient volume of monomer was present to fill the cracks completely. Also they showed a linear relationship between the amount of monomer delivered to the crack site and the average diameter of microcapsules for a given weight fraction. It is to be noted here that the fracture testing protocol of TDCB specimens employed by the researchers in the group of White and coworkers to evaluate the healing efficiency is not a perfectly autonomic process of achieving healing. It involves keeping the cracked faces of the specimens in contact by external intervention after the first loading for certain periods before subsequent loading. Further, healing efficiency as determined by the mode I fracture test protocol of TDCB resin samples in [[3], [49], [50], [51], [52], [53], [54]], involves calculating the ratio of critical loads of the same modified sample (incorporated with healing agents) during the first (virgin) and second (healed) loading. No comparison is made with respect to neat regular samples (not incorporated with healing agents) in the definition of

healing efficiency in these works. Incorporation of foreign materials like microcapsules and catalysts can alter the base mechanical property of the neat sample. Depending on the various factors, the base mechanical properties might improve or degrade compared with the neat samples due to the inclusion of foreign materials as found in [[50], [51]]. This likely alterations in the base mechanical property reflected in the first (termed as virgin) loading of the modified sample (incorporated with healing agents) might give a wrong perception about the true healing performance. This is discussed in detail with different possible scenario analysis in chapter 5.

Kirkby et al. [54], researchers in the same group of White and Sottos [3], instead, investigated healing of epoxy aided by embedded shape memory alloy (SMA) wires. The embedded SMA wires that bridged the fracture plane of the TDCB specimens (as shown in figure 2.13) were activated after fracture by passing DC current through it.

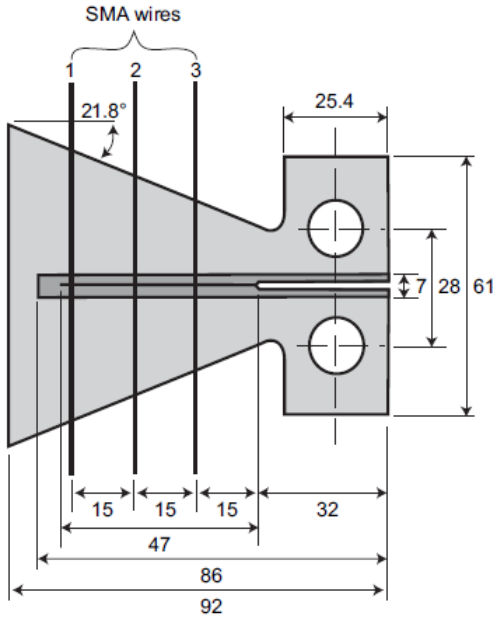

Figure 2.13 TDCB geometry; samples were prepared with three SMA wires perpendicular to the crack plane, spaced uniformly. The distance units are mm [54]

The activation of the SMA wires increased the temperature of the local matrix to 80ºC and generated an axial recovery force to close the crack during the healing period which substituted the requirement of manual clamping of the cracked surfaces to achieve significant healing. The comparison in healing performance with and without embedded SMA wires is shown in figure 2.14. The improvement was attributed to the reduction in crack volume due to the axial forces generated by activated SMA wires. They also observed that an over-delivery of healing agent of at least a factor of two is required to ensure complete filling of the crack and the highest healing

efficiency [54]. The healing process investigated, however, is not autonomic as manual activation of SMA wires is required after the fracture event.

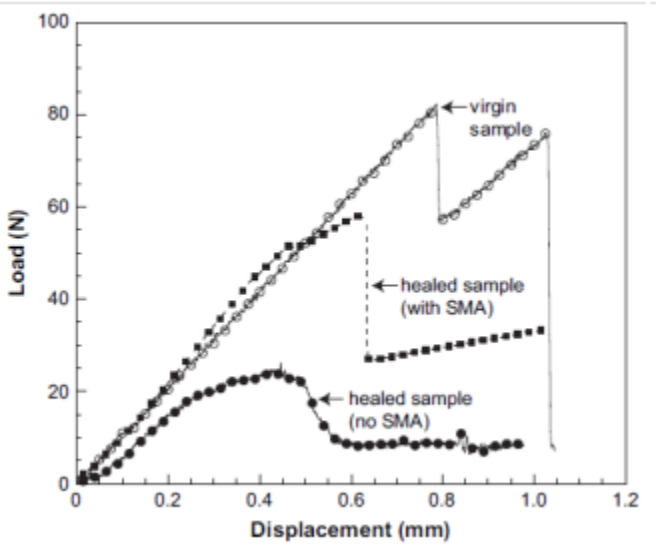

Figure 2.14 Load-displacement curve of the epoxy TDCB fracture specimen containing DCPD microcapsules, Grubbs catalyst and SMA wires [54]. Virgin sample actually refers to the modified resin sample (with healing agents) during the first loading of the fracture test method

One of the earliest investigations dealing with the healing (DCPD/Grubbs system) of fiber reinforced composites (FRC) was carried out by Kessler et al. [[56], [57]], in the research group of White and Sottos [3]. They employed the fracture-heal-fracture approach in the fracture testing of double cantilever beam (DCB) geometry (figure 2.15 a) specimen [56] and width-tapered double cantilever beam (WTDCB) geometry (figure 2.15 b) specimen [57] to evaluate the healing efficiency of the glass/epoxy [56] and carbon/epoxy [57] composites.

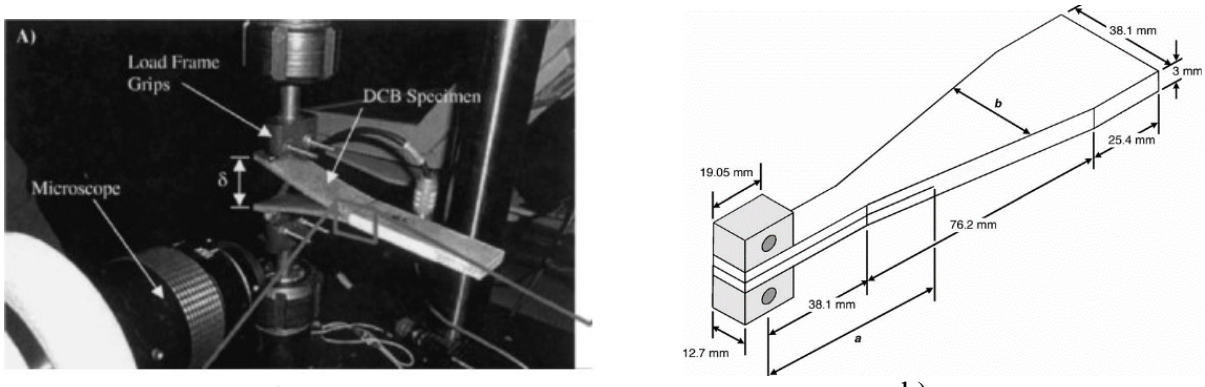

a) b)

Figure 2.15 a) DCB specimen during testing [56] and b) schematic of WTDCB specimen [57]

Fracture testing of DCB specimens [56] involves the direct measurement of fracture toughness through several calculation steps using approximations estimating the initial crack lengths. Healing efficiency is evaluated by comparing the fracture toughness of the modified specimens during the first and second loadings. Fracture testing of (WTDCB) geometry specimens [57], on the other hand, is perceived to make the energy release rate independent of crack lengths leading to direct evaluation of healing efficiency simply by comparing the critical loads during the first and second loadings according to equation 1.

$$\eta = \sqrt{\frac{G_{IC}^{Healed}}{G_{IC}^{Virgin}}} = \frac{K_{IC}^{Healed}}{K_{IC}^{Virgin}} = \frac{P_{IC}^{Healed}}{P_{IC}^{Virgin}} \quad \text{..... (1) [57]}$$

Where, G, K and P values represent the critical strain energy release rate, critical stress intensity factor and the critical loads during the first (termed as virgin) loading and second (termed as healed) loading respectively.

Three groups of specimens were manufactured and tested in these works as shown and explained in figure 2.16.

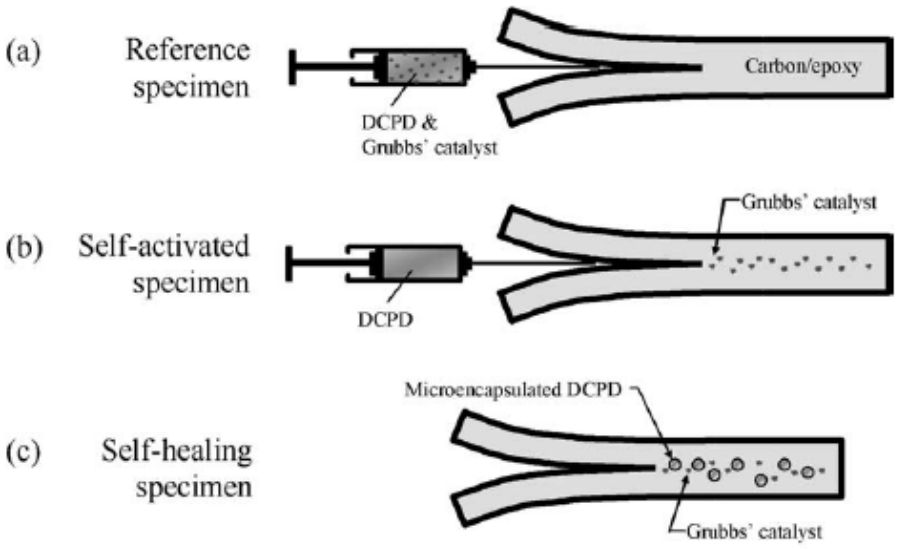

Figure 2.16 a) Reference specimen where catalyzed healing agent is manually injected into the delamination after first loading; b) Self-activated specimen where catalyst is already embedded in the matrix and only monomer is manually injected into the delamination and c) Self-healing specimen where both encapsulated monomer and catalyst are embedded into the matrix [57]

During the fracture testing of the specimens, the delaminated faces after the first loading was kept clamped with modest pressure during the healing period (48 hours) before the second loading. A maximum healing efficiency of 67% for reference specimens (manually injected catalyzed DCPD) and a maximum of only 19% healing efficiency for the self-activated GFRP specimens (manually injected uncatalyzed DCPD), were achieved in [56]. In another work [57], an average healing efficiency of 99% for reference specimens and 73% for self-activated CFRP specimens, based on equation 1, was reported. Clearly, the demonstrated healing for the reference and self-activated specimens is completely manual. Even for the 'self-healing' specimens the delaminated faces were kept clamped during the healing period which is a form of considerable manual intervention and the healing efficiency was only 38% [57]. The achievement of healing in these works is thus not autonomic.

Further, the efficiency values reported in [[56], [57]] were based on comparing the averages of the critical parameters (fracture toughness [56], critical loads [57]) of the same category specimens (e.g self-activated modified specimens) during the first and second loading which, in fact, is not the true index of the healing performance. The true index of healing performance should be realized by comparing the critical parameters between the modified (with healing agent) and regular (without healing agents) specimens.

Patel et al. [58], the researchers in the same group of White and Sottos [3], investigated the healing performance of glass/epoxy composite panels subjected to drop weight impact loads. Healing was first evaluated by fluorescent labeling of damage and image processing and then by compression after impact (CAI) testing. A 51% reduction in crack length and 97% recovery of residual compressive strength (quality) is reported in the work. However, the healing performance was calculated by comparing the values with the modified non healing control specimen (C-III) which was already incorporated with DCPD microcapsules and wax microspheres without catalyst; not with the neat regular specimens as shown in figure 2.17. Incorporation of foreign materials into CIII specimens might reduce the properties of the host material furnishing high efficiency values. From a practical point of view, the comparison of performance of self-healing specimens (SH) to neat regular specimens is more fair in a sense that it represents the true index of improvement due to healing. Further, it was not clear whether the characteristic mechanical properties of the regular panels was sacrificed, in this work, with lower

compaction pressure (4.8 kPa for regular panels compared to 95.8 kPa for modified panels) applied during the manufacturing of composite specimens with compression molding process.

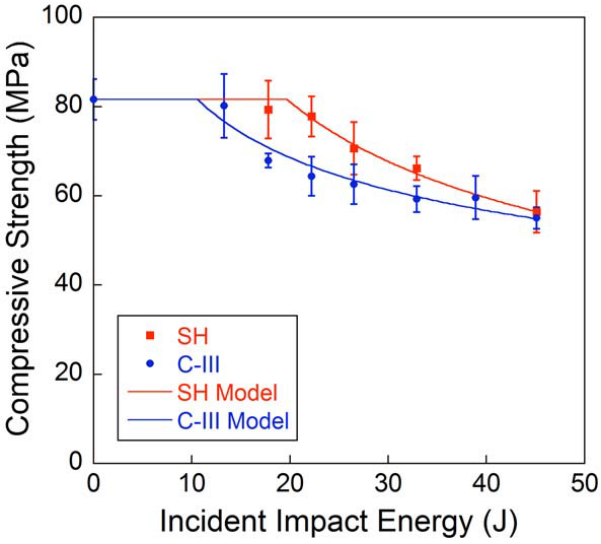

Figure 2.17 Residual compressive strength (RCS) for non-healing control panels (C-III, micro-encapsulated DCPD and wax microsphere, no catalyst) and self-healing panels (SH, microencapsulated DCPD and catalyst) versus nominal incident impact energy. Error bars are ±one standard deviation. Also plotted is a fit to RCS [58]

O'Brien and White [59] assessed the healing of microencapsulated DCPD/Grubbs system for the delamination of fiber reinforced composite skin/stringer flange debond specimen as shown in figure 2.18.

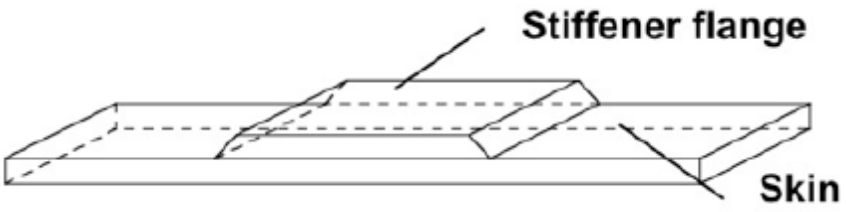

Figure 2.18 Skin/stiffener flange debond specimen configuration [59]

They [59] employed an interlayer approach to produce the modified prepregs in order to fabricate the specimens. In the interlayer approach, the microcapsules (10-100 μm) and catalyst

were dispersed in the regular base resin bath to produce modified resin. The modified resin was then deposited onto a carrier fabric on the top of each composite layer (containing the regular base resin only) to produce the prepregs as in figure 2.19 [59].

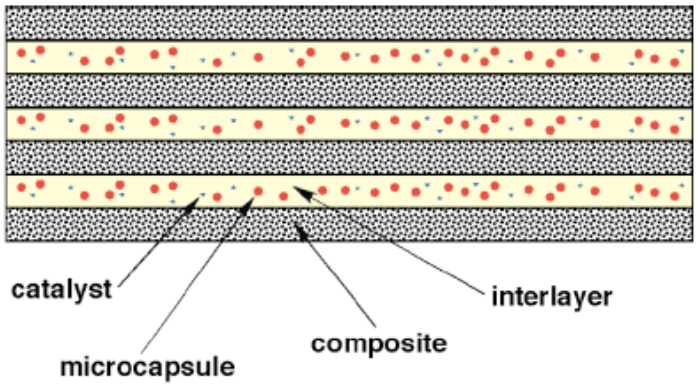

Figure 2.19 Self-healing (modified) prepreg [59]

With the flexure-heal-flexure approach they [59] found no considerable recovery of structural properties in the specimens in which the cracked faces were not pressed together during the healing period before the second loading. Even no visual evidence of healing was observed in this case. They achieved up to 96% recovery of original peak loads for the specimens for which the cracked faces were kept closed by reverse bending for 48 hours. The interleaf layer of the modified resin was shown to increase the thickness and weight of the laminate reducing its fiber volume fraction. The delamination cracks were also seen to be migrated to the top of the interface layer limiting the encounter mechanism necessary to initiate self-healing. They pointed out that a significant time and pressure was necessary to achieve a considerable recovery of properties with this DCPD/Grubbs system. They suggested exploring new healing agents that can heal rapidly under load with minimal contact (no external pressure) and can survive autoclave temperature and pressure cure cycles. They also suggested reducing the microcapsule size that can be incorporated into the interstices of fibers in the FRPC instead of adding an interleaf layer.

It is again to be reminded here that DCPD may not be suitable for low temperature applications as it freezes around 10^{o}C. This is probably the reason that no work involving low temperature self-healing using DCPD monomer alone is found in literature.

The interesting observations and recommendations made in [59] along with the unsatisfactory healing performance of microencapsulated DCPD/Grubbs system in several other studies discussed above, with regards to autonomic structural healing of FRPC, prompts the researchers to search for alternative healing agents with superior properties. The following section reviews some of these studies found in literature.

b) Healing agents other than DCPD/Grubbs system

Jin et al. [60] investigated a dual microcapsule epoxy-amine based healing system of high temperature epoxy samples. One type of microcapusules contained curing agent and the other contained diluted epoxy resin. Quality of healing was characterized by the recovery of fracture strength using modified TDCB epoxy specimens. Specimens were allowed to heal for 48 hours at room temperature following the virgin fracture test without any external intervention as mentioned in [60]. A maximum of 91% healing efficiency at 15 wt% (6wt% epoxy, 4wt% curing agent) microcapsules concentration was reported in the work. However, the efficiency of healing was observed to be reduced significantly with increasing time after healing the reason of which was attributed to the possible leakage/instability of amine microcapsules. This drawback might limit the use of the healing agents for practical applications.

Group of Zhang et al. in several works [[61], [62], [63], [64], [65]] explored different healing agents for studying healing of thermosets. They encapsulated epoxy [[61], [62], [63]] and hardener [63] as healing agents and used dispersed hardener [61] and catalyst [62] to impart healing capability to GFRP [[61], [63]] and epoxy matrix [62]. However, quality encapsulation of epoxy and its subsequent flow into the crack plane at room temperature might become difficult due to its high viscosity as they mentioned. In [64], they encapsulated a single component healing agent, glycidyl methacrylate (GMA) which remains as a low viscosity liquid at ambient temperature. Fracture tests of TDCB epoxy specimens revealed nearly full recovery of mechanical properties as shown in figure 2.20.

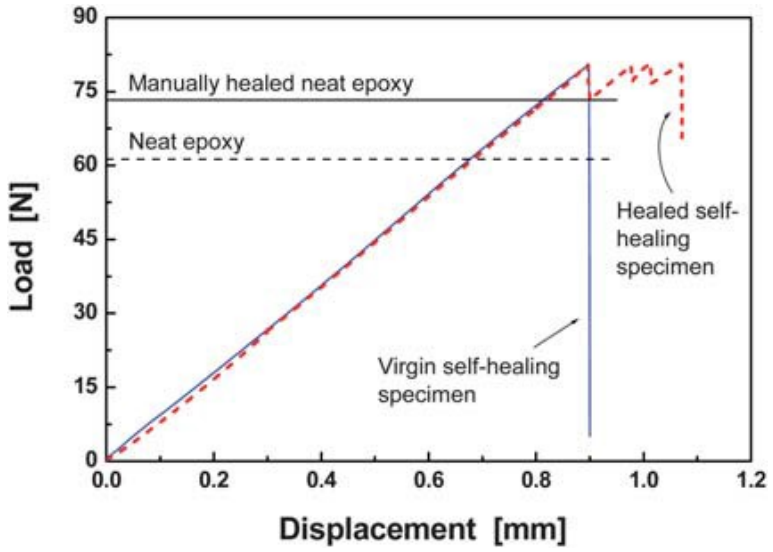

Figure 2.20 Typical load-displacement curves recorded during TDCB tests. The fracture loads of both unfilled epoxy and manually healed unfilled epoxy specimens are shown in the form of horizontal lines as references. Healing of the fractured specimens was conducted at 25 C for 72 h. [64]

Recently, in another work, they [65] successfully microencapsulated styrene (much lower viscosity than epoxy monomer) as well as benzoyl peroxide (BPO), the initiator of styrene polymerization, which were incorporated into epoxy matrix. Significant healing (more than 60%) was reported to be achieved at room temperature without any manual intervention in [[62], [63], [64], [65]].

Caruso et al. [[66], [67]] investigated healing of epoxy resins using encapsulated solvents. In their preliminary work [66], they demonstrated healing of epoxy matrix incorporated with encapsulated chlorobenzene solvent with 82% healing efficiency measured by fracture test of TDCB specimens where the fractured surfaces were manually kept intimately closed. In a later work [67], they encapsulated epoxy monomer in solvents and found better efficiency of healing than in the previous case [66] that consisted microcapsules containing solvent only. In a more recent work, Neuser et al. [68] observed that the residual reactivity of host epoxy matrix which is a prerequisite for solvent assisted healing of thermosets, decreases significantly with exposure and increasing uptake of solvent. Almost no residual reactivity was found for the epoxy samples prepared at the saturation level of the solvent [68]. It thus seems that the host epoxy matrix requires remaining partially cured for the solvent assisted healing to be achieved. In other words,

the mechanical properties of the host matrix are possibly compromised in order to impart healing functionality to the matrix through solvent healing.

It is to be noted here that, in the above studies by other research groups, healing efficiency is also evaluated by the same protocol as in [[3], [49], [50], [51], [52], [53], [54], [56], [57]] where there is a scope for improving the protocol. In the current work, a suitable protocol for evaluating the healing performance under realistic loading condition is developed.

The alternative healing agents explored in the above works [[61], [62], [63], [64], [65], [66], [67]] although showed autonomic structural healing for some cases, none of them are really suitable for low temperature applications where the healing agents must remain liquid at the low temperatures. Thus, in the current work, 5E2N which is known to have low freezing point (-80^{o}C), is being investigated for autonomic structural self-healing for low temperature applications.

Besides the number of healing approaches discussed above, several other healing approaches like utilizing reversible Diels-Alder reaction scheme [[69], [70], [71], [72], [73]] and embedding materials in the form of particles (or fibers) as healing agent into the thermoset matrix [[74], [75], [76]] has been investigated by different groups of researchers. However, these approaches require external heating to initiate healing, thus are not autonomic. Many of the other studies, like [[77], [78], [79], [80], [81], [82], [83], [84]], found in literature were dedicated to exploring non-structural healing using various healing strategies. Further discussions on these studies are not covered as the current work deals with autonomic structural healing of FRPC composites.

Table 1 summarizes the key studies of healing discussed in the literature review section, in terms of different category of healing and methods employed to evaluate its performance. The key differences of these works with the current work are also discussed after the illustrations in table 1.

Table 2-1. Summary of key studies investigating different category of healing and methods employed for evaluating healing performance

Healing approach	Healing agents	Specimen	Method	Form of external intervention	Healing efficiency	Category of healing		Ref.
						Autonomic Vs Semi-autonomic	Structural Vs Non-structural	
Hollow fiber	epoxy/ hardener [2]	GFRP	CAI	Heating (60°C), vacuum treatment	10%	Semi-autonomic	Structural	[29]
	epoxy /acetone /hardener [2]	GFRP	Dye penetrant, FAI	-	10%[1]	Autonomic	Structural	[31]
	epoxy /hardener [2]	GFRP, CFRP	FAI	Heating (100°C)	87%	Semi-autonomic	Structural	[28]
Hollow channel /Micro-vascular network	DCPD /Grubbs	Epoxy coating-substrate	Flexure-Heal-Flexure	Manual filling of monomer	60%	Semi-autonomic	Non-structural	[35]
	epoxy /hardener [2]	Epoxy coating-substrate	Flexure-Heal-Flexure	Repeated cyclic loading to enhance mixing of fluid	50-100%	Semi-autonomic	Non-structural	[36], [37], [38]
Micro-encapsulation	DCPD /Grubbs	TDCB Epoxy	Fracture-Heal-Fracture	Fractured surfaces kept into contact	Up to 90%[1]	Semi-autonomic	Structural	[49], [50], [51]. [52]
	DCPD /Grubbs	TDCB Epoxy	Fracture-Heal-Fracture	Activation of SMA wire	80%[1]	Semi-autonomic	Structural	[54]
	DCPD /Grubbs	GFRP CFRP	Fracture-Heal-Fracture	Clamping of delaminated faces	Up to 38%[1]	Semi-autonomic	Structural	[56] [57]
	DCPD /Grubbs	GFRP	fluorescent labeling, CAI	-	Up to 97%[1]	Autonomic	Structural	[58]
	DCPD /Grubbs	CFRP	Flexure-Heal-Flexure	Cracked faces kept closed manually	Up to 96%[1]	Semi-autonomic	Structural	[59]

[1] Not calculated based on comparing the values with regular specimens (i.e. neat specimens without any healing agents and its containers). [2] Healing agents are not suitable for low temperature applications.

Table 2.1 Summary of key studies investigating different category of healing and methods employed for evaluating healing performance (cont'd)

Healing approach	Healing agents	Specimen	Method	Form of external intervention	Healing efficiency	Category of healing		Ref.
						Autonomic Vs Semi-autonomic	Structural Vs Non-structural	
Micro-encapsulation	Epoxy /hardener[2]	TDCB epoxy	Fracture-Heal-Fracture	-	91%[1]	Autonomic	Structural	[60]
	Epoxy /hardener[2]	SENB Epoxy, GFRP	Fracture-Heal-Fracture	Clamping of fractured surfaces, Heating (130C)	111% (epoxy) 68% (GFRP)	Semi-autonomic	Structural	[61]
	Epoxy /hardener[2]	Epoxy	FAI	Cracked surfaces kept into contact	76%	Semi-Autonomic	Structural	[62]
	Epoxy /hardener[2]	GFRP	Acoustic microscope	-	100%	Autonomic	Non-structural	[63]
	Glycidyl methacrylate[2]	TDCB epoxy	Fracture-Heal-Fracture	-	100%	Autonomic	Structural	[64]
	Styrene /initiator[2]	Epoxy	Impact strength	-	60%	Autonomic	Structural	[65]
	Epoxy /solvent[2]	TDCB epoxy	Fracture-Heal-Fracture	Cracked surfaces kept into contact	82%[1]	Semi-Autonomic	Structural	[66], [67]

[1] Not calculated based on comparing the values with regular specimens (i.e. neat specimens without any healing agents and its containers)

[2] Healing agents are not suitable for low temperature applications

Analyzing the above table, it can be observed that the studies exploring the hollow fiber approach mainly deal with structural healing but the method of achieving healing is not autonomic [[25], [28]]. In contrast, the quality of autonomic structural healing achieved in [29] was poor (only 10%). On the other hand, the demonstrations of healing for the hollow channel/microvascular network approach [[31], [32], [33], [34]] were mostly for non-structural semi-autonomic healing. The demonstration of healing for microencapsulation approach using DCPD/Grubbs system [[40], [41], [42], [43], [44], [45], [46], [47], [48], [49]] are mostly for semi-autonomic structural healing. Conversely, autonomic structural healing with high healing efficiency [97%] was claimed to be achieved in [3] for unreinforced modified (incorporated with healing agents) epoxy samples. However, the efficiency value was not based on comparison with the regular samples (i.e. neat specimens without any foreign materials) similar as in many other studies [[49], [50], [51]. [52], [54], [56], [57], [58], [59], [60]]. This prompts for establishing a suitable protocol for evaluating the healing performance of FRPC based on comparing with the regular samples under realistic loading conditions in a truly autonomic fashion without any manual intervention. Autonomic structural healing with high healing efficiency was achieved in some studies [[62], [63], [64]] exploring microencapsulation approach using alternative healing agents other than DCPD/Grubbs system. However, the alternative healing agents, like epoxy, possess some limitations including great difficulties in quality encapsulation, reduced flow ability in the crack plane due to high viscosity and consequently, for its unsuitability for low temperature applications where the healing agents must remain liquid at the low temperatures. Thus, it is noted that none of the healing systems studied in various investigations really demonstrated the potential for autonomous structural healing for low temperature applications. In the current work, autonomic structural healing of microencapsulated 5E2N/Grubbs system is being investigated for its known superior properties than DCPD/Grubbs system and suitability for low temperature applications.

2.3 5-Ethylidene-2-norbornene (5E2N) as a candidate for microencapsulated healing agent

DCPD/Grubbs catalyst based microencapsulated healing system has been investigated extensively by the group of White and coworkers [[49]- [54]; [56]- [59]]. DCPD used as the healing agent in these studies requires to be cured for around 48 hours at the presence of comparatively large amount (up to 5%) of catalyst to achieve substantial healing efficiency. The

large amount of expensive Grubbs catalyst and the long period of cure time are not desirable in practical applications. DCPD also has a melting point of around 10°C, which means that the healing mechanism proposed may not work by freezing of the healing agent below the temperature. Development of healing agent with low freezing point is thus essential [9]. According to Yin et al. [61], higher temperature and longer lasting time might result in polymerization of DCPD monomer leading to its invalidation. Further, the rate of healing is compromised in the usual case where inhibitors are used to prevent early polymerization [8].

Lee et al. [9] characterized DCPD as well as 5E2N as healing agent for polymer composites using differential scanning calorimetry (DSC), TGA and dynamic mechanical analysis (DMA). In the study, they found that 5E2N have advantages as a healing agent because, when cured under same conditions as DCPD, it reacts much faster in the presence of a much lower amount of catalyst, has low freezing point, and produces a resin that has a higher value of glass transition temperature (Tg). The characteristics of the low freezing point and high reactivity of 5E2N are essential for further development of self-healing concept toward practical use in polymeric composites [9].

Mauldin et al. [8] showed, as in figure 2.21, that ethylene norbornene (ENB) monomers has much superior shear storage modulus than DCPD and gain its maximum shear storage modulus at a much faster rate than DCPD.

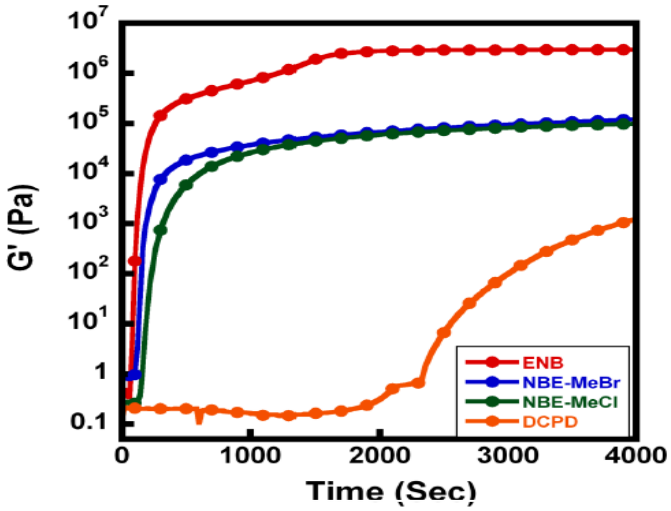

Figure 2.21 Evolution of shear storage modulus (G') of various healing agents using a modified rheokinetic technique (ENB = Ethylidene Norbornene, NBE-MeBr = 5-Norbornene-2-methylbromide, NBE-MeCl = 5-Norbornene-2-methylchloride, DCPD = Dicyclopentadiene) [8]

Liu et al. [85] investigated the blend of various proportions of DCPD and 5E2N (ENB) as candidates for healing of polymer composites using DSC and DMA. They observed that DCPD and ENB are miscible in all proportions and the blending results in the desired lowering of the melting point of DCPD. They have suggested a blend of DCPD and 5E2N at a ratio of 1:3 to be a potential candidate for healing agent which can combine high rigidity of DCPD after cure and fast reaction rate, much lower catalyst requirement and low temperature capabilities of 5E2N. Recently, Raimondo et al. [86] showed that a blend of ENB with up to 5% DCPD was not phase separated at low temperature (-50^{o}C). However, in this work, no mechanical test was carried out at low temperature. Unfortunately, no other published paper investigating the effect of low temperature on self-healing of composites is found in literature.

The 5E2N/Grubbs catalyst healing system can thus overcome some of the limitations of extensively studied DCPD/Grubbs system and possesses a great potential for a wide range of applications including in the low temperature environment. The current work, thus investigates the 5E2N/Grubbs system for the autonomic structural self-healing of CFRP composites for low temperature applications.

CHAPTER 3

Synthesis of Microcapsules and Investigation of the Effect of Processing Parameters on their Quality Characteristics

3.1 Introduction

The current research is aimed at evaluating the self-healing performance of CFRP composite both at room and low temperatures using microencapsulated 5-Ethylidene-2-norbornene (5E2N) and Grubbs catalyst as healing agents. To accomplish the objective, three major stages are envisaged. These steps are the fabrication of samples, creating controlled damage to the samples and observing the effect of healing. Each of these stages is subjected to various issues, challenges and constraints. For the fabrication stage, the first issue is to synthesize the microcapsules and the challenge is to control their quality characteristics.

In this chapter, the procedure of synthesis of microcapsules and the associated issues and challenges are discussed. The role of different ingredients used in the microencapsulation process was studied. The effect of agitation speed and SLS concentration on the quality of microcapsules are investigated. Finally, an optimum combination of agitation speed-SLS concentration is established through numerous synthesis trials.

3.2 Synthesis of microcapsules and the key roles of different ingredients used in the encapsulation process

The first and one of the most important tasks of this work is to encapsulate the self-healing monomer in suitable polymeric shells and establishing control on their quality in terms of their average size, size distribution, thermal stability, monomer content, shell thickness, surface morphology et cetera. These characteristics of microcapsules are known to influence capsule rupture behavior, healing agent release and the healing performance of composites [87]. Preliminary synthesis runs of microcapsules were carried out to be familiar with different steps of the process and the mechanism and the roles of different ingredients used were studied through literature survey. The materials, processes, and the outcome of the preliminary synthesis

runs as well as the mechanism and the roles of different ingredients used in the microencapsulation process are described below.

3.2.1 Materials, processes and preliminary synthesis runs

The core material 5E2N, the shell materials melamine, urea and formaldehyde (37 wt%) and the stabilizing agent polyvinyl alcohol (PVA) and the surfactant sodium dodecyl sulphate (SDS or SLS) were purchased from Sigma-Aldrich, Canada.

5E2N is encapsulated in poly melamine urea formaldehyde (PMUF) shells using in-situ polymerization technique according to the flowchart in figure 3.1 [88].

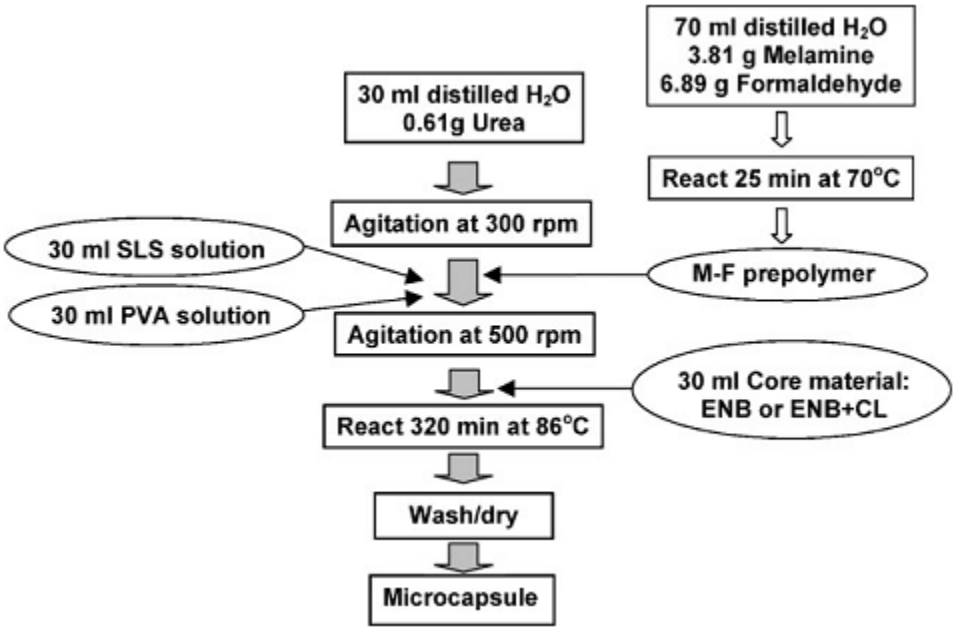

Figure 3.1 Procedure to synthesize the MUF microcapsules containing Ethylidene-norbornene (ENB). [88]

The procedure described in [88] was followed during the preliminary runs to be familiar with different steps of the process. The encapsulation procedure in accordance with [88] is described below.

Aqueous SLS (0.5%) and PVA (6.3 wt%) solution was first prepared in beakers by heating at 70°C for 20 minutes and 2 hours, respectively, on a hot plate with magnetic stirrer. Specified amount (as in figure 3.1) of melamine and formaldehyde was then taken in 70 ml deionized water in a 250 ml beaker. The ingredients were then mixed and heated for 25 minutes at 70°C to form melamine-formaldehyde prepolymer. The prepolymer was cooled down to room temperature for subsequent use. In another reaction beaker partially submerged in an oil bath

kept on a hot plate, specified amount of urea, SLS and PVA (as in figure 3.1) were mixed with 30 ml deionized water using a three-bladed stirrer at a speed of 300 rpm.

The melamine-formaldehyde prepolymer was then added to the mixture together which constitute the microcapsule shell materials in hydrophilic aqueous phase. The microcapsule core material, 5E2N, which is hydrophobic, was then added to the mixture in a slow stream under continuous stirring to form oil-in-water emulsion. The stirring speed was then raised to the desired value. At this stage, the emulsion was optionally ultra-sonicated to form fine emulsion. The emulsion was then allowed for some time to become stable and kept under continuous stirrer agitation. Heat was then applied to the emulsion in the reaction beaker through the oil bath kept on a hot plate equipped with a temperature controller. The heating rate was adjusted in the hot plate and specified temperature [86^{o}C] was set in the temperature controller. The set-up is shown in figure 3.2.

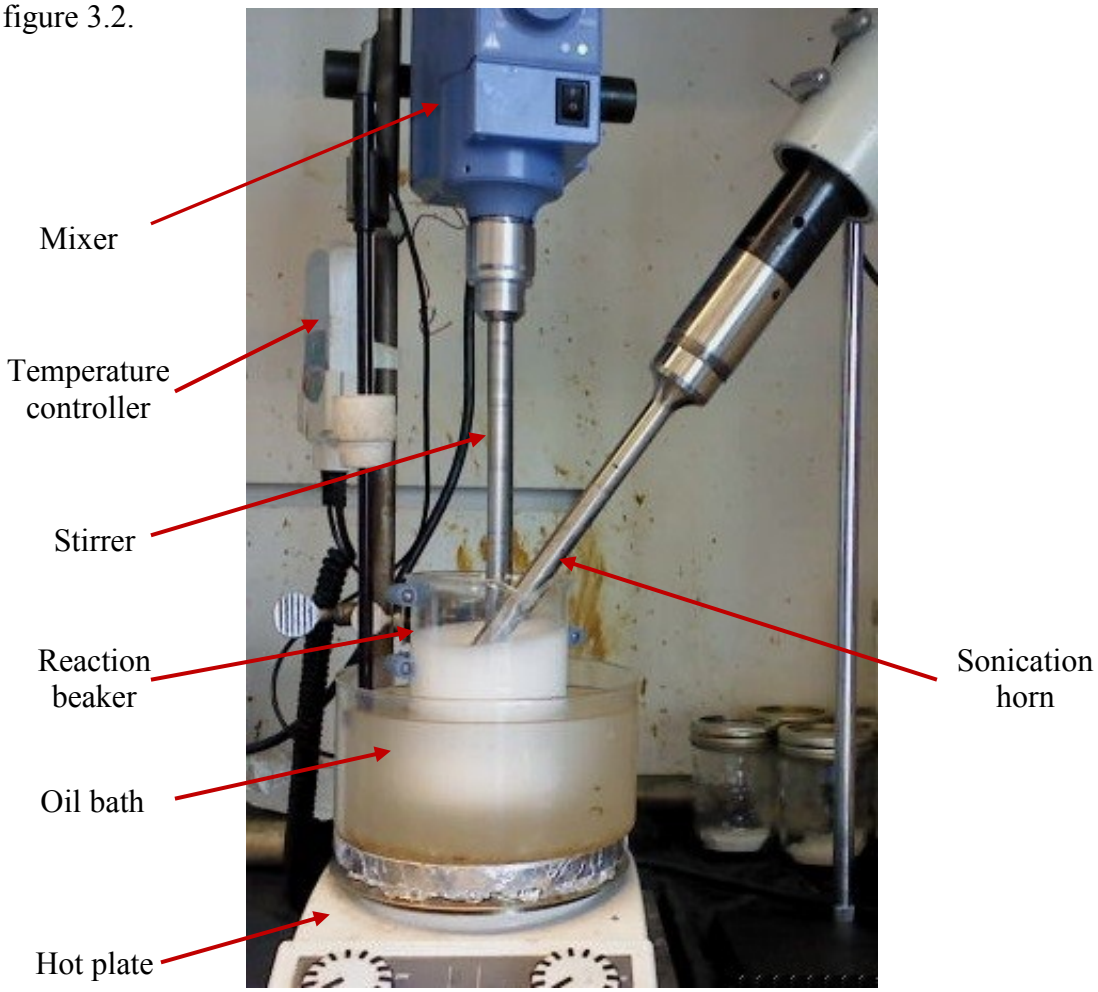

Figure 3.2 Set-up for the synthesis of microcapsules by in-situ polymerization method [sonication is introduced optionally].

After the temperature reached to the desired value, the emulsion was kept at this temperature for 5 hours with continuous agitation to complete the polymerization reaction. After that, the heating and stirring was stopped and the reaction product was cooled down to room temperature. Fresh deionized water was then added to it and kept for some time. The spherical microcapsules containing the 5E2N monomer in its core were then accumulated on the top of the mixture due to the density differences as shown in figure 3.3. Most of the dross produced during the in situ emulsion polymerization reaction were settled at the bottom.

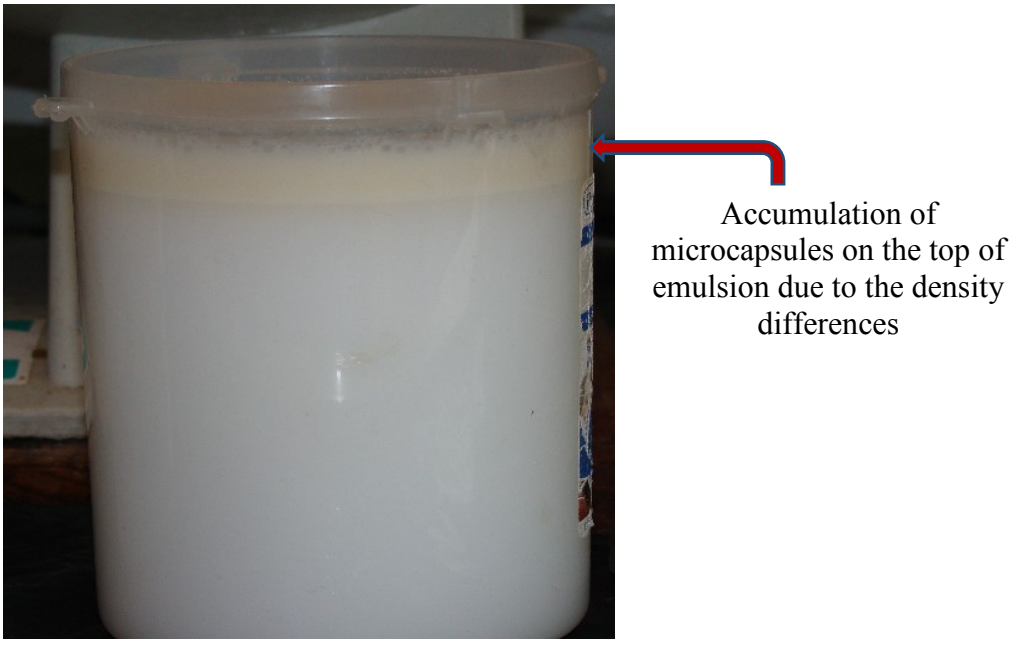

Figure 3.3 Accumulation of microcapsules on the top of the mixture

The microcapsules were collected from the top of the mixture and washed and filtered repeatedly before drying in the air to obtain free flowing individually separated microcapsules as shown in figure 3.4 (a) and (b).

(a) (b)

Figure 3.4 a) Filtering of microcapsules after washing and b) freely flowing particles indicating successful synthesis of microcapsules

After repeating several synthesis runs according to figure 1, microcapsules were obtained with 500 rpm agitation speed. The microcapsules were taken on a glass slide and observed under optical microscope. The images of the microcapsules were examined with image analysis software ImageJ [89] and the diameter of the individual microcapsules were measured. More than 500 microcapsules were individually measured to obtain its average diameter and the distribution of its sizes. The optical image of microcapsules produced with 500 rpm agitation speed and the distribution of sizes of microcapsules is shown in figure 3.5 (a) and (b).

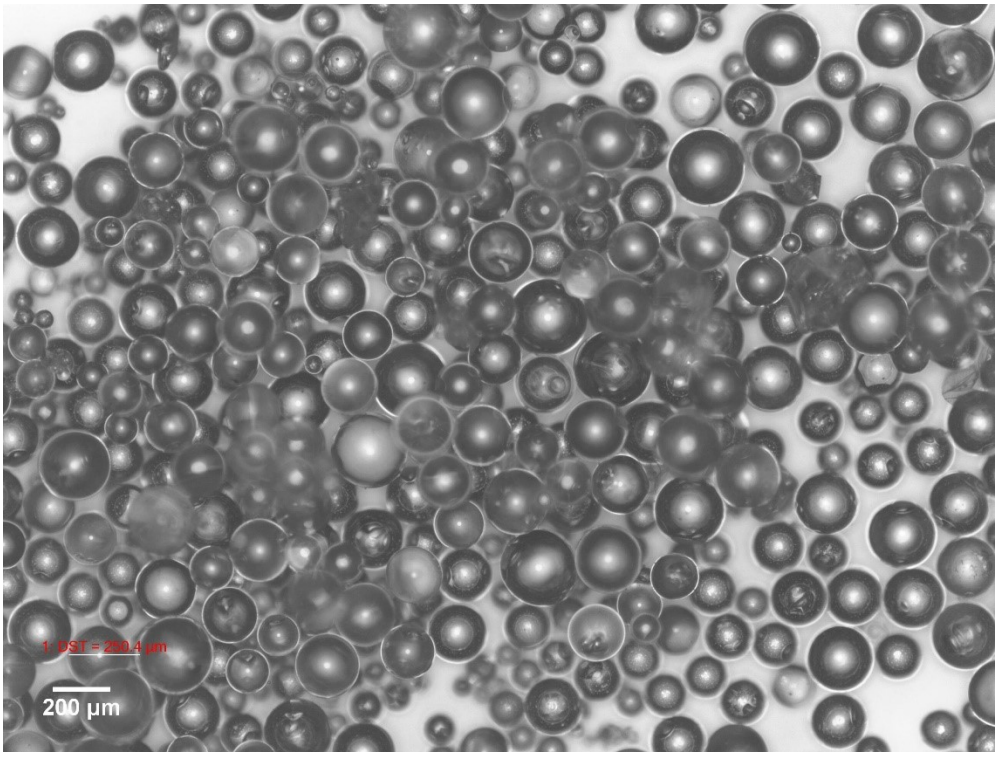

(a)

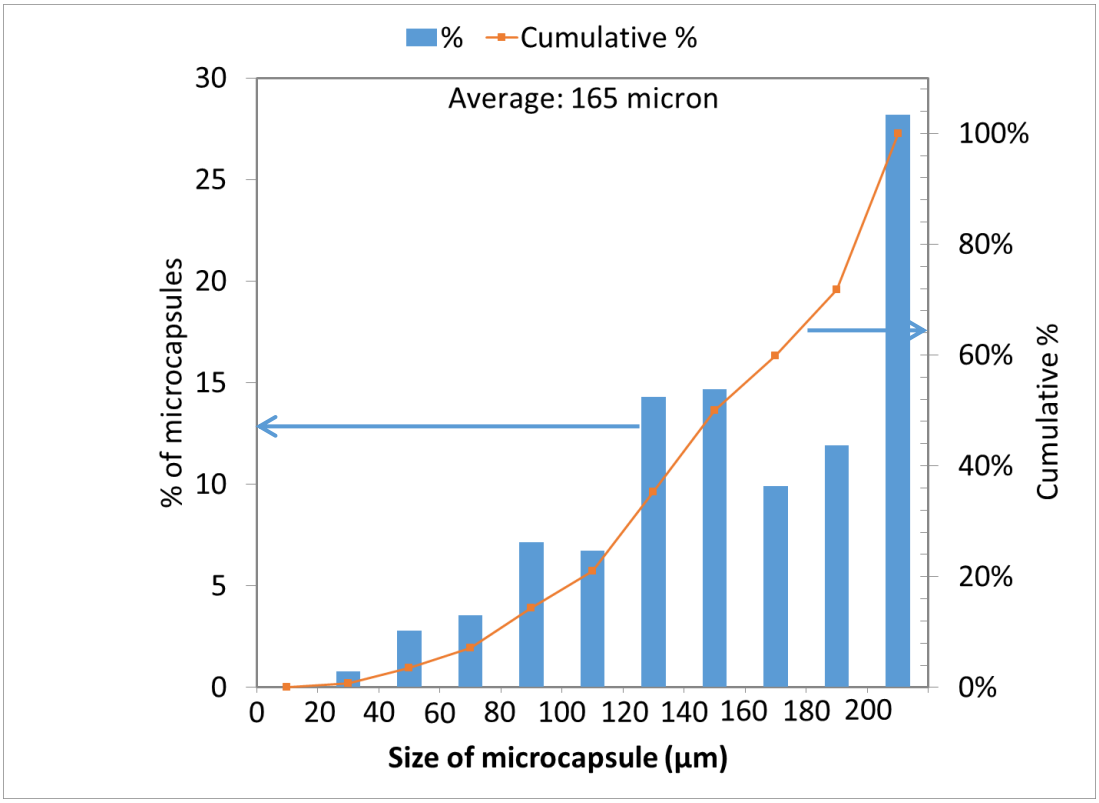

(b)

Figure 3.5 a) Microcapsule synthesized according to flowchart in figure 1 and with 500 rpm agitation speed and b) their distribution of sizes (diameters)

The optical image in figure 3.5(a) confirms that separated individual microcapsules having solid spherical shells with different sizes are successfully produced in the encapsulation process as described in figure 3.1. The vertical bars in the graph (figure 3.5(b)) indicate the percentage of total microcapsules available in a specific size range. For example, from the graph, it can be seen that about 28% of the total microcapsules are larger than 200 µm. About 30% (15 +15) of microcapsules falls within the size range 120-160 µm. The connected lines in the graph, on the other hand, indicates the cumulative percentage of the microcapsules in the specified size ranges. For example, it can be observed from the cumulative percentage that about 15% of the microcapsules are less than 100 µm. Thus, from figure 3.5(b), it is observed that microcapsule synthesized with 500 rpm agitation speed produces microcapsules of average diameter 165 µm with relatively wide distribution of sizes ranging from 20 µm to more than 200 µm.

3.2.2 Understanding the mechanism and the role of different ingredients used in the encapsulation process

In order to establish control on the quality of microcapsules produced by the above procedure, it is necessary to understand the mechanism and roles of different ingredients used in the encapsulation process. This is realized by a brief survey of literature involving similar encapsulation process.

The microencapsulation process is carried out using the principles of in-situ polymerization taking place in oil-in-water emulsions [90]. Broadly, the formation of microcapsules involves two key steps. The first key step is the creation of oil-in-water emulsion (emulsification) and the second key step is the formation of microcapsule shells (shell formation) [91]. In the first step, the hydrophobic core material (5E2N) is emulsified with the hydrophilic aqueous solution of shell materials (Urea, Melamine and Formaldehyde) using mechanical stirring (or ultra-sonication, homogenizer etc.) with suitable emulsifier (SLS) and stabilizing agent (PVA). In the emulsion, liquid 5E2N remains as the dispersed phase and the aqueous solution of shell materials (with water, surfactant and stabilizer) remains as the continuous phase. In the second step, polymerization of shell materials is carried out preferentially at the interface of the emulsion bubbles producing a film as microcapsule shells [91] around the liquid droplet of 5E2N. The size distribution of the microcapsules is determined in the emulsification step. However, the morphology and other physical properties of microcapsules are determined in the shell formation step [92].

The role of different reagents used in the microencapsulation process is described below.

5E2N

5E2N is a colorless liquid (at room temperature) monomer which is capable of undergoing Ring Opening Metathesis Polymerization (ROMP) reaction with Grubbs catalyst (described in other chapter) for self-healing applications. It has a freezing point around -80°C [93] and boiling point around 146°C [94]. 5E2N has the formula C_9H_{12} and its chemical structure is shown in figure 3.6.

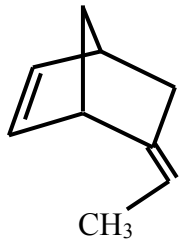

Figure 3.6 5-ethylidene-2-norbornene (5E2N) [94]

The liquid 5E2N acts as the hydrophobic oil phase in the oil-in-water emulsion in the microencapsulation process and it is the core material of the microcapsules.

Urea, Melamine and Formaldehyde

Urea is a white solid crystalline substance obtained as small granular particles from supplier (Sigma Aldrich). Its melting point is 132°C. It is highly soluble in water [94]. Urea has the formula $CO(NH_2)_2$ and its chemical structure is shown in figure 3.7 [95].

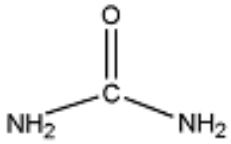

Figure 3.7 Urea [95]

Melamine is a white solid substance obtained as powdered form from supplier (Sigma Aldrich). Its melting point is 300°C [94]. It is moderately soluble in water. Melamine has a formula $C_3H_6N_6$ and its chemical structure is shown in figure 3.8.

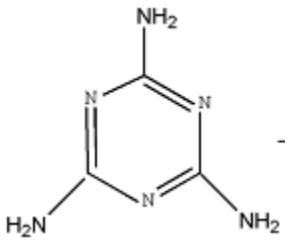

Figure 3.8 Melamine [95]

Formaldehyde solution (37 wt %) is obtained as a colorless clear liquid (at room temperature). It is completely soluble in water. Fromaldehyde has a formula HCHO and its chemical structure is shown in figure 3.9.

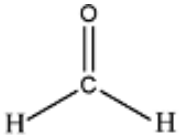

Figure 3.9 Formaldehyde [95]

The mixture of the three above reagents (together with water, surfactant and stabilizing agents) constitute the continuous hydrophilic phase in the oil-in-water emulsion and undergoes polymerization upon heating [8] to form the shell of the microcapsules during the microencapsulation process. The polymerization of the reagents is a poly condensation reaction (loss of small molecules like water during the reaction) according to the scheme shown in figure 3.10

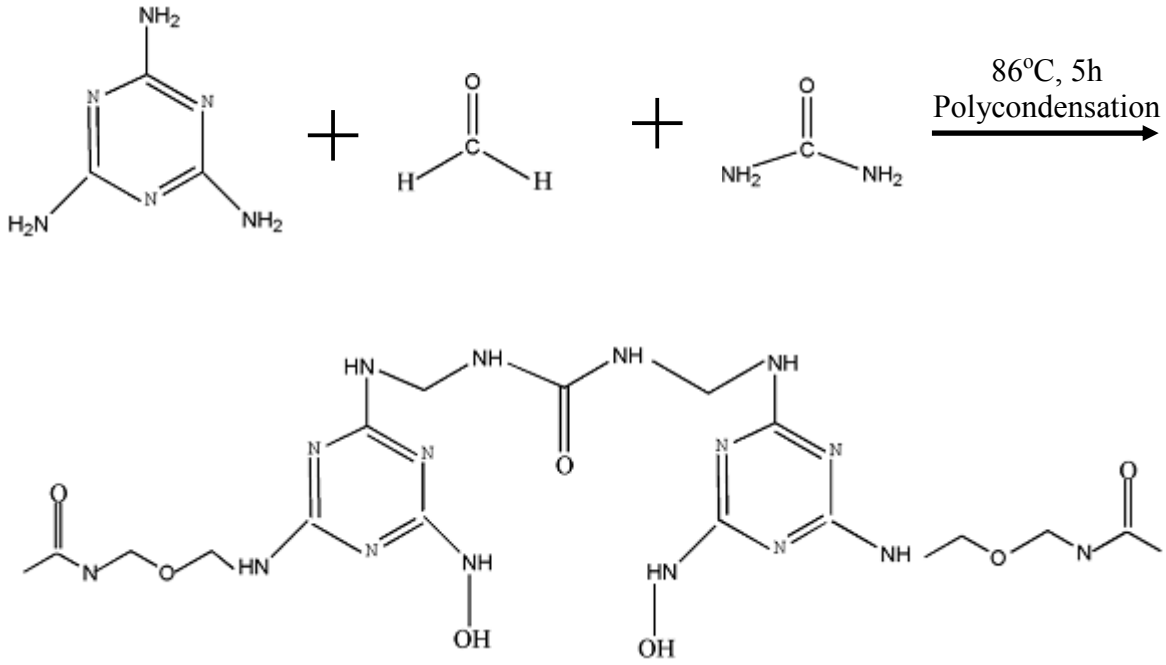

Figure 3.10 Reaction scheme of PMUF [95]

Urea, melamine and formaldehyde together form the shell of the microcapsules during the microencapsulation process.

Sodium Lauryl Sulphate (SLS)

SLS is received as white solid with small rod like structures. It is soluble in water. Different concentrations of aqueous SLS solution (0.5 wt% - 3 wt%) were prepared by dissolving specified amount of SLS with deionized water at 70°C for 20 minutes under continuous stirring. SLS has a formula $CH_3(CH_2)_{11}OSO_3Na$ [94] and its chemical structure is shown in figure 3.11.

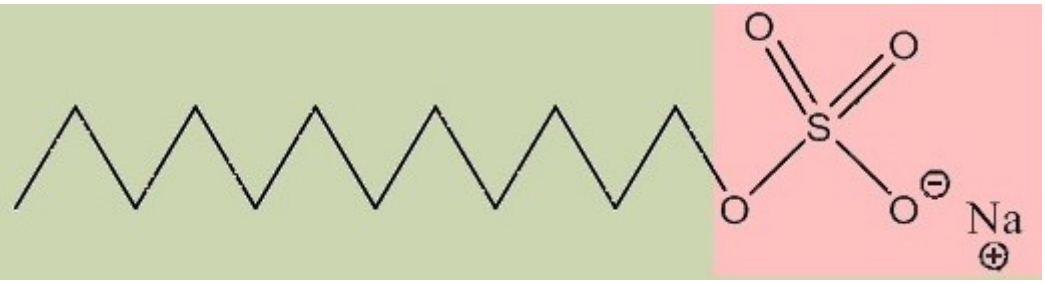

Figure 3.11 Sodium Lauryl Sulphate (SLS) [96]

SLS is used as an emulsifying agent and surfactant in the microencapsulation process. SLS, like other emulsifying agents, has both hydrophilic and hydrophobic part in their chemical structure. The sulphate head group in the structure [shown in figure 3.11] is hydrophilic and water soluble, while, the 12 carbon long chain in the tail is hydrophobic and water insoluble [96]. The hydrophilic part is thus attracted to the aqueous phase (made of shell materials) and the hydrophobic part is attracted to the oil phase (made of 5E2N) of the oil-in-water emulsion thus maintaining a hydrophilic-hydrophobic balance of the emulsion. The emulsifying agent, SLS, concentrates at and is adsorbed onto the oil:water interface to provide a protective barrier around the dispersed hydrophobic droplets [97] of 5E2N in the emulsion. SLS, having a negative charge at the sulphate head group which is sufficiently soluble in water, is also classified as anionic surfactant [96]. In addition to the protective barrier, SLS stabilizes the emulsion by reducing the interfacial tension between oil and aqueous phase. It also enhances the emulsion stability by imparting a charge on the droplet surface thus reducing the physical contact between the droplets and decreasing the potential for coalescence [[92], [97]]. The formation and quality of microcapsules is thus greatly affected by the presence of SLS in the microencapsulation process.

Polyvinyl alcohol (PVA)

PVA having molecular weight of 85000-124000 is a crystalline colorless solid obtained from sigma aldrich. 6.3 wt% of aqueous PVA solution was prepared by dissolving specified amount of PVA and deionized water at 70^{o}C for 2 hours under continuous stirring.

PVA has a formula [-CH_2CHOH-]n and its chemical structure is shown in figure 3.12.

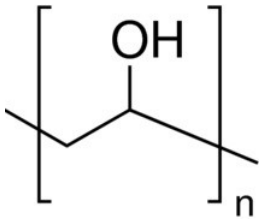

Figure 3.12 Polyvinyl alcohol (PVA) [94]

PVA is also an excellent emulsifying agent and used in conjunction with SLS to aid in the emulsification of the oil-in-water emulsion in the microencapsulation process. Aqueous solution of PVA with high molecular weight increases the viscosity of the emulsion and contributes in stabilizing the emulsion droplets.

The combination of PVA and SLS solution used in the microencapsulation process is believed to have significant effect on the average size, size distribution and the overall quality of the microcapsules.

3.3 Investigating the effect of processing parameters on the quality of microcapsules

Numerous synthesis runs of microcapsules were carried out primarily in order to establish control on the quality characteristics of microcapsules. The intention here is to establish sufficient control on the process of encapsulation so as to produce quality microcapsules with desired properties. This is achieved by understanding the effect of process variables on the quality of microcapsules. The microcapsule size, for example, is shown to be controlled by agitation rate during the similar microencapsulation process in several earlier works [[98], [99], [100], [101]]. However, the core and shell materials as well as the emulsion system (e.g. the emulsifying agents, stabilizing agents etc.) used in those works were different for different applications. As the current encapsulation process involves different emulsion systems with different core and shell materials for self-healing applications, the effect of processing variables

should be different. The 5E2N monomer is first encapsulated in PMUF shells by Liu et al. [88] with mechanical impeller and later with porous glass emulsification technique by the same group of researchers [102]. However, the effect of stirring speed and the concentration of emulsifier (SLS) on the quality of microcapsules were not studied in those works. The effect of these two variables on the quality of microcapsules containing 5E2N monomer in PMUF shells are thus studied in the current work. The agitation speed of the impeller and the concentration of SLS were varied, one at a time, while keeping all other processing conditions same as in figure 3.1, during the encapsulation process, to understand their effect on the quality of microcapsules. Finally, an optimum combination of agitation speed-SLS concentration is established through numerous synthesis trials. The results are discussed below.

3.3.1 Effect of agitation speed

Increasing the rotation speed of stirrer in the emulsion during the microencapsulation of 5E2N in PMUF shells is expected to produce smaller size microcapsules as observed in similar other works [[98], [99], [100], [101]]. In order to verify this, agitation speed was increased from 500 rpm to 1000 rpm while keeping the SLS concentration fixed at 0.5 wt% and all other processing conditions same as in figure 3.1. The resulting microcapsules were observed under optical microscopes and SEM to determine their average size, size distribution and surface morphology. The results are discussed below.

500 rpm (0.5 wt% SLS)

The microcapsules produced at 500 rpm during the preliminary runs are already shown in figure 3.5 (a) with their size distribution in 3.5 (b). For convenience in discussion, it is shown again below.

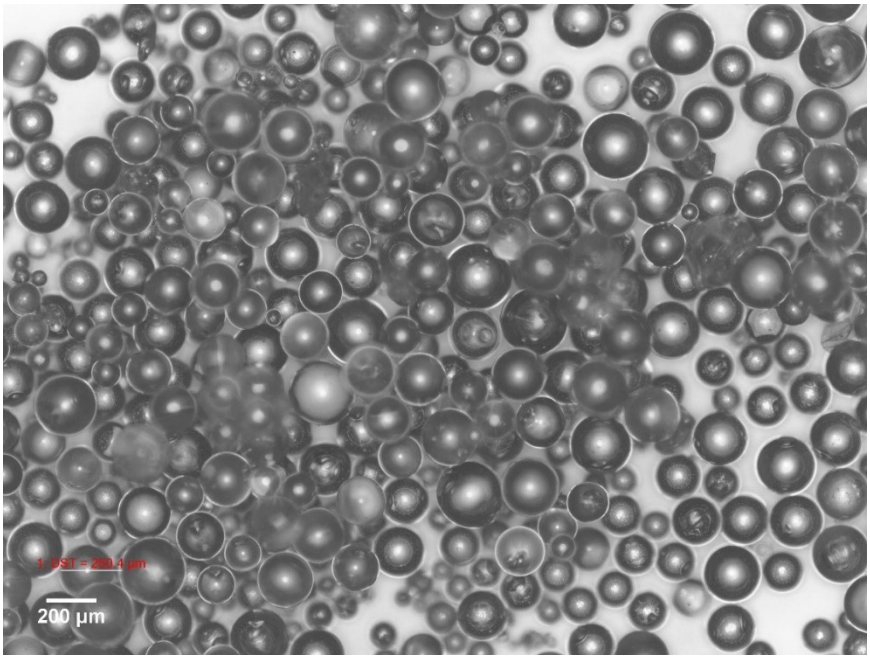

(a)

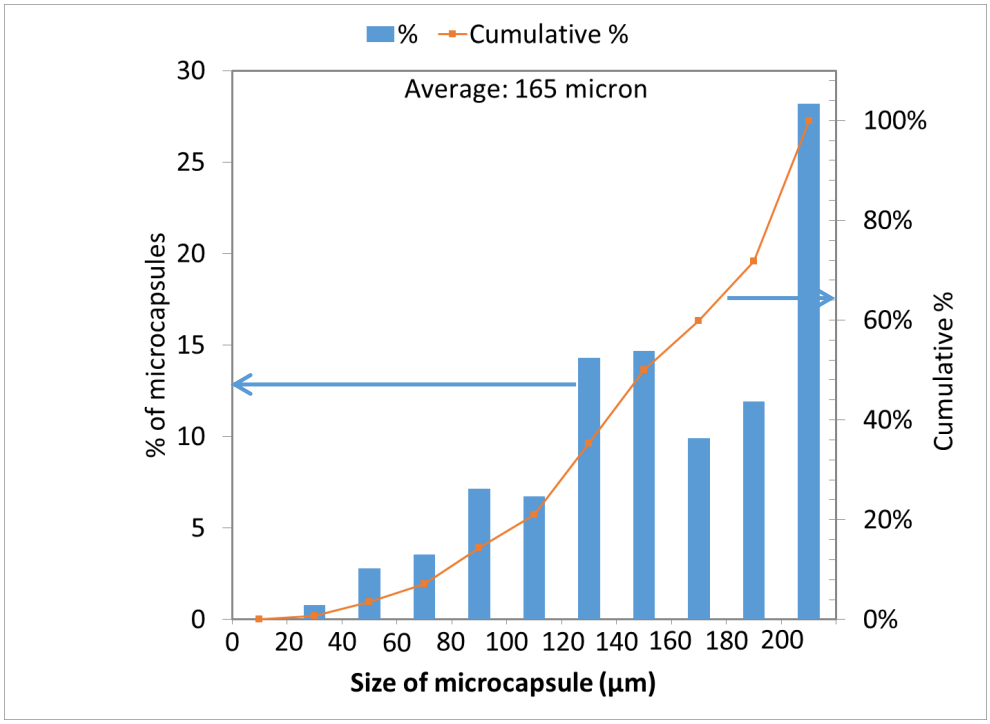

(b)

Figure 3.5. a) Microcapsules produced with 500 rpm agitation speed keeping the SLS concentration fixed at 0.5 wt% and b) their size distribution

The microcapsules produced have a core-shell structure with smooth inner surface and rough outer surface as shown in figure 3.5 (c).

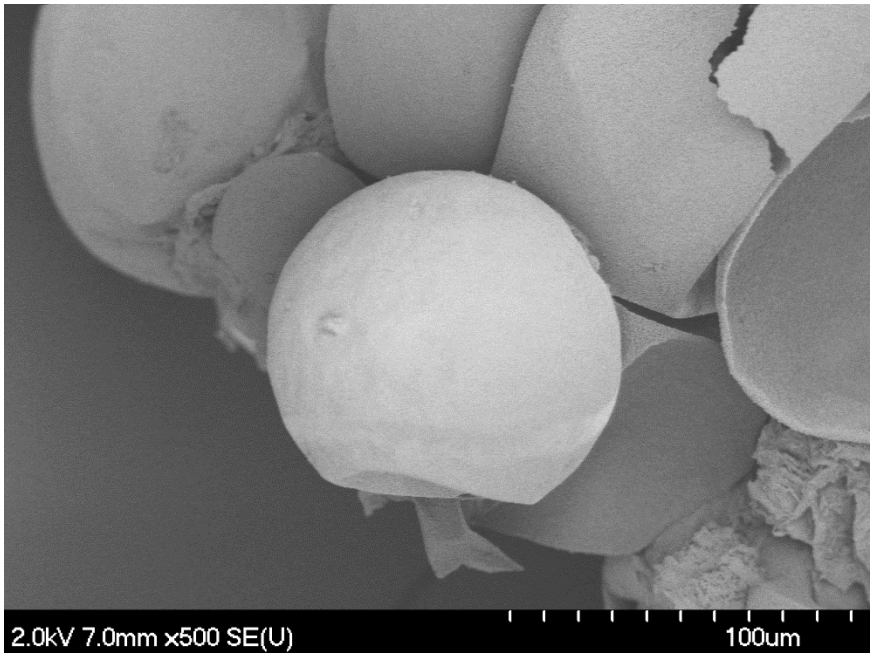

Figure 3.5. c) Core-shell structure of microcapsules

The inner and outer surface morphology of the microcapsules as observed under SEM is shown in figure 3.5 (d) and (e) respectively.

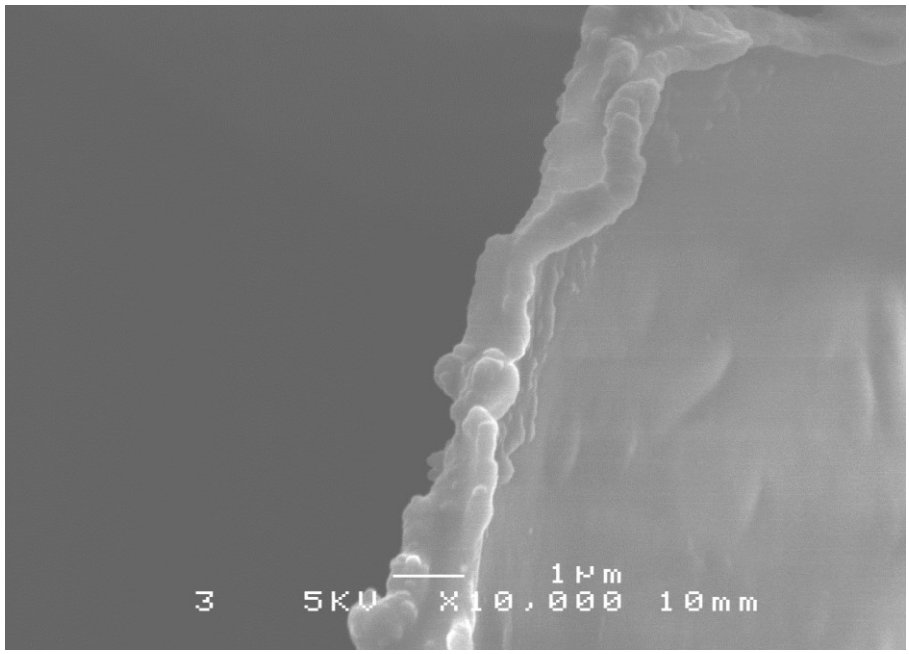

Figure 3.5. d) Smooth inner surface of microcapsules

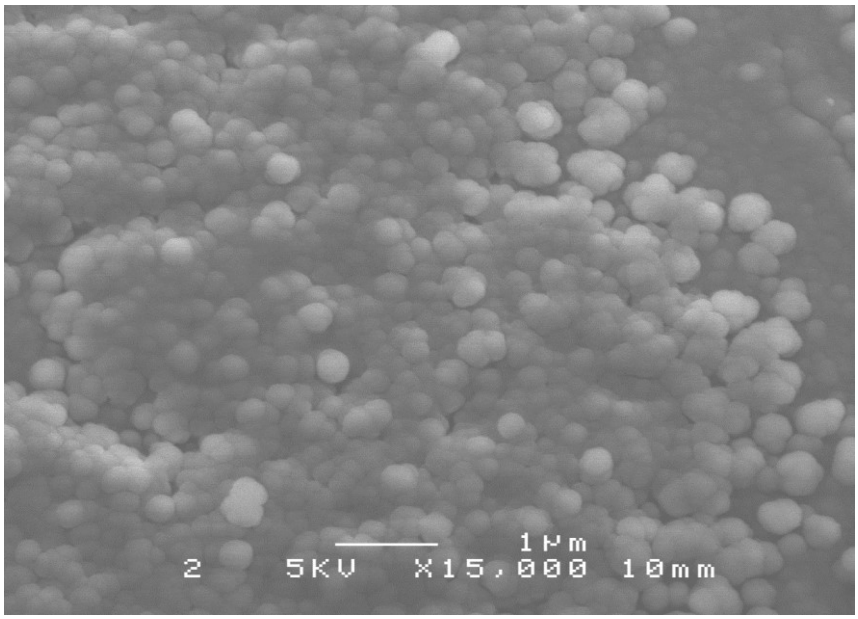

Figure 3.5. e) Rough outer surface of microcapsule shell

The inner surface of the microcapsules was smooth and the outer surface was observed to be rough and patterned with relatively coarse nanoparticles deposits. The nanoparticles attached to the outer surface of the microcapsules are believed to be made of PMUF which has been formed during the in situ polymerization of the shell materials as observed in other works [[87], [103]] The shell thickness of the microcapsules as observed under SEM is shown in figure 3.5 f).

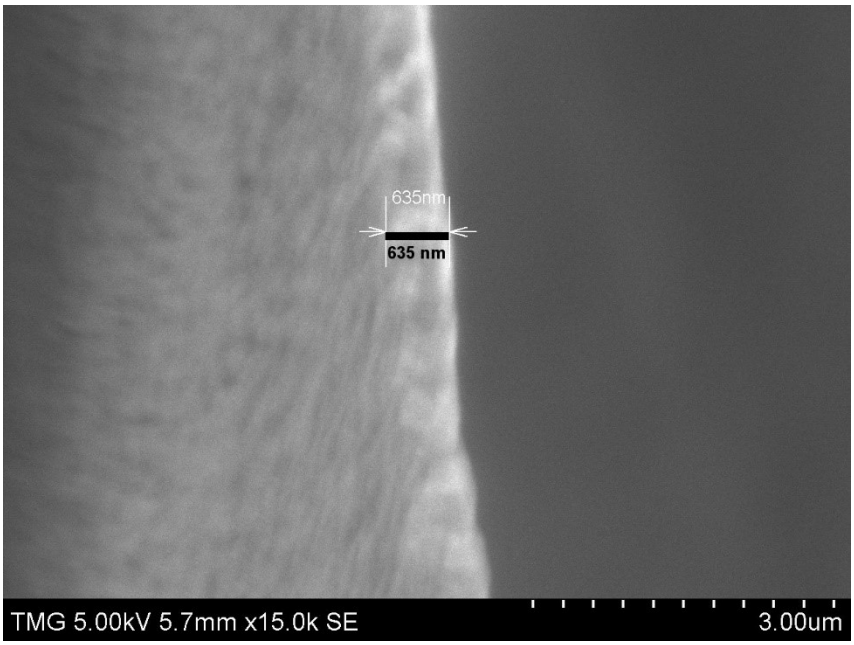

Figure 3.5. f) Thickness of the microcapsule shell

The shell thickness of the microcapsules were measured to be in the range of 500-700 nm as shown in figure 3.5 (f). A shell thickness of urea formaldehyde (UF) microcapsules in the range of 220 nm found in the work of [87] was perceived to be sufficiently robust to survive handling, manufacture of self-healing polymer providing excellent storage and release properties for self-healing applications [87]. The range of shell thickness of PMUF microcapsules obtained in [102] was 400-600 nm and obtained in [88] was 700-900 nm.

600 rpm (0.5 wt% SLS)

Microcapsules were produced by increasing the agitation speed to 600 rpm while keeping the SLS concentration fixed at 0.5 wt% and all other processing conditions same as in figure 3.1. The microcapsules produced are shown in figure 3.13 (a) with their size distribution shown in figure 3.13 (b).

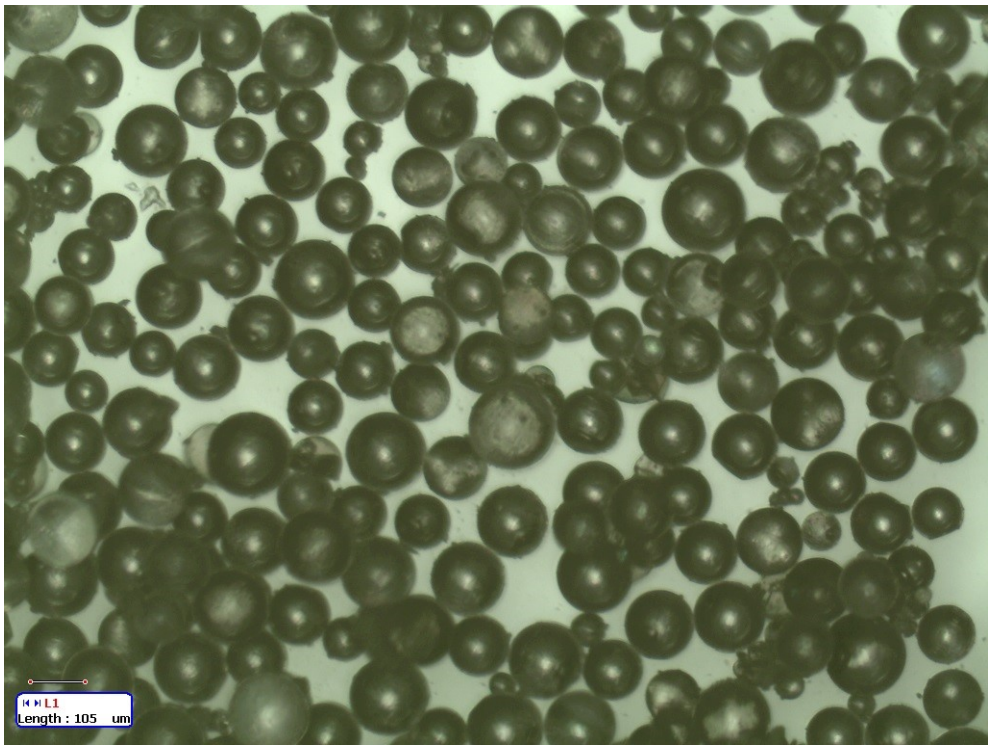

(a)

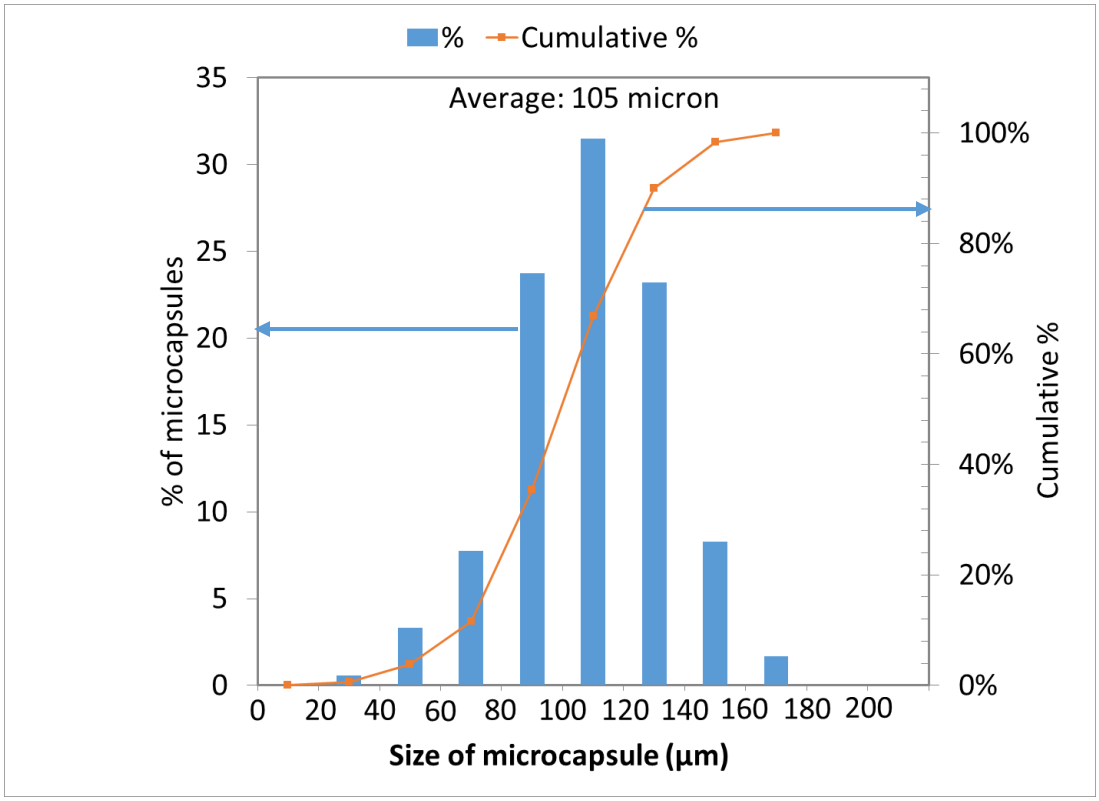

(b)

Figure 3.13 a) Microcapsules produced with 600 rpm agitation speed keeping the SLS concentration fixed at 0.5 wt% and b) their size distribution

From figure 3.13 b), it can be seen that the average size of the microcapsules is 105 μm with more than 30% of the microcapsules have diameters between 100 μm-120 μm. It is also interesting to note that more than 75% (31 +23+23) of the microcapsules produced are within the size range of 80 μm-140 μm which can be considered roughly as a fair distribution of sizes around the average value. Thus, by comparing the figures 3.5 b) and 3.13 b), it can be seen that increasing the agitation speed from 500 rpm to 600 rpm, the average size of the microcapsules reduces from 165 μm to 105 μm. The increase in agitation speed also improves the distribution of sizes with a larger percentage of microcapsules remain in the vicinity of the average value of diameter.

Obtaining individually separated smaller microcapsules with 600 rpm agitation speed, however, required increased number of washing cycles to remove the dross from the microcapsule compared to microcapsules obtained with 500 rpm agitation speed. This implies that more dross are produced with increasing agitation speed which makes it difficult to wash and filter out the individually separated microcapsules. Dross, produced during the encapsulation process, is the sticky materials which is found on the surface of the microcapsules and tends to hold several microcapsule glued together. This makes it difficult to separate out the individual microcapsules, even, by increased number of washing cycles.

The surface morphology of the microcapsules was observed similar as in figure 3.5 (e) with less coarse nanoparticles attached at the outer surface. The shell thickness was also observed to be in the range of 500-700 nm, similar as in the case of 500 rpm microcapsules as shown in figure 3.5 (f).

800 rpm (0.5 wt% SLS)

Attempts to further reducing the average size of the microcapsules by merely increasing the agitation speed did not work as expected. Microcapsules were produced by increasing the agitation speed to 800 rpm while keeping the SLS concentration fixed at 0.5 wt% and all other processing conditions same as in figure 3.1. The microcapsules produced are shown in figure 3.14.

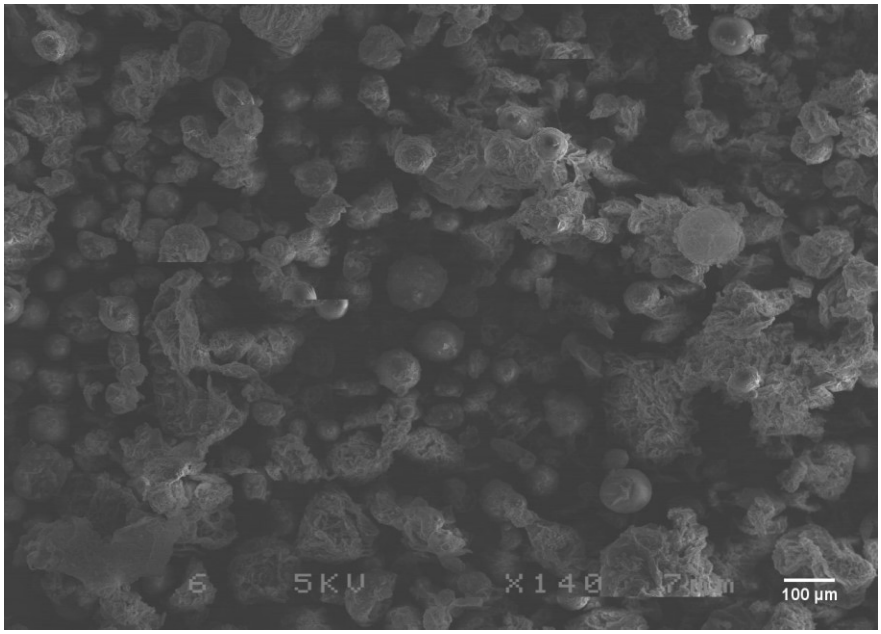

Figure 3.14 Microcapsules obtained with 800 rpm agitation speed keeping the SLS concentration fixed at 0.5 wt% showing lot of dross produced during the in situ polymerization of the shell materials which sticks to the surface of the microcapsules

As the average size of the microcapsules further decreases with increasing agitation speed, the dross produced during the polymerization reaction of the shell materials in the emulsion system tends to stick to the microcapsule surface as shown in the SEM image in figure 3.14. This dross could not be cleared even with multiple washing cycles. With decreasing size, the tendency of agglomeration among the microcapsule increases rapidly and it becomes extremely difficult to individually separate them out. Even some modified washing methods (like using fine spray of water, washing with SLS solution, washing in a sonicating bath, vacuum centrifugation etc.) did not contribute much in separating the individual microcapsules once the microcapsules were synthesized. The sticky dross attached to the microcapsule surface can act as impurities and can create many problems including poor dispersion into resin, improper adhesion to the matrix, and insufficient release of the core content during self-healing applications. The microcapsules, thus, cannot be used for self-healing applications and, hence, the other quality characteristics of the microcapsules are not investigated further. Further increase of agitation speed have similar results and agglomeration of microcapsules was observed.

The possible explanation of producing more dross and increasing difficulty with washing and filtering of microcapsules produced by increasing agitation speed at a fixed low SLS

concentration (0.5 wt%) can be realized by understanding the function of SLS in the process. As discussed earlier, SLS, as an emulsifier and surfactant, serves two main purposes. One is to form a protective layer around the core droplets stabilizing the emulsion and other is to reduce the interfacial tension between the core material (oil phase) and shell material (aqueous phase) interface. The SLS also can give negative charges to the core droplets which repulse each other to stay separated in the emulsion and prevent coalescence. As the speed of agitation increases, the average sizes of the emulsion droplets decrease which means that the total surface area of the droplet increases. However, a fixed concentration of SLS supplies a fixed number of SLS molecules in the emulsion which might not be sufficient to entirely cover up the increased surface area of the emulsion droplets. Thus, the emulsifier and surfactant function of SLS might not be properly served due to the lack of sufficient SLS molecules present in the emulsion causing coalescence of droplets and instability in the emulsion.

Thus, for a given SLS concentration, the main effect of increasing agitation speed is the reduction of average size of microcapsules with improved size distribution. The surface morphology and shell thickness remains similar as at lower speeds. However, microcapsules become increasingly sticky and difficult to separate as their average size decreases with increasing agitation speeds.

3.3.2 Effect of SLS concentration

In order to find the effect of SLS concentration, microcapsules were produced at a fixed agitation speed of 600 rpm with increasing the concentration of SLS from 0.5 to 1.5 wt% while keeping all other processing conditions same as in figure 3.1. The resulting microcapsules were observed under optical microscopes and SEM to determine their average size, size distribution and surface morphology. The results are discussed below.

0.5 wt% SLS (600 rpm)

The characteristics quality of microcapsules produced with 0.5 wt% SLS concentration at a fixed agitation speed of 600 rpm is already discussed in section 3.3.1. The characteristics quality of microcapsules produced with other concentrations of SLS studied is described below.

1 wt% SLS (600 rpm)

Microcapsules produced with SLS concentration of 1 wt% at a fixed agitation speed of 600 rpm is shown in figure 3.15 (a) along with their size distribution in figure 3.15 (b).

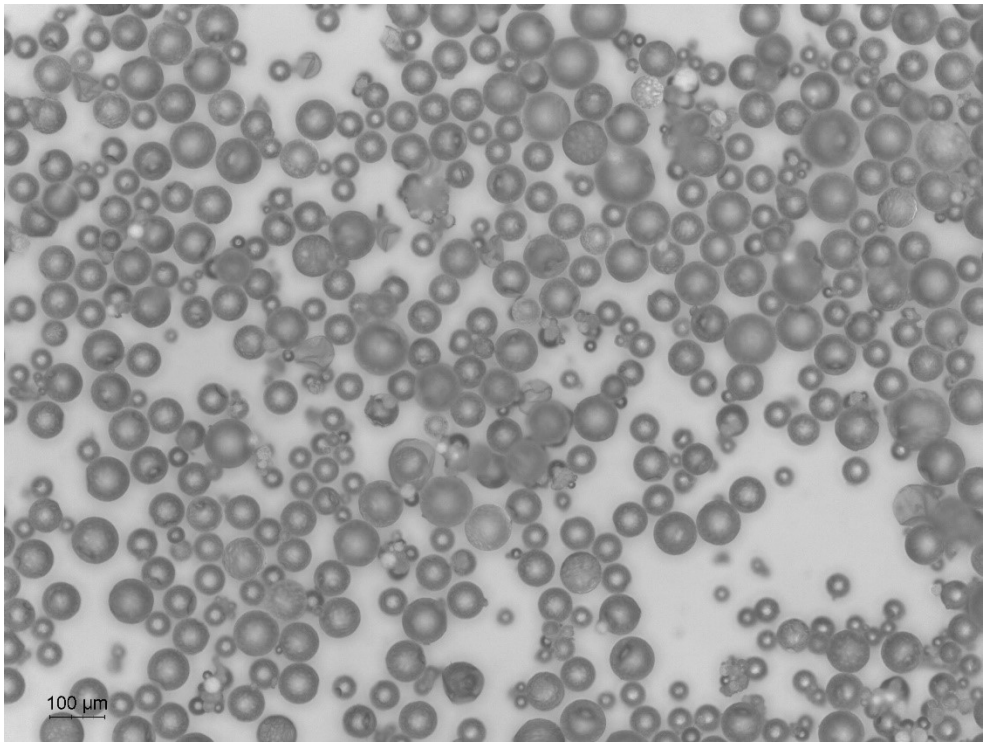

(a)

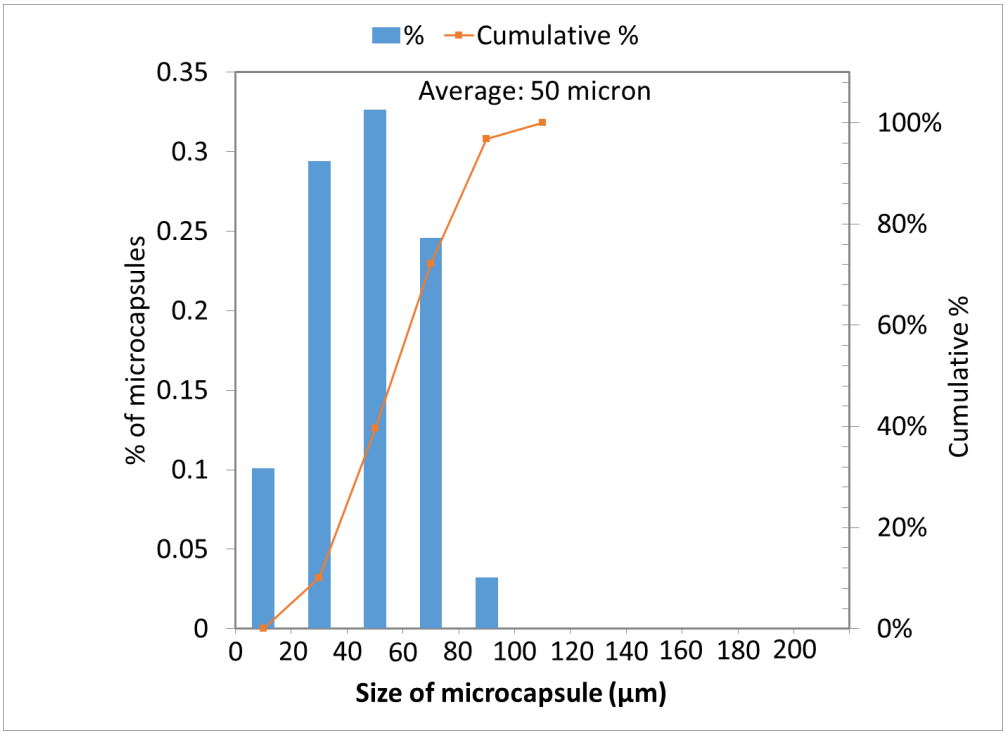

(b)

Figure 3.15 a) Microcapsules produced with SLS concentration of 1 wt% keeping the agitation speed fixed at 600 rpm and b) their size distribution

From figure 3.15 b), it can be seen that the average size of the microcapsules is 50 µm with more than 30% of the microcapsules have diameters between 40 µm-60 µm. It is also interesting to note that more than 86% (29 +33+24) of the microcapsules produced are within the size range of 20 µm-80 µm which can be considered as a fair distribution of sizes around the average value. Thus, by comparing the figures 3.13 b) and 3.15 b), it can be seen that increasing the SLS concentration from 0.5 wt% to 1 wt% while keeping the agitation speed fixed at 600 rpm, the average size of the microcapsules produced reduces from 105 µm to 50 µm. The distribution of sizes of microcapsules remains similar as in 0.5 wt% with the average value shifted to the smaller microcapsule diameters. Increased concentration of SLS offers greater reduction of interfacial tension between the oil and aqueous phases of the emulsion which possibly allows the formation of smaller emulsion droplets leading to the formation of smaller microcapsules [6].

The surface morphology of microcapsules obtained with 0.5 wt% and 1 wt% of SLS at the given agitation speed of 600 rpm are compared in figure 3.16 (a) and (b)

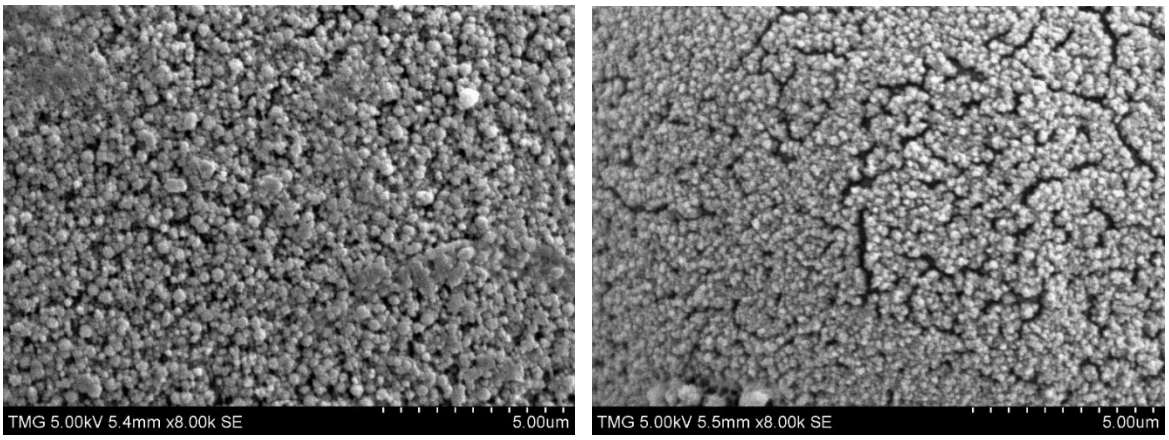

(a) 600 rpm (0.5 wt% SLS) **(b) 600 rpm (1 wt% SLS)**

Figure 3.16 Comparison of surface morphology of microcapsules produced with 600 rpm agitation speed with a) 0.5 wt% SLS and b) 1 wt% SLS

The outer surface of the microcapsules produced with 0.5 wt% SLS, as shown in figure 3.16 (a) is patterned with relatively coarse nanoparticles. The surface also looks more compact than that of 1 wt% microcapsule surface. The outer surface of microcapsules produced with 1 wt% SLS, as shown in figure 3.16 (b), on the other hand, are patterned with finer nanoparticles but with more cracks. Core liquid monomers can diffuse through the crack networks of the outer surface of microcapsule shells. Thus, increasing the concentration of SLS at a lower agitation

speed can actually degrade the microcapsule quality. Compact surface morphology and rough out surface with finer attached nanoparticles is beneficial for self-healing applications due to improved containment capability and improved adhesion properties to the matrix.

The shell thickness of microcapsules obtained with 0.5 wt% and 1 wt% of SLS at the given agitation speed of 600 rpm are compared in figure 3.17 (a) and (b).

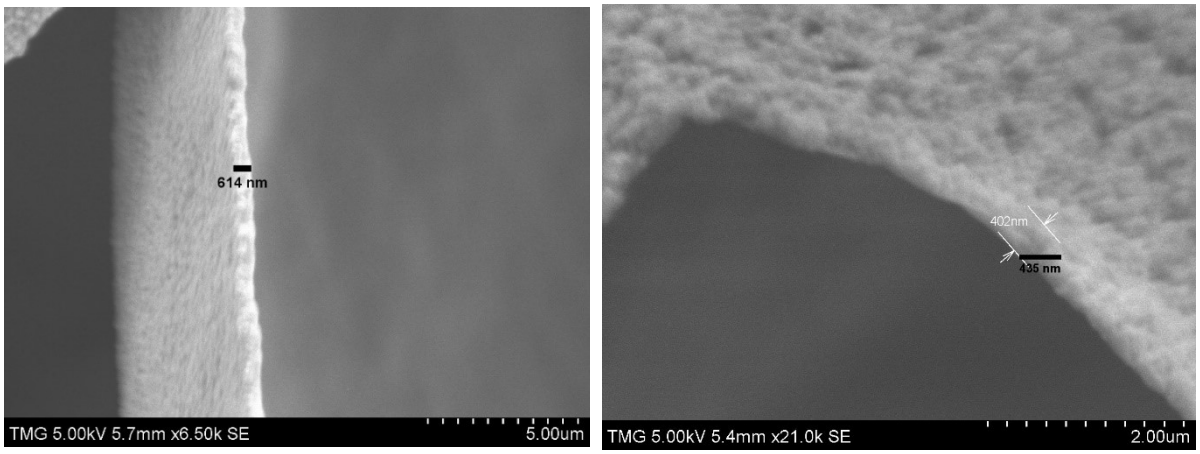

(a) 600 rpm (0.5 wt% SLS) **(b) 600 rpm (1 wt% SLS)**

Figure 3.17 Comparison of shell thickness of microcapsules produced with 600 rpm agitation speed with a) 0.5 wt% SLS and b) 1 wt% SLS

The shell of the microcapsules produced with 0.5 wt% SLS is observed thicker (614 nm) than that of the microcapsules produced with 1 wt% SLS (402 nm) as can be seen in figure 3.17 (a) and (b).

Thus, the clear effect of increasing the concentration of SLS at a given agitation speed is the reduction of the average size of microcapsules with decreasing shell thickness. However, the shell thickness remains within the desirable range as discussed in [87]. Increasing SLS concentration at a lower speed (600 rpm) also tends to produce microcapsule with cracks on the surface which is not desirable for self-healing applications.

1.5 wt% SLS (600 rpm)

Further increase of SLS concentration to 1.5 wt% at the given speed of 600 rpm led to unsuccessful microencapsulation as shown in figure 3.18.

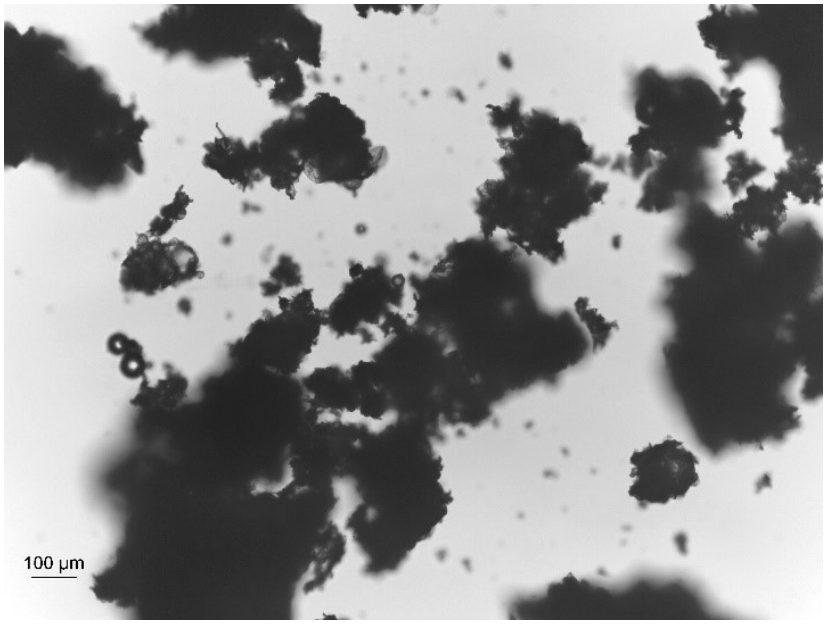

Figure 3.18 Unsuccessful microencapsulation with 1.5 wt% SLS at 600 rpm

It can be explained by understanding the role of SLS in the microencapsulation process. As discussed in section 3.2.2, the hydrophilic head and the hydrophobic tail of the SLS molecule are attracted, respectively, to the aqueous and oil phase of the emulsion thus maintaining a hydrophilic-hydrophobic balance of the emulsion. Increasing the SLS concentration possibly shifts the balance to the hydrophilic side of the emulsion due to the surfactant properties of SLS. The aqueous phase, being too much hydrophilic with increasing SLS concentration, possibly limits sufficient wetting of the oil phase droplets resulting in unsuccessful encapsulation. More investigation is necessary to confirm the explanation.

From the above results it is concluded that for a given SLS concentration, increasing agitation speed reduces the average size of microcapsules. However, microcapsules become increasingly sticky and difficult to separate as their average size decreases. On the other hand, for a given low agitation speed, increasing SLS concentration to some limit also reduces the average size of microcapsules while affecting the surface morphology of the microcapsules. Further, increase of SLS concentration beyond this limit at a given speed led to unsuccessful encapsulation. The above results led to the assessment that there might be an optimum concentration of SLS for a given speed range in order to have successful encapsulation of the core 5E2N with PMUF shells with desired quality characteristics of the microcapsules.

Numerous synthesis trials of microencapsulation led to the establishment of the optimum combination of agitation speed and SLS concentration. The optimum combination of speed-SLS concentration possibly gives the correct hydrophilic-hydrophobic balance of the emulsion leading to successful encapsulation with desired quality of microcapsules. The microcapsules successfully produced with those optimum combinations of speed-SLS concentration and their quality characteristics are shown and discussed in the subsequent sections.

3.3.3 Optimum combinations of agitation speed and SLS concentration

Efforts were made in reducing the average size (diameter) of the microcapsules while maintaining the desired quality characteristics of microcapsules. The effect of different average size on the healing performance of composites is intended to be investigated in this work. Agitation speed of the stirrer and the SLS concentration are found to be the main controlling factors in reducing the average size of the microcapsules. With numerous trials of microcapsule synthesis, it was found that increasing the concentration of SLS and slightly decreasing the amount of PVA solve the problem of stickiness and agglomeration of microcapsule as its average size decreases with increasing agitation speed while maintaining the desired quality of microcapsules. The microcapsules successfully produced with those optimum combinations of speed-SLS concentration found through this investigation are discussed below.

850 rpm-1 wt% SLS

Figure 3.19 (a) and (b) show microcapsules along with their distribution of sizes produced with 850 rpm, using 1wt% SLS and a slightly decreased amount of PVA (28ml instead of 30 ml), while keeping the other parameters same as in figure 3.1.

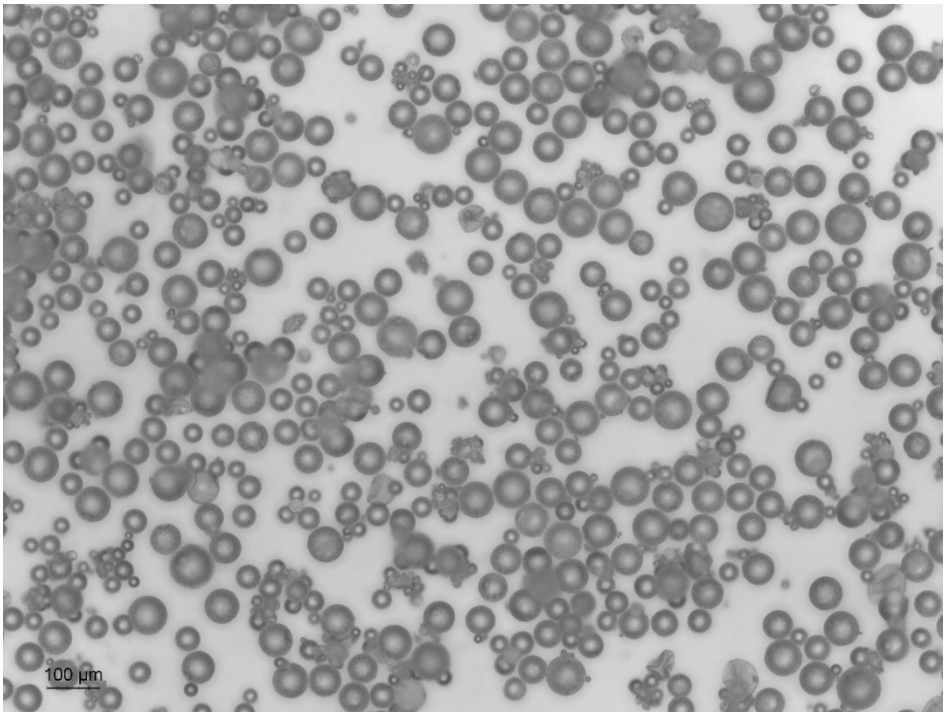

(a)

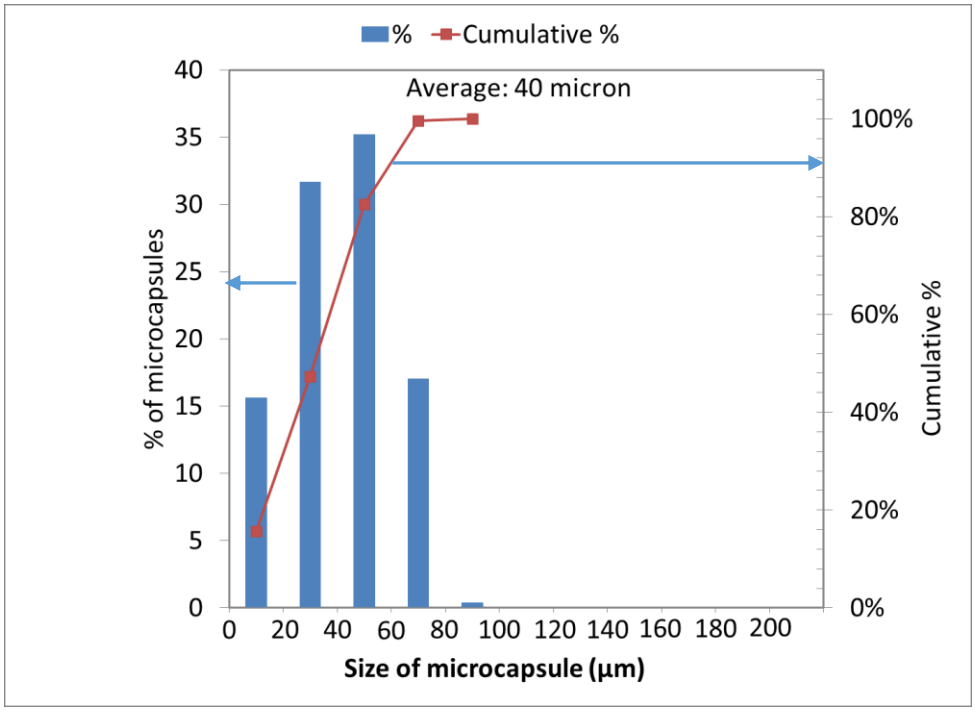

(b)

Figure 3.19 a) Individually separated small microcapsules (average diameter 40 µm) produced with 850 rpm agitation speed and 1 wt% SLS and b) their size distribution

Figure 3.19 (a) shows that the combination of 850 rpm-1wt% SLS with a slight decrease in the amount of PVA solved the problem of stickiness and produced individually separated free flowing smaller microcapsules of average size 40 micron. The distribution of sizes in figure 3.19 (b) shows that about 65% of microcapsules fall in the size range of 20-60 μm which is in the close vicinity of the average value (40 μm). It can be further observed from the graph in 3.19 (b) that about 16% of the microcapsules have sizes below 20 μm while about 80% of microcapsules are smaller than 60 μm which indicate a good and desired narrow size distribution.

950 rpm-1.5 wt% SLS

Figure 3.20 (a) and (b) show successful synthesis of microcapsules of average size 30 μm produced with 950 rpm agitation speed and 1.5 wt% SLS.

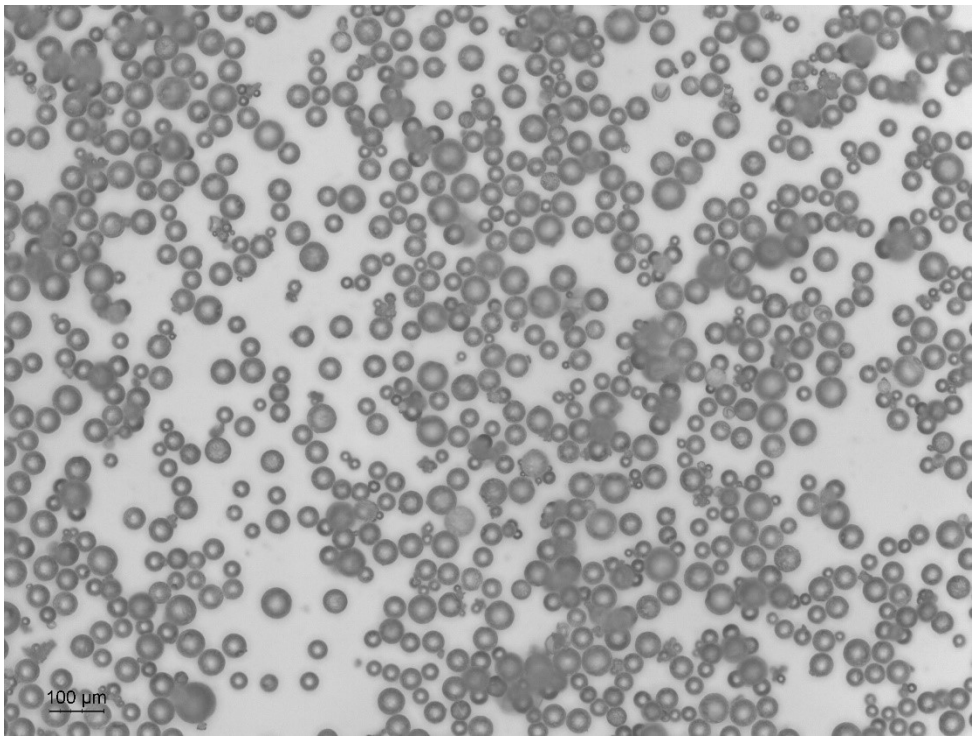

(a)

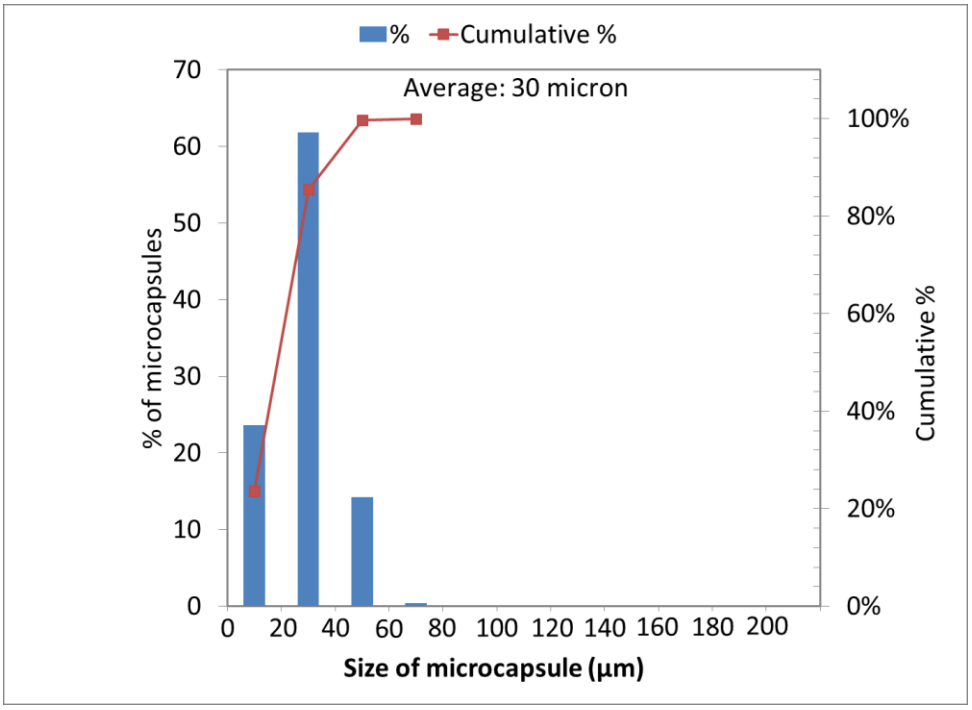

(b)

Figure 3.20 a) Successful synthesis of small microcapsules (average diameter 30 µm) produced with 950 rpm agitation speed and 1.5 wt% SLS and b) their distribution of sizes

The distribution of sizes in figure 3.20 (b) show a very good narrow distribution where most of the microcapsules remain in the close vicinity of average value. This again confirms that, increasing the agitation speed along with increasing the concentration of surfactant successfully reduces the average size of microcapsules while solving the problem of stickiness and agglomeration with improved the distribution of sizes.

1200 rpm-2 wt% SLS

Figure 3.21 (a) and (b) show the microcapsules produced with 1200 rpm agitation speed along with 2wt% SLS and 22ml PVA (instead of 30 ml).

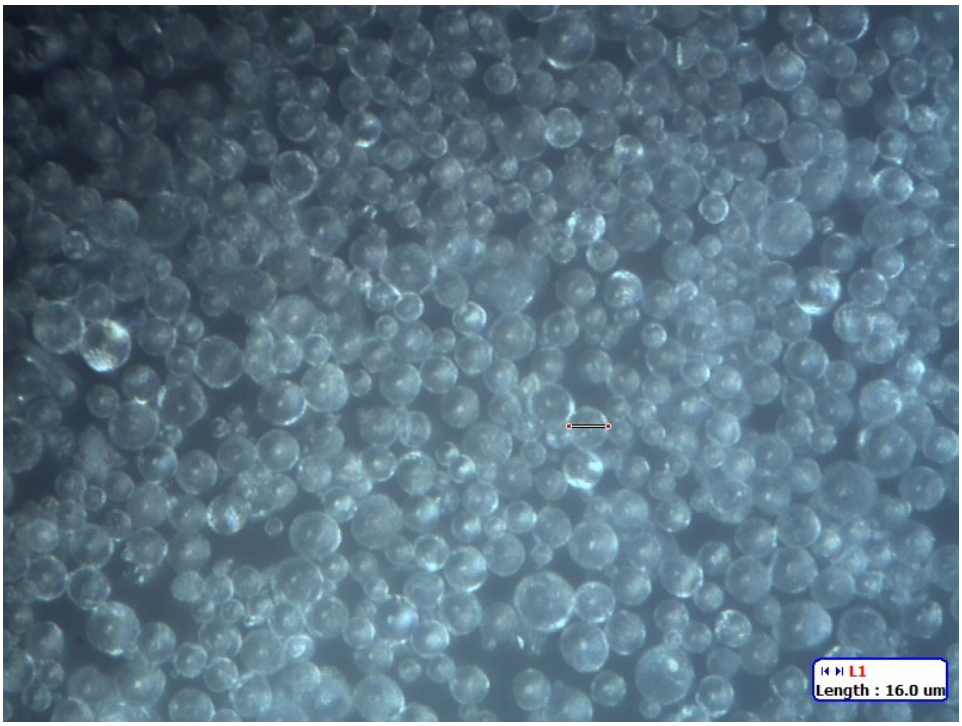

(a)

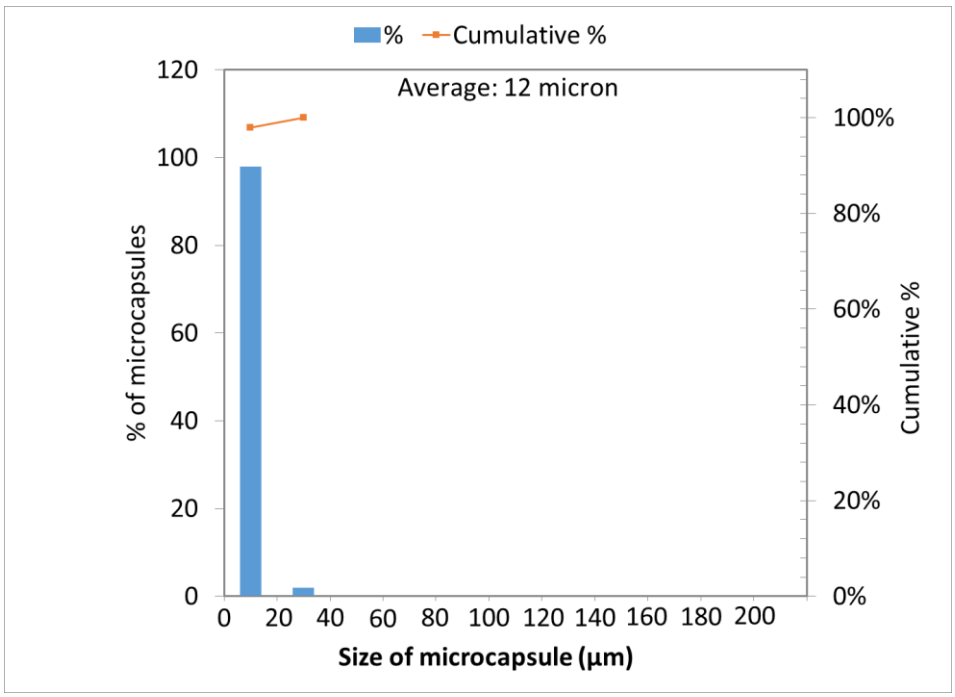

(b)

Figure 3.21 a) Successful synthesis of small microcapsules (average diameter 12 µm) produced with 1200 rpm agitation speed and 2 wt% SLS and b) their distribution of sizes

The average size of the microcapsules with this combination of processing parameters was found to be 12 μm. The distribution of sizes, as shown in figure 3.21 (b), is excellent with almost all the microcapsules remain in the same size range (0-20 μm).

The surface morphology of the microcapsules obtained with the optimum combination of agitation speed-SLS concentration are compared in figure 3.22.

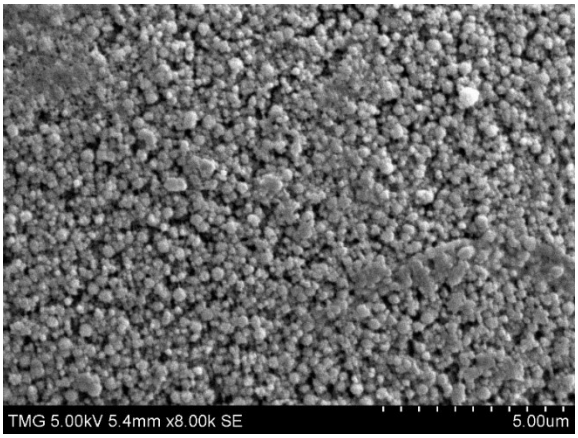

(a) 600 rpm 0.5 wt% SLS

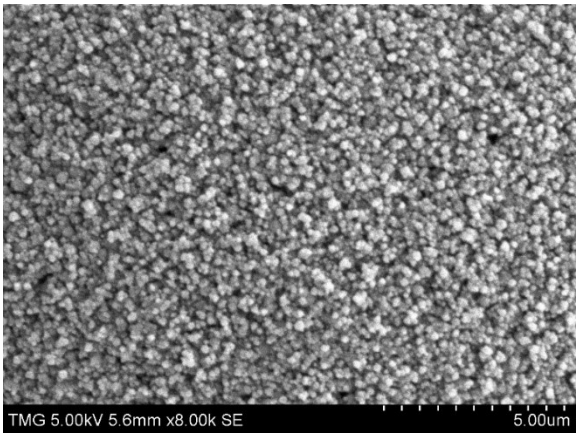

(b) 850 rpm 1 wt% SLS

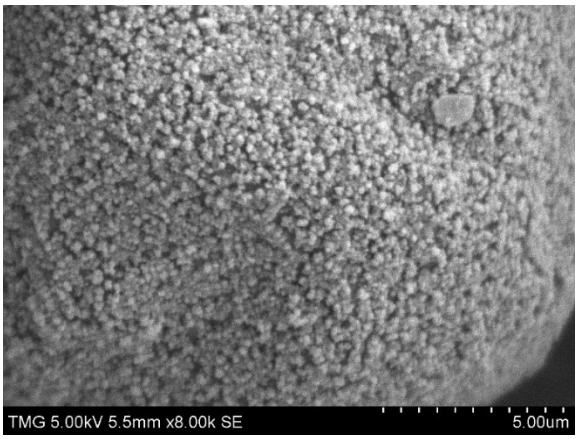

(c) 1200 rpm 2 wt% SLS

Figure 3.22 Comparison of surface morphology of microcapsules obtained with optimum agitation speed-SLS concentration a) 600 rpm-0.5 wt%, b) 850 rpm-1 wt% and c) 1200 rpm-2wt%

The surface of the microcapsules are observed to be compact and patterned with precipitated PMUF nanoparticles. With the combined increase in agitation speed and SLS concentration, the nanoparticles on the outer surface of microcapsules become finer and the compactness of the

microcapsules tends to be increased with less porosity which is desirable for good adhesion properties and self-healing performance.

The shell thickness of the microcapsules obtained with the optimum agitation speed-SLS concentration are compared in figure 3.23.

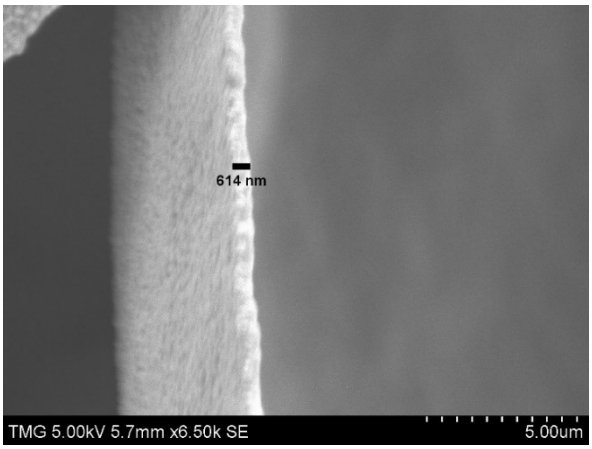

(a) 600 rpm 0.5 wt% SLS

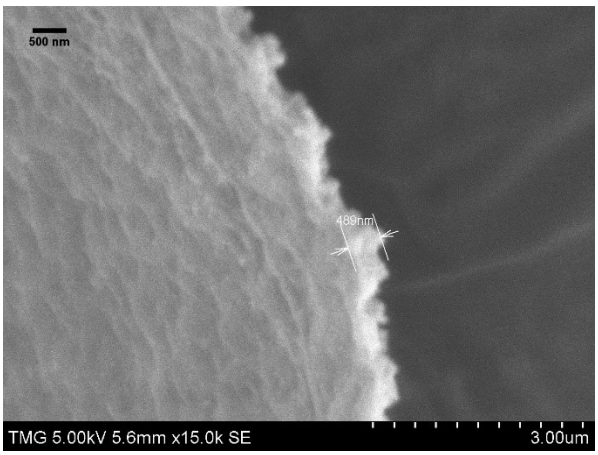

(b) 850 rpm 1 wt% SLS

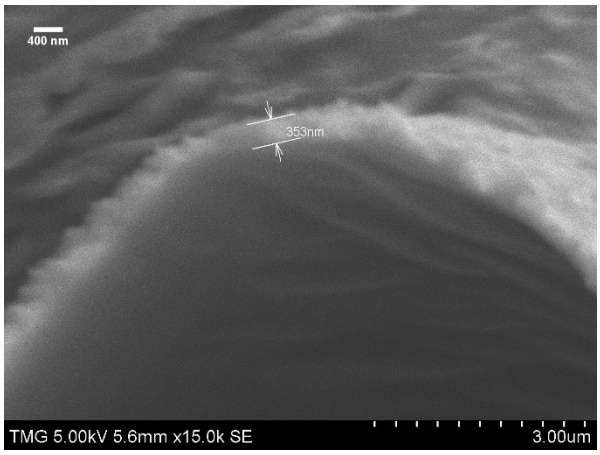

(c) 1200 rpm 2 wt% SLS

Figure 3.23 Comparison of shell thickness of microcapsules obtained with optimum agitation speed-SLS concentration a) 600 rpm-0.5 wt%, b) 850 rpm-1 wt% and c) 1200 rpm-2wt%

With increasing speed-SLS concentration, the shell thickness of the microcapsules decreases with decreasing average size of microcapsules. The shell thicknesses of microcapsules obtained with 600 rpm-0.5 wt% SLS, 800 rpm-1wt% SLS and 1200 rpm-2wt% SLS combinations are in the range of 500-700 nm, 400-500 nm and 300-400 nm respectively. The lowest shell thickness

obtained with 1200 rpm-2 wt% SLS combination is still in the desired range for handling and manufacturing of composites for self-healing applications.

Thus, with the numerous trials of synthesis runs, the optimum combination of agitation speed and SLS concentration for producing individually separated free flowing microcapsules of average size ranging from around 200 µm down to 15 µm with desired quality characteristics is established through this investigation.

Figure 3.24 shows the relationship between the average size of microcapsules, agitation speed and concentration of surfactant (SLS) for obtaining individually separated free flowing microcapsules with good quality characteristics.

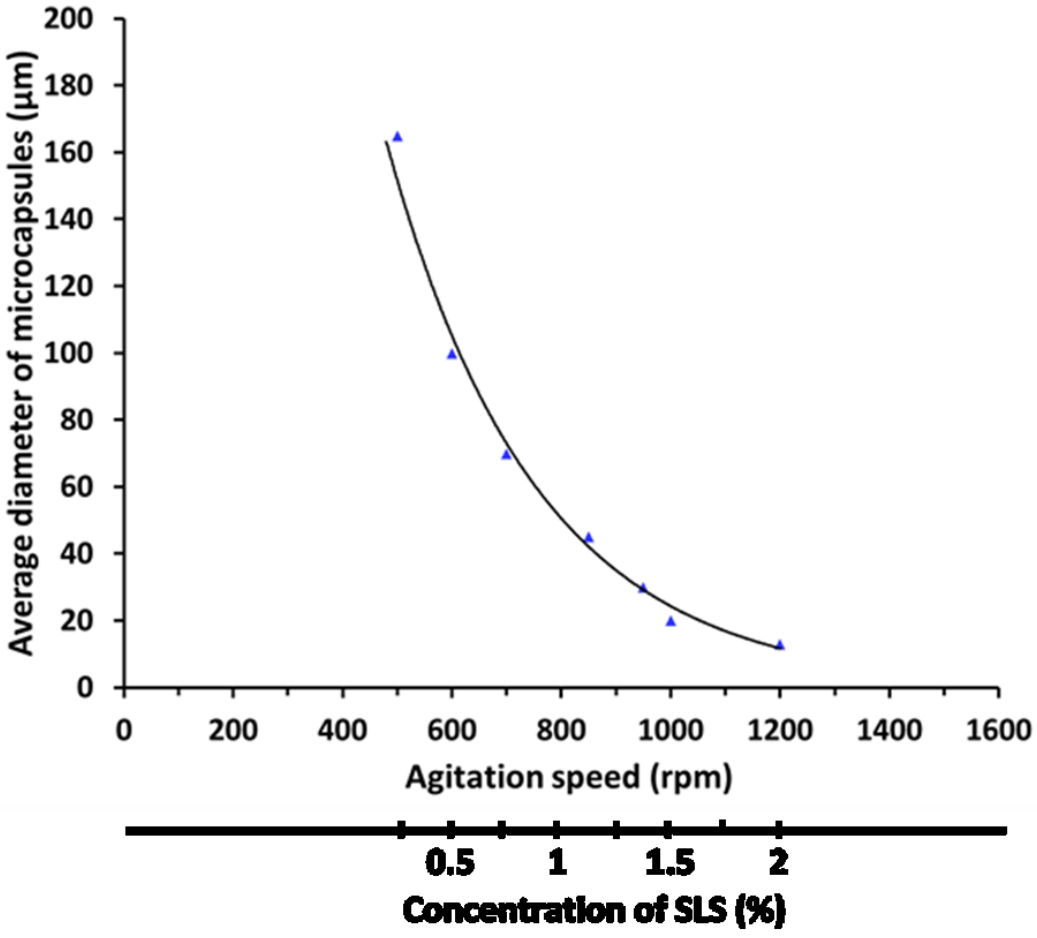

Figure 3.24 Optimum combination of agitation speed-SLS concentration for successful production of free-flowing individually separated microcapsules with desired quality characteristics

The average size of the microcapsules could not be significantly reduced further by simply increasing the agitation speed of the stirrer. Sonication with certain power and duration was needed to further reduce the average size of the microcapsules. However, individually separated free flowing small microcapsules (in the vicinity of average size 1 μm) could not be obtained in a similar way by increasing the concentration of the SLS during the encapsulation process. The small microcapsules (in the vicinity of average size 1 μm) formed in the reaction were not accumulated at the top of the mixture due to the density differences and it was extremely difficult to filter out the whole emulsion. Further efforts are necessary to obtain free flowing microcapsules of average size in the vicinity of 1 μm and less.

3.4 Thermal stability and core monomer content of microcapsules

Thermal stability of microcapsules and the monomer content inside the microcapsule shells are two key quality characteristics of microcapsules. Thermogravimetric Analysis (TGA) was carried out for the microcapsules synthesized by the encapsulation process with the established optimal combinations of agitation speed-SLS concentration to investigate its thermal stability and core monomer content. About 20 mg of microcapsule sample was put into the TGA (TA Q50 series) cell and the parameters are set in the program using a heat and hold method. The program is run under controlled nitrogen flow and the changes is sample mass is continuously recorded. A representative TGA curve is shown in figure 3.25.

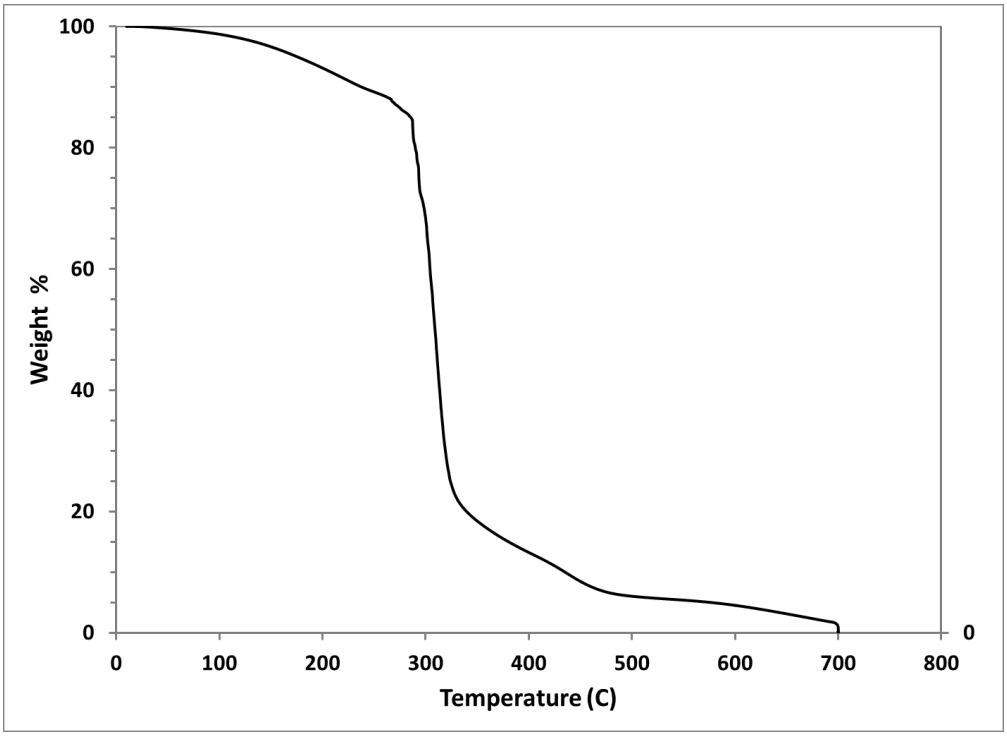

Figure 3.25 Typical TGA curve showing the thermal stability and core content of microcapsules

The temperature is increased up to 700°C with a heating rate of 20°C/min. The temperature is held constant at this temperature for about one hour to finish the analysis. The curve shows that the weight of microcapsules remains almost same until the temperature reached 100°C. About 15% loss of weight was observed between 100°C and 285°C which might be associated with the diffusion and evaporation of the core materials through the microcapsule shells due to its thermal degradation with increasing temperature as observed by Liu et al. [88]. A small portion of the weight loss at this temperature range might also be due to the evaporation of high volatile compounds from the PMUF shell materials [104]. It is to be noted here that the core 5E2N has a boiling point of around 146°C [94]. That means, after the temperature is reached to the boiling point of the core materials, vapor pressure inside the microcapsule continues to build-up with increasing temperature and put pressures on the wall of the microcapsules. This results in an additional 60% rapid loss of weight between 285°C and 325°C which, according to [88], might be associated with sudden rupture or explosion of the shells causing rapid release of the vaporized core materials. The rate of weight loss slows down between around 325°C to 460°C and the residue is decomposed beyond this temperature. Thus from the TGA analysis it is found

that the microcapsules are fairly stable up to the rupture and release of the vaporized core materials. Based on the above analysis, more than 75% of the total weight of microcapsule is estimated to be the monomer contained within the microcapsules.

3. 5 Concluding remarks

Microcapsules containing liquid 5E2N in the core with PMUF shells have been synthesized using the established procedure in literature. The key role of each ingredients used in the emulsion microencapsulation process is understood through literature studies. Melamine, urea and formaldehyde reacts to form the shells of the microcapsules around the liquid 5E2N droplets which forms the core of the microcapsule in the microencapsulation process. SLS serves as an excellent emulsifying agent and surfactant and used in conjunction with PVA to aid in the emulsification of the oil-in-water emulsion in the microencapsulation process. The effect of agitation speed and SLS concentration on the quality characteristics of microcapsules is investigated. The quality of produced microcapsules in terms of average size, size distribution, surface morphology and shell thickness are compared. For a given SLS concentration, the main effect of increasing agitation speed is found to be the reduction of average size of microcapsules with improved size distribution. The surface morphology and shell thickness remains similar as at lower speeds. However, microcapsules become increasingly sticky and difficult to separate as their average size decreases with increasing agitation speeds. On the other hand, the clear effect of increasing the concentration of SLS at a given agitation speed is the reduction of the average size of microcapsules with decreasing shell thickness. Surface morphology is also affected with SLS concentration. The outer shell of microcapsules are found to be patterned with finer nanoparticles with more cracks on it when produced with relatively high concentration of SLS at a lower fixed agitation speed. Finally, an optimum combination of speed-SLS concentration is established through numerous synthesis trials in the investigation.

Microcapsules produced with optimum process parameters (agitation speed and SLS concentration) meets the desired quality standard of microcapsules with good thermal stability and core monomer content. The results of the investigation can be utilized to produce microcapsules of required average size with desired quality characteristics. Among these microcapsules two different average sizes are selected to investigate their effect on self-healing of FRPC composites discussed in the subsequent chapters.

CHAPTER 4

Preliminary Experiments

4.1 Introduction

Numerous trials of synthesis of microcapsules were carried out to study the effects of different processing parameters and to establish control on the quality characteristics of microcapsules. After successfully establishing control on the quality characteristics of the microcapsules, the next key issues were to demonstrate the feasibility of self-healing with the current materials system (5E2N and Grubbs catalyst) and to find a suitable protocol to evaluate the self-healing performance of fiber reinforced polymer (FRP) composites subjected to realistic loadings. Several preliminary experiments were carried out to address the issues.

The feasibility of self-healing with the current materials system was first demonstrated by visually observing the healing of crack network that was created on unreinforced epoxy samples impacted with high velocity projectiles. Once, the self-healing of cracks on unreinforced epoxy sample created with realistic loadings (such as impact of projectiles) was demonstrated with the current materials system, the next issues were how to quantify it realistically, especially, for the FRP composite systems. Initiatives to quantify the self-healing of unreinforced epoxy sample involved measuring the fraction of the length of the crack networks that was observed to be healed under optical microscope. This is described in detail in the following sections.

For the fiber reinforced composites, however, it was not practically possible to visually observe and measure the fraction of healed region in the composites as the cracks created on the FRP composites mostly remained in the sub-surface locations in the form of delamination and other forms of damages. Further, it is necessary to measure how much of a selected mechanical property (e.g. strength or stiffness) is recovered through self-healing. The alternative initiatives to quantify self-healing, thus, involved measuring some mechanical properties of regular (not incorporated with microcapsules and catalysts) and modified (incorporated with microcapsules and catalysts) FRP composites of different architectures subjected to some damages under realistic loadings (like impact, bending etc.) and later compare those properties after being allowed to heal. Several methods were implemented in the preliminary experiments for this purpose. The methods and the preliminary results are discussed in this chapter.

4.2 Demonstration of self-healing of resin sample (without reinforcement)

In order to demonstrate the feasibility of self-healing with the microencapsulated 5E2N/Grubbs catalyst system, cured resin samples (without fibers) incorporated with microcapsules and catalyst were impacted with high velocity projectiles. The damage created and the subsequent healing is visually observed and analyzed using image reconstruction method.

4.2.1 Fabrication of modified resin sample and impact condition

Modified resin samples were prepared by mixing epoxy (EPON 828), curing agent, microcapsules and Grubbs catalyst using vacuum centrifugation method. The mixture was then poured into a silicone mold and cured. The cured sample was then polished and shot with projectile using a high velocity gas gun *[105]* as shown in figure 4.1.

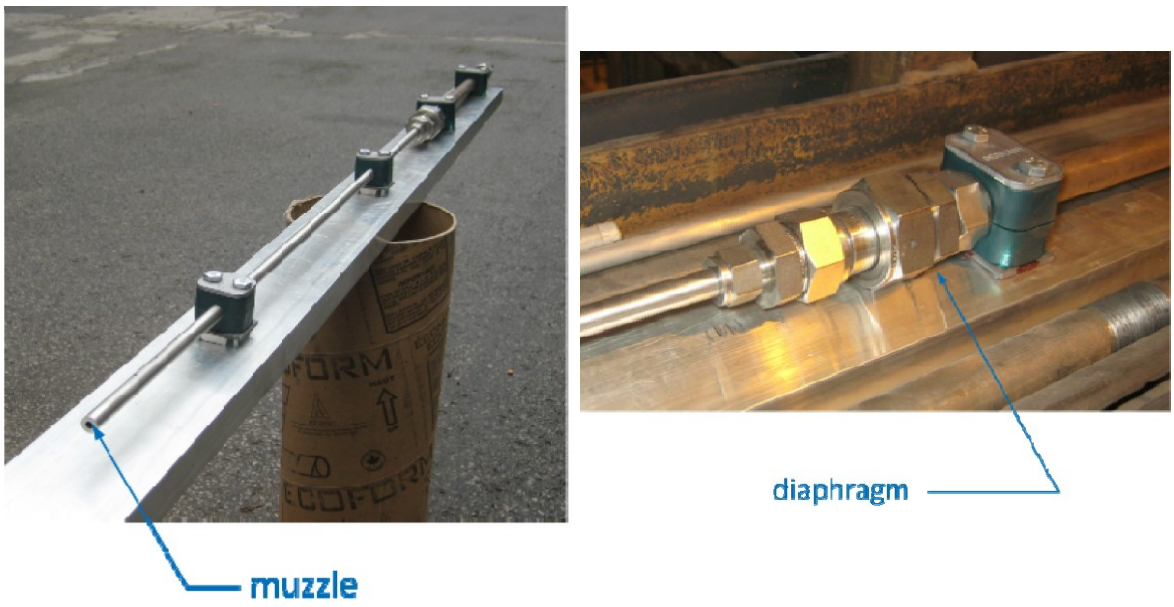

Figure 4.1 Single stage gas launcher [105]

The dimensions of the resin sample and shot conditions are given as follows:

Dimensions of the resin sample: 50.8 mm X 50.8 mm X 4.8 mm

Projectile material: Aluminum

Projectile dia: 1.8 mm

Projectile mass: 15 mg

Projectile speed: (600 ± 50) m/sec

The high velocity projectile impact on the modified resin sample created a crater on one side and a network of cracks on the other side as shown in figure 4.2 a) and b).

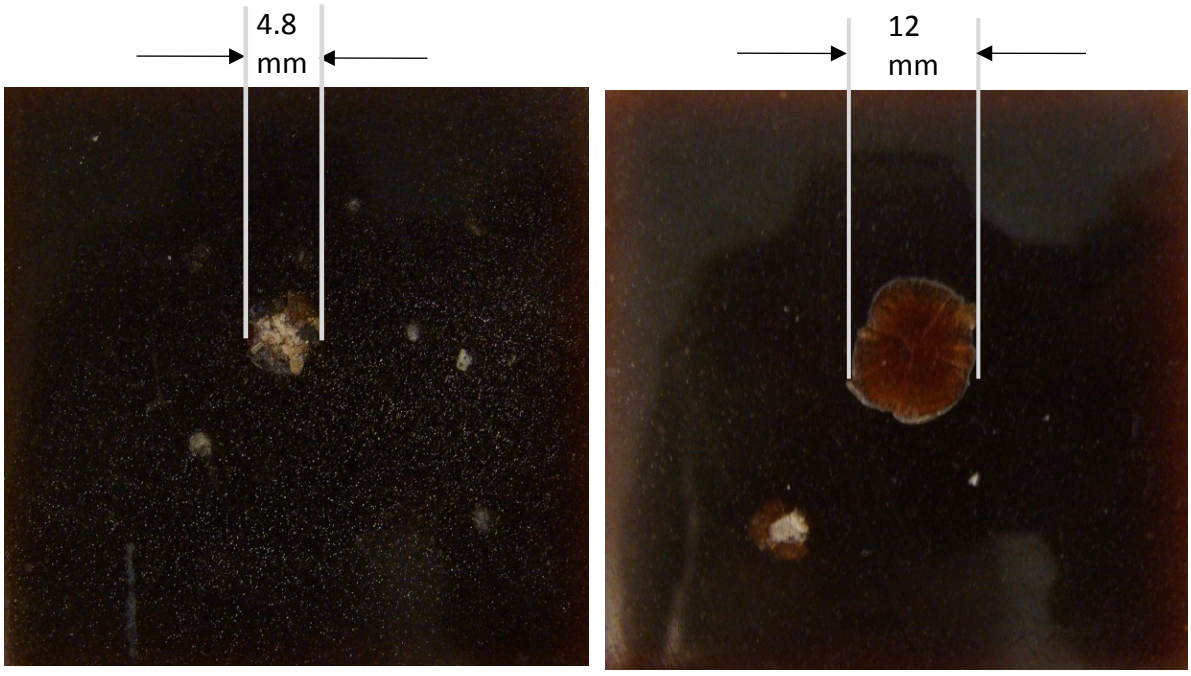

Figure 4.2 Photograph of the modified resin sample after impact a) side of the impact and b) opposite side of the impact

After allowing certain time for healing, the crack network thus created on the opposite side of the sample was observed under Optical Microscope (OM) for analysis.

4.2.2 Observation and analysis of self-healing

Encounter of microcapsules with propagating cracks and filling of the cracks with self-healed polymer are revealed in the series of observations made with OM as shown in figure 4.3 a) - f).

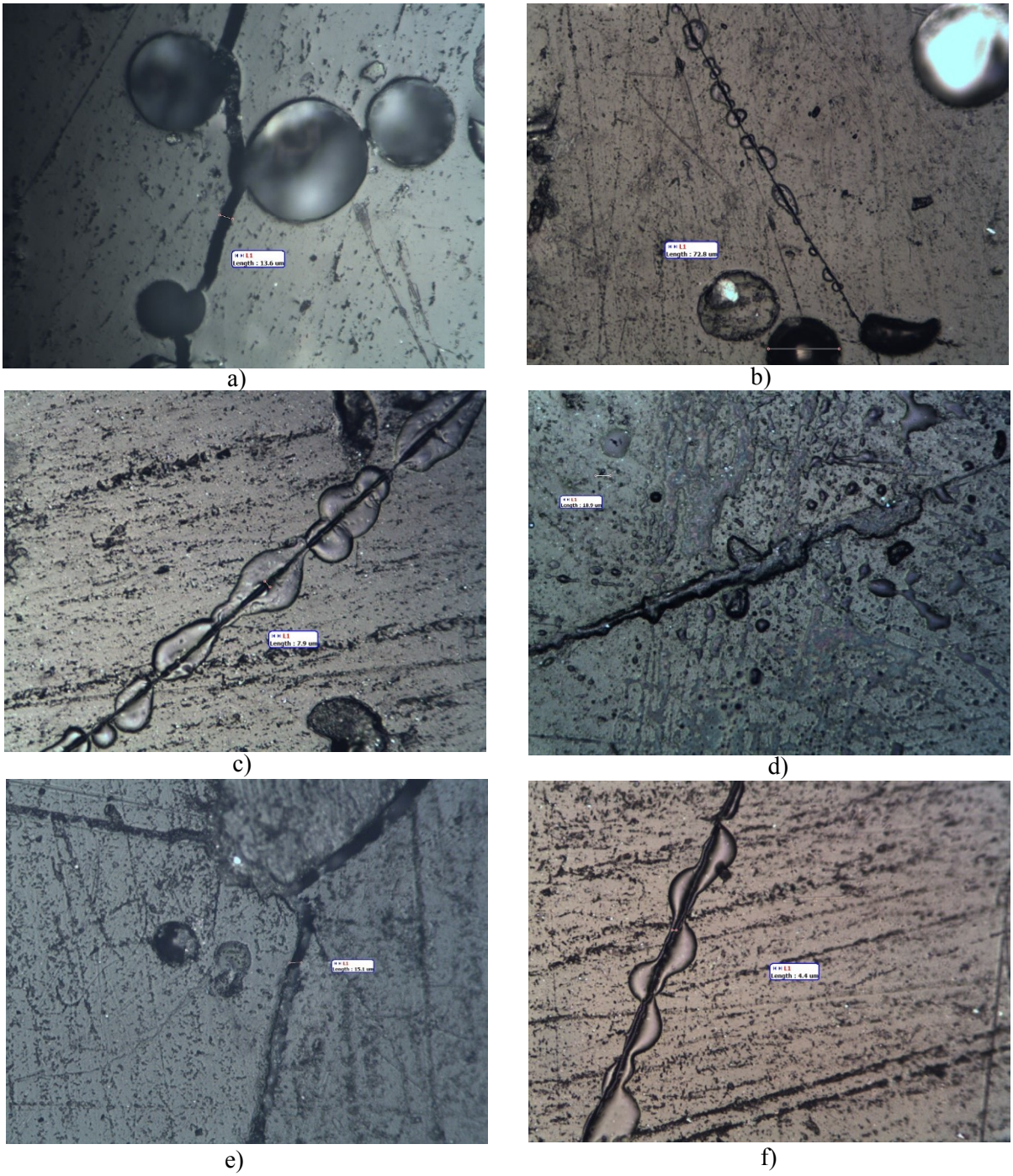

Figure 4.3 Optical micrographs of the crack networks on the impacted modified resin sample showing examples of a) encounter of microcapsules with a propagated crack and b-f) cracks healed by monomer which oozed out from broken microcapsules and subsequent polymerization

The optical micrographs in figure 4.3 demonstrate, successfully, the self-healing of cracks created on the resin samples under realistic loading and without any manual assistance for healing.

In order to make a quantitative analysis, it was necessary to have a sufficiently enlarged image of the damaged region of the sample on the opposite side of the impact as shown in figure 4.2 b). For this purpose, the damaged region was observed at a fixed magnifications under OM and series of images captured were reconstructed to reproduce the entire damaged region all together.

The lowest magnification used for this purpose was 6.3X. With this magnification, only a portion of the damaged region could be captured at a time. Several images (8-10) were then captured in order to cover the whole damaged region. Every image represents a certain portion of the damaged region and contains some overlapped region. These images were then carefully arranged in order to reconstruct the image of the entire damaged region. The reconstructed image of the damaged region on the opposite side of the sample at magnification of 6.3X is shown in figure 4.4.

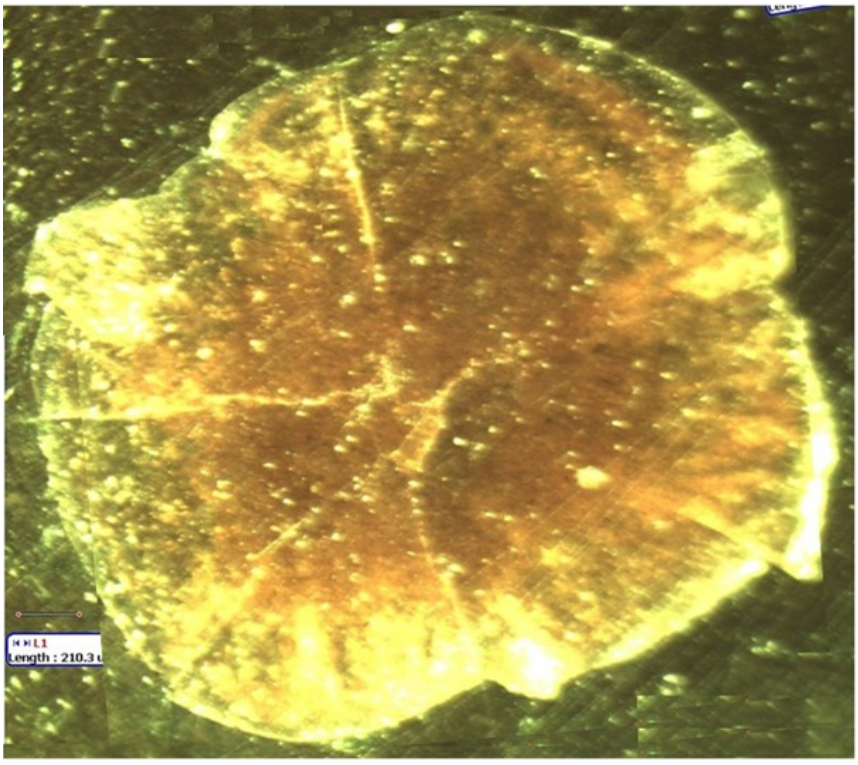

Figure 4.4 Reconstructed image of the damaged region under 6.3X magnification

Figure 4.4 shows better view of the damaged region compared to the digital photograph shown in figure 4.2 b) although it was not sufficient to make a quantitative analysis. Thus, the same procedures were followed with higher magnifications (10X, 16X, 25X). With increasing magnifications, each captured image could only capture a decreasing area/portion of the damaged region and requires an increasing number of images to be captured to reconstruct the entire region making the reconstruction tedious. However, it was found that, even with 25X magnification, the crack network could not be observed satisfactorily to make a quantitative analysis.

The details of the cracks can, however, are observed with a minimum 50X magnification. With this magnification, more than 200 images were captured to cover the entire damaged region. The images were then reduced to 25% relative to the original size while maintaining the aspect ratio. These images were then arranged on a 3ft X 3ft power point slide (which is equivalent to a poster size paper) to reconstruct the whole damaged region in a single image. The reconstructed image (downsized to accommodate into the paper) is shown in figure 4.5.

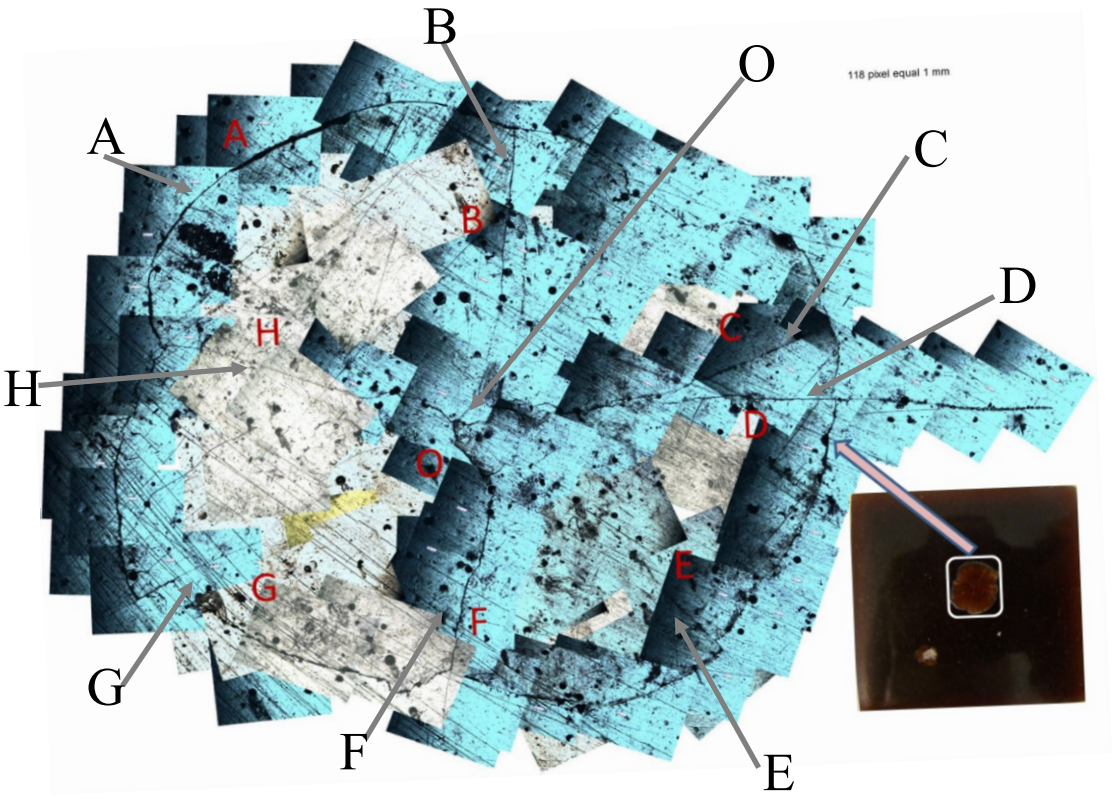

Figure 4.5 Reconstructed image (downsized to accommodate to the paper) of the damaged region at the opposite side of the impacted modified resin sample. Each crack branched out from the centre is indicated by letters (B-H) and the crack in the outer circumference is indicated by letter A.

With the reconstructed image, each individual crack could be identified on the damaged region. The damaged region is surrounded by a major crack which is designated as crack A. The crack at the center of the region is designated as crack O. The other cracks are designated similarly from crack B to crack H. The network of cracks, illustrated with letters (A-H) in figure 4.5, was then analyzed and their dimensions (length) were obtained using image analysis software (ImageJ) [89].

Healing of the cracks, as shown in figure 4.3 and the smaller dimension (width) of the cracks, however, could not still be satisfactorily observed with this reconstructed image. Thus, each crack identified on the reconstructed image was again followed under OM at higher magnifications to find the healed portions and to measure the width of the cracks at different locations. Self-healing of the resin sample was then quantified by determining the fraction of the total crack length that was visibly filled with healed polymer.

With reference to the reconstructed image in figure 4.5, the quantitative measurements and analysis of the cracks are given below:

Crack A

Between cracks H and B (see figure 4.5)

Length = 9.9 mm

Average width = 9 µm

Healed length = 0.8 mm

Between cracks B and C

Length = 7.7 mm

Average width = 9 µm

Healed length = Not observed

Between cracks C and D

Length = 1.6 mm

Average width = 7 µm

Healed length = Not observed

Between cracks D and E

Length = 5.5 mm

Average width = 9 µm

Healed length = Not observed

Between cracks E and F

Length = 5.7 mm

Average width = 5 μm

Healed length = 0.3 mm

Between cracks F and G

Length = 6 mm

Average width = 12 μm

Healed length = 0.5 mm

Between cracks G and H

Length = 5 mm

Average width = 11 μm

Healed length = 0.4 mm

The total circumferential length of crack A = 41.5 mm.

Total healed length of crack A = 2.3 mm

Percentage of healed length = 5 %

To measure the length of the cracks, the curves were divided into small segments and the lengths of each segment were measured. Similarly, average width of the cracks were calculated by measuring width in various locations of a crack.

Crack B

Length = 5.4 mm

Average width = 3 μm

Healed length = 1.1 mm

Percentage of healed length = 20.4%

Crack C

Length = 6.2 mm

Average width up to the mid length (measured from the center to the outer circumference of the damaged region) = 12 μm

Average width from the mid length to the end of the crack (measured from the center to the outer circumference of the damaged region) = 4 μm

Healed length = 5.8 mm

Percentage of healed length = 93.5 %

Crack D

Length = 7.4 mm

Average width = 10 μm

Healed length = 2.2 mm

Percentage of healed length = 29.7 %

Crack E

Length = 4.2 mm

Average width = 2 μm

Healed length = 1.2 mm

Percentage of healed length = 28.6 %

Crack F

Length = 5.1 mm

Average width = 18 μm

Healed length = 0.1 mm

Percentage of healed length = 2 %

Crack G

Length = 2.6 mm

Average width = 3 μm

Healed length = 0.3 mm

Percentage of healed length = 11.5 %

Crack H

Length = 5.4 mm

Average width up to the mid length (measured from the center to the outer circumference of the damaged region) = 7 μm

Average width from the mid length to the end of the crack (measured from the center to the outer circumference of the damaged region) = 2 μm

Healed length = 2.1 mm

Percentage of healed length = 38.9 %

Crack O

Length = 6.3 mm

Average width = 9 μm

Healed length = 1 mm

Percentage of healed length = 15.9%

In summary,

Total number of cracks observed = 9

Total crack length = (41.5 + 5.4 + 6.2 + 7.4 + 4.2 + 5.1 + 2.6 + 5.4 + 6.3) mm = 84.1 mm

Total healed length = (2.3 + 1.1 + 5.8 + 2.2 + 1.2 + 0.1 + 0.3 + 2.1 + 1) mm = 16.1 mm

Healing efficiency defined as the fraction/percentage of the total crack length that was healed = 19 %

In addition to demonstrating and quantifying self-healing, the investigation also led to the observations that self-healing seems to perform better when

i) The propagating cracks intersect as many microcapsules as possible releasing sufficient amount of monomer into the crack to fill it up, and

ii) The crack width is in the order of around 10-15 μm.

After the successful demonstration of self-healing in resin (without reinforcement) sample with the current healing agents (5E2N/Grubbs catalyst), the next issues were to determine how much of a selected mechanical property (e.g. strength and stiffness) of FRP composite is provided by the healed material. Further, it was necessary to investigate and establish realistic methods of imparting damage to the composites and loading procedures to evaluate self-healing performance. Several methods were preliminary investigated for this purpose and are discussed in the following sections.

4.3 Investigation of self-healing of FRP composites

Several methods were employed to investigate the self-healing of FRP composites. The methods involve fabrication of regular (without healing agents) and modified (with healing agents) FRP composites, creation of controlled damages to it with realistic loadings and measuring the mechanical properties after allowing to heal the damages. These are discussed in the following sections.

4.3.1 Flexure After Impact (FAI)

This procedure can also be termed as impact-heal-flexure approach. In this approach, damages in the FRP composite samples were first created by controlled impact of projectiles shot from the available high velocity gas gun. Delaminations created in the samples were then

analyzed by visual observations. The damages created on the sample were then allowed to heal after which it is loaded in flexure using standard testing methods (ASTM D7264 [106]) to measure its flexural properties. Flexural properties of the undamaged control samples were also measured to compare it with the properties of healed samples.

Fabrication of composite samples and impact conditions

Regular (without healing agents) and modified (with healing agents) composite panels were manufactured using the hand lay-up method with autoclave molding. For the manufacturing of regular composite panel, layers of the carbon fabric were impregnated with regular epoxy matrix (containing epoxy and curing agent only). On the other hand, layers of the carbon fabric were impregnated with modified epoxy matrix (containing epoxy, microcapsules, catalyst and curing agent) for manufacturing modified composite panel. During the lay-up, a thin strip of teflon was introduced in between the 4th and 5th layer of the $[0_2/90_2]_S$ laminate. This teflon strip acts as an artificial flaw which is introduced in order to stimulate controlled delamination in the samples during high velocity impact of projectiles. The laminate construction is shown in figure 4.6.

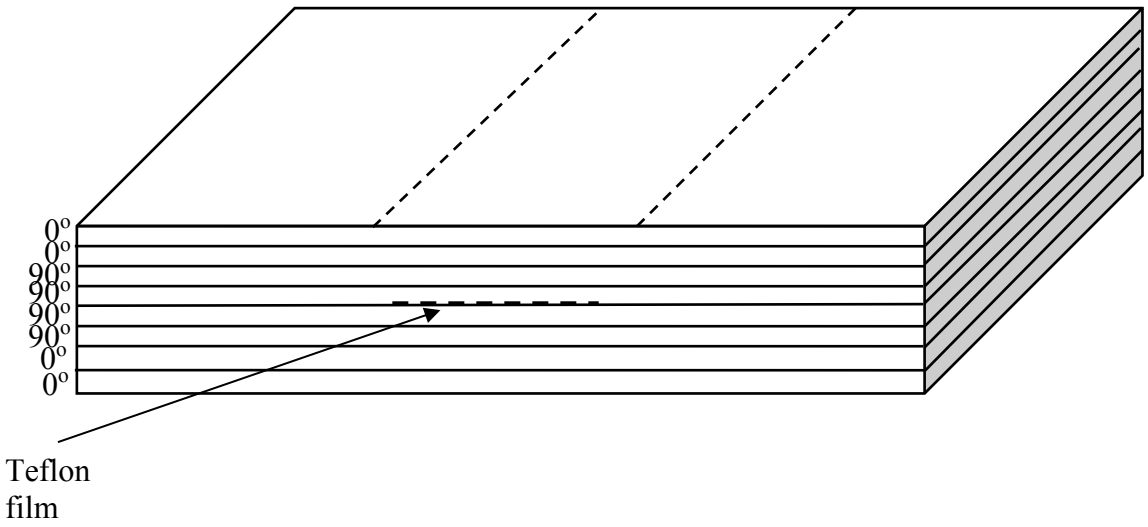

Figure 4.6 $[0_2/90_2]_S$ Laminate construction with artificial flaws. Projectiles travel from bottom to top. Layers are also counted in the same direction; bottom (1), top (8).

From these composite laminates, the 3-point bending samples were prepared according to the guidelines of ASTM D7264 specifications. The composite samples are shown in figure 4.7.

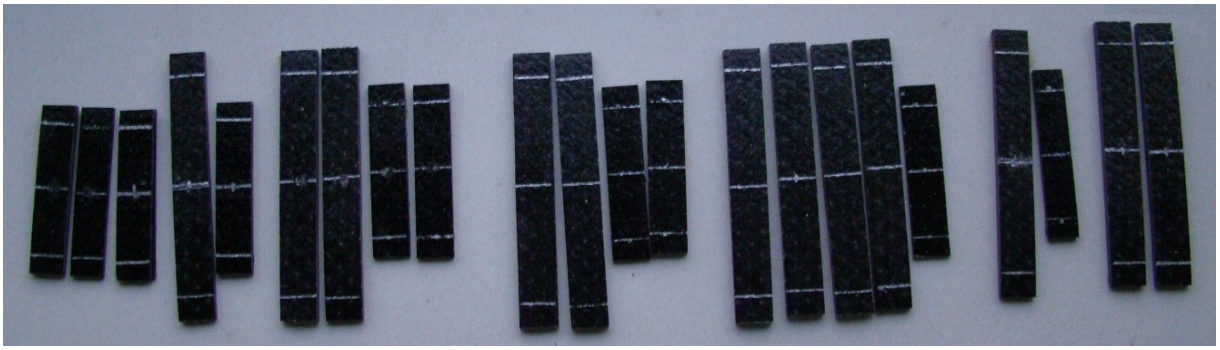

Figure 4.7 3-point bending samples prepared from regular and modified carbon/epoxy composite panels

The modified composite samples were typically 60% thicker than the regular composite samples due to the incorporation of healing agents into the matrix. The modified samples were thus cut longer than the regular samples (as shown in figure 4.7) to keep the same span to thickness ratio according to the ASTM standard. Some of these composite samples were shot with projectiles with varying impact energy using a high pressure gas gun.

The samples were attached between two rigid supports with sealant tape as shown in figure 4.8. The samples were then shot by projectiles (made of aluminum and polycarbonate) with different speeds (ranging from 300 m/s to 550 m/s) to vary the impact energy.

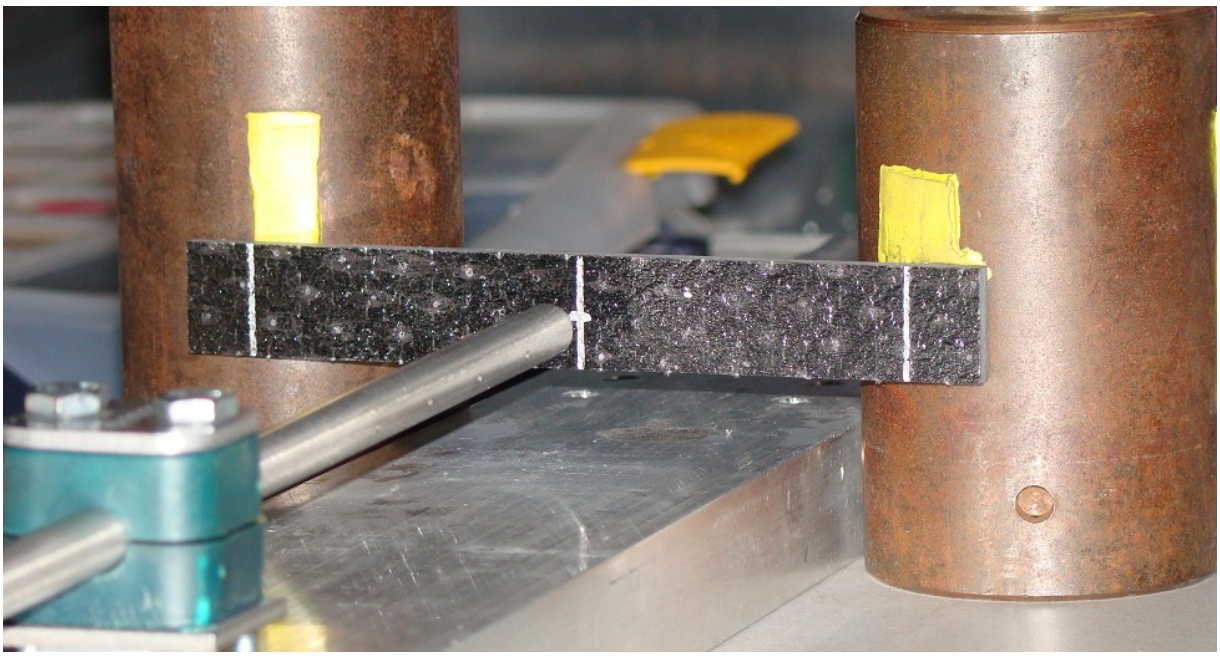

Figure 4.8 Shooting set up for the composite samples

The impact energy was calculated according to

$$E_{im} = \frac{1}{2}mv^2 \quad \text{---------- (4.1)}$$

where,

E_{im} represents the impact energy (joule);

m represents the mass of projectile (gm/1000),

v represents the velocity of projectiles (m/s) which was controlled by varying the diaphragm thickness.

The velocity of projectiles was obtained based on the calibration curves as shown in figure 4.9.

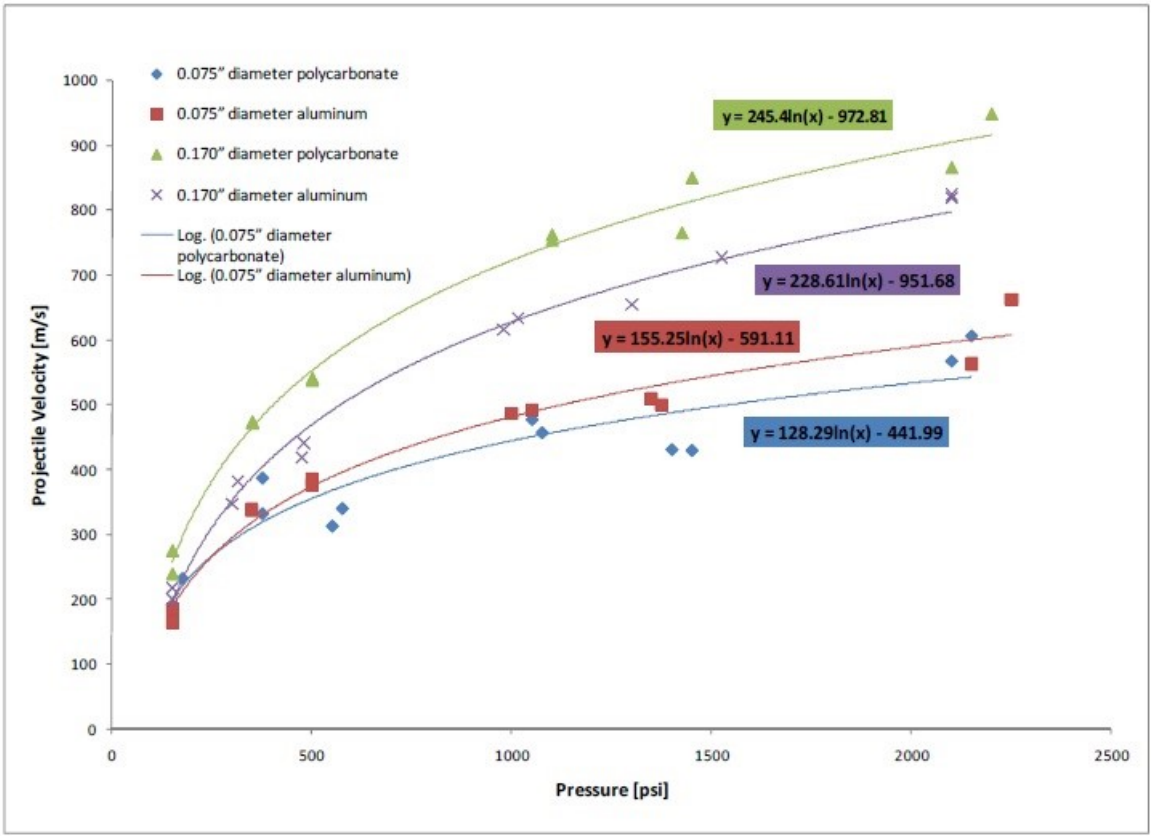

Figure 4.9 Calibration curves for the velocity of projectiles in high pressure gas gun [105]

Analysis of damage created on the samples by the impact of projectiles

The delamination created on the composite samples due to the impact of high velocity projectiles were first analyzed by visual observations. Close observations of the edges of the composite samples revealed a systematic pattern of delamination created by the impact of projectiles. The schematic of the typical delamination pattern for regular shot samples is given in figure 4.10.

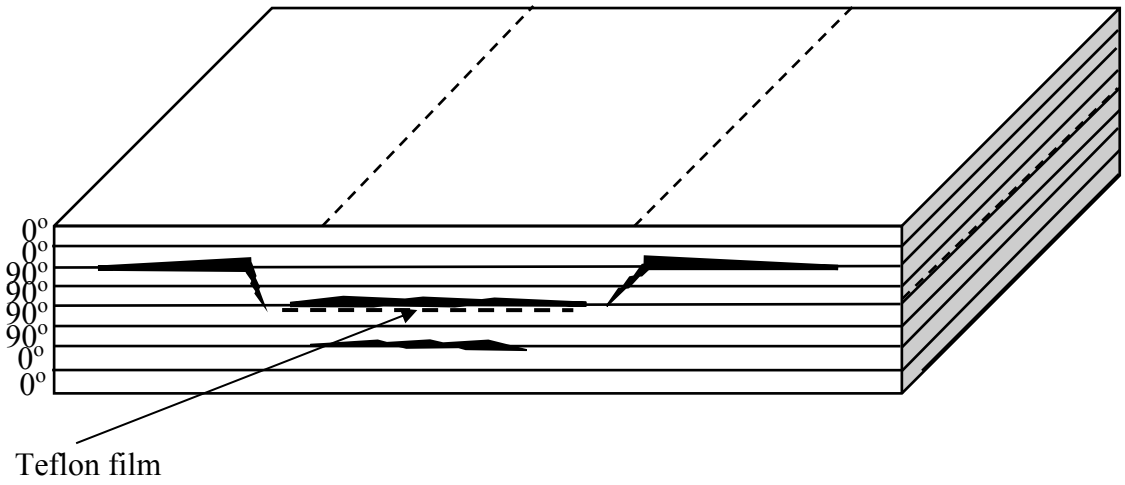

Figure 4.10 Typical delamination pattern of regular $[0_2/90_2]_S$ composite sample with artificial mid-layer flaw under high velocity impact. Projectiles travel from bottom to top. Layers are also counted in the same direction; bottom (1), top (8).

At relatively lower impact energy, the delamination is mainly observed at the 0/90 interfaces and the interface of the induced flaw (teflon insert). Relatively minor delamination is created at the 0/90 interface (between 2nd and 3rd layer) which is closer to the site of impact (bottom surface in figure). An independent delamination is also created in the mid layer interface (between 4th and 5th layer) where the teflon strip is located. This delamination jumps from both ends of the teflon insert up (from bottom to top direction in which the shot projectile travels) to the next 0/90 interface (between 6th and 7th layer) which is furthest away from the site of impact. The delamination at this interface (between 6th and 7th layer) then travels along the length of the sample in both directions away from the induced flaw. The most severe delamination (in terms of length and width of separation between the layers) is always observed at the farthest 0/90 interface away from the site of impact.

The modified composites (incorporated with healing agents), on the other hand, show somewhat similar pattern but less severe delamination under comparable and relatively small impact energy. Further, no jumps of the cracks which connects two delaminations between two different interfaces is observed for modified samples. Incorporation of healing agents into the modified composites possibly make it more ductile to absorb more strains before delamination jumps to the next interface. The schematic of typical delamination pattern for modified shot samples is given in figure 4.11.

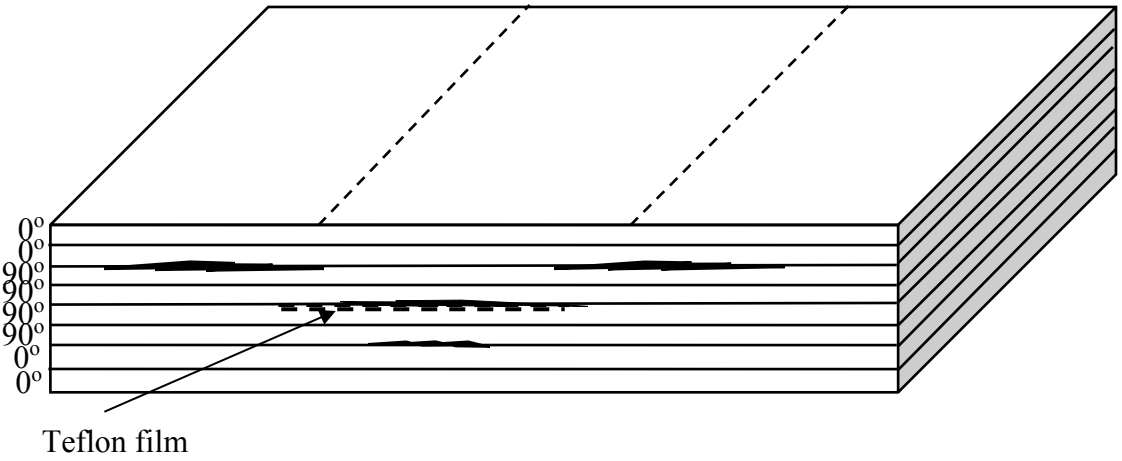

Figure 4.11 Typical delamination pattern of modified [$0_2/90_2$]$_S$ composite sample with artificial mid-layer flaw under high velocity impact. Projectiles travel from bottom to top. Layers are also counted in the same direction; bottom (1), top (8).

After allowing the damaged composite samples to heal, the samples were loaded in flexure according to ASTM D7264 to measure their residual flexural properties (strength and stiffness). Flexural properties of the undamaged control samples were also measured to compare with the properties of healed samples.

3-point bending test

Figure 4.12 shows a composite sample undergoing flexural test on MTS machine equiped with a three point bending fixture.

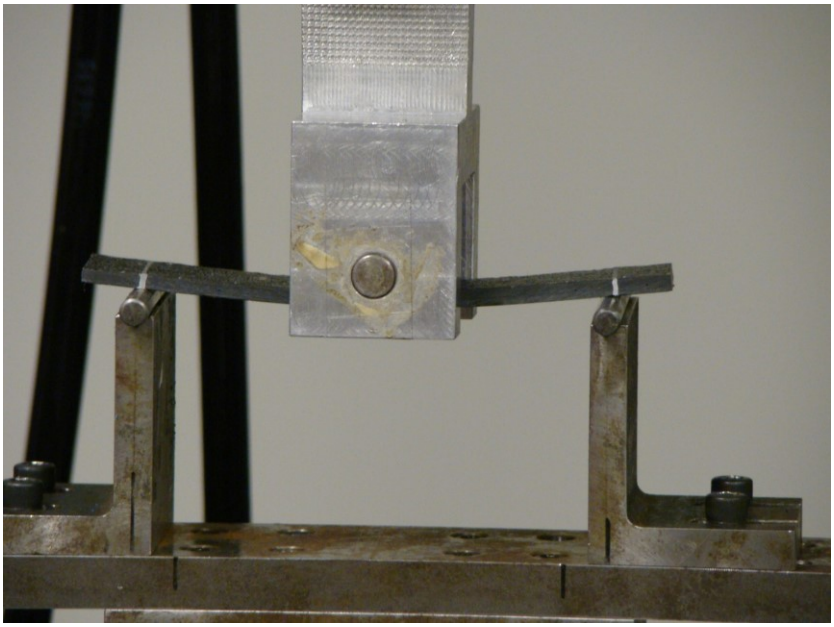

Figure 4.12 A composite sample undergoing flexural test on MTS machine equipped with three-point bending fixture

The load-displacement curves for the regular and modified composite samples shot with different impact energies with high velocity projectiles are shown in figure 4.13 and 4.14.

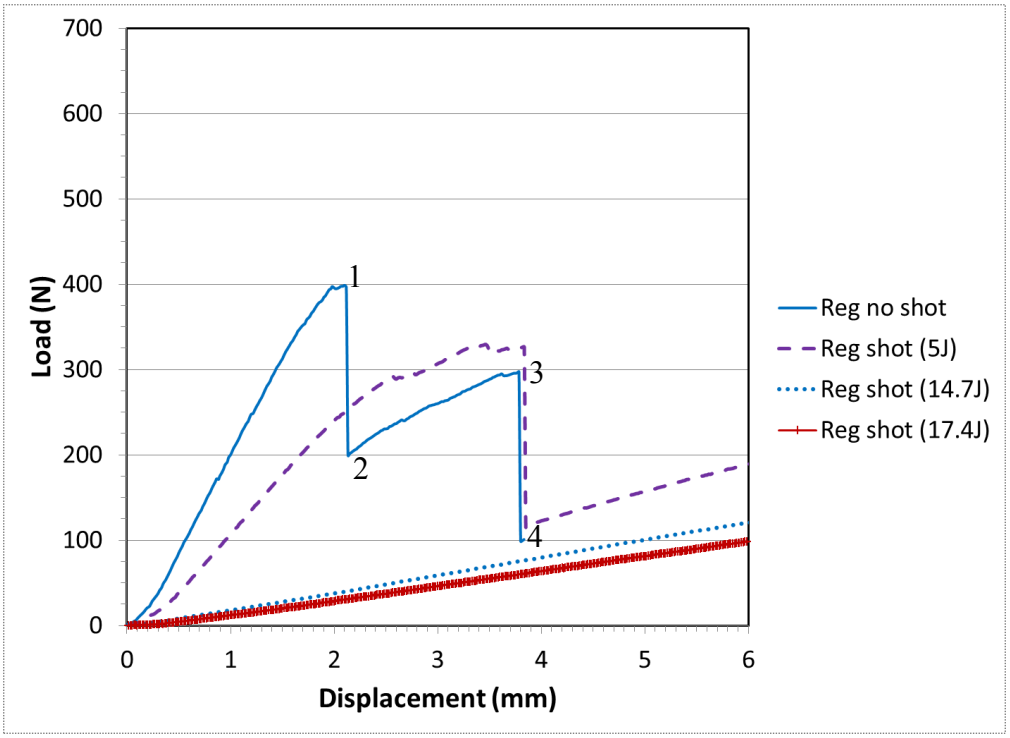

Figure 4.13 Load-displacement curves for regular composite samples after being shot with different impact energy with high velocity projectiles.

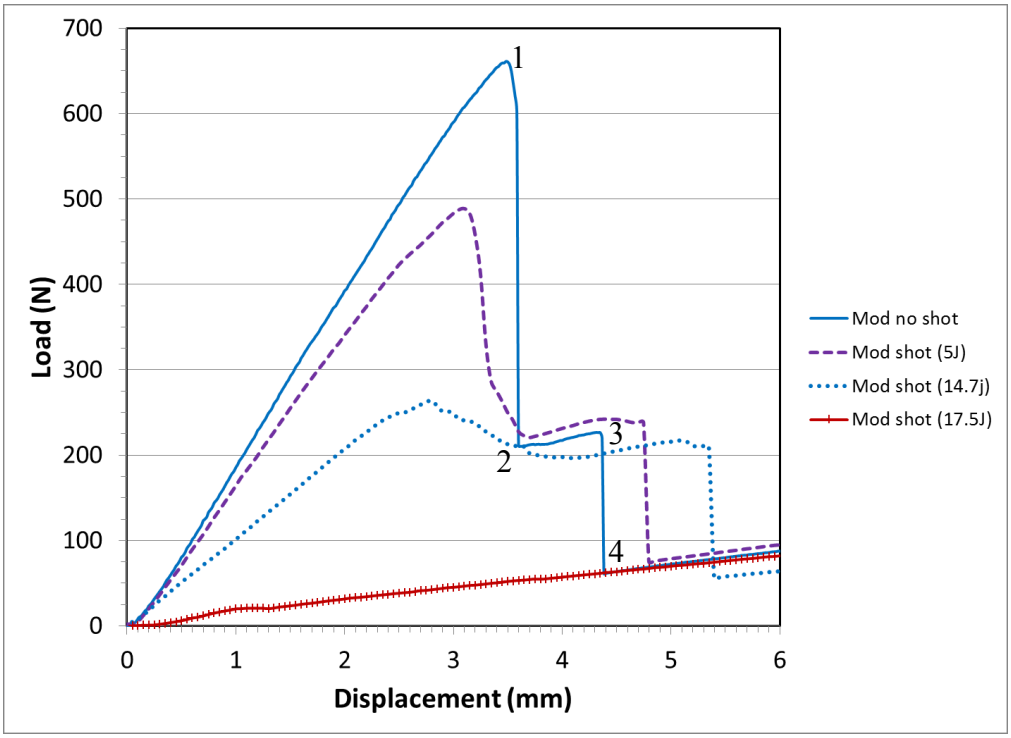

Figure 4.14 Load-displacement curves for modified composite samples after being shot with different impact energies with high velocity projectiles.

It is obvious from figures 4.13 and 4.14 that for both regular and modified composites, the no- shot samples have the highest load carrying capacity. As the impact energy increases the load carrying capacity decreases. Also, the slopes of the curves, which points to the stiffness of the samples, decrease with increasing impact energy. It is due to the fact that the increasing impact energy produces progressively larger amount of damages which, correspondingly, reduces the load carrying capacity and the stiffness of the samples. For the no-shot specimens, initially, the load increases with increasing displacement. At the peak load (point 1), delamination is created (initiation) at the middle layer of the samples where the artificial flaw (teflon film) is located (figure 4.10). The delamination at the middle layer then propagates along the length of the sample and the load continues to drop. The propagation of delamination at the mid layer is stopped near the ends of the teflon insert marking the end of the propagation stage (point 2). The slope of the 1-2 line depends on the speed of propagation of delamination at the middle layer. For high speed of the propagation, this slope is almost vertical. At point 2, the load continues to increase a bit with ongoing displacement up to point 3 until the delamination appears at the outer

0/90 interface. The line 3-4 is the result of propagation of delamination at the outer 0/90 interface along the length of the samples. Again, the slope of line 3-4 depends on how fast the delamination is propagating at this layer. At point 4, the delamination is arrested at one of the support pins. If the loading is continued after point 4, the load continues to increase a bit until the delamination overcomes the resistance at the support pin and propagates to the end of the sample length separating two faces completely at one of its ends. Other shot samples under three-point bending shows similar stages of load-displacement curves as shown in figures 4.13 and 4.14. The absolute values of the peak loads in figure 4.13 and 4.14, however, should not be compared as the modified samples are significantly thicker than the regular samples caused by the incorporation of healing agents (microcapsules and catalyst) into the modified composites. Instead, the residual stiffness of the samples is calculated according to

$$E = \frac{L^3 m}{4bh^3} \text{ ----------(4.2)}$$

Where, E is the residual modulus of the sample (GPa),

m is the slope of the load-displacement curve (N/mm).

b is width of the samples which is kept the same for both regular and modified samples (mm),

h is the thickness of the samples (mm) and

L is the span length (mm)

The ratio (L/h) is also kept fixed for both regular and modified composite samples according to the ASTM D7264 standard.

From equation, (4.2), it can be understood that residual modulus of the samples (E) is directly proportional to the corresponding slope of the load-displacement curves(m) as the other parameters (L/h) and b are kept constant for the regular and modified samples. Thus the comparison of the values of (E) between regular and modified composites might be fairer even the thicknesses of the two types of the samples are significantly different.

Thus, the residual stiffness retained by the composite samples after subjected to impact of projectiles with varying impact energy and subsequent healing (for modified composites) compared with regular samples (no healing ability) is shown in figure 4.15.

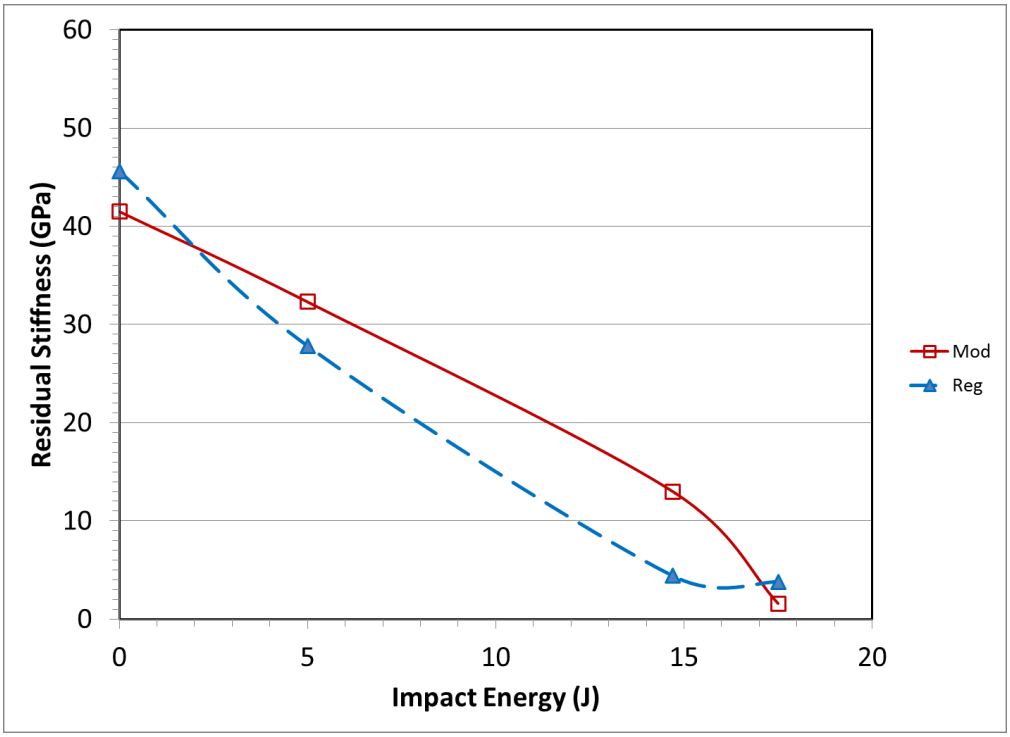

Figure 4.15 Residual stiffness retained by the composite samples after subjected to damage by impact and subsequent healing (modified composites) compared with regular samples (no healing ability)

Figure 4.15 shows that stiffness of the modified no-shot (impact energy = 0) composite sample closely matches the stiffness of the regular no-shot composite sample. It indicates that incorporation of healing agents into the modified composites does not affect its stiffness. However, the residual stiffness retained by the modified samples after healing is greater than the residual stiffness retained by the regular samples subjected to projectile shot up to the impact energy of 15J. This improved retention of residual stiffness of modified composites is possibly due to the self-healing of cracks by the healing agents incorporated into the modified composites.

The residual strength, on the other hand, is calculated according to

$$\sigma = \frac{3pL}{bh^2} \quad \text{---------- (4.3)}$$

Where, σ is the residual flexural strength (MPa) and,

p is the peak load (N) in the load-displacement curve.

From equation, (4.3), it can be realized that, even the parameters (L/h) and b are kept constant for the regular and modified samples, the residual strength of the samples (σ) is still a function of the parameter $\left(\frac{p}{h}\right)$ which is not independent of thickness(h). Thus, comparison of the values of (σ) between regular and modified composites might not be fair. Instead, the values of the parameter $\left(\frac{p}{h}\right)$ is plotted against the impact energy in figure 4.16, for the regular and healed modified composites subjected to projectile impact.

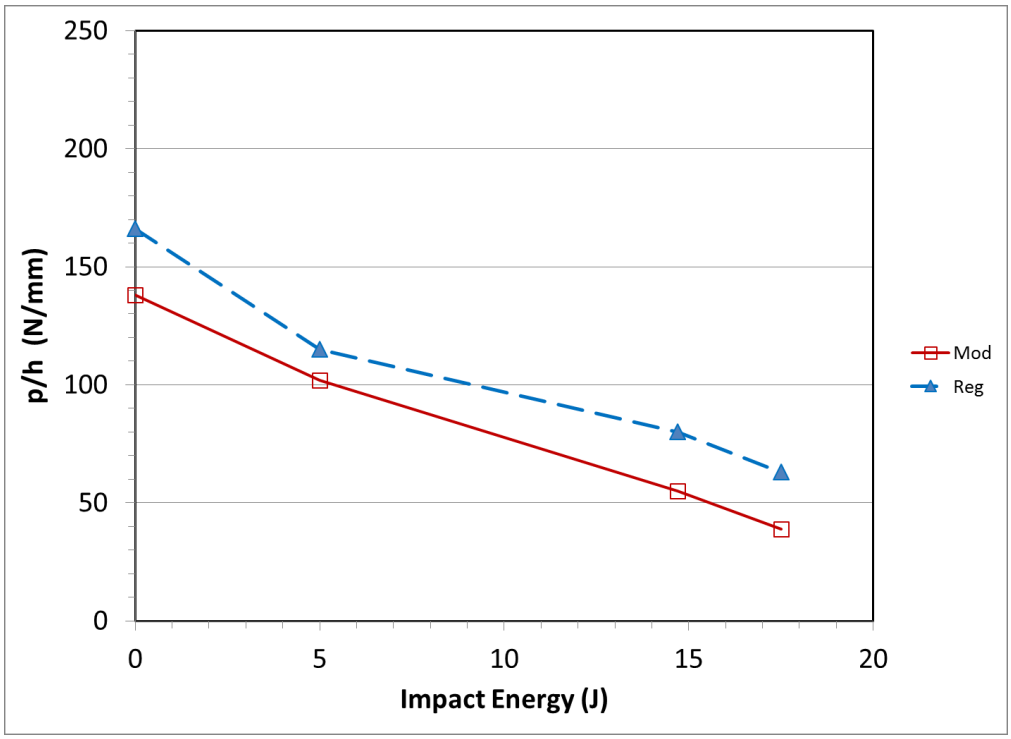

Figure 4.16 Peak loads per unit thickness (p/h) retained by the composite samples after subjected to damages by impact and subsequent healing (modified composites) compared with regular samples

Figure 4.16 indicates that the values of the parameter $\left(\frac{p}{h}\right)$ for the modified composite samples remained lower than that of regular samples at a given impact energy. However, due to the dependence of the flexural loads on the geometry (thickness) of the samples [106], the effect of self-healing could not be clearly extracted from the above figure.

Residual flexural strengths of the composites, further, could not be directly compared because of its dependence on the thickness of the samples [even the parameters (L/h) are kept constant] which are significantly different in the regular and modified composite samples. Thus, it is concluded that the effect of self-healing might not be extracted accurately from the strength based approach. A fracture based approach which usually deals with determining material properties independent of geometry (thickness) of samples would probably, be a better choice for the evaluation of healing performance of FRP composites.

4.3.2 Flexure after Flexure (FAF)

As one of the objectives of the current work is to evaluate the self-healing performance of composites by a realistic loading procedure, the other procedure that was followed during the preliminary investigations also involved strength based approach while trying to minimize the difference in thickness between the regular and modified samples. The procedure can also be termed as flexure-heal-flexure approach. In this approach, damages in the FRP composite samples were first created by controlled bending of the composites instead of impact of projectiles. Delaminations created by the bending of the samples were then allowed to heal by unloading after which the samples are loaded again in three point bending according to ASTM D7264 [106] to measure its residual flexural properties. The difference in the fabrication of composite samples and the test procedures that followed are described in the following sections.

Fabrication of composite samples

New regular and modified composite samples were fabricated using the same method described in the previous section except the fact that only layers containing the dissimilar interfaces (i.e. only the 0/90 interfaces) and the mid 90/90 interface (where the teflon film was inserted) in the modified samples were impregnated with modified resin containing relatively high concentration (15 wt%) of microcapsules (see figure 4.6). The other layers (like the 0/0 and 90/90 interfaces) of the modified samples were impregnated with regular resin. This was done to minimize the difference in thickness between the regular and modified composite samples and the delaminations were found to operate mainly on the dissimilar interfaces of the composites. Even with this modification, the modified composite samples were found to be about 45% thicker than the regular samples. The span to thickness ratio of the two types of samples were thus kept constant according to ASTM D7264 [106] for measuring the flexural properties of the samples with the new test schemes.

The FAF test schemes that were employed in the preliminary investigation are described below.

Test scheme 1

The first test scheme that was employed for the evaluation of healing performance is depicted in figure 4.17

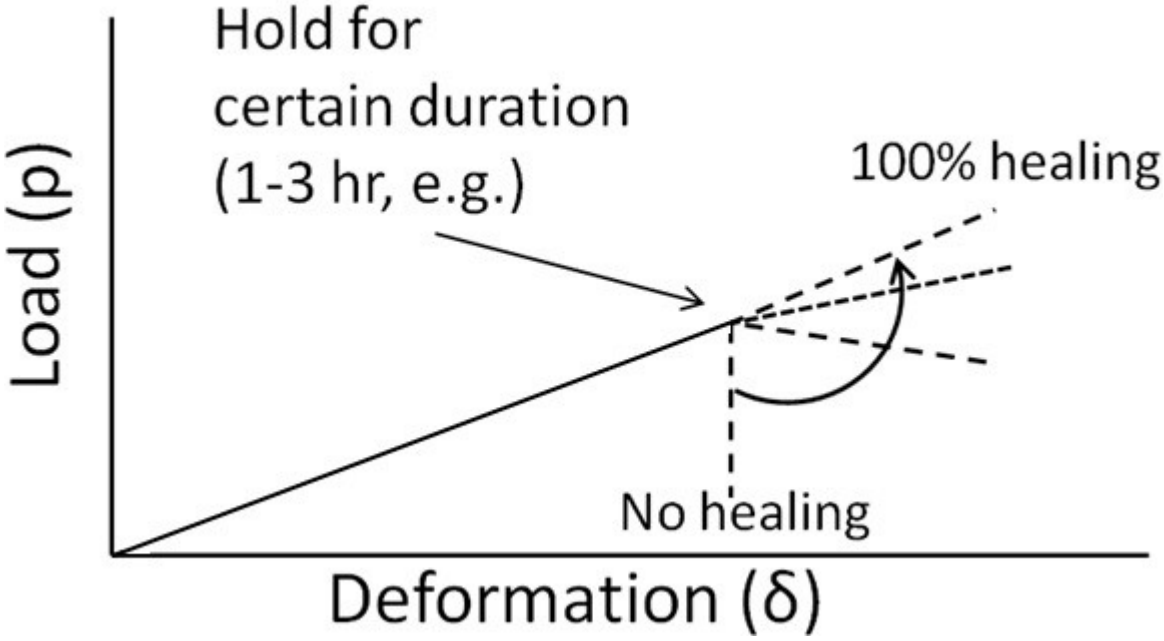

Figure 4.17 Test scheme 1 under FAF protocol for evaluation of self-healing performance

In the test scheme 1 under the FAF protocol, it was proposed that the modified samples would be first loaded under 3-point bending test arrangement according to ASTM. The load would continue to increase with increasing displacement. At the instant, the initiation of delamination is observed, the same load would be maintained on the sample by halting the displacement for a while to allow time for self-healing as shown in figure 4.17. After certain time, the load would be increased again with increasing displacement. Intuitively, 100% self-healing would be assigned if the load continues to increase maintaining the same slope during the second loading. On the other hand, no healing (0%) would be assigned if the load drops vertically down when loading continues. Anything in between this envelope would be assigned proportionate percentage of self-healing.

Several tests were made following the above scheme. The typical load-displacement curve with this test scheme 1 is shown in figure 4.18.

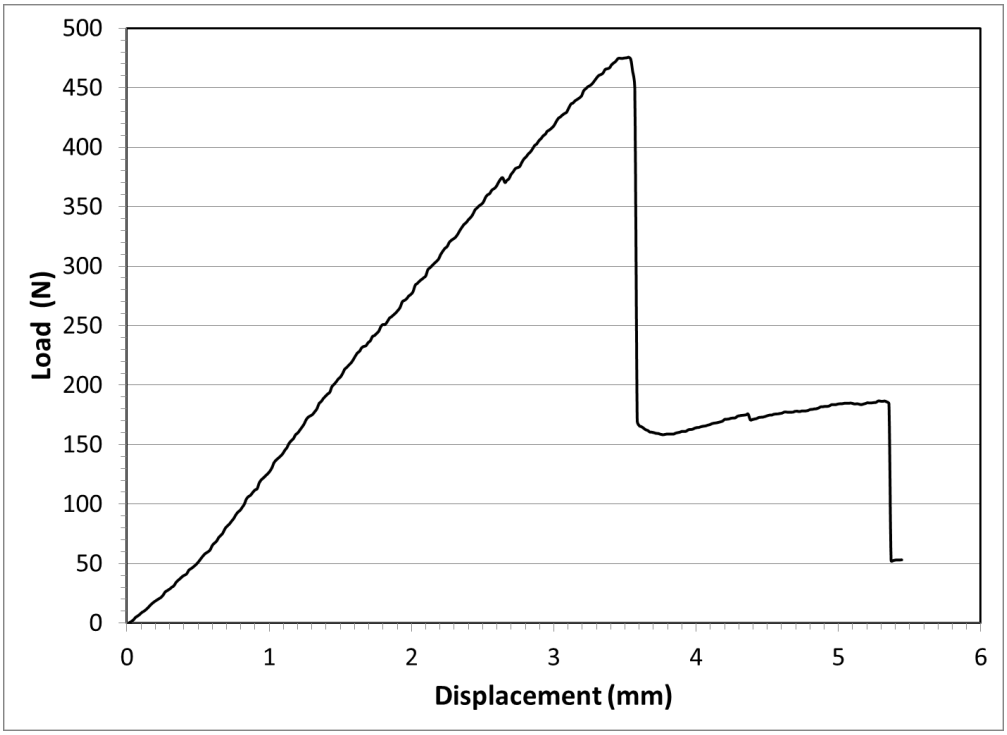

Figure 4.18 Typical load-displacement curve with the proposed test scheme 1 under FAF protocol for evaluation of self-healing performance

Figure 4.18 indicates that, the proposed test scheme was not possible to maintain in practice. It was intended that, the load would be held constant (by halting the displacement) at the instant when the delamination is just initiated. The displacement was halted at the peak load but the delamination propagated very fast reducing the load as evidenced in the vertical drop of the load in figures 4.18. The effect of self-healing could not be demonstrated in this case as large delamination already occurred in the composite sample. In order to better control the fast propagation of delamination, the displacement rate was reduced from a typical 1 mm/min down to 0.1 mm/min. Even, with this low displacement rate, the propagation of delamination could not be controlled by halting the displacement of the sample at the peak load. Thus the test scheme was modified which is described below.

Test scheme 2

The modified test scheme is shown in figure 4.19.

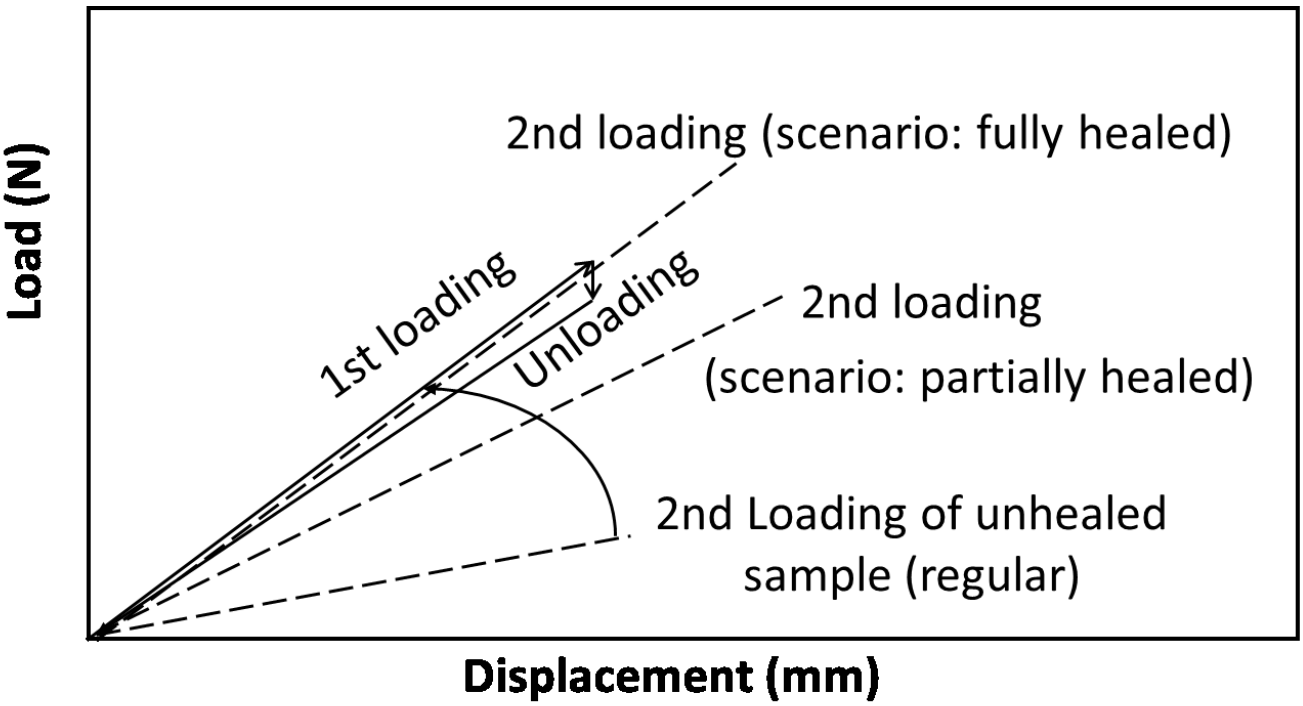

Figure 4.19 Test scheme 2 under FAF protocol for evaluation of self-healing performance

According to the new test scheme 2, as depicted in figure 4.19, it was proposed that the modified samples would be first loaded until a delamination is initiated. The sample would be video recorded to look for the event of initiation of delamination during the first loading. The samples would then be unloaded immediately instead of keeping under the same load as in scheme 1. After unloading, certain time would be allowed to heal the delamination. After healing, the samples would be loaded again. The flexural properties (residual strength and stiffness) would be determined and compared for the regular and modified samples for the first and second loading using the equations (4.2) and (4.3) to evaluate the self-healing performance.

Several tests were made following the new test scheme 2 under FAF protocol. The typical load-displacement curves for the regular and modified composite samples with this test scheme 2 is shown in figure 4.20.

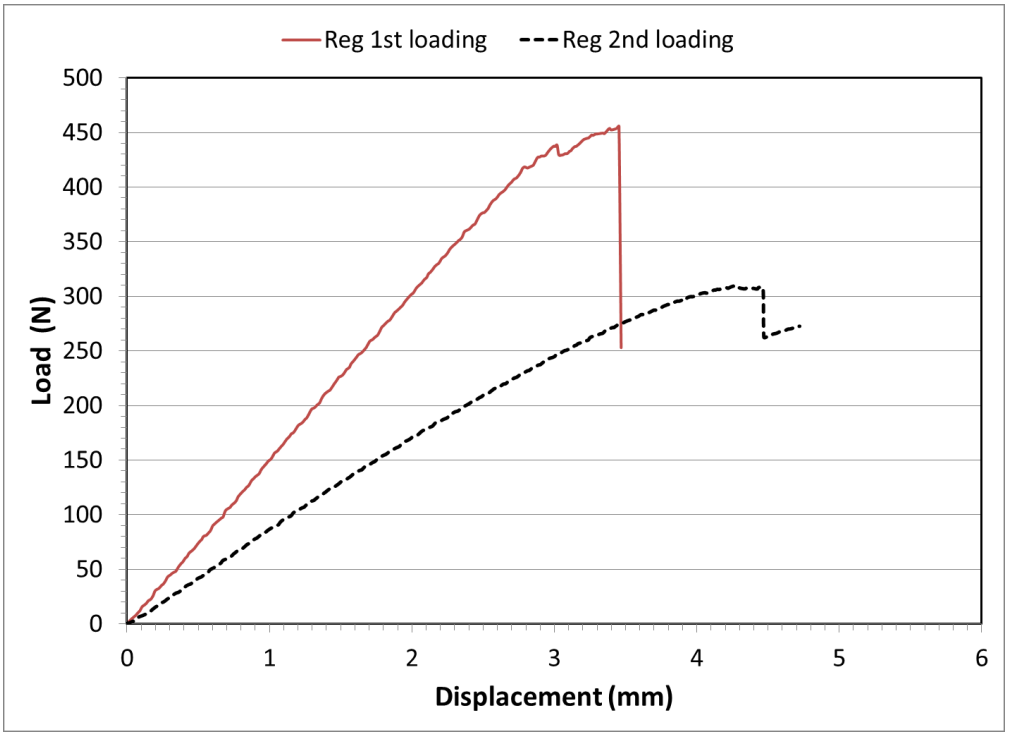

a)

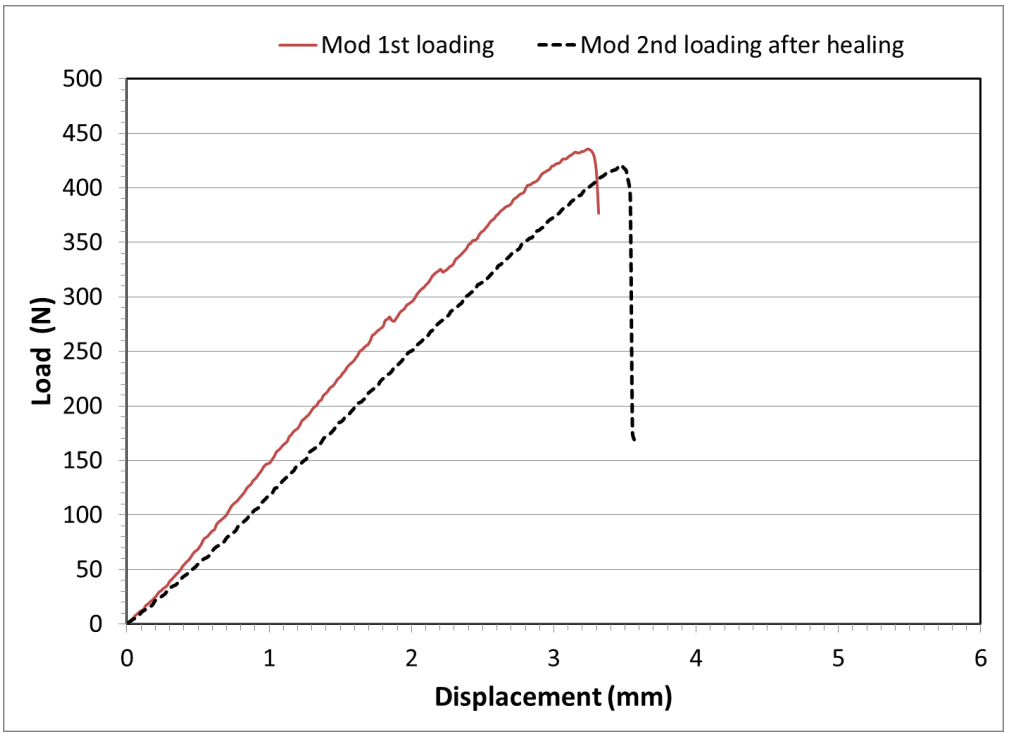

b)

Figure 4.20 Typical load-displacement curves for a) regular samples and b) modified samples with the proposed test scheme 2

During running the test of the regular and modified samples under the test scheme 2, the video of the test was monitored to detect the initiation of delamination in the samples. As soon as the delamination was observed in the video, the samples were unloaded. A duration of 24 hours was allowed for modified samples for healing without any manual intervention before it was reloaded. Comparing figures 4.20 a) and b) it can be observed that, the slope of the load-displacement line in the second loading decreased more drastically in the regular samples than in the modified samples which is possibly due to the self-healing of delamination. The residual stiffness's of the samples were calculated according to equations (4.2) and compared between the regular and modified composites as shown in figure 4.21. The comparison of residual stiffness between regular and modified samples according to equation (4.2) might be fairer even the modified samples were significantly thicker (about 45%) than the regular samples for reasons discussed earlier.

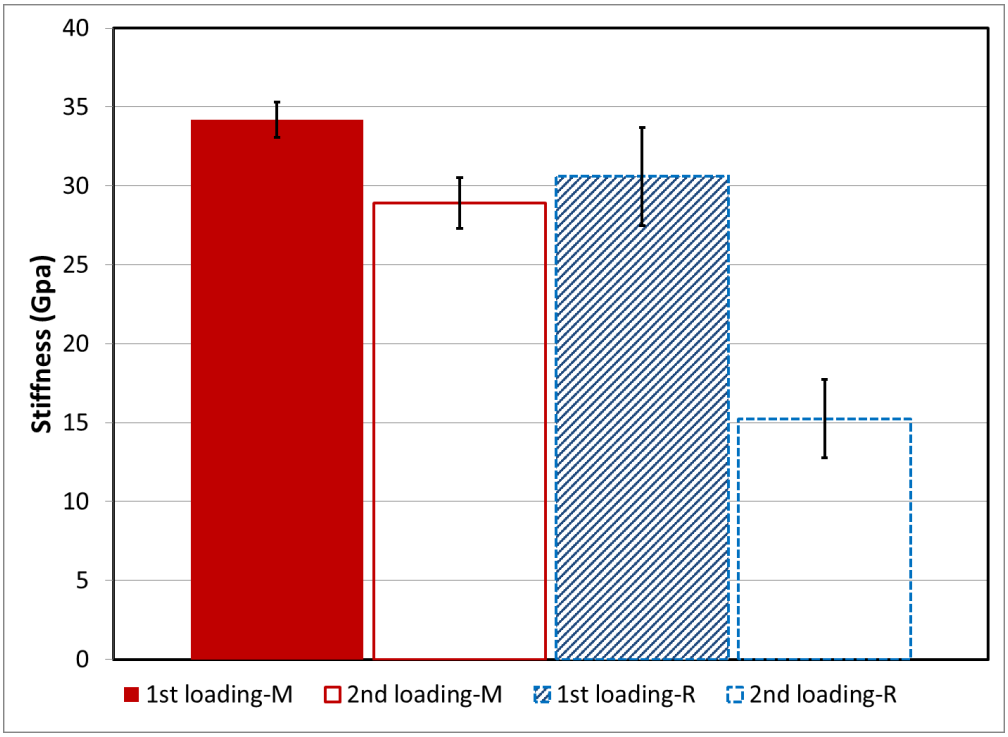

Figure 4.21 Comparison of stiffness of the regular and modified composite samples during the first loading and second loading under the test scheme 2. M refers to modified and R refers to regular composite samples. Error bars represent one standard deviation.

Figure 4.21 shows that the original stiffness of modified sample in first loading closely matches the original stiffness of regular sample in first loading. This indicates that the

incorporation of healing agents into modified composites did not reduce its stiffness. The figure also shows that residual stiffness of the regular sample in 2nd loading is about 50% less than its original stiffness in first loading. On the other hand, residual stiffness of the modified sample in 2nd loading is only about 15% less than its original stiffness in first loading. This improved retention of residual stiffness of modified composites might be due to the self-healing of cracks by the healing agents incorporated into the modified composites. However, it should be noted that, during the first loading of the composite samples, the amount of extension of delamination from the pre-implanted teflon insert could not be controlled as desired. Thus, the length of delamination in the regular and modified samples was not equal which also might affect the residual stiffness value obtained during the second loading. Thus, the effect of self-healing might not be accurately extracted from the test scheme.

Further comparing figures 4.20 a) and b) it can be observed that the modified composite samples under second loading can retain most of the peak load of the 1st loading. The absolute values of the peak loads in figure 4.20 a) and b), however, should not be compared as the modified samples are significantly thicker than the regular samples caused by the incorporation of healing agents (microcapsules and catalyst) into the modified composites. Further, a plot of $\left(\frac{p}{h}\right)$ versus displacement might give an incorrect comparison of slopes of the lines for regular and modified composite samples due to the thickness differences. Instead, the values of the term $\left(\frac{p}{h}\right)$ is calculated for the peak loads achieved during the tests for the regular and modified samples and are compared in figure 4.22.

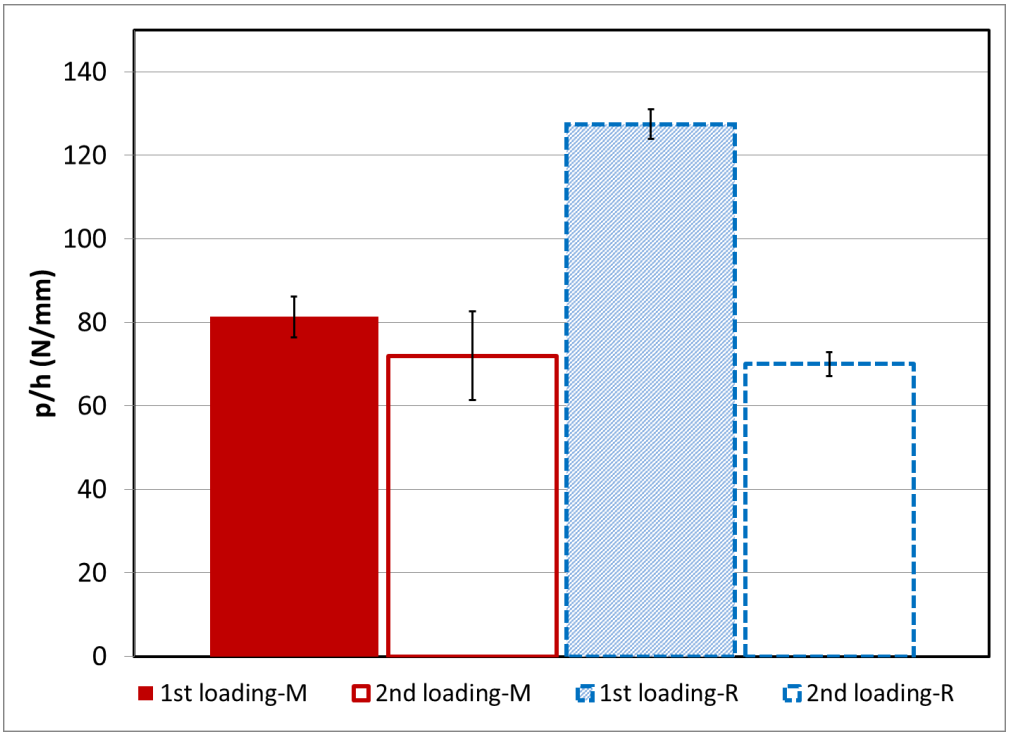

Figure 4.22 Peak loads per unit thickness (p/h) retained by the regular and modified composite samples during the first and second loading under the test scheme 2. M refers to modified and R refers to regular composite samples. Error bars represent one standard deviation.

The values of the term, $\left(\frac{p}{h}\right)$ in the first loading are found to be significantly less in the modified composite samples than regular samples tested under test scheme 2. This might be due to the incorporation of relatively high concentration (15 wt%) of microcapsules in the modified composite samples. The values of the term, $\left(\frac{p}{h}\right)$, however, remains similar in the second loading for the regular and modified samples as can be seen in figure 4.22. Similarly as discussed earlier, the effect of self-healing could not be clearly extracted from the above figure due to the dependence of the flexural loads on the geometry (thickness) of the samples [106]. A fracture based approach which usually deals with determining material properties independent of geometry (thickness) of samples would probably, be a better choice for the evaluation of healing performance of FRP composites

4.4 Concluding remarks

It is concluded from the above preliminary investigations that the effect of self-healing of FRP composites might not be extracted accurately from the strength based approach. A fracture based approach which usually deals with material properties independent of geometry of samples would probably, be a better choice for the evaluation of healing performance.

In 2014, ASTM international formally approved a new standard test method for the determination of mode II interlaminar fracture, or delamination, toughness of unidirectional FRP composites [107]. The method is based on calibration of compliance of the composite sample with crack lengths under three point bending set up and provides values of mode II fracture toughness (G_{II}^{C}) which is independent of geometry of the samples. It was shown that the compliance calibration method produces G_{II}^{C} values with accuracies of ±1.5% for carbon epoxy samples with $21 \leq L/h \leq 47$ where L and h are the span length and thickness of the samples [107]. The fracture based approach thus resolves the key issues (like the variation of thickness of samples, possible crack length dependence of flexural stiffness etc.) of the strength based approach investigated in the preliminary experiments. This method of determining G_{II}^{C} of the FRP composites, thus, matches well within the framework of the current work one of the objectives of which is to establish a protocol of evaluating the healing performance of composites under realistic loading conditions. Thus a new protocol based on the measurement of G_{II}^{C} according to ASTM D7905/7905M-14 [108] is proposed to evaluate the healing performance of FRP composites. This is discussed in detail in the next chapter.

CHAPTER 5

Protocol for Evaluating Self-Healing Performance of FRPC and Scenario Analysis

5.1 Introduction

Self-healing performance of polymer composite samples is evaluated by different protocols by different groups of researchers. These include impact-healing-compression approach in a Compression After Impact (CAI) test [[29], [58]], impact-healing-flexure approach in Flexure After Impact (FAI) test [[31], [32]], flexure-healing-flexure approach in flexure test [59]and fracture-healing-fracture approach in mode I fracture test protocol [[56]- [61]]. As the study of healing in composites involves cracks to be healed, it might be more relevant to analyze it based on fracture mechanics approach rather than strength of materials approach. Thus, the comparison of fracture properties of the composites might be more appropriate in determining and comparing its healing performance. While, mode I type crack propagation is common during interlaminar fracture of laminated composites, mode II type fracture is more relevant in many cases depending on the actual load conditions. Mode II delamination in laminates is a major matrix-controlled failure mode induced by out-of-plane shear stresses frequently encountered in composite structures. As a fundamental failure mode, mode II delamination strongly influences a wide range of structural behavior under out-of-plane loading, especially that due to surface loading such as impact [109]. Further, three-point bending of sample with crack is the load scenario that typically induces mode II fracture [110]. In current work, healing performance of CFRP composites is thus finally evaluated by measuring and comparing the mode II fracture toughness representing realistic loading conditions with and without healing.

5.2 Assessment of the mode I fracture test protocol and definition of a new protocol

In most of the research works studying the microencapsulated self-healing of polymers, healing efficiency is used as a parameter to indicate and compare the healing performance of different self-healing systems. Healing efficiency, is determined by measuring the strain energy

release rates (independent of crack length achieved by suitable geometry of samples) of resin (without fibers) samples [[49]- [66]] and FRPC samples [[56], [57]] in mode I fracture during the first (crack generation) and second (healed) loading as depicted in figure 5.1.

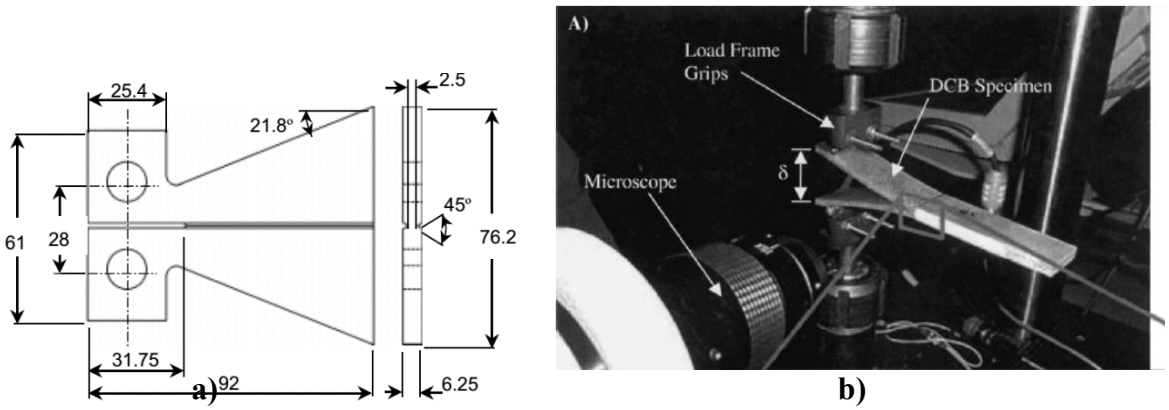

Figure 5.1 Mode I fracture testing of a) resin (without reinforcement) sample [51] and b) FRPC sample [56]

Specified time is allowed after the first loading to achieve healing after which the second loading is carried out. After the crack propagates in the first loading, the two crack surfaces are brought into contact to allow for healing for certain duration before the second loading [52]. In [57], the cracked surfaces of the FRPC samples were held together by a bar clamp after the first loading, to achieve healing. Healing efficiency is determined according to the following equation:

$$\eta = \sqrt{\frac{G_{IC}^{Healed}}{G_{IC}^{Virgin}}} = \frac{K_{IC}^{Healed}}{K_{IC}^{Virgin}} = \frac{P_{IC}^{Healed}}{P_{IC}^{Virgin}} \quad \text{.....(5.1) [57]}$$

Where, G, K and P values represent the critical strain energy release rate, critical stress intensity factor and the critical loads during the first (termed as virgin) loading and second (termed as healed) loading, respectively, of the same specimen [57].

It is to be noted here that in the process of determining healing efficiency, it was required to manually bring the crack surfaces together after the crack propagates in the first loading in order to achieve significant healing. Kirkby et al. [54], researchers in the same group of White and Sottos [3], investigated healing of epoxy specimen aided by embedded shape memory alloy (SMA) wires. The embedded SMA wires that bridged the fracture plane of the TDCB specimens

were activated after first loading by passing DC current through it. The activation of the SMA wires increased the temperature of the local matrix to 80^{o}C and generated an axial recovery force to close the crack during the healing period which substituted the requirement of manual clamping of the cracked surfaces to achieve significant healing. O'Brien and White [59]assessed the healing of microencapsulated DCPD/Grubbs system for the delamination of fiber reinforced composite skin/stringer flange debond specimen. With the flexure-heal-flexure approach they found no considerable recovery of structural properties in the specimens in which the cracked faces were not pressed together during the healing period. Even no visual evidence of healing was observed in this case. They achieved up to 96% recovery of original peak loads for the specimens for which the cracked faces were kept closed by reverse bending for 48 hours. In real applications, it might not be feasible to bring two cracked surfaces of a part in contact in order to achieve healing. Practically, the process of achieving self-healing should be free from any manual intervention to fall into the type of autonomic self-healing.

Another point to be noted here that healing efficiency is determined , as in equation (1), by the ratio of critical loads of the same modified sample (incorporated with healing agents) during the first (virgin) and second (healed) loading. No comparison is made with respect to neat samples (with no incorporation of foreign materials like the healing agents). Incorporation of foreign materials like microcapsules and catalysts can alter the base mechanical property of the neat sample. Depending on the various factors, the base mechanical properties might improve or degrade due to the inclusion of foreign materials. Keller and Sottos [49], Brown et al. [[50], [51]] and Rule et al. [52] investigated the effect of microcapsule properties on the modified (healing agent incorporated) epoxy specimen. They found that microcapsules if adequately bonded to the matrix can actually improve its fracture toughness contrary to the presence of voids or other poorly bonded particles which tend to reduce the same. Keller and Sottos [49] found that geometry and fill content of microcapsules also influence the toughening mechanism of the matrix. However, they found a continuous reduction in strength of the epoxy specimen with increasing wt% of microcapsules. They pointed out that good adhesion of the microcapsules with the matrix is essential for encounter of microcapsules and its subsequent rupture by the approaching matrix crack triggering self-healing [49]. These possible changes in the base mechanical properties of the matrix due to the inclusion of healing agents are not reflected in the healing efficiency equation (equation 1) as it only compares the critical loads of the same

modified sample (incorporated with healing agents) during the first (virgin) and second (healed) loading.

In the current work, mode II fracture toughness of CFRP composites are directly measured according to ASTM D7905-7905M-14 standard using a compliance calibration method [108]. Two values of fracture toughness were measured from each sample. The fracture toughness obtained with the propagation of delamination from the pre-implanted insert (acting as artificially introduced initial crack) is termed as NPC (Non-pre-cracked) fracture toughness. The fracture toughness obtained afterwards with the propagation of delamination from the naturally occurred initial crack is termed as PC (Pre-cracked) fracture toughness. The specimens are arranged in a three point bending fixture according to the arrangements in figure 5.2. For the NPC (No precrack) test, one end of the teflon insert acts as the starter crack tip. The crack length is measured from the left support roller to the crack tip. This crack length is kept the same for the subsequent PC (precrack) test. During the first (NPC) loading, the crack extends from the end of the teflon insert as shown in figure 5.2 (a). After the crack extension during NPC loading, the sample is unloaded and allowed for healing. After healing period, second (PC) loading is carried out. During the second loading (PC test), the sample is repositioned to keep the new crack tip at a same distance from the left support roller (Figure 5.2 c). Fracture toughness is then calculated according to data reduction procedure described in [108]. The procedure is elaborated in detail in chapter 6.

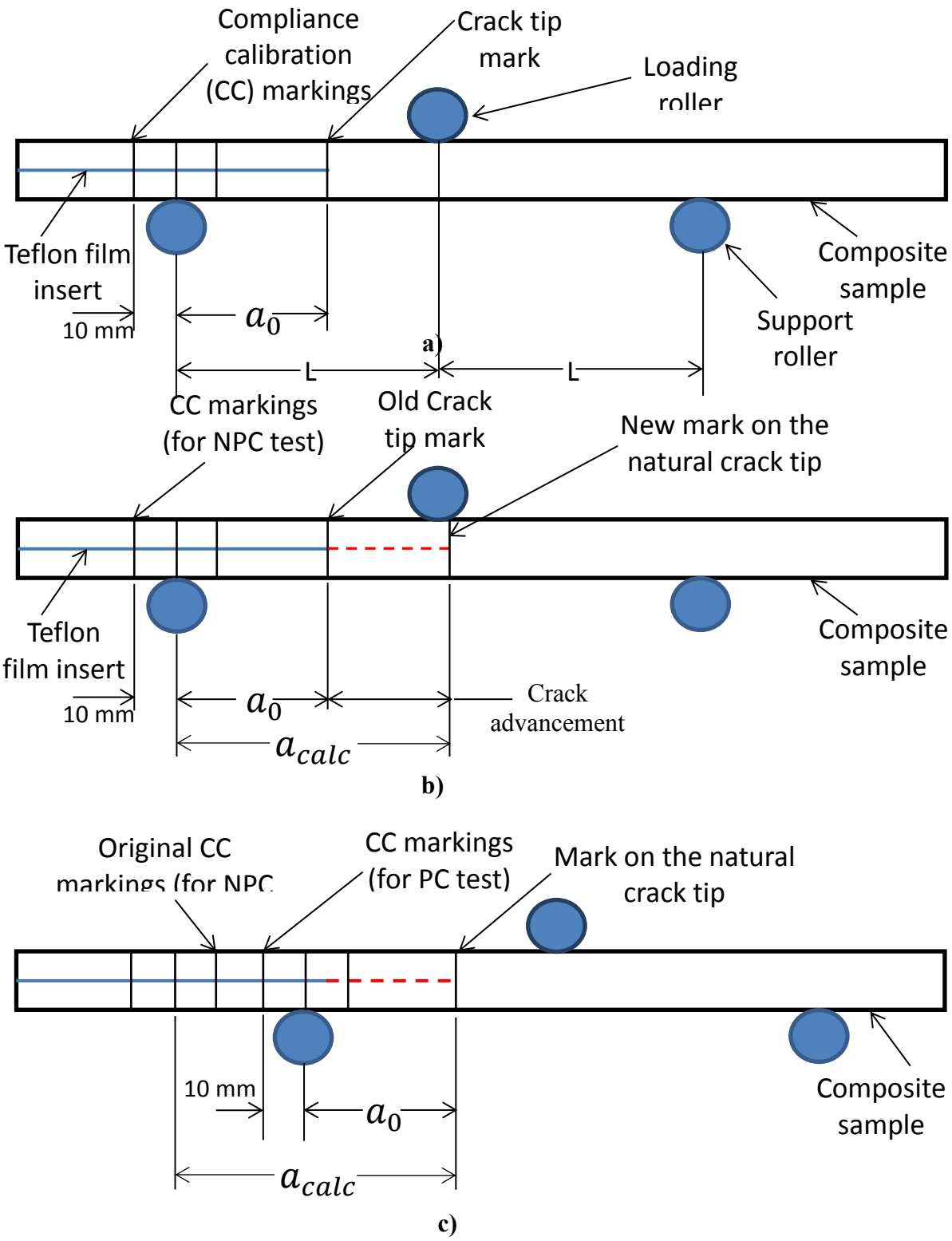

Figure 5.2 Schematic of the composite sample showing the relative positions of the tip of the crack a) before the NPC fracture loading b) After the NPC fracture loading and c) before the PC fracture loading [108].

In the new proposed protocol, healing performance is evaluated by measuring and comparing the mode II fracture toughness of regular neat (no foreign materials incorporated) and modified (healing agents incorporated) FRPC samples during the first (NPC) and second (PC) loadings without any manual intervention for achieving healing. Healing performance index, instead of healing efficiency, is defined as in equations (2)-(4), by comparing the fracture toughness of regular and modified samples during the first and second loading.

Self-healing performance is evaluated using the following equations:

$$PI = \eta_h - \Delta\varphi \tag{2}$$

Where

PI refers to performance index of healing

η_h refers to relative healing efficiency and

$\Delta\varphi$ refers to toughening (or weakening) effect

$$\eta_h = \frac{(G_{II,PC}^C)_M - (G_{II,PC}^C)_R}{(G_{II,NPC}^C)_R - (G_{II,PC}^C)_R} \tag{3}$$

and

$$\Delta\varphi = \frac{(G_{II,NPC}^C)_R - (G_{II,NPC}^C)_M}{(G_{II,NPC}^C)_R} \tag{4}$$

Here,

G_{II}^C refers to strain energy release rate measured during the NPC and PC tests, and

R and *M* refer to regular (without healing agents) and modified (with healing agents) specimens respectively. The elaboration of the equations is given in the following subsections.

The notable differences between the new protocol and the existing protocol for evaluating healing performance can be summarized as follows:

a) The new protocol involves mode II fracture which composite structures are frequently encountered with under realistic loading conditions (like impact or bending)

b) In this protocol, healing is achieved in an autonomic manner after the NPC (crack generation) test. No external intervention (like pressing the cracked surfaces together) was made to influence or trigger self-healing.

c) The new protocol calculates relative healing efficiency which is obtained by comparing the fracture performances of both the regular and modified composite samples after healing. It involves testing of two types of samples (regular and modified) in NPC and PC configurations. That is, a total of four measurements of the fracture toughness is necessary to evaluate the healing performance. In the existing protocol, only two measurements of fracture toughness of one type of sample (modified) are required to evaluate healing performance.

d) The new protocol includes the toughening (or weakening) effect of incorporating healing agents into composite samples in the definition of healing performance index. The existing protocol does not include this effect in the healing efficiency definition. It should be realized that, in an actual multi-layered composite part, healing agents need to be incorporated in every interface as the exact location of crack initiation might not be known. However, during a test of a coupon sample, healing agents is usually incorporated into the known weaker interface. Thus, in a composite test coupon, the effect of incorporating healing agents might not be too evident in contrast to the actual composite part. Thus, this effect should always be considered in the evaluation of healing performance for practical applications.

5.2.1 Elaboration of healing performance index and definition of conventional healing efficiency

The ultimate purpose of imparting self-healing functionality to regular (the matrix without healing agents) composite parts is to regain its original mechanical properties when cracks form in it due to some damage events. A regular composite part will only be replaced with a modified (the matrix incorporated with healing agents) composite part, when it is expected to show better fracture performance. In other words, self-healing application will be deemed attractive only when the overall fracture performance of modified composite parts (replacing the regular composite parts) is improved compared to regular composite parts. Healing efficiency, as defined in equation (1), does not consider this comparative improvement of fracture performance. It only

indicates the ratio of critical loads when a crack first propagates through the modified matrix (first loading) and when it propagates through the healed matrix (second loading) of the same modified composite samples. That means, even if the healing efficiency has a large value, 96% e.g. as in [59], it might not guarantee that it is an attractive and desired result. This is specially, true, if the initial mechanical properties of the modified composite part is significantly degraded due to the inclusion of healing agents. As discussed previously, the inclusion of healing agents can either degrade or improve initial mechanical properties depending on various factors like size, concentration, mechanical properties and bonding effectiveness of the healing agents (microcapsules and catalysts). These effects cannot be seen in the current healing efficiency value.

Healing performance index, as in equation (2), on the contrary, has two terms. One is relative healing efficiency term defined in equation (3). The other is the toughening (or weakening) effect defined in equation (4). In order to realize the advantages of the new protocol, it is necessary to define the conventional healing efficiency based on mode II fracture toughness which is the counterpart of existing protocol. Thus,

Conventional healing efficiency is defined as,

$$\eta_{h,c} = \frac{\left(G^{C}_{II,PC}\right)_{M}}{\left(G^{C}_{II,NPC}\right)_{M}} \tag{5}$$

Where, M refers to modified (with healing agents) composite samples.

Conventional healing efficiency as defined by equation (5) is equivalent to the healing efficiency defined in equation 1 based on mode I fracture toughness. From here on, the symbol G^{C}_{II} will be omitted for simplicity. A qualitative comparison of the conventional healing efficiency and healing performance index is made in the following subsections.

5.3 Qualitative comparisons of healing performance index and conventional healing efficiency

The terms used for defining healing efficiencies are indicated in figure 5.3.

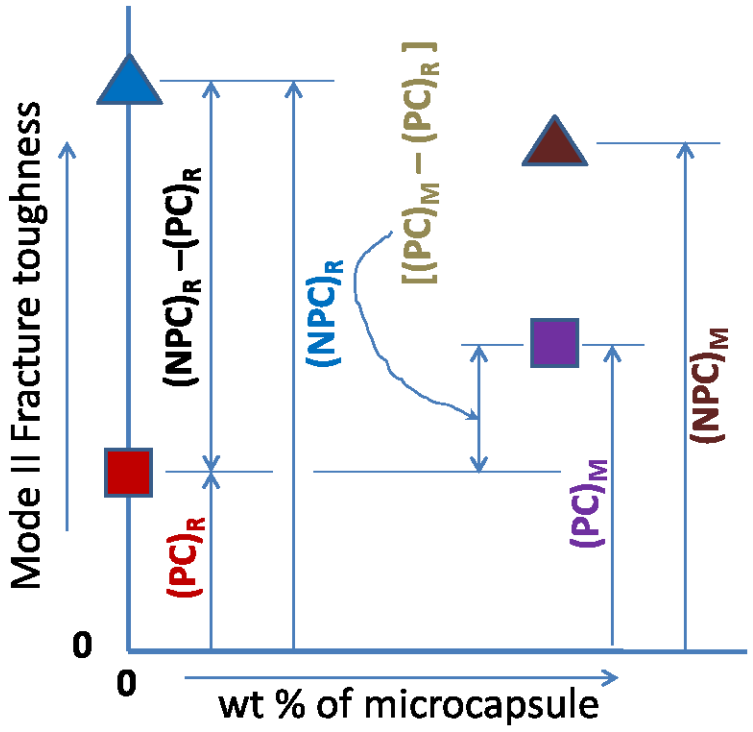

Figure 5.3 Terms used in the healing performance indicators

In figure 5.3, horizontal axis represents wt% of microcapsules used in composite samples. Vertical axis represents the mode II fracture toughness during first loading (NPC) and second loading (PC-after time allowed for healing). Rectangles and triangles represent the measured values (qualitatively) of the NPC and PC fracture toughness, respectively. The composite samples containing no healing agents (0 wt% microcapsules) are termed as regular samples and the composite samples which contain healing agents (certain wt% of microcapsules) are termed as modified samples. Figure 5.3 thus represents one regular and one modified sample tested for NPC and PC fracture toughness. Equations (2)-(5) are rewritten in simpler forms (omitting the common symbol G_{II}^{C}) below.

$$\boldsymbol{PI = \eta_h - \Delta\varphi} \qquad (2)$$

$$\Delta\boldsymbol{\varphi} = \frac{(NPC)_{\boldsymbol{R}} - (NPC)_{\boldsymbol{M}}}{(NPC)_{\boldsymbol{R}}} \quad (4')$$

$$\boldsymbol{\eta_h} = \frac{(PC)_{\boldsymbol{M}} - (PC)_{\boldsymbol{R}}}{(NPC)_{\boldsymbol{R}} - (PC)_{\boldsymbol{R}}} \quad (3')$$

$$\eta_{\mathrm{h,c}} = \frac{(PC)_{\mathrm{M}}}{(\mathrm{NPC})_{\mathrm{M}}} \quad (5')$$

It is to be noted that PC fracture toughness of regular sample $[(PC)_{\boldsymbol{R}}]$ is usually always lower than NPC fracture toughness of regular sample $[(NPC)_{\boldsymbol{R}}]$ as indicated in figure 5.3. This is because, the sample already contains a real sharp precrack during the PC test while there was no real precrack (teflon insert) during the preceding NPC test as shown in figure 5.2.

For a comparative scenario analysis, let us assume that, the PC fracture toughness of regular sample is (m*100) % of NPC fracture toughness. i.e.

$$(PC)_{\boldsymbol{R}} = m(NPC)_{\boldsymbol{R}} \quad \text{where, } 0 < m < 1 \quad (7)$$

As there are no healing agents (microcapsules or catalysts) in regular samples, this value remains fixed. The NPC and PC fracture toughness of modified samples, however, will vary according to the wt% of microcapsules used in the samples. Let us again assume that, the fracture toughness values of modified samples will either remain the same, will increase or decrease a certain percentage compared to regular samples. This variation of NPC fracture toughness of modified samples with respect to regular samples is due to the toughening (or weakening) mechanisms in effect for the inclusion of healing agents. This is, however, not directly related to the Ring Opening Metathesis Polymerization (ROMP) reaction between the 5E2N monomer and Grubbs catalyst (self-healing) as the monomer still remains encapsulated within the unbroken microcapsules during the NPC test. On the contrary, the variation of PC fracture toughness of modified samples with respect to regular samples is the direct effect of self-healing, i.e., the ROMP reaction between the monomer released from the broken microcapsules and catalyst dispersed in the sample. The effect of these possible variations on the healing performance index and conventional healing efficiency are discussed in the following scenario analysis.

5.3.1 Scenario analysis

Case I:

Let in the first case, we assume that NPC fracture toughness of modified samples remain the same as NPC fracture toughness of regular samples. That is,

$$(NPC)_{\boldsymbol{M}} = (NPC)_{\boldsymbol{R}} \tag{8}$$

and PC fracture toughness varies according to following scenario

a) PC of modified sample also remains the same as regular sample

$$(PC)_{\boldsymbol{M}} = (PC)_{\boldsymbol{R}} \tag{9}$$

In this scenario both, NPC and PC fracture toughness remain the same as NPC and PC fracture toughness of regular samples, respectively. That means, the modified samples have exactly the same fracture performance as regular samples. It implies that, there is no need to replace the regular composite part as there is no advantage of incorporating healing agents in it. Now, let us see what the healing efficiencies defined by equations (2)-(5) tell us about this scenario.

From equation (7) and (9), we get

$$(PC)_{\boldsymbol{M}} = m(NPC)_{\boldsymbol{R}} \tag{9a}$$

By definition, relative healing efficiency is given by

$$\eta_h = \frac{(PC)_{\boldsymbol{M}} - (PC)_{\boldsymbol{R}}}{(NPC)_{\boldsymbol{R}} - (PC)_{\boldsymbol{R}}} \tag{3}$$

Replacing the relations from equations (7) and (9a) in equation (3), we get

$$\eta_h = \frac{m(NPC)_{\boldsymbol{R}} - m(NPC)_{\boldsymbol{R}}}{(NPC)_{\boldsymbol{R}} - \boldsymbol{m}(NPC)_{\boldsymbol{R}}} = 0 \tag{3a}$$

Again, by definition, the toughening effect is given by

$$\Delta\varphi = \frac{(NPC)_{\boldsymbol{R}} - (NPC)_{\boldsymbol{M}}}{(NPC)_{\boldsymbol{R}}} \tag{4}$$

Replacing the relation from equation (8) in equation (4), we get

$$\Delta\varphi = \frac{(NPC)_{\boldsymbol{R}} - (NPC)_{\boldsymbol{R}}}{(NPC)_{\boldsymbol{R}}} = 0 \quad (4a)$$

Further, by definition, healing performance index is given by

$$PI = \eta_h - \Delta\varphi \quad (2)$$

Replacing the values from (3a) and (4a), in equation (2), we finally get

$$PI = \eta_h - \Delta\varphi = 0 \quad (2a)$$

By definition, conventional healing efficiency, on the other hand, is given by

$$\eta_{\mathrm{h,c}} = \frac{(PC)_{\mathrm{M}}}{(\mathrm{NPC})_{\mathrm{M}}} \quad (5)$$

Replacing the relation from equations (8) and (9a) in equation (5), we get

$$\eta_{\mathrm{h,c}} = \frac{m(NPC)_{\mathrm{R}}}{(\mathrm{NPC})_{\mathrm{R}}} = m \quad (5a)$$

Thus, healing performance index gives the correct signal in this scenario (*PI =0*) indicating that there is no need to replace the regular composite part as there is no advantages of incorporating healing agents in it. Conventional healing efficiency, on the contrary, show a positive healing efficiency value (= *m*), in this scenario, indicating advantages of incorporating healing agents and suggesting for a possible replacement of regular composite part with modified ones. It is an inappropriate signal, in this scenario, given by the conventional healing efficiency based on the previous argument that the modified sample has exactly the same NPC and PC fracture performance as that of NPC and PC fracture performance of regular sample, respectively. As an example, for a likely value of m =0.4, equation (5a) indicates that conventional healing efficiency is 40%. Equation (2a), on the contrary, indicates that the healing performance index is still zero in this scenario defined by equations (8) and (9).

b) PC of modified sample increases (n*100) % compared to PC of regular sample, i.e.

$$(PC)_{\boldsymbol{M}} = (1+n)(PC)_{\boldsymbol{R}} \quad \text{where,} \quad 0 < n < (1\text{-}m)/m \quad (10)$$

From equation (7) and (10), we get

$$(PC)_{\boldsymbol{M}} = m\,(1+n)(NPC)_{\boldsymbol{R}} \tag{10a}$$

By definition, relative healing efficiency is given by

$$\eta_h = \frac{(PC)_{\boldsymbol{M}} - (PC)_{\boldsymbol{R}}}{(NPC)_{\boldsymbol{R}} - (PC)_{\boldsymbol{R}}} \tag{3}$$

Replacing the relations from equations (7) and (10a) in equation (3), we get

$$\eta_h = \frac{m(1+n)(NPC)_{\boldsymbol{R}} - m(NPC)_{\boldsymbol{R}}}{(NPC)_{\boldsymbol{R}} - \boldsymbol{m}(NPC)_{\boldsymbol{R}}}$$

Or, $$\eta_h = \frac{m(NPC)_{\boldsymbol{R}}\{\mathbf{1}+\boldsymbol{n}-\mathbf{1}\}}{(NPC)_{\boldsymbol{R}}(\mathbf{1}-\boldsymbol{m})}$$

Or, $$\eta_h = \frac{mn}{(\mathbf{1}-\boldsymbol{m})} \tag{3b}$$

Again, by definition, the toughening effect is given by

$$\Delta\varphi = \frac{(NPC)_{\boldsymbol{R}} - (NPC)_{\boldsymbol{M}}}{(NPC)_{\boldsymbol{R}}} \tag{4}$$

Replacing the relation from equation (8) in equation (4), we get

$$\Delta\varphi = \frac{(NPC)_{\boldsymbol{R}} - (NPC)_{\boldsymbol{R}}}{(NPC)_{\boldsymbol{R}}} = 0 \tag{4b}$$

Further, by definition, healing performance index is given by

$$PI = \eta_h - \Delta\varphi \tag{2}$$

Replacing the values from (3b) and (4b), in equation (2), we finally get

$$PI = \frac{mn}{(\mathbf{1}-\boldsymbol{m})} - 0$$

Or, $$PI = \frac{mn}{(\mathbf{1}-\boldsymbol{m})} \tag{2b}$$

By definition, conventional healing efficiency, on the other hand, is given by

$$\eta_{h,c} = \frac{(PC)_M}{(NPC)_M} \quad (5)$$

Replacing the relation from equations (8) and (10a) in equation (5), we get

$$\eta_{h,c} = \frac{m\,(1+n)(NPC)_R}{(NPC)_R}$$

Or, $$\eta_{h,c} = m(1+n) \quad (5b)$$

For the cases of $0 < m < 1$ and $0 < n < (1-m)/m$, conventional healing efficiency in equation (5b) always gives higher values than healing performance index in equation (2b). For some likely fixed values of m (m= 0.3 to 0.5), figure 5.4 (a)-(c) show the comparison of conventional healing efficiency and healing performance index for increasing values of n as given by equations (2b) and (5b).

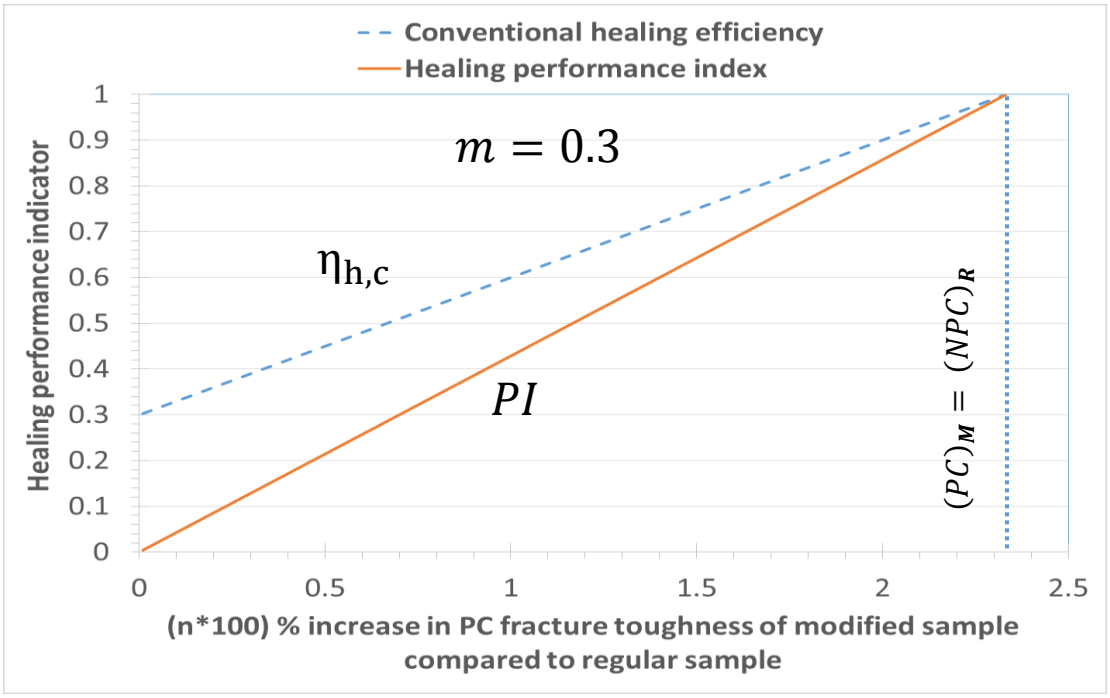

a)

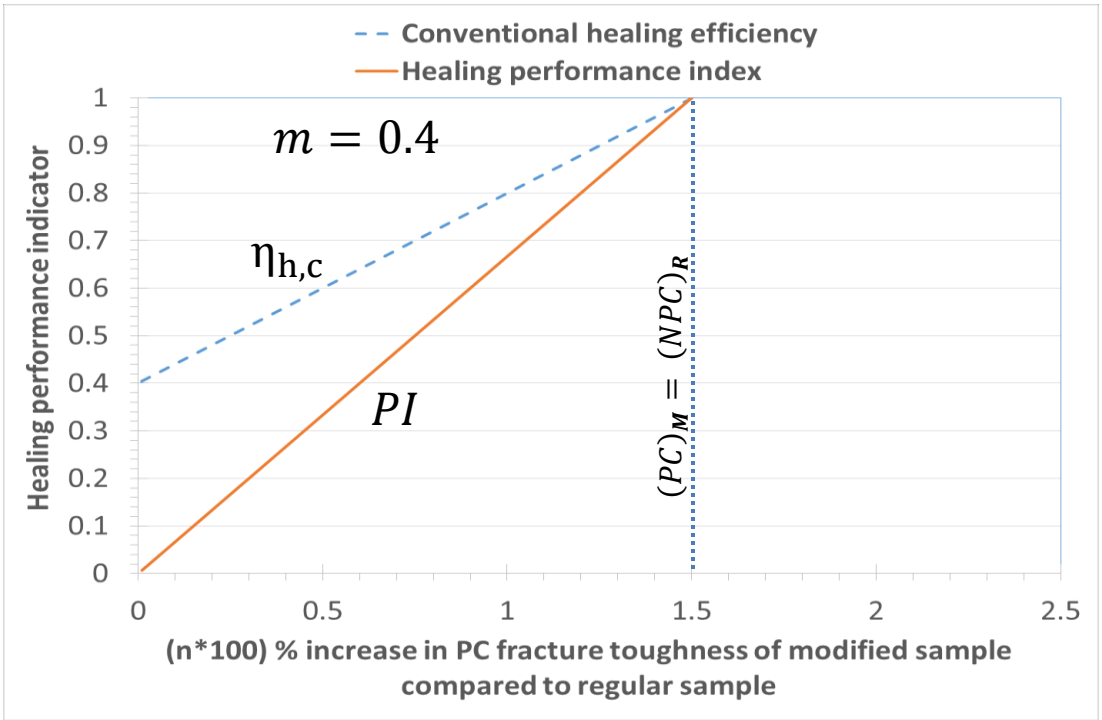

b)

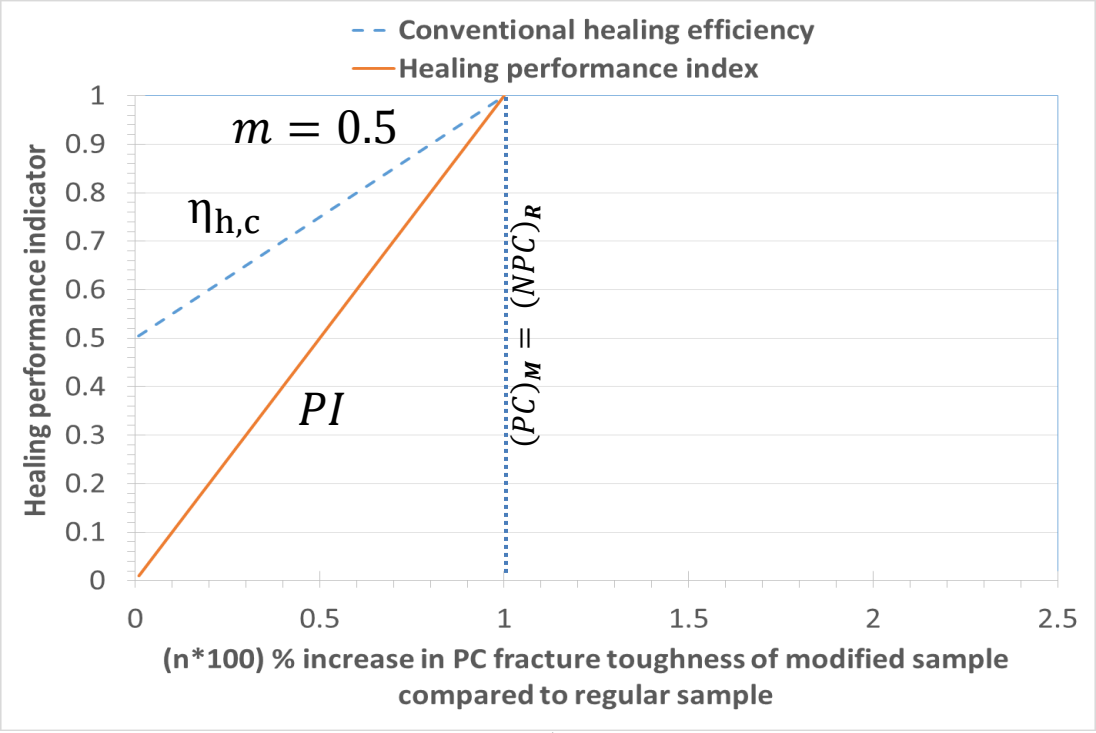

c)

Figure 5.4 Comparison of conventional healing efficiency, $\eta_{h,c}$ Vs healing performance index PI, for fixed values of m equals to a) 0.3, b) 0.4 and c) 0.5 according to equations (2b) and (5b). m is the % decrease of NPC fracture toughness of regular sample when a real precrack is present.

Comparing the figures in 5.4 (a)-(c), it can be observed that, conventional healing efficiency,$\eta_{h,c}$ significantly overestimates the healing performance as compared to healing performance index (*PI*) until PC fracture toughness of modified sample $[(PC)_{\mathrm{M}}]$ equals the NPC fracture toughness of regular sample $[(NPC)_{\mathrm{R}}]$. This situation $[(PC)_{\mathrm{M}} = (NPC)_{\mathrm{R}}]$, in fact, implies that the modified cracked sample is capable of restoring the original fracture toughness of a regular uncracked sample after healing.

c) PC of modified sample decreases (n*100) % compared to PC of regular sample, i.e.

$$(PC)_{\boldsymbol{M}} = (1-n)(PC)_{\boldsymbol{R}} \quad \text{where,} \quad 0 < n < 1 \tag{11}$$

Similar to scenario (b), it can be shown that, for the current scenario,

Relative healing efficiency as defined by equation (3) becomes

$$\eta_h = \frac{-mn}{(\mathbf{1}-\boldsymbol{m})} \tag{3c}$$

The toughening effect as defined by equation (4) becomes

$$\Delta\varphi = 0 \tag{4c}$$

Further, the healing performance index as defined by equation (2) becomes

$$PI = \frac{-mn}{(1-m)} \tag{2c}$$

Finally, the conventional healing efficiency as defined by equation (5) becomes

$$\eta_{\mathrm{h,c}} = \mathrm{m}(1-\mathrm{n}) \tag{5c}$$

For the likely cases of $0 < m < 1$ and $0 < n < 1$, conventional healing efficiency as in equations (5c) always give a positive value while healing performance index as in equation (2c) always gives a negative value. The ultimate purpose of imparting healing functionality to modified composite parts is to achieve better PC fracture toughness than a regular sample after a crack has been formed in it. If the opposite happens, that is, if the PC fracture toughness of modified sample becomes less than PC fracture toughness of regular sample, the purpose of incorporating healing agents in composites is failed. This is an undesired situation in terms of self-healing. In this scenario, healing performance index and relative healing efficiency as

defined by equations (2) and (3) give a negative value effectively signaling an undesired situation. In other words, getting a negative value of relative healing efficiency and healing performance index would suggest that there is no reason to replace a regular composite part with modified ones. Even in this scenario, the conventional healing efficiency defined in equations (5) shows a positive value which might give rise to a confusion about the decision to replace an existing regular composite part.

Thus, in all of the above scenarios, the healing performance index effectively aids in making a go/no go decision for a possible replacement of an existing regular composite part with a modified composite part incorporated with healing agents.

Case II:

Let in the second case, we assume that PC fracture toughness of modified samples remain the same as PC fracture toughness of regular samples, i.e.,

$$(PC)_{\boldsymbol{M}} = (PC)_{\boldsymbol{R}} \tag{12}$$

and, NPC fracture toughness of modified sample varies according to scenario described below. It is to be reminded here that, equation (12) itself indicates an undesired situation in terms of self-healing, as the ultimate purpose of self-healing is to have improved fracture performance compared to regular composites when a crack is generated in the composite part. That is, the PC fracture toughness of modified sample should always be higher than PC fracture toughness of regular sample in order for the self-healing to be an attractive option. In the following scenario analysis, we can see how the healing performance indicators handle this undesired situation.

d) NPC of modified sample increases (p*100) % compared to NPC of regular sample, i.e.

$$(NPC)_{\boldsymbol{M}} = (1+p)(NPC)_{\boldsymbol{R}} \quad \text{where, } 0 < p < 1 \tag{13}$$

From equation (7) and (12), we get

$$(PC)_{\boldsymbol{M}} = m(NPC)_{\boldsymbol{R}} \tag{13a}$$

By definition, relative healing efficiency is given by

$$\eta_h = \frac{(PC)_M - (PC)_R}{(NPC)_R - (PC)_R} \tag{3}$$

Replacing the relations from equations (7) and (13a) in equation (3), we get

$$\eta_h = \frac{m(NPC)_{\boldsymbol{R}} - m(NPC)_{\boldsymbol{R}}}{(NPC)_{\boldsymbol{R}} - m(NPC)_{\boldsymbol{R}}} = 0 \quad (3d)$$

Again, by definition, the toughening effect is given by

$$\Delta\varphi = \frac{(NPC)_{\boldsymbol{R}} - (NPC)_{\boldsymbol{M}}}{(NPC)_{\boldsymbol{R}}} \quad (4)$$

Replacing the relation from equation (13) in equation (4), we get

$$\Delta\varphi = \frac{(NPC)_{\boldsymbol{R}} - (1+p)(NPC)_{\boldsymbol{R}}}{(NPC)_{\boldsymbol{R}}}$$

Or, $$\Delta\varphi = \frac{(NPC)_{\boldsymbol{R}}(\boldsymbol{1-1-p})}{(NPC)_{\boldsymbol{R}}}$$

Or, $$\Delta\varphi = -p \quad (4d)$$

Further, by definition, healing performance index is given by

$$PI = \eta_h - \Delta\varphi \quad (2)$$

Replacing the values from (3d) and (4d), in equation (2), we finally get

$$PI = 0 - (-p)$$

Or, $$PI = p \quad (2d)$$

In this scenario, we can see that the improvement in fracture performance due to self-healing (achieved by the ROMP reactions of monomer and catalyst), as indicated by the relative healing efficiency term $\boldsymbol{\eta_h}$, is zero. The positive value of healing performance index (PI), however, indicates the overall improvement of fracture performance which is due to the toughening mechanisms of the healing agents in effect. The improvement of this fracture performance (equal to p) is, however, the sole contribution of the toughening mechanisms of the microcapsules as indicated by the value of $\Delta\boldsymbol{\varphi}(= -p)$ and not related to the self-healing (polymerization reaction of monomer and catalyst) reaction. Intuitively, a negative value of $\Delta\boldsymbol{\varphi}$ indicates toughening effect whereas a positive value of $\Delta\boldsymbol{\varphi}$ indicates weakening effect of healing agents incorporated in modified samples.

By definition, conventional healing efficiency, on the other hand, is given by

$$\eta_{h,c} = \frac{(PC)_M}{(NPC)_M} \tag{5}$$

Replacing the relation from equations (13) and (13a) in equation (5), we get

$$\eta_{h,c} = \frac{m(NPC)_R}{(1+p)(NPC)_R}$$

Or, $$\eta_{h,c} = \frac{m}{(1+p)} \tag{5d}$$

For a likely fixed value of m (m= 0.4), figure 5.5 shows the comparison of conventional healing efficiency and healing performance index for increasing values of p as given by equations (2d) and (5d).

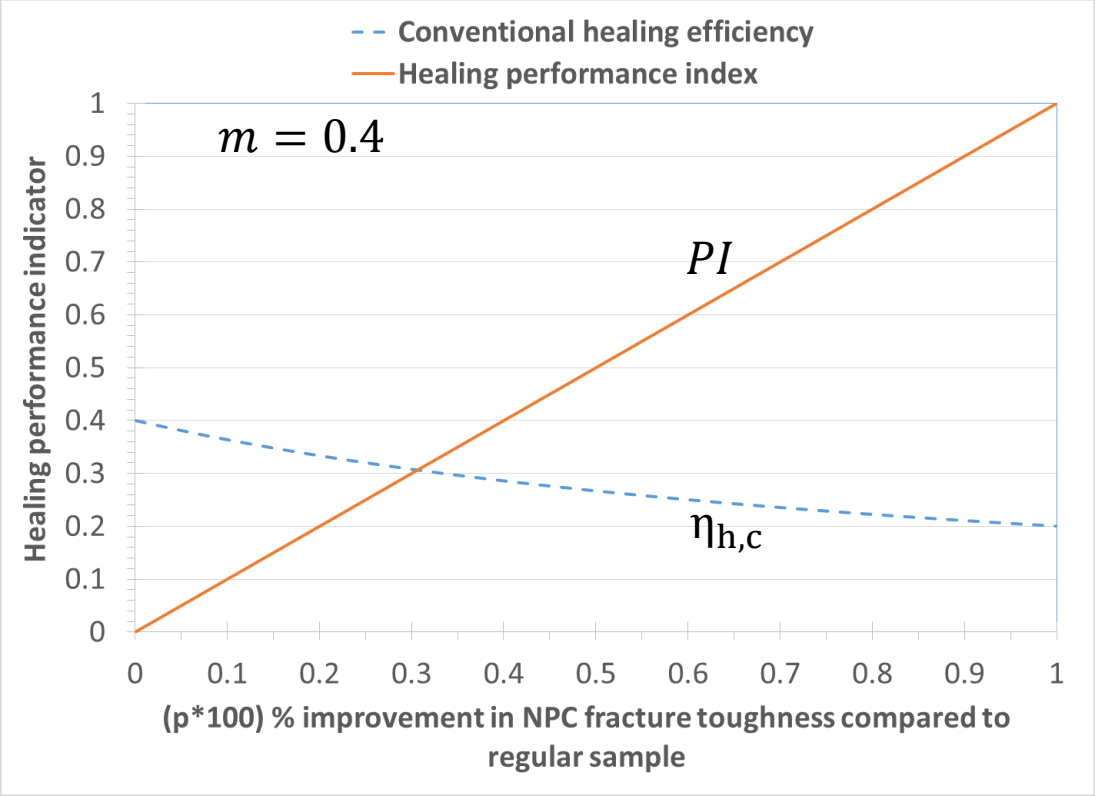

Figure 5.5 Comparison of conventional healing efficiency, $\eta_{h,c}$ Vs healing performance index PI, for fixed values of m according to equations (2d) and (5d). m is the % decrease of NPC fracture toughness of regular sample when a real precrack is present.

From figure 5.5, it can be observed that, as the NPC fracture toughness of modified sample improves compared to regular sample (i.e. p increases), the conventional healing efficiency decreases. This is a wrong signal and counter-intuitive. Healing performance index,PI, on the other hand, increases with the increase in p which is expected. That means, it accounts for the toughening effect of the healing agents which expectedly translates into higher PI values. Further, it can be realized here that positive values of conventional healing efficiency, in this scenario, neither signifies an improvement of fracture performance due to the self-healing reaction (as the PC fracture toughness of modified sample remains the same as the PC fracture toughness of regular sample in this scenario) nor due to the toughening effect of the healing agents. On the other hand, positive values of performance index ($PI = p$) along with the zero values of relative healing efficiency ($\boldsymbol{\eta_h = 0}$), in this scenario, confirm the fact that there is no contribution of self-healing (due to ROMP reaction) although there is an overall improvement in fracture performance due to the toughening effect of healing agents incorporated into the modified sample. Thus, the performance index, as defined in equation (2), can effectively differentiate the contributions from self-healing reaction and toughening effect.

e) NPC of modified sample decreases (p*100) % compared to regular sample, i.e.

$$(NPC)_{\boldsymbol{M}} = (1-p)(NPC)_{\boldsymbol{R}} \quad \text{where, } 0 < p < 1 \tag{14}$$

Similar to scenario (d), it can be shown that, for the current scenario,

Relative healing efficiency as defined by equation (3) becomes

$$\eta_h = 0 \tag{3e}$$

The toughening effect as defined by equation (4) becomes

$$\Delta\varphi = p \tag{4e}$$

Further, the healing performance index as defined by equation (2) becomes

$$PI = -p \tag{2e}$$

In this scenario, the negative healing performance index (PI) value indicates that there is an overall degradation of fracture performance due to the weakening effect ($\boldsymbol{\Delta\varphi = p}$) of the healing

agents incorporated in the modified samples.

Finally, the conventional healing efficiency as defined by equation (5) becomes

$$\eta_{h,c} = \frac{m}{(1-p)} \tag{5e}$$

For a likely fixed value of m (m= 0.4), figure 5.6 shows the comparison of conventional healing efficiency and healing performance index for increasing values of p as given by equations (2e) and (5e).

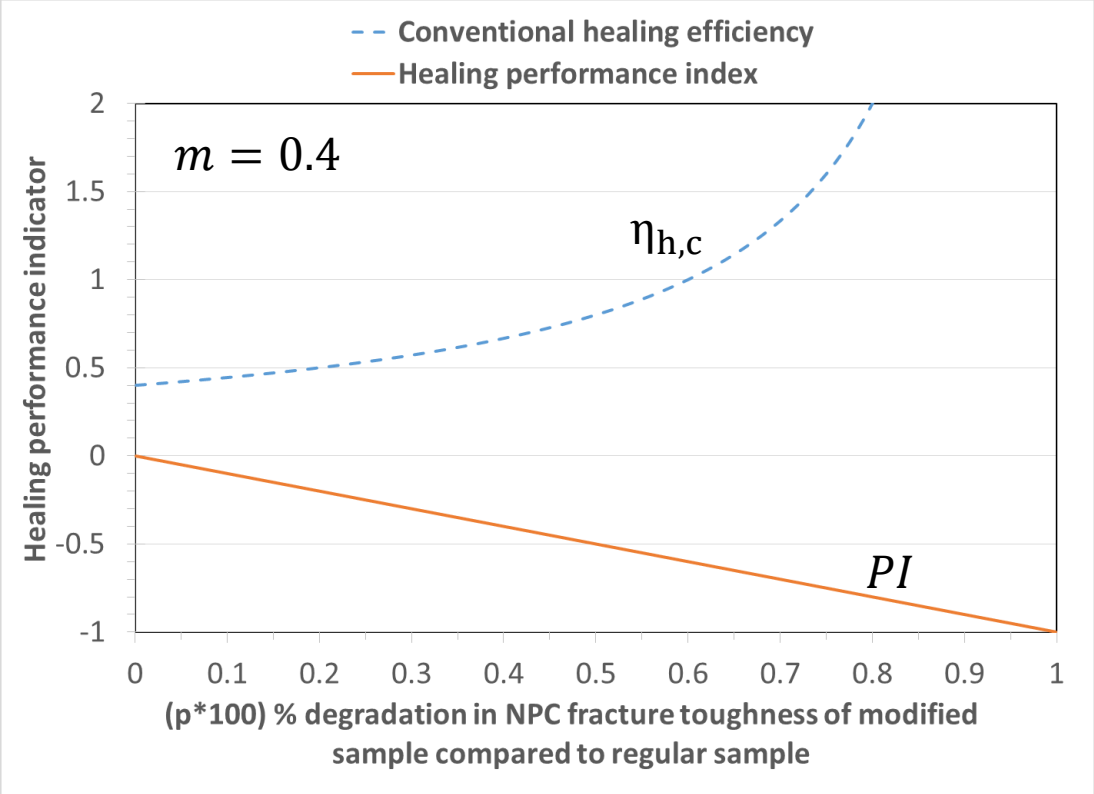

Figure 5.6 Comparison of conventional healing efficiency, $\eta_{h,c}$ Vs healing performance index PI, for fixed values of m according to equations (2e) and (5e). m is the % decrease of NPC fracture toughness of regular sample when a real precrack is present.

Figure 5.6 shows that as the NPC fracture toughness degrades (i.e. p increases), the value of conventional healing efficiency increases. The more the NPC fracture toughness degrades, more the value of conventional healing efficiency increases. This is, in fact, happens in any other scenario for a fixed value of PC fracture toughness of modified sample. This is one of the greatest limitations of the conventional healing efficiency. The degradation of NPC fracture

toughness due to the incorporation of healing agents is a very likely situation in many cases and conventional healing efficiency gives an opposite signal indicating that the healing situation is actually improved. This is indeed, a wrong signal and counter-intuitive. Healing performance index,PI, on the other hand, decreases with the increase in p, as shown in figure 5.6, which is expected. That means, it accounts for the weakening effect of the healing agents which expectedly translates into lower PI values. Again, positive values of conventional healing efficiency, in this scenario, neither signifies an improvement of fracture performance due to the self-healing reaction (as the PC fracture toughness of modified sample remains the same as the PC fracture toughness of regular sample in this scenario) nor due to the weakening effect of the healing agents. On the other hand, negative values of performance index ($PI = -p$) along with the zero values of relative healing efficiency ($\boldsymbol{\eta_h} = 0$), in this scenario, confirm the fact that there is no contribution of self-healing (due to ROMP reaction) although there is an overall degradation in fracture performance due to the weakening effect of healing agents incorporated into the modified sample.

Thus, it can be realized from the above discussions that, healing performance index, unlike the conventional healing efficiency, always gives a correct signal representing the desired or undesired situations in terms of self-healing.

In reality, composite parts may not perform exactly according to the above scenarios. Rather, a combination of the above scenarios would be operative practically. The NPC fracture toughness may increase or decrease in combination with the increase or decrease of the PC fracture toughness of the modified sample. The results discussed above would then be superimposed depending on the actual scenario in effect.

5.4 Summary of the distinguishing features of the new protocol versus existing protocol for evaluating healing performance

From the analysis of the basic scenarios discussed above, it is clear that healing performance index as defined by equations (2)-(4) handles all the above possible scenarios better than conventional healing efficiency definitions. The characteristic features and advantages of healing performance index over the conventional healing efficiency can be summarized as follows:

i) Any positive value of performance index always represents an improvement in fracture performance over regular composites. A negative value of performance index, on the other

hand, warns that there is no advantage of incorporating healing agents into composites. On the contrary, conventional healing efficiency always gives a positive value which may or may not represent an improvement of fracture performance over regular samples.

ii) Healing performance index separates the contribution of self-healing (ROMP reaction of monomer and catalyst) and toughening (or weakening) effect of incorporating healing agents (microcapsules and catalyst particles) in the composite sample. The contribution of self-healing is demonstrated by the relative healing efficiency term, $\boldsymbol{\eta_{h,}}$ as defined by equation (3). The contribution of toughening (or weakening) effect is demonstrated by $\Delta\boldsymbol{\varphi}$ as defined by equation (4). The numerical values of healing performance index thus represents real physical phenomena. Conventional healing efficiency, on the other hand, cannot differentiate these effects and its numerical value may not represent a real physical phenomenon.

iii) Relative healing efficiency term in healing performance index sets up a threshold value for PC fracture toughness of modified sample (equals to PC fracture toughness of regular sample) at or below which the healing performance is not acceptable as indicated by its zero or negative values [scenario (a), (c)-(e)]. Conventional healing efficiency, on the other hand, always shows a positive healing efficiency and can, in fact, show a significantly high value even if the healing performance is not attractive as discussed in scenario (e) and indicated in figure 5.6.

iv) A possible toughening or weakening effect of incorporating healing agents into the modified sample is correctly translated into higher or lower values, respectively, of healing performance index. Conventional healing efficiency, on the contrary, resolves these effects in opposite way. That is, a toughening effect reduces the healing efficiency, and more alarmingly, a likely weakening effect increases the healing efficiency as discussed in scenario (d) and (e) and indicated in figures 5.5 and 5.6. The more the weakening effect, the higher is the conventional healing efficiency (figure 5.6). This fact can make the conventional healing efficiency an unreliable index indicating self-healing performance.

v) Conventional healing efficiency always gives higher values than healing performance index in neutral cases where there is no significant weakening or toughening effect as discussed in scenario (b) and indicated in figures 5.4 (a)-(c).

vi) The healing performance index, unlike the conventional healing efficiency, always gives a correct signal representing the desired or undesired situations in terms of self-healing. It thus

effectively aids in making a go/no go decision for a possible replacement of an existing regular composite part with a modified composite part incorporated with healing agents.

vii) Finally, in the new protocol, no manual intervention is made to trigger or influence healing after the crack is generated in the sample.

Thus, a better protocol of evaluating healing performance of composites which represents the true improvement of healing performance over regular composites under realistic loading condition is established.

CHAPTER 6

Investigation of Self-healing of FRP Composites at Room Temperature

6.1 Introduction

Mode II delamination in laminates is a major matrix-controlled failure mode induced by out-of-plane shear stresses frequently encountered in Fiber Reinforced Polymer (FRP) composite structures. As a fundamental failure mode, mode II delamination strongly influences a wide range of structural behavior under out-of-plane loading, especially that due to surface loading such as impact [109]. Further, three-point bending of sample with crack is the load scenario that typically induces mode II fracture [110]. In current work, healing performance of FRP composites is thus evaluated by measuring and comparing the mode II fracture toughness representing realistic loading conditions with and without healing. This chapter describes the procedure of measuring the mode II fracture toughness of regular (without healing agents) and modified composites (with healing agents) and discusses the obtained results in relation to self-healing. Fractographic analysis was done by a series of observations of fracture surfaces of composites to understand the self-healing behavior.

6.2 Fabrication of composite samples

Fiber reinforced carbon/epoxy samples were fabricated for self-healing experiments. Two types of fiber reinforced carbon/epoxy composite samples were fabricated. Regular composite samples do not contain any healing agents. Modified, composite samples, on the other hand, contains healing agents. The fiber reinforced composite samples were used for mode II fracture tests.

The formulation of regular (without healing agents) and modified (with healing agents) epoxy matrix and the procedure of fabricating fiber reinforced composite samples are discussed in details below.

6.2.1 Formulation of epoxy matrix

Two types of epoxy matrix were formulated for manufacturing epoxy (without reinforcement) samples and fiber reinforced composite laminates. These are the regular epoxy matrix (without healing agents) and modified epoxy matrix (with healing agents). Regular epoxy matrix was formulated by mixing EPON 828 (a bisphenol-A based epoxide resin, Miller Stephenson Chemical Co.) and Epicure 3046 (an amidoamine room temperature curing agent, Miller Stephenson Chemical Co.) at a concentration of 100:47 (by weight). Epicure 3046 curing agent provides a working life of several hours, yet cures to handling strength overnight at room temperature. Good strength properties are achieved within three days and essentially complete cure is obtained within two weeks at room temperature. According to the manufacturer recommendation, comparable mechanical properties are also obtained when cured for 16 hours at 25^{o}C and post cured for 2 hours at 100^{o}C. For the formulation of regular (no healing agents) epoxy matrix, an appropriate amount of the resin and the curing agent were mixed in a container by stirring first with a wooden stick. The container was then placed in a vacuum mixer and the rotation speed of the mixer, time and vacuum were set. Mixing of the resin and curing agent was carried out with vacuum applied for several minutes intermittently (to avoid raising the temperature of the mixture) until a smooth, transparent, air bubble free mixture was obtained. For the formulation of modified epoxy matrix, a modified route of mixing was followed in order to incorporate the healing agents (microcapsules and catalysts) into it. For the modified epoxy matrix, appropriate amount of catalyst (1 wt% of the total weight of epoxy and curing agent) was first dispersed into the EPON 828 resin in a container by stirring it with a wooden stick for several minutes. The container was then placed in the vacuum mixer and spun at a relatively high set speed (up to 2000 rpm) intermittently for several minutes to disperse the catalyst uniformly in the resin. Appropriate amount of microcapsules were then added into the catalyst-resin mixture, stirred and dispersed in the same way in the vacuum mixer but with relatively low rotation speed (up to 1200 rpm) to avoid breaking of microcapsules due to high shear. At the last step, appropriate amount of the curing agent was added to the catalyst-resin-microcapsule mixture, stirred and spun with the same speed (1200 rpm) as with the microcapsules with vacuum applied for several minutes intermittently until a smooth, air bubble free mixture was obtained. The regular (without healing agents) and modified (with healing agents) epoxy matrix thus formulated were used to fabricate fiber reinforced composite samples.

6.2.2 Fabrication of FRP composite samples

As stated earlier, two types of fiber reinforced carbon/epoxy composite samples were manufactured. One type is the regular carbon/epoxy composite samples without self-healing capabilities. The other type is the modified carbon/epoxy composite samples with self-healing capabilities. Fiber reinforced carbon/epoxy composite panels were manufactured by hand lay-up with autoclave molding process. Unidirectional carbon fabric (Fiber Glast Development Corp.) was used as reinforcement. Twelve 300 X 200 mm rectangles were first cut from the carbon fabric. For the manufacturing of regular composite panel, each of the twelve layers of the carbon fabric was impregnated with regular epoxy matrix (formulation is described in the previous section) using a plastic applicator and stacked on top of one another on an aluminum flat tool surface kept on a lay-up table. A Teflon (polytetrafluoroethylene, PTFE) film strip was placed at one edge at the middle of the twelve layers (i.e. between the sixth and seventh layer interfaces) across its width to act as a site of crack initiation. The configuration of the composite samples with pre-implanted teflon insert is termed as NPC (Non-pre-cracked) configuration. After finishing the stacking of twelve layers, a porous release film was placed on top of it followed by a bleeder layer to allow the excess resin to bleed during compaction. A breather layer was placed on top of it to facilitate vacuum. A caul plate was then placed on top of the laminate to distribute the vacuum and the subsequent applied pressure evenly on the composite. The entire assembly was sealed with vacuum bag using sealant tape. A vacuum valve was installed on the vacuum bag on the tool surface slightly away from the stacked composite layers to avoid jamming of the valve during bleeding of the excess resin. The vacuum bag assembly is shown in figure 6.1.

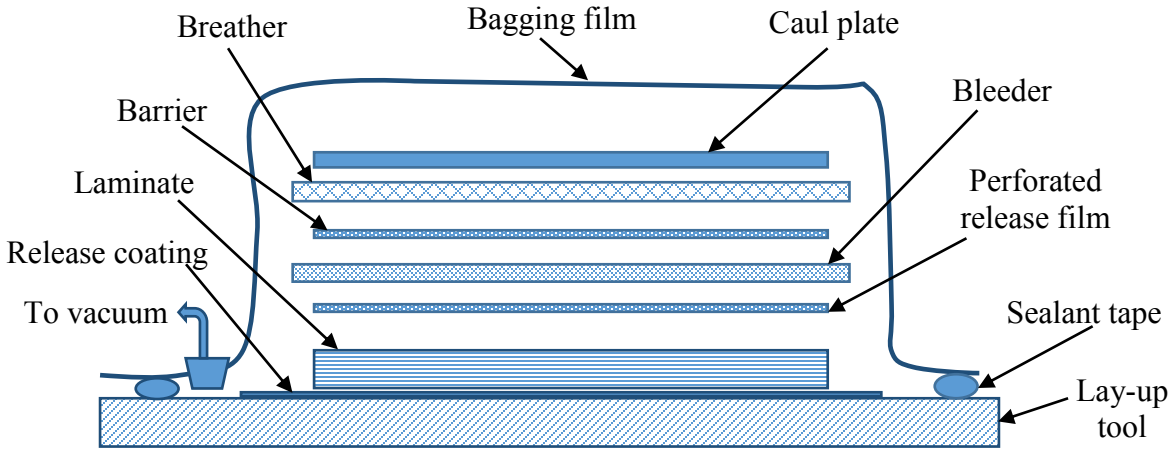

Figure 6.1 Vacuum bagging assembly

The aluminum plate with the vacuum bagged assembly was then connected to the vacuum line and put inside the autoclave. The composite was initially cured in the autoclave at room temperature for 72 hours with the vacuum and pressure (50 psi) applied. The panel was then removed from the autoclave and kept at room temperature for another two weeks for complete curing according to the recommendations of the supplier of the curing agent. The panel was then post cured at 100^{o}C in an oven for 2 hours. Epicure 3046, used as the curing agent in this work, is a room temperature curing agent and according to the supplier recommendation, a complete cure is obtained within two weeks at room temperature. Further, the composites were chosen to be cured at room temperature to avoid degradation of Grubbs catalyst which is known to be sensitive to prolonged exposure to high temperature. In the Differential Scanning Calorimetry (DSC) analysis of the composite samples as shown in figure 6.2, no major heat flow event is detected which confirms a complete curing of the samples.

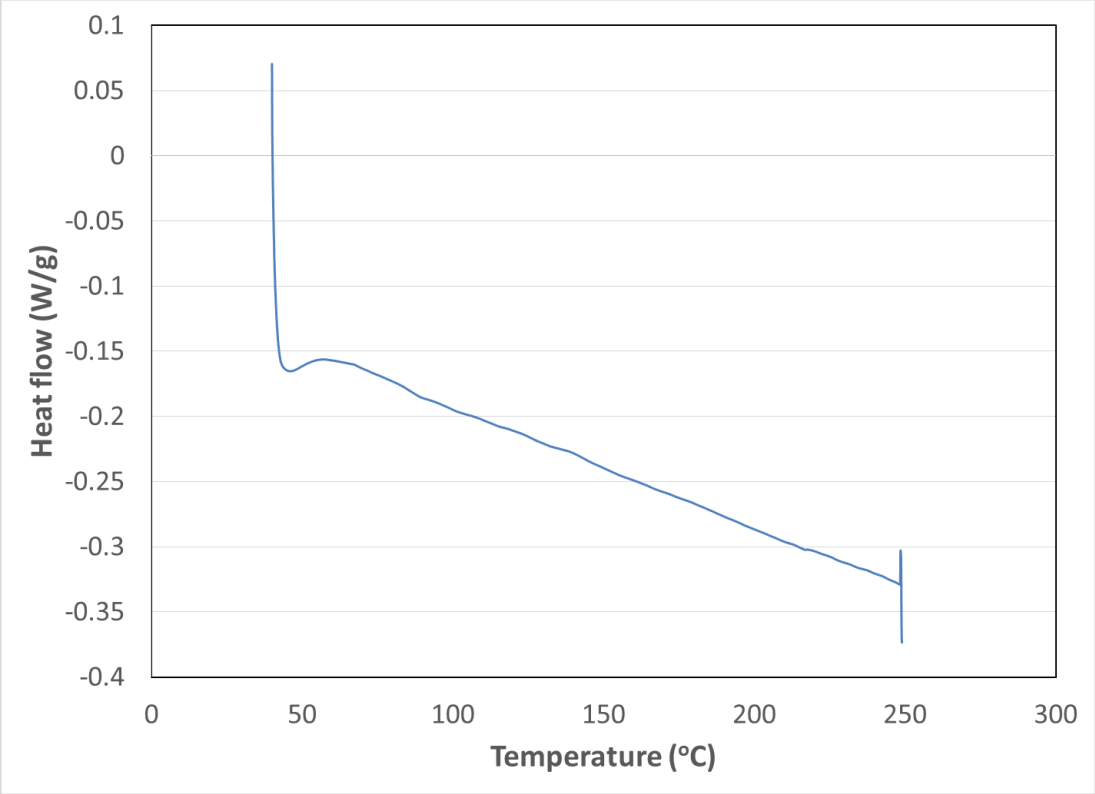

Figure 6.2 Typical DSC curve for composite samples showing a complete curing of the samples

The same procedure was followed to manufacture the modified composite panels (with self-healing capability) except that the center two layers were impregnated with modified epoxy matrix (incorporated with healing agents. Its formulation is described in the previous section).

Besides the regular (contained no microcapsules) composite panels, different modified composite panels (incorporated with microcapsules and catalyst) were fabricated varying the average size and concentration of microcapsules. Two different average sizes (100 μm and 45 μm) and 3 different concentrations [2 wt% (2.3 vol%), 5 wt% (5.7 vol%) and 8 wt% (9.1 vol%) of the modified epoxy] of microcapsules were chosen for investigation. The viscosity of modified epoxy increases with increasing concentration of microcapsules and above 8wt% it becomes very difficult to process and uniformly disperse it during the lay-up leading to poor quality of composite laminate. Table 6.1 indicates the different types of composite panels that were manufactured for mode II fracture testing both at room temperature and cold (-40^{o}C) temperature.

Table 6-1. Categories of composite panels manufactured with mid layer teflon insert (NPC configuration) for mode II fracture tests (at room temperature and cold

Designation of the types of composite panels (NPC configuration) manufactured	Conc. of MC contained in the panels wt% (vol%)	Avg. size of MC (μm)	Number of panels manufactured		
			For RT test	For CT test	Total
I	0 (0)	-	01	01	02
II	2 (2.3)	100	01	01	02
III	5 (5.7)	100	01	01	02
IV	8 (9.1)	100	01	01	02
V	2 (2.3)	45	01	-	01
VI	5 (5.7)	45	01	-	01
VII	8 (9.1)	45	01	01	02

MC: Microcapsules**; RT:** Room Temperature**; CT:** Cold (-40°C) temperature**;**
Avg.: Average**; Conc.:** Concentration

Samples with specified dimensions according to ASTM D7905-7905M-14 standard [108] were cut from each panel manufactured using water-cooled diamond saw. All composite samples fabricated were, thus, of NPC configuration (contained a pre-implanted teflon film insert). The schematic of NPC configuration of the sample is shown in section 6.3.

6.3 Fracture test procedure and measurement of mode II fracture toughness of composites

Mode II fracture toughness of fiber reinforced composites was directly measured according to ASTM D7905-7905M-14 standard using a compliance calibration method [108]. Fracture testing of the composite samples was conducted on a standard MTS machine equipped with a three point bending fixture. Data for the instantaneous loads and displacements are continuously recorded at a specified interval during the progression of the test through the data acquisition system. Two values of fracture toughness were measured from each sample. The fracture toughness obtained with the propagation of delamination from the pre-implanted insert (acting as artificially introduced initial crack) is termed as NPC (Non-pre-cracked) fracture toughness. The

fracture toughness obtained afterwards with the propagation of delamination from the naturally occurred initial crack is termed as PC (Pre-cracked) fracture toughness. The corresponding configurations of the cracks are termed as NPC configuration and PC configuration, respectively. The displacement controlled loadings during the tests are similarly termed here as NPC loading for NPC test and PC loading for PC test, respectively. The samples are allowed to heal for 24 hours in-between the completion of the NPC test and beginning of PC test.

The teflon film insert at the mid plane of the composite sample (which was introduced during manufacturing) acts as an artificial initial crack for NPC test. NPC fracture toughness is determined by propagating this artificial initial crack during the displacement controlled first fracture loading (NPC loading) of the sample. Thus, after the NPC test, a naturally occurred crack is present in the composite sample. PC fracture toughness is determined by further propagating this naturally occurred crack during the displacement controlled second fracture loading (PC fracture loading) of the same sample.

The configurations of composite samples and the procedure of determining the two values of fracture toughness are explained, separately, in detail below.

NPC (Non pre-cracked) test

NPC fracture toughness is calculated using the load and displacement data obtained during the NPC test of the composite sample in a three point bending set up as shown in figure 6.3 using a compliance calibration method according to ASTM D7905D-7905M [108].

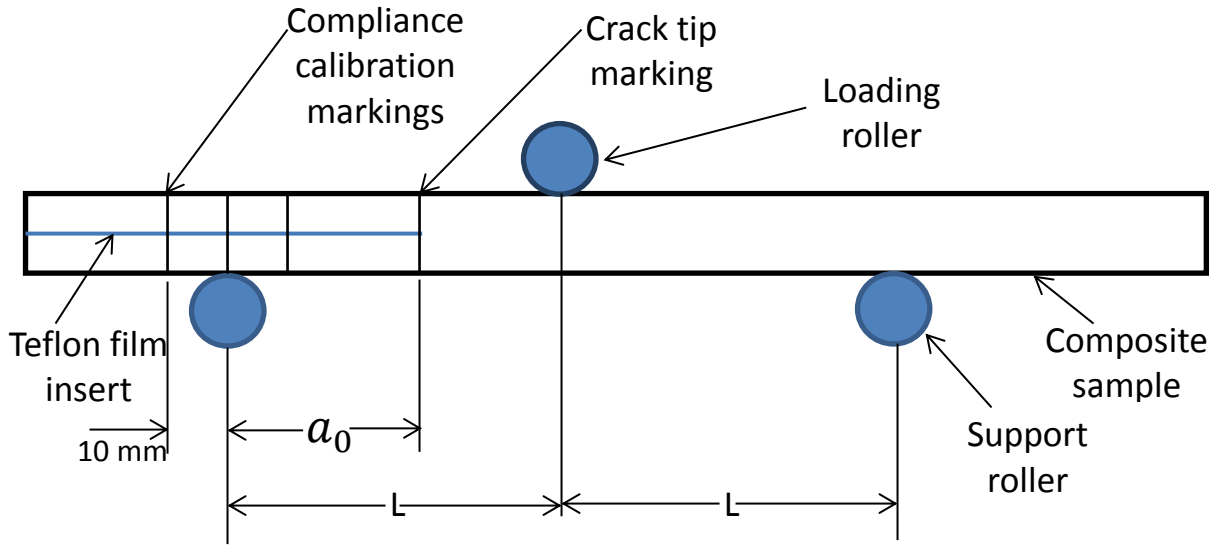

Figure 6.3 Composite sample, fixture and dimensions for NPC test [108]

Before starting the NPC test, the relative positions of the loading and support rollers in the fixture are adjusted such that the loading roller remains exactly at the center/middle of the support span (distance between the support rollers, 2L =101mm in figure 6.3). Before placing the sample on the fixture, the tip of the teflon insert (acting as an artificial crack) on the sample is first marked at its edge with a vertical line using a marker. The other three compliance calibration markings are done similarly at a distance of a_0 (= 35 mm), $(a_0 + 10)$ mm, and $(a_0 - 10)$ mm from the tip of the teflon insert as shown in figure 6.3. The composite sample is then placed between the support rollers such that the left support roller touches the marking at $(a_0 - 10)$ mm on the sample (see figure 6.3; the crack length is defined as the distance between the tip of the artificial crack and the middle of the left support roller). The sample is then loaded at this crack length (= 25 mm) with the displacement control mode at a rate of 0.5 mm/min until a certain predetermined load (equal to 50% of the expected critical load at this crack length) is reached and then unloaded. This concludes the first NPC compliance loading. The sample is then repositioned in the fixture such that the left support roller touches the marking at $(a_0 + 10)$ mm on the sample (see figure 6.3). The sample is loaded similarly at this crack length (=45 mm) until a certain predetermined load (equal to 50% of the expected critical load at this crack length) is reached and unloaded. This concludes the second NPC compliance loading. It is to be noted that during the two compliance loadings of the sample with two different crack lengths, the artificial crack is not allowed to propagate. Finally, the sample is repositioned again in the fixture such that the left support roller touches the marking at a_0 on the sample. The sample is loaded at this crack length (=35 mm) until the artificial crack propagates and then unloaded at the same displacement rate of 0.5 mm/min. Data for the instantaneous loads and displacements for this final unloading is also recorded to determine the unloading compliance (i.e. slope of the displacement vs load line). This concludes the NPC fracture loading and marks the end of the NPC test. As an example, a typical calculation procedure for determining the NPC fracture toughness is discussed here with actual data obtained during the NPC test of a composite sample. A typical displacement Vs load data obtained through the NPC test of a composite sample are plotted in figure 6.4.

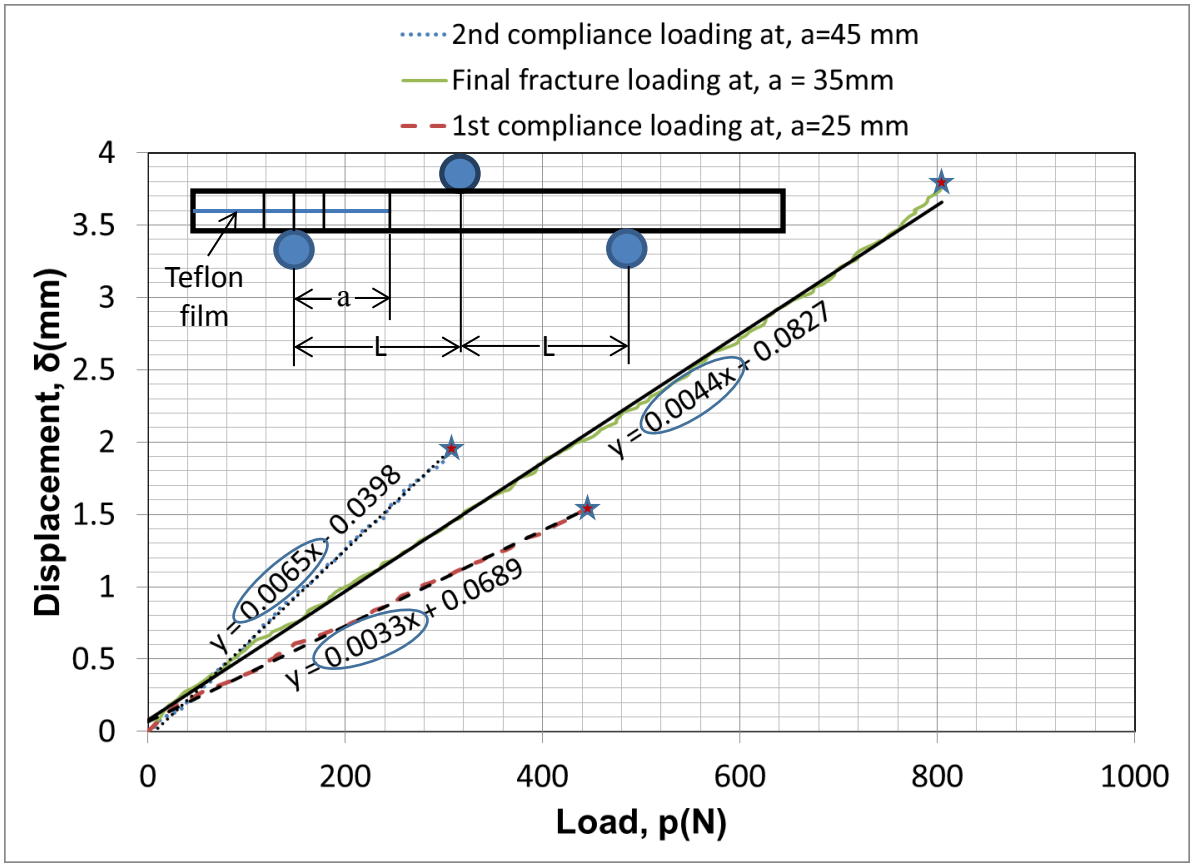

Figure 6.4 Typical plot of displacement Vs load data obtained in a NPC test of a composite sample to determine the compliances at different crack lengths. The sample configuration for the NPC test is shown in the inset of the graph. The peak load achieved during the compliance and fracture loadings are highlighted with star symbols. The calculated compliance value for each crack length is also shown encircled inside the graph.

The compliances determined from the plot (circled values in figure 6.4) were then plotted vs the corresponding crack length cubed (a^3) as shown in figure 6.5.

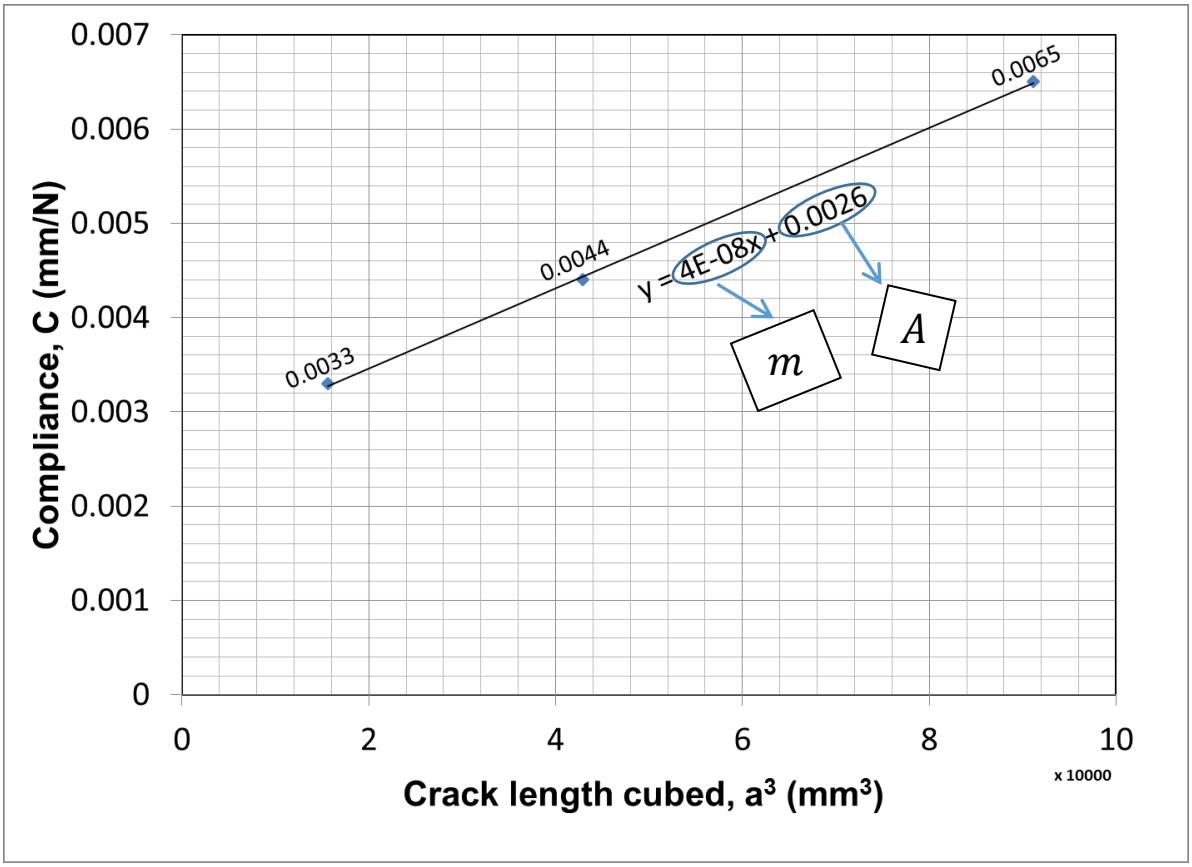

Figure 6.5 Plot of compliance Vs crack length cubed (a^3) to determine the compliance parameters. The compliance values (y-axis values) indicated in the graph are taken from the previous graph in figure 6.4. The compliance parameters are calculated from the slope (m) and the y-axis intercept (A) of the line shown in the graph.

The compliance relationship with crack length of the sample is expressed in the form

$$C = A + ma^3 \quad \text{.....(6.1 a) [108]}$$

Where,

C----------Compliance; (mm/N)

A----------y-axis intercept of the plot of compliance Vs a^3; (mm/N)

m----------Slope of the line in the plot of compliance Vs a^3; [1/(N.mm^2)]

a----------Crack length (mm)

A, and m are termed as the compliance calibration parameters.

The mode II fracture toughness is determined according to the equation

$$G_{II}^{C} = \left(\frac{p^2}{2B}\right) * \left(\frac{\partial C}{\partial a}\right)|_{(a=a_0)} \quad \text{.....(6.2) [108]}$$

where,

G_{II}^{C} ----------Strain energy release rate (N/mm)

p ---------- Peak load (N) achieved during the NPC fracture loading

B ----------Width of the sample (mm)

a_0 ----------Crack length at which the fracture loading is carried out

From equation (6.1 a)

$$\left(\frac{\partial C}{\partial a}\right)|_{(a=a_0)} = 3ma_0^2 \quad \text{.....(6.3)[[108]}$$

Combining equations (6.2) and (6.3), we get

$$G_{II}^{C} = \frac{3ma_0^2p^2}{2B} \quad \text{.....(6.4) [108]}$$

Practically, the value of the fracture toughness obtained by equation (6.4) is first taken as a candidate toughness G_Q. If the percentages of G_Q $(\%G_Q)$ that were achieved during the compliance loadings satisfy $15 \leq \%G_Q \leq 35$, the candidate toughness value is accepted as $G_{II}^{C} = G_Q$ [108].

For the current example, the values of the parameters at the right hand side of equation 6.4 are given below.

$m = (4\text{E-}08)\ (1/\text{Nmm}^2)$ [See figure 6.5]

$a_0 = 35\ (\text{mm})$ [The crack length at which the fracture loading is carried out]

$p = 804\ (\text{N})$ [See figure 6.4]

$B = 20\ (\text{mm})$ [Width of the sample]

Putting the above values in equation (6.4), we can first calculate a candidate toughness

$G_Q = 2.38\ (\text{N/mm})$, or,

$G_Q = 2380$ (J/m^2) ……(6.5) [108]

Validation

The percentages of G_Q $(\%G_Q)$ that were achieved during the compliance loadings are given by

$$\%G_{Q,j} = \left[\frac{100\ (P_j a_j)^2}{(P_{max} a_0)^2}\right]; \text{j} = 1, 2 \text{……......(6.6) [108]}$$

Where,

$\%G_{Q,j}$ ------Two values of G_Q associated with two compliance loadings

P_{max} ------Peak value of the force achieved during the fracture loading (see figure 6.4)

P_j ----------Peak value of the forces achieved during compliance loadings at a_j (see figure 6.4); and

a_j ---------- jth crack length used during the compliance loading.

For the current example, the values of the parameters in the right hand side of equation (6.6) are given below

$a_0 = 35\ mm$

$P_{max} = 804\ N$ (see figure 6.4)

i) for the first compliance loading

$a_1 = 45mm$

$P_1 = 313\ N$ (see figure 6.4)

Putting these values in equation 6.6,

$\%G_{Q,1} = 25\%$ which remains in the validity range $15 \leq \%G_{Q,1} \leq 35$

ii) for the second compliance loading

$a_2 = 25mm$

$P_1 = 452\ N$ (see figure 6.4)

Putting these values in equation 6.6,

$\%G_{Q,2} = 16\%$ which remains in the validity range $15 \leq \%G_{Q,2} \leq 35$

As the $\%G_Q$ achieved during both the compliance loadings satisfy the validity criteria$15 \leq \%G_Q \leq 35$, the candidate toughness value G_Q obtained in equation (6.5) is accepted as

$$G_{II}^{C} = G_Q = 2380 \text{ (J/m}^2\text{)} \quad \text{.....(6.7)}$$

Thus, the procedure for determining the NPC fracture toughness of a composite sample using the compliance calibration method according to ASTM D7905/7905M is described above. At least three samples for each category of composite samples with NPC configurations were tested following the above procedure and the average values of $G_{II,NPC}^{C}$ are determined.

Determination of the location of the natural crack tip

Figure 6.6 shows the schematic of the composite sample before and after the NPC test showing the advancement of delamination from the pre-implanted insert and the relative location of the natural crack tip.

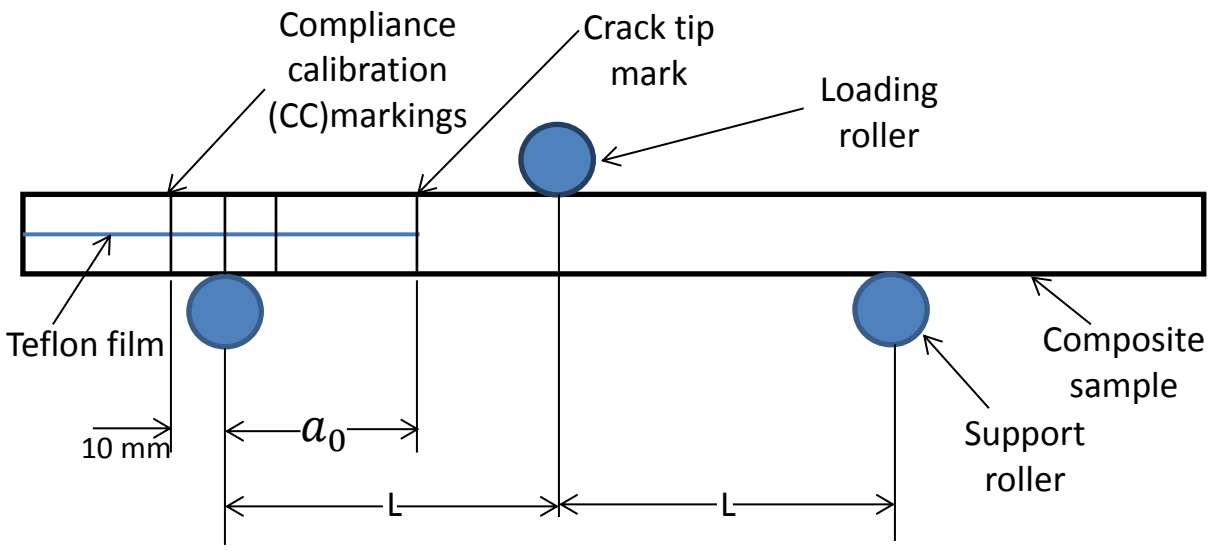

a)

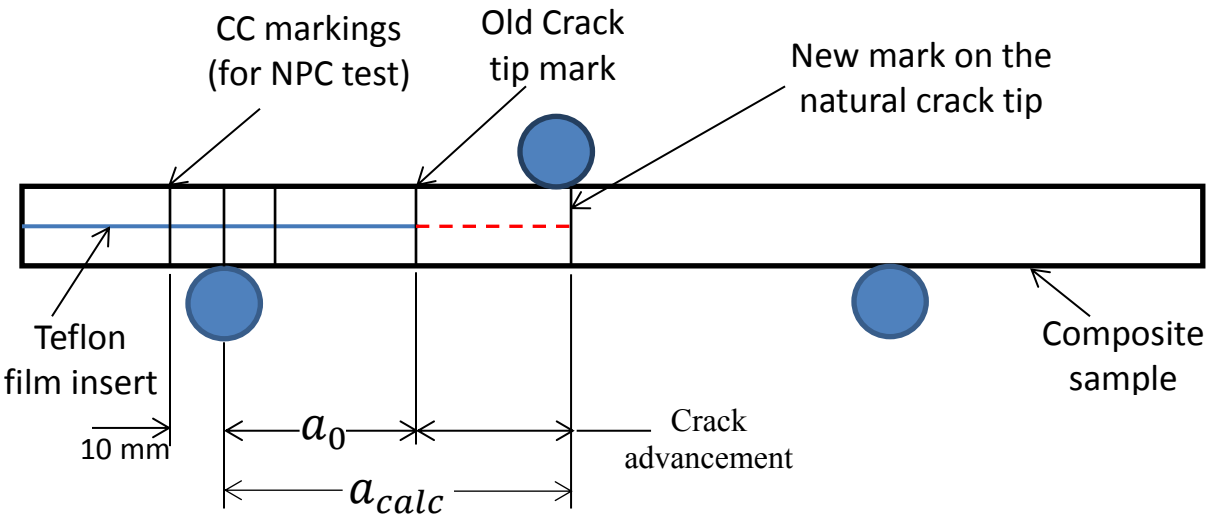

b)

Figure 6.6 Schematic of the composite sample showing the relative position of the tip of the a) artificial crack (pre-implanted insert) before the NPC fracture loading and b) natural crack after the NPC fracture loading. Dotted line represents the natural crack created due to the NPC fracture loading [108]

Figure 6.6 shows that the delamination has been advanced from its pre-implanted insert (artificial crack) after the NPC test of the composite sample. However, the exact location of the new crack (now called a natural crack) tip is often difficult to locate by mere visual observation.

Instead, the location of the tip of the natural crack (a_{calc}) is calculated from the unloading data of the NPC fracture test according to equation

$$a_{calc} = \left(\frac{C_u - A}{m}\right)^{1/3} \quad \text{.....(6.8) [108]}$$

Where,

a_{calc} ----------Distance between the locations of the tip of the natural crack and the left support roller in the NPC fracture test setting (mm) as shown in figure 6.6 b).

A and m ----------The compliance parameters as shown in figure 6.5

C_u ----------Compliance determined from the unloading line of the NPC fracture test (mm/N) (shown in figure 6.7 below)

For the current example, figure 6.7 shows the plot of displacement Vs. load data obtained during the unloading after the NPC fracture loading.

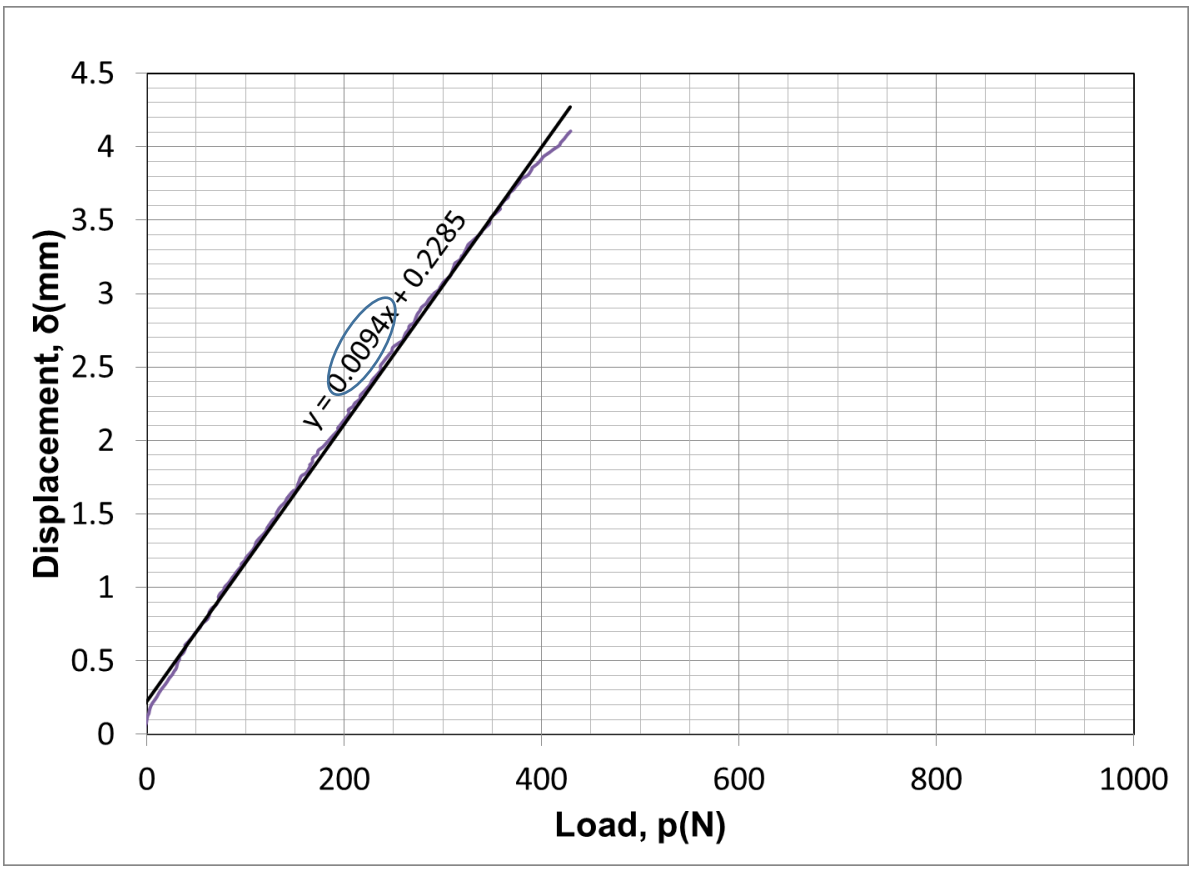

Figure 6.7 Unloading compliance (C_u) determined from the displacement-load data obtained during the unloading after the NPC fracture loading. The unloading compliance value for the current example is encircled inside the graph.

Thus, for the current example,

C_u= 0.0094 mm/N

m = (4E-08) (1/Nmm^2) [See figure 6.5]

A = 0.0026 mm/N [See figure 6.5]

Putting these values in equation (6.8), we get

a_{calc} = 55.4 mm

As, the crack length during the fracture loading

a_0 = 35 mm

Thus, the crack advancement (see figure 6.6 b) is given by

$(a_{calc} - a_0) = 20.4$ mm

This location of the natural crack tip is further verified by close visual observations, adjusted if seems necessary and marked on the composite sample (see figure 6.6 b) for the subsequent PC test as recommended in the ASTM standard [108].

In summary, NPC test consists of three loadings of a composite sample which contains a pre-implanted teflon insert as an artificial crack. Among the three loadings, two are compliance loadings where the artificial crack is not allowed to propagate and the other one is fracture loading where the artificial crack is allowed to propagate. Fracture loading is carried out at a specific crack length ($a_0 = 35$ mm) while the two compliance loadings are carried out at crack lengths 10 mm below (i.e. $a = 25$ mm) and 10 mm above (i.e. $a = 45$ mm) the fracture crack length. Data for the instantaneous loads and displacements are recorded for the two compliance loadings, one fracture loading and final fracture unloading during the NPC test. The amount of crack advancement is calculated from the unloading compliance. This advancement of crack during the NPC test creates the precrack that is used for the PC test. The tip of this natural crack is marked with a vertical line on the composite sample for the subsequent PC test. The composite sample is allowed to heal for 24 hours at targeted environment before the PC test is carried out.

PC (Pre-cracked) test

Once the NPC test of the composite sample is completed, the samples are kept inside a zipped plastic bag to minimize mainly the moisture effect and kept at room temperature (RT) for 24 hours to allow the self-healing reaction (between the monomer oozed out of broken microcapsules and the dispersed catalyst) at the crack plane to complete before the PC test. Regular composite samples (without healing agents), however, do not require healing time. They are, however, also kept inside the zipped plastic bag and kept in RT for 24 hours before the PC test. For cold temperature tests, the samples are kept in a dry ice chamber maintained at -40^{o}C for 24 hours to allow for healing in cold temperature. The cold temperature experiment is described in chapter 7. After 24 hours, the samples are loaded into the three point bending fixture of the MTS machine. PC fracture toughness is calculated using the load and displacement data

obtained during the PC test of the composite sample in a three point bending set up as shown in figure 6.8.

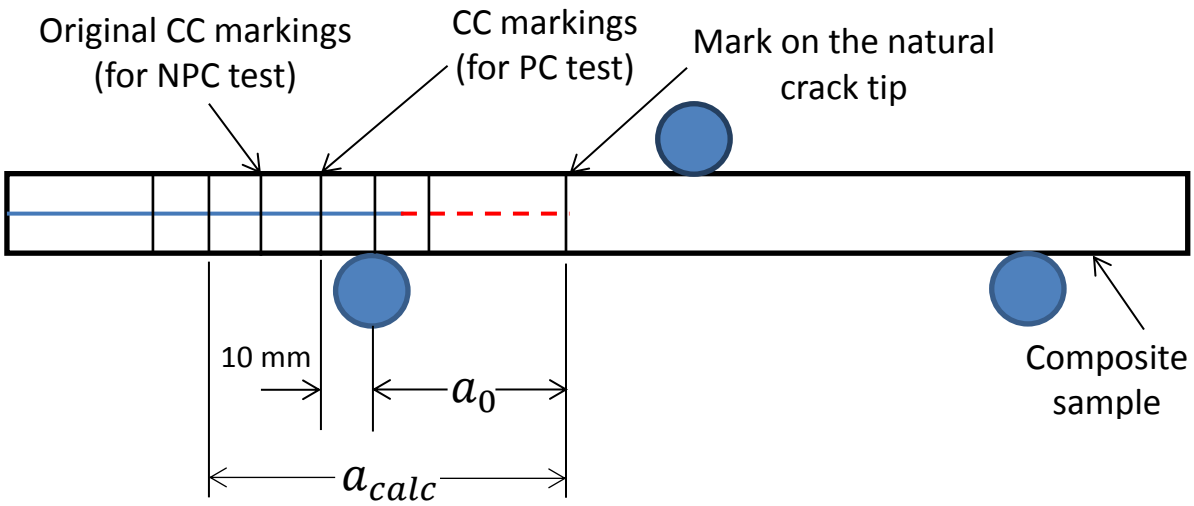

Figure 6.8 Schematic of the composite sample showing the relative position of the tip of the natural precrack for the PC fracture loading. Dotted line represents the natural crack created during the NPC fracture loading [108]

Before placing the sample on the fixture for PC test, new PC compliance calibration markings are put on the sample at a distance of a_0 (= 35 mm), $(a_0 + 10)$ mm, and $(a_0 - 10)$ mm from the tip of the natural precrack (that were created during the NPC fracture loading) as shown in figure 6.8. The composite sample is then placed between the support rollers such that the left support roller touches the new PC marking at $(a_0 - 10)$ mm on the sample. The sample is then loaded at this crack length (= 25 mm) with the displacement control mode at a rate of 0.5 mm/min until a certain predetermined load (equal to 50% of the expected critical load at this crack length) is reached and then unloaded. This concludes the first PC compliance loading. The other PC compliance loading at $(a_0 + 10)$ mm, and the PC fracture loading at $(a_0 = 35$ mm) is carried out and the value of PC fracture toughness is determined similarly as described for NPC test. At least three samples for each category of composite samples are tested with PC configurations following the above procedure and the average values of $G^C_{II,PC}$ are determined. During the PC compliance loading, the natural precrack is not allowed to propagate while during the PC fracture loading it is allowed to propagate. The amount of crack advancement is, however, not required to calculate, in the case of PC test.

A summary of the types of tests performed at room temperature and low temperature (-40°C) with different types of FRP composite samples (Type I-VII) indicating the designation of the individual test result are listed in table 6.2. Table 6.2 summarizes the designation of the test results (fracture toughness values) that would be obtained with the kind of tests performed (NPC and PC) at room temperature and low temperature (-40°C) on different types of composite samples (I-VII) containing varying average size and concentration of microcapsules. The experimental set up for low temperature tests are described in chapter 7.

Table 6-2. Summary of the type of tests performed at RT and CT (-40°C) with different types of composite samples (I-VII) indicating the designation of individual test results

Types of composite samples	Kind of tests performed at room temperature and low temperature (-40°C) on each type of sample and the designation of the test results			
	RT		CT	
	Non Pre-cracked $G^{C}_{II,NPC}$	Pre-cracked $G^{C}_{II,PC}$	Non Pre-cracked $G^{C}_{II,NPC}$	Pre-cracked $G^{C}_{II,PC}$
I	NPC (0%)	PC (0%)	NPC (0%)	PC (0%)
II	NPC(2%,100 µm)	PC(2%,100 µm)	NPC(2%,100 µm)	PC(2%,100 µm)
III	NPC(5%,100 µm)	PC(5%,100 µm)	NPC(5%,100 µm)	PC(5%,100 µm)
IV	NPC(8%,100 µm)	PC(8%,100 µm)	NPC(8%,100 µm)	PC(8%,100 µm)
V	NPC(2%,45 µm)	PC (2%,45 µm)	-	-
VI	NPC(5%,45 µm)	PC (5%,45 µm)	-	-
VII	NPC(8%,45 µm)	PC (8%,45 µm)	NPC(8%,45 µm)	PC(8%, 45 µm)

MC: Microcapsules; RT: Room Temperature; CT: Cold (-40°C) temperature

Thus, the value of NPC fracture toughness of regular type I sample (containing no microcapsules) is termed as NPC (0%). The value of PC fracture toughness of the same type sample is termed as PC (0%). Similarly, the value of NPC fracture toughness of modified type VII sample (containing 8wt% microcapsules of average size 45 µm), for example, is termed as NPC (8%, 45 µm) and so on. The NPC and PC fracture toughness is generally designated as $\boldsymbol{G^{C}_{II,NPC}}$ and $\boldsymbol{G^{C}_{II,PC}}$, respectively.

6.4 Results and Discussions

A representative load-displacement curves for the NPC and PC fracture loading of composite samples and the corresponding NPC and PC fracture toughness values as determined according to the procedure described above are shown and discussed in section 6.4.1. The effect of inclusion of microcapsules of different average size on the NPC fracture toughness and the effect of self-healing on the PC fracture toughness measured at room temperature are discussed in the subsequent sections.

6.4.1 Elaboration of representative load-displacement curves and measured values of fracture toughness of regular (Type I) composite sample as example

Figure 6.9 shows a representative load-displacement curve for the NPC and PC fracture loading of regular sample (Type I) as an example.

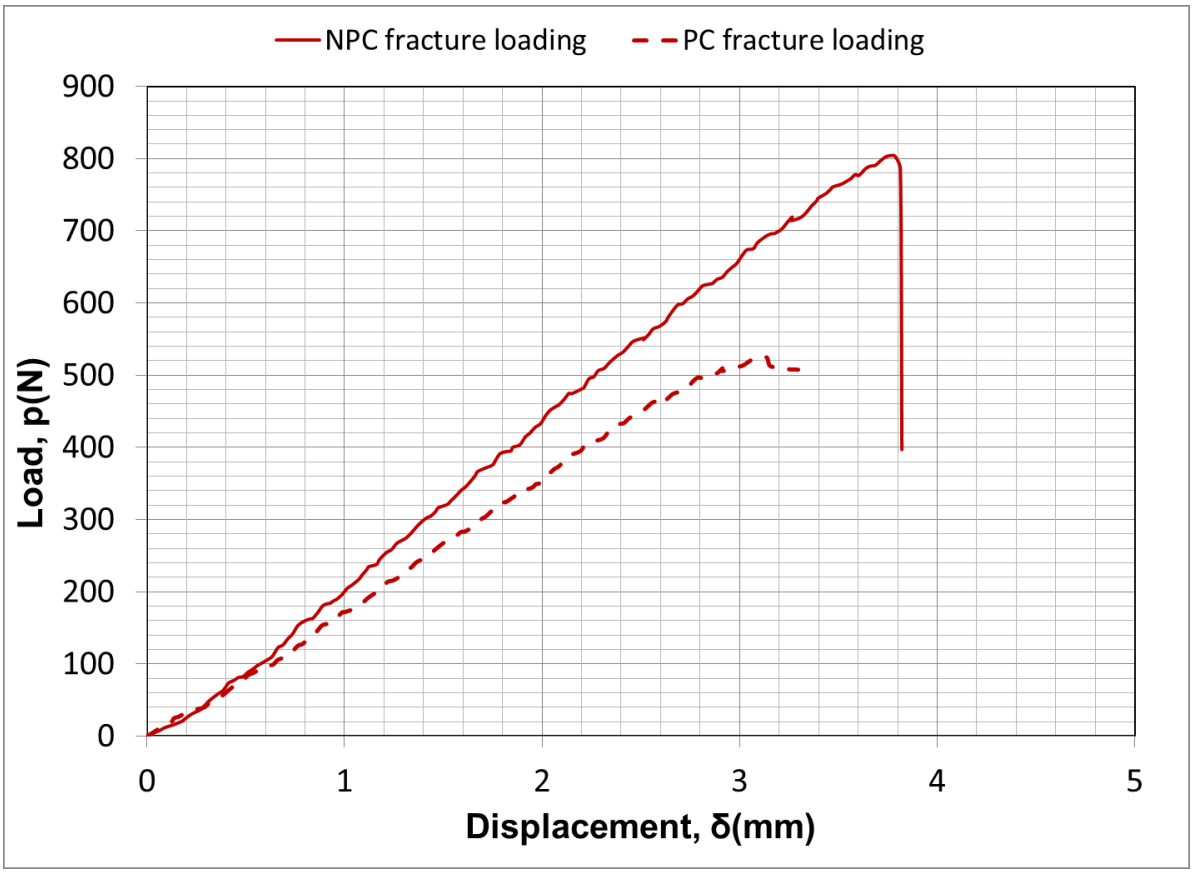

Figure 6.9 Representative load-displacement curves for the NPC and PC fracture loading of regular (Type I) composite samples

From the load-displacement curve in figure 6.9, it is observed that during the NPC fracture loading, the load increases linearly up to a displacement of about 3.8 mm and then suddenly drops which is also associated with a loud cracking sound implying rapid crack propagation. The nearly vertical drop of the load implies a high speed of crack propagation. The load-displacement curve during PC fracture loading of the same composite sample, on the other hand, shows also a linear increase of load up to a displacement of about 3.1 mm after which the load drops and the slope of the line changes more smoothly. This drop in load and the change in slope is also associated with a mild cracking sound implying an advancement of the PC crack. However, the speed of crack propagation is slower than NPC fracture loading as implied by the smoother change in the slope. When comparing the linear portions of the NPC and PC curves, it can be observed that both the slopes and the peak value of PC curve are substantially lower than the slope and the peak value, respectively, of the NPC curve. This difference is because of the fact that there is no real precrack in the composite sample during the NPC test. A pre-implanted teflon film acts as an artificial crack starter and delamination is propagated from this pre-implanted insert during the NPC test (see figure 6.3). On the contrary, a naturally occurred sharp crack already exists during the PC test and delamination is propagated from this sharp natural crack (see figure 6.8). The existence of the naturally occurred sharp crack makes the slope and the peak value of the PC line substantially lower than the NPC line. The same is true for the speed of crack propagation. As no natural sharp precrack exists in the NPC configuration, the composite sample can absorb substantial strain energy before it propagates at a high speed (vertical drop of load). However, the existence of a naturally occurred sharp crack in the PC configuration allows the sample to absorb smaller strain energy before its slower extension. With the above comparisons of the representative load-displacement curves, it can be estimated that PC fracture toughness ($G_{II,PC}^{C}$) is smaller than the NPC fracture toughness ($G_{II,NPC}^{C}$). The actual values of $G_{II,NPC}^{C}$ and $G_{II,PC}^{C}$ are, however, determined using the compliance calibration method discussed before and are shown in figure 6.10.

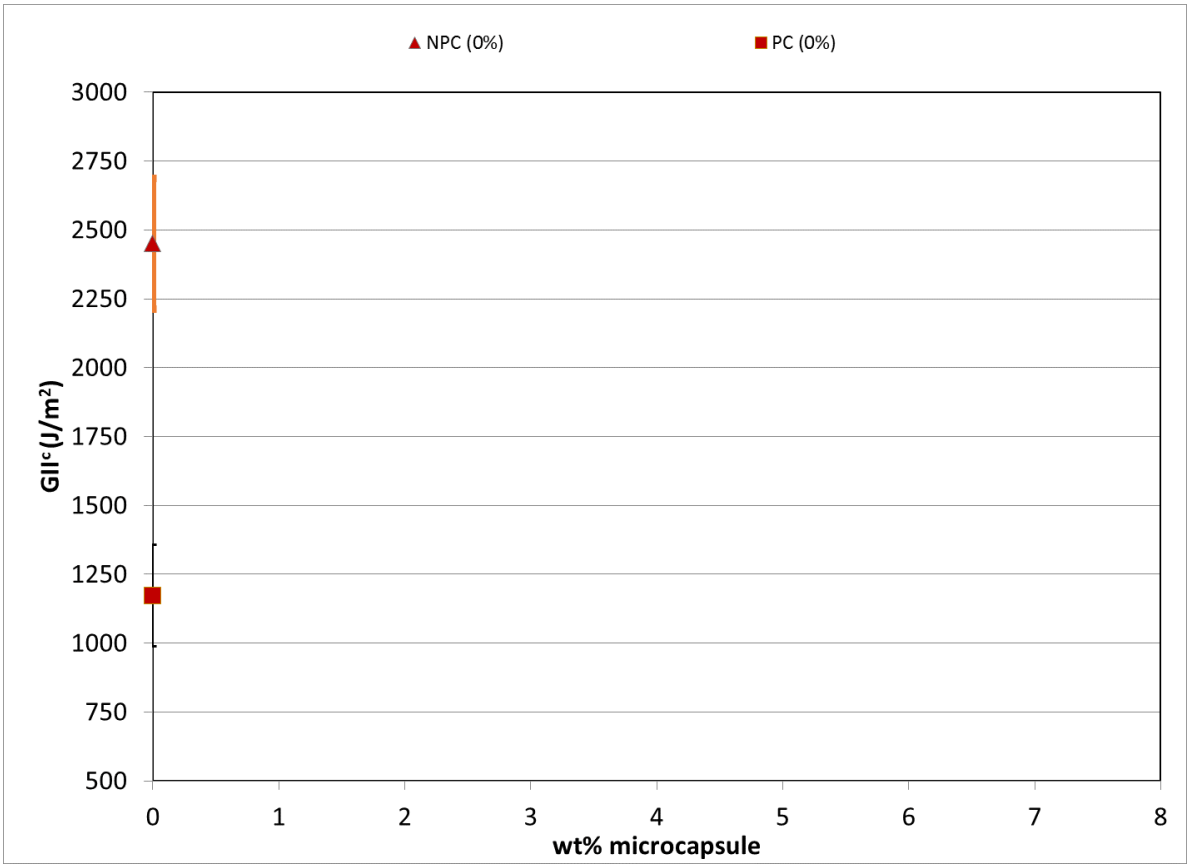

Figure 6.10 NPC and PC fracture toughness of regular (Type I) composite samples designated as NPC (0%) and PC (0%), respectively. Error bars represent one standard deviation of measured values. The scale and spacing of the graph are chosen for later comparisons.

Figure 6.10 shows the NPC and PC fracture toughness of composite samples as a function of concentration of microcapsules for later comparisons. It is observed from the figure that there is almost 50% reduction in fracture toughness when a natural pre-crack exists in the regular (Type I) sample compared to the same sample (Type I) without a natural pre-crack (i.e. PC fracture toughness is about 50% of NPC fracture toughness). Percentage reduction of fracture toughness of the composite sample from NPC to PC configuration is calculated as

$$\% \text{ Red. (NPC-PC)} = \frac{(G^C_{II,NPC} - G^C_{II,PC})}{G^C_{II,NPC}} \quad \text{.....(6.9)}$$

Thus, the drastic reduction of fracture toughness with PC configuration is, ultimately, the effect of having a sharp natural pre-crack (which is not healed due to the absence of healing agents) in the regular sample (Type I). The idea of incorporating healing agents (i.e.

microcapsules and catalysts) into the composite samples of different types (II, III…..VII) is to heal this natural pre-crack as much as possible to improve its PC fracture toughness. In doing so, however, the original NPC fracture toughness might have been compromised by the incorporation of microcapsules and catalyst particles into the samples. An optimum average size and concentration of microcapsules for incorporating into modified composite samples (Type II-VII) is searched for, in this work, which would improve the PC fracture toughness as much as possible while would not degrade the NPC fracture toughness substantially, compared to type I sample.

The effect of inclusion of varying concentration of different sizes of microcapsules into the composite sample is determined by comparing the NPC fracture toughness of different types of samples (Type II, III……VII) with the NPC fracture toughness of type I sample. Similarly, the effect of self-healing is determined by comparing the PC fracture toughness of different types of samples (Type II, III……VII) with the PC fracture toughness of type I sample. These effects are discussed in the following sections.

6.4.2. Effect of inclusion of microcapsules on the NPC fracture toughness of composite samples

As a reminder, regular composite sample (Type I) contains no microcapsules and catalysts. Modified composite samples (Type II, III……..VII) contain microcapsules and catalysts. The NPC fracture toughness is the value of fracture toughness obtained with the advancement of delamination from the pre-implanted insert. No self-healing takes place yet during the NPC test even for modified samples as the natural crack is just generated during this test. Thus, when comparing the NPC fracture toughness of regular (Type I) and modified composite samples (Type II-VII), it represents the effect of incorporating those foreign healing agent particles into the modified composite samples since the only difference between the two types of samples is the presence (modified) or absence (regular) of those foreign healing agent particles.

The effects of inclusion of microcapsules on the NPC fracture toughness of modified composite samples (Type II, III……..VII) measured at room temperature are discussed below.

Effect of concentration of larger microcapsules (average size 100 µm) on the NPC fracture toughness

The values of the NPC fracture toughness ($G^C_{II,NPC}$) of the composite samples (Type I, II, III and IV) as a function of concentration of microcapsules of average size 100 µm are shown in figure 6.11.

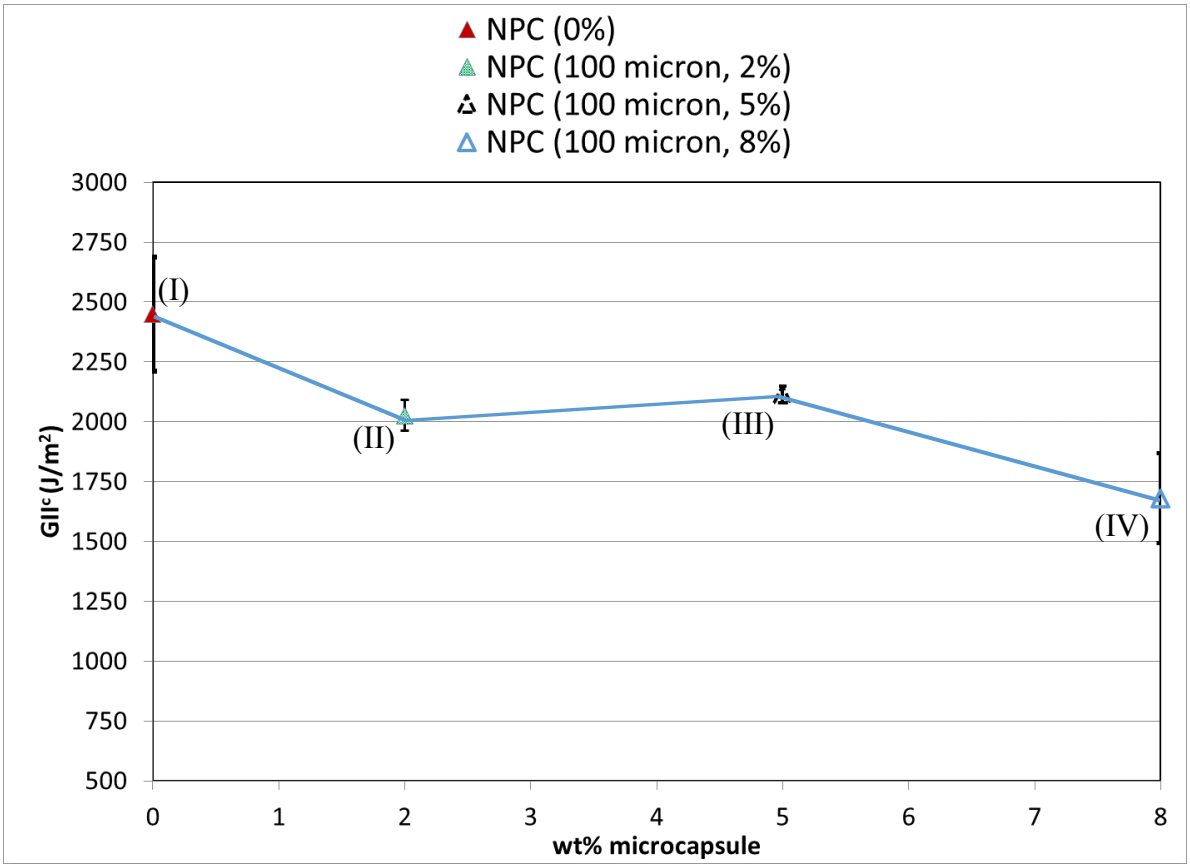

Figure 6.11 NPC fracture toughness of composite samples as a function of concentration of microcapsules of average size of 100 µm. Error bars represent one standard deviation of measured values.

Figure 6.11 shows that incorporation of varying concentration of microcapsules (average size 100 µm) tend to reduce the NPC fracture toughness ($G^C_{II,NPC}$). The values of $G^C_{II,NPC}$ of modified composite samples of type II, III and IV [containing certain wt% of larger microcapsules (average size 100 µm)] are always less than the values of $G^C_{II,NPC}$ of regular composite samples of type I (containing no microcapsules). NPC fracture toughness is reduced by 17% in type II sample, 14% in type III sample and 31% in type IV sample compared with type I sample. In

other words, the values of $G_{II,NPC}^{C}$ are reduced by 17%, 14% and 31% when incorporated with 2wt%, 5 wt% and 8 wt% of larger microcapsules (average size 100 μm), respectively, in the composites.

Percentage reduction in NPC fracture toughness due to incorporation of microcapsules in the composite samples is calculated as

$$\%\,\boldsymbol{red.}_{(\boldsymbol{NPC})} = \frac{(G_{II,NPC}^{C})_{\boldsymbol{R}} - (G_{II,NPC}^{C})_{M})}{(G_{II,NPC}^{C})_{\boldsymbol{R}}} \times \mathbf{100} \text{ ----------(6.10)}$$

where,

$(G_{II,NPC}^{C})_{\boldsymbol{R}}$---------- NPC fracture toughness of regular composite sample (Type I) not incorporated with microcapsules, and

$(G_{II,NPC}^{C})_{\boldsymbol{M}}$----------NPC fracture toughness of modified composite (Type II-VII) sample incorporated with certain wt% of microcapsules

The observation of reduction of fracture toughness of modified (incorporated with microcapsules of average size 100 μm) fiber reinforced composite samples is consistent with the observations made by Keller and Sottos [49], Brown et al. [[50], [51]] and Rule et al. [52] who investigated the effect of microcapsule properties on the modified (incorporated with microcapsules) epoxy (without fibers) sample. They [[49]- [52]] found that poorly bonded particles tend to reduce the mode I fracture toughness of epoxy specimen. They observed a continuous reduction in strength of the epoxy specimen with increasing wt% of microcapsules [49]. According to [50], weak bonding of particles act as voids in composites. However, they concluded that microcapsules if adequately bonded to the matrix can actually improve its fracture toughness. The observations made by [[49]- [52]] prompts to think debonding of microcapsules as one of the key reasons for the observed reduction in $G_{II,NPC}^{C}$ of fiber reinforced composites in the current work. Representative fracture features of the modified composites (Type II-IV containing certain wt% of microcapsules of average size 100 μm) as observed under SEM, is shown in figure 6.12. It shows the evidence of matrix-microcapsule debonding which occurs during the crack propagation leaving deep impressions of microcapsules on the fracture surface.

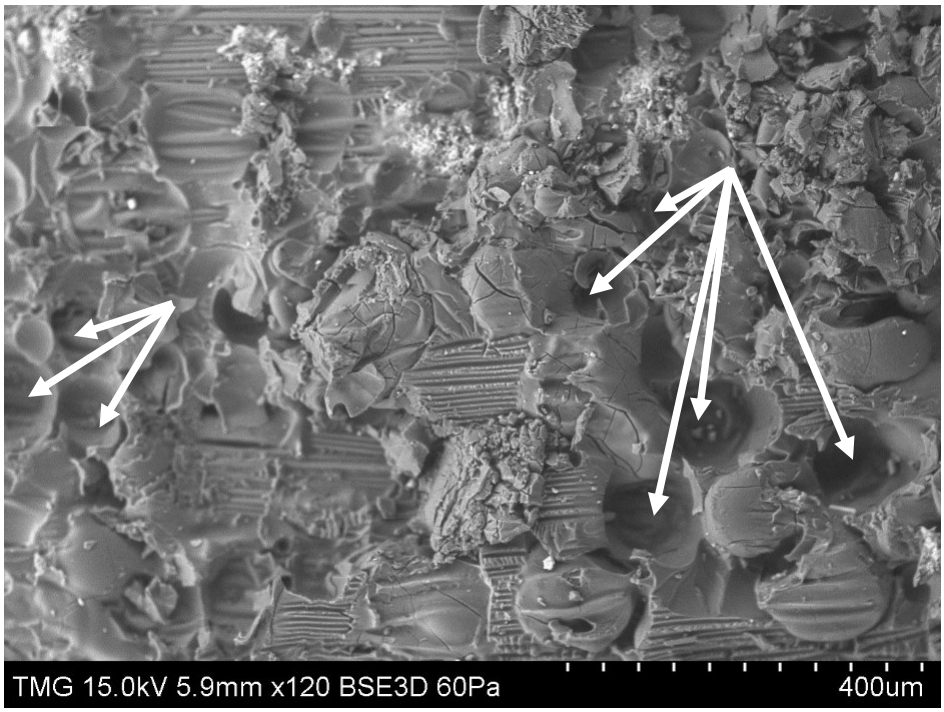

Figure 6.12 Matrix-microcapsule debonding during crack propagation leaving deep impression of microcapsules on the fracture surface.

As the larger microcapsules (average size 100 μm) tend to debond from the matrix, as revealed in figure 6.12, increasing the concentration of larger microcapsules beyond 5wt% reduces its NPC fracture significantly as shown in figure 6.11.

Thus, it is concluded that larger microcapsules (average size 100 μm) tend to form weaker bonding with the matrix which eventually leads to debonding from the matrix during the mode II crack propagation within composites. This results in significant degradation of NPC fracture toughness above the concentration of 5wt%. Brown [50] observed that the fracture behavior of epoxy with poor microcapsule bonding was identical to samples containing similar concentration of voids showing significant reduction in fracture toughness which is consistent with the observations in the current work. In his analytical models, Lauke [111] concluded that size and size distributions of particles might have significant influence on the fracture toughness of polymer composites resulting from the particle debonding, voiding and yielding of the polymer. In addition to the average size and size distribution, the morphology and shell thicknesses of the larger microcapsules, as investigated in the current work and discussed in chapter 3, might also contribute to the weaker matrix-microcapsule bonding in the composites. More research is

necessary to understand the effects of these factors on the bonding behavior of microcapsules with polymer matrix composites.

Effect of concentration of small microcapsules (average size 45 µm) on the NPC fracture toughness

The values of the NPC fracture toughness ($G_{II,NPC}^{C}$) of the composite samples as a function of concentration of small microcapsules of average size 45 µm are shown in figure 6.13.

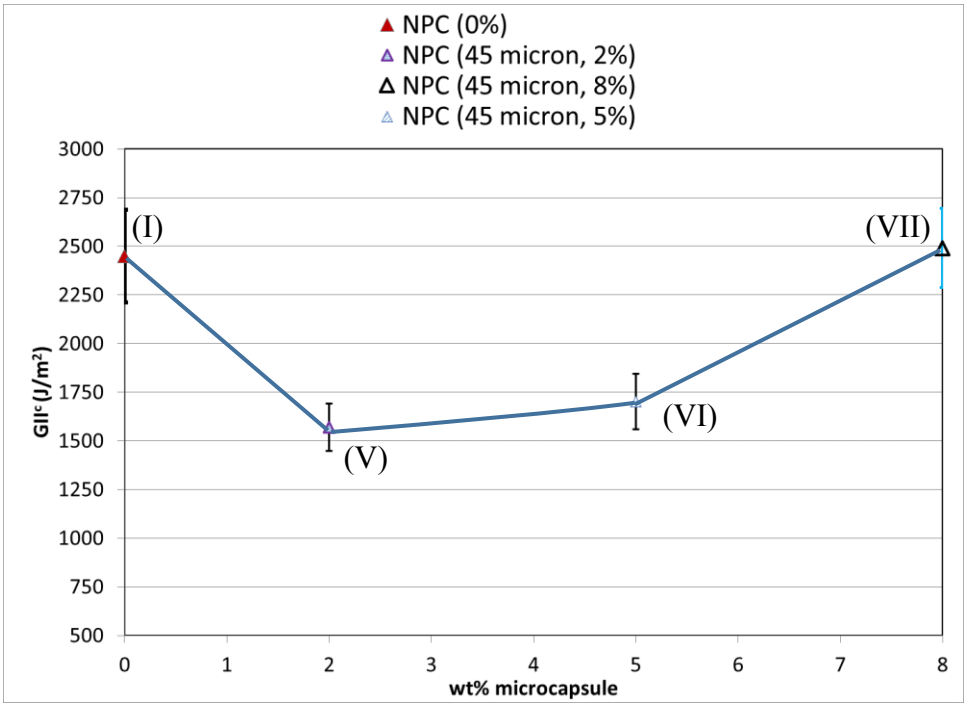

Figure 6.13 NPC fracture toughness of composite samples as a function of concentration of microcapsules of average size of 45 µm. Error bars represent one standard deviation of measured values.

Figure 6.13 shows that, incorporation of small microcapsules (average size 45 µm) up to 5 wt% reduces the NPC fracture toughness ($G_{II,NPC}^{C}$) of the samples of type V and VI compared with sample type I. However, incorporation of higher concentration (8wt%) of small microcapsules does not reduce the value of $G_{II,NPC}^{C}$ of sample type VI. Compared with type I sample, 35% reduction in NPC fracture toughness is observed in type V sample, 30% reduction in type VI sample and almost no reduction in type VII sample is observed. In other words, the values of $G_{II,NPC}^{C}$ are reduced by 35% and 30% when incorporated with 2wt% and 5 wt% of

small microcapsules (average size 45μm), respectively, in the composites. The value of $G_{II,NPC}^{C}$, however, is not affected by incorporation of 8 wt% small microcapsules in the composites.

SEM observations of fracture surface of the modified composites (containing microcapsules of average size 45 μm) shows good matrix-microcapsule bonding as shown in figure 6.14 a) and b).

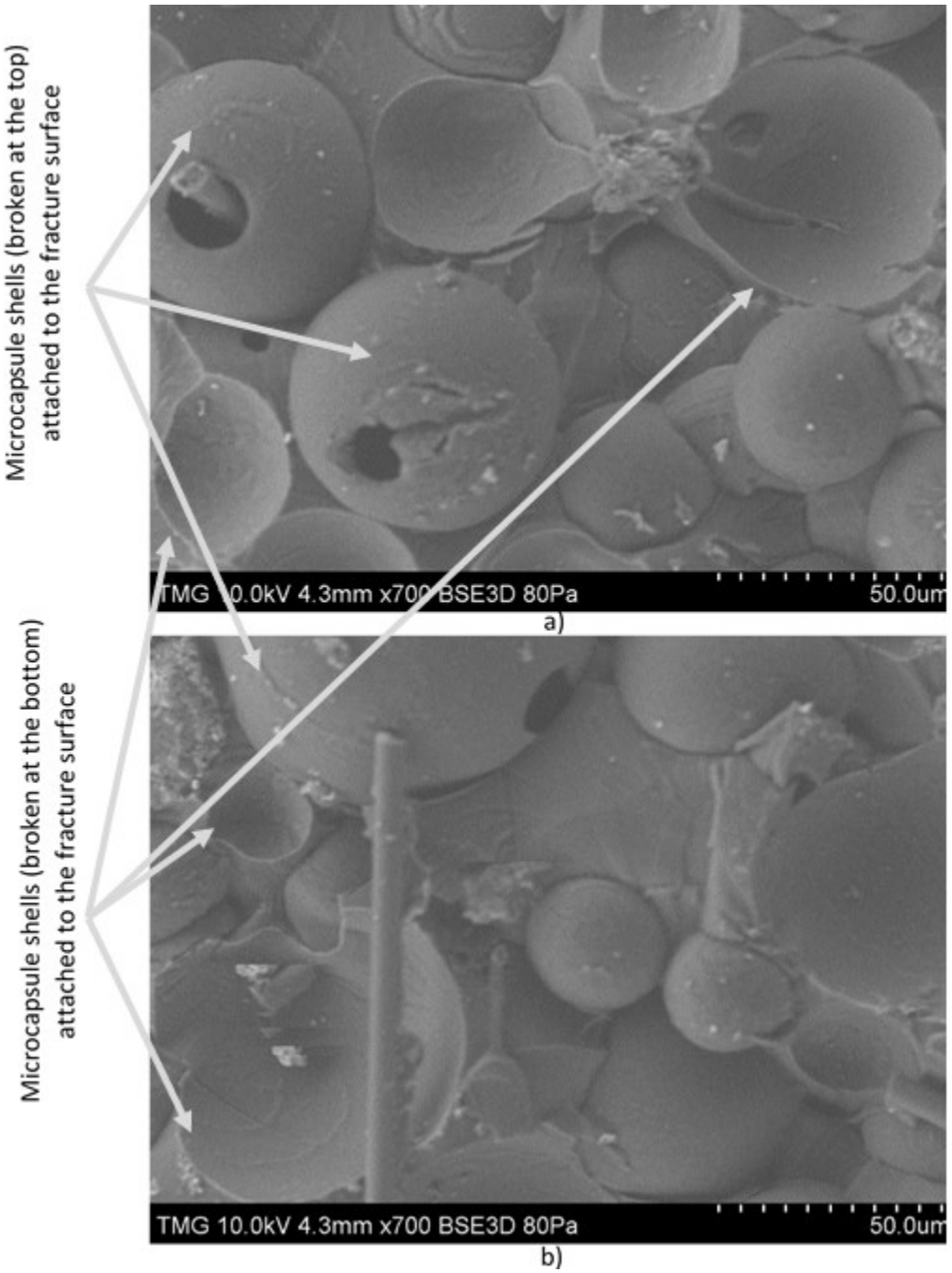

Figure 6.14 a) and b). SEM micrographs showing good bonding of smaller microcapsules (average size 45 μm) with the matrix on the fracture surface.

SEM micrograph with higher magnification (2700X) in figure 6.15 shows, more clearly, broken shells of smaller microcapsules (average size 45 μm) still attached to the fracture surface.

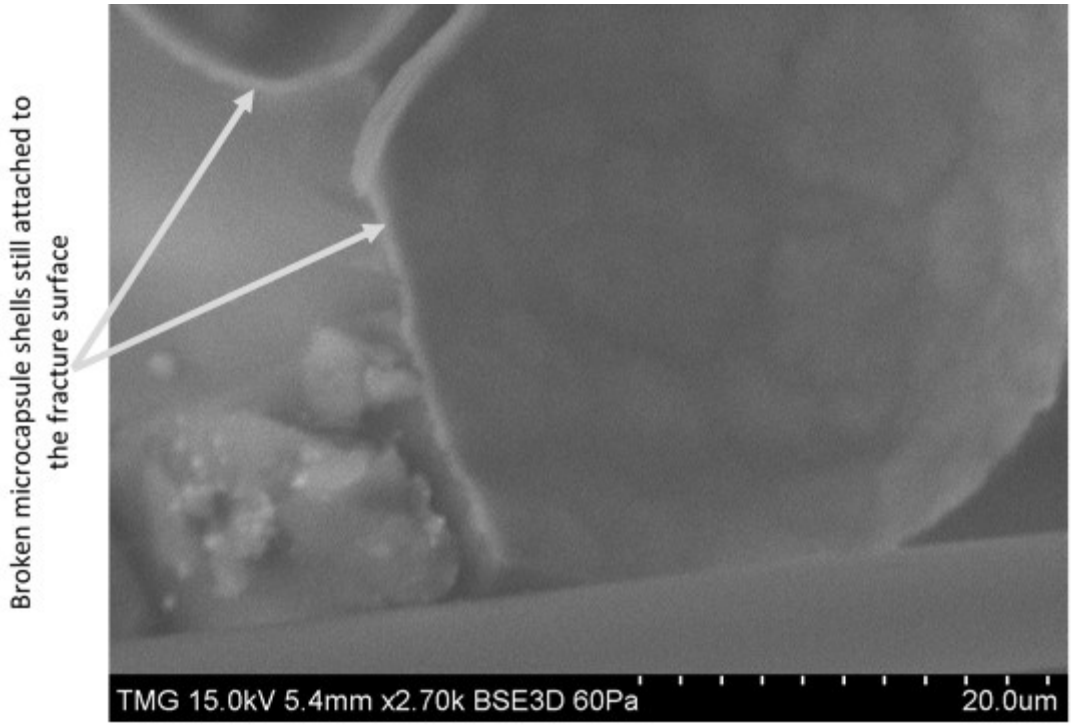

Figure 6.15 SEM micrograph (2700X) showing broken shells of smaller microcapsules (average size 45 μm) still attached to the fracture surface.

As pointed out earlier, the size, size distribution, morphology and shell thicknesses of the microcapsules which are shown to be different for larger and smaller microcapsules as investigated in the current work and discussed in chapter 3, might have significant effects on the matrix-microcapsule bonding and requires more research works to understand the behavior.

The good bonding between matrix and small microcapsules (average size 45 μm) does not, however, explain the reduction of NPC fracture toughness of modified composites of type V and VI as shown in figure 6.13. In order to find possible reasons for this, fracture surfaces of the composite samples near the NPC crack fronts were observed under SEM. Figure 6.16 shows the fracture surfaces of the composites of type V, VI and VII samples near their NPC crack fronts (i.e. at the edge of the teflon insert).

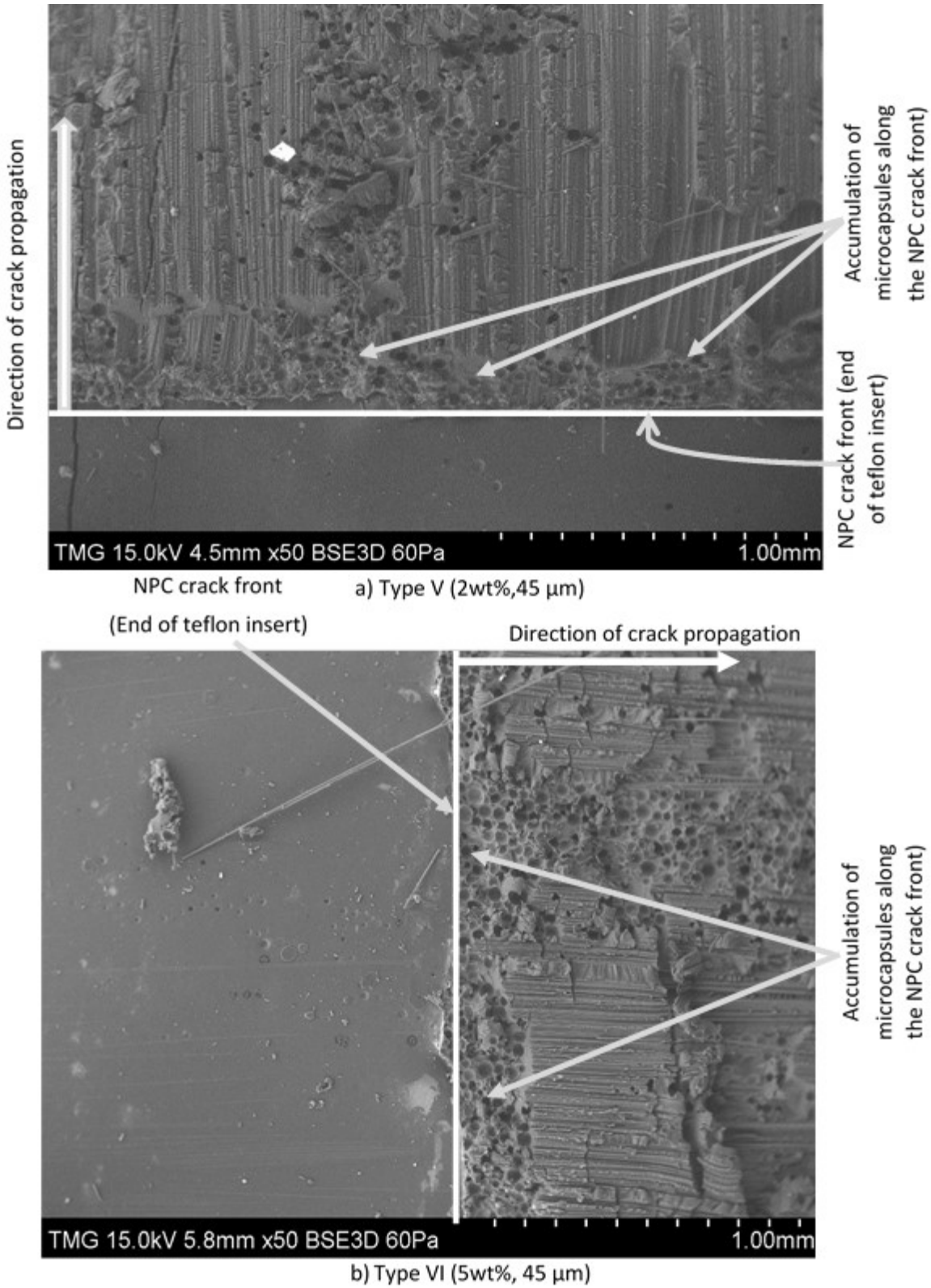

Figure 6.16 SEM micrographs showing features of fracture surface near NPC crack front of modified composite samples containing a) 2wt% (Type V) b) 5wt% (Type VI) and c) 8wt% (Type VII) microcapsules of average size 45 µm

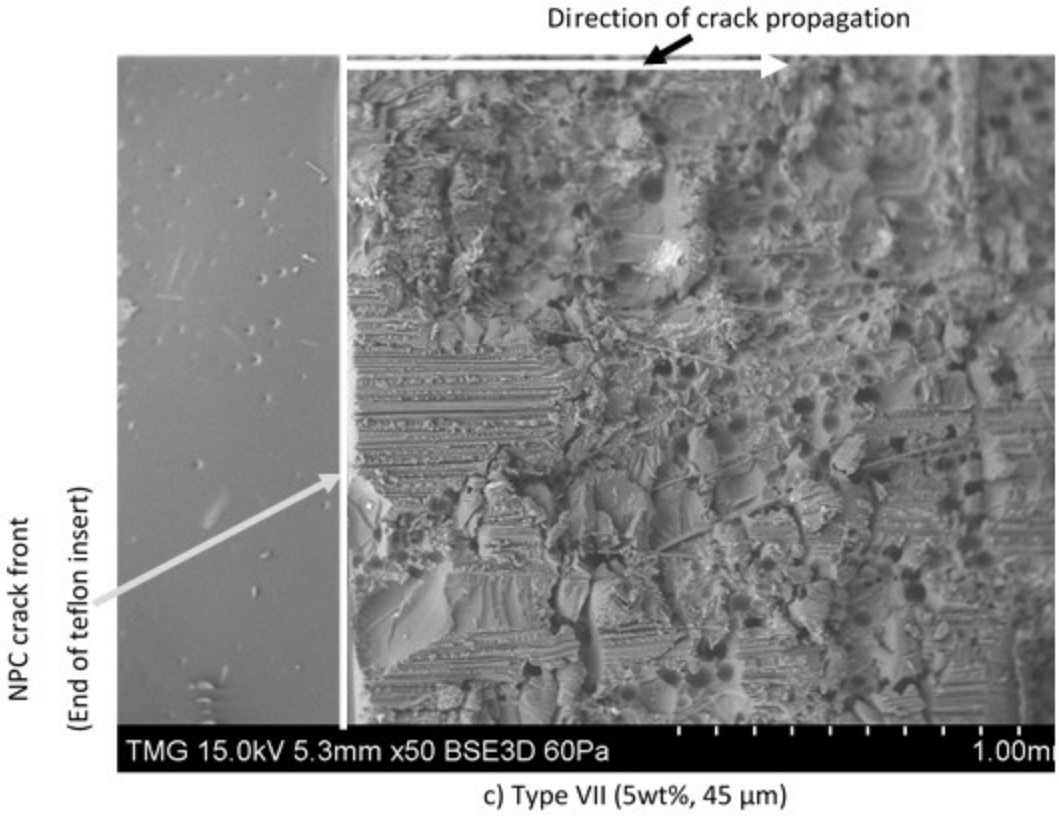

Figure 6.16. SEM micrographs showing features of fracture surface near NPC crack front of modified composite samples containing a) 2wt% (Type V) b) 5wt% (Type VI) and c) 8wt% (Type VII) microcapsules of average size 45 µm

Figure 6.16 a), b) reveals that extra resin, rich in microcapsule concentration, are accumulated at the NPC crack front and its vicinity of the type V and type VI samples. Figure 6.16 c), however, does not show such accumulation of microcapsule-rich extra resin at the NPC crack front of type VII samples. This explains the reason why significant degradation of NPC fracture toughness occurred in type V and type VI samples, but not with type VII samples as shown in figure 6.13. The accumulation of microcapsule-rich extra resin at a preferred location (tip of the teflon film insert) possibly causes stress concentration weakening the NPC crack front. It significantly reduces the NPC fracture toughness the value of which is obtained by the advancement of this crack front. As no such accumulation is observed in type VII samples, no significant reduction in NPC fracture toughness is observed.

The accumulation of microcapsules and extra resin at the vicinity of NPC crack front (teflon insert) occurred during the hand lay-up. During hand lay-up, modified epoxy incorporated with

the microcapsules were first poured upon the mid-layer of carbon fibers and then spread and infused it over the layer with a hand applicator. Teflon film (with a thickness of about 15 micron) was located at one end of the layer across its width as shown in figure 6.17. During the lay-up, the epoxy poured on the layer is drawn with the applicator along the length (and width) direction of the layer in both way (towards the teflon film starting from the other end and starting from the teflon film end towards the other end. The schematic of the process is shown in figure 6.17.

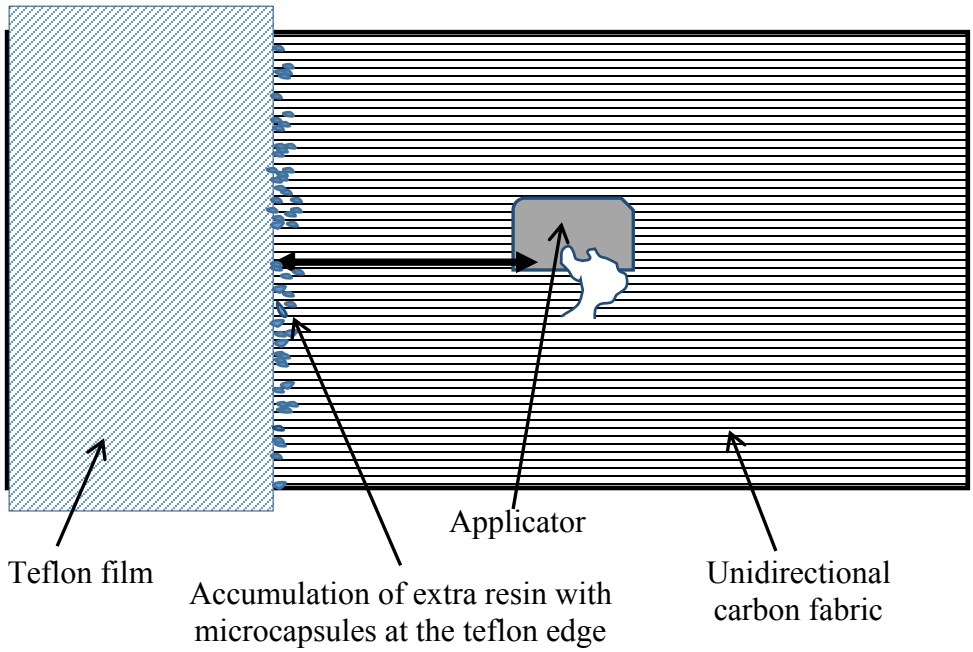

Figure 6.17 Schematic of lay-up method showing accumulation of microcapsules at the tip of the teflon film insert (NPC crack front) of composite samples

During drawing the modified epoxy incorporated with healing agents to the left of the composite layer with the applicator moving towards the teflon film, modified epoxy gets obstructed at the teflon edge. Repeated drawing of the epoxy toward the teflon film starting from the other end of the layer results in accumulation of extra resin incorporated with microcapsules at its edge. This accumulation of microcapsules at a preferred location (tip of the teflon film insert) causes stress concentration which drastically reduces its NPC fracture toughness. Once the problem in manufacturing the laminate was identified, proper care was taken to avoid the accumulation of extra resin with microcapsules at a preferred location. It was done by avoiding the drawing of the modified epoxy to the left where teflon film was placed. Instead, the epoxy was drawn with the applicator repeatedly starting from the teflon end to the right towards the other end of the layer. This allowed smoother infusion of modified epoxy over the layer without

any obstruction. As the modified epoxy was not obstructed at the edge of the teflon film in this amended lay-up procedure, there was no accumulation of extra resin with microcapsules at a preferred site (NPC crack front). Type VII composite samples (8wt%, 45 μm) were made according to the amended lay-up practice and the NPC crack front was found to be free from accumulation of extra resin with microcapsules as shown in figure 6.16 c) before.

It is thus observed through the investigation that significant deterioration of NPC fracture toughness can be caused by issues related to manufacturing of modified composites even the matrix-small microcapsule (45 μm) bonding is good. The manufacturing issues are, however, controllable once identified. No degradation of NPC fracture toughness is observed in type VII sample even with the high concentration (8wt%) of small microcapsules (average size 45 μm) due to the good matrix-microcapsule bonding as evidenced in figures 6.14 and 6.15 shown before.

Effect of average size of microcapsules on the NPC fracture toughness

The effect of average size of microcapsules on the NPC fracture toughness of modified composites can be extracted by simply comparing the figures 6.11 and 6.13 which is shown in figure 6.18.

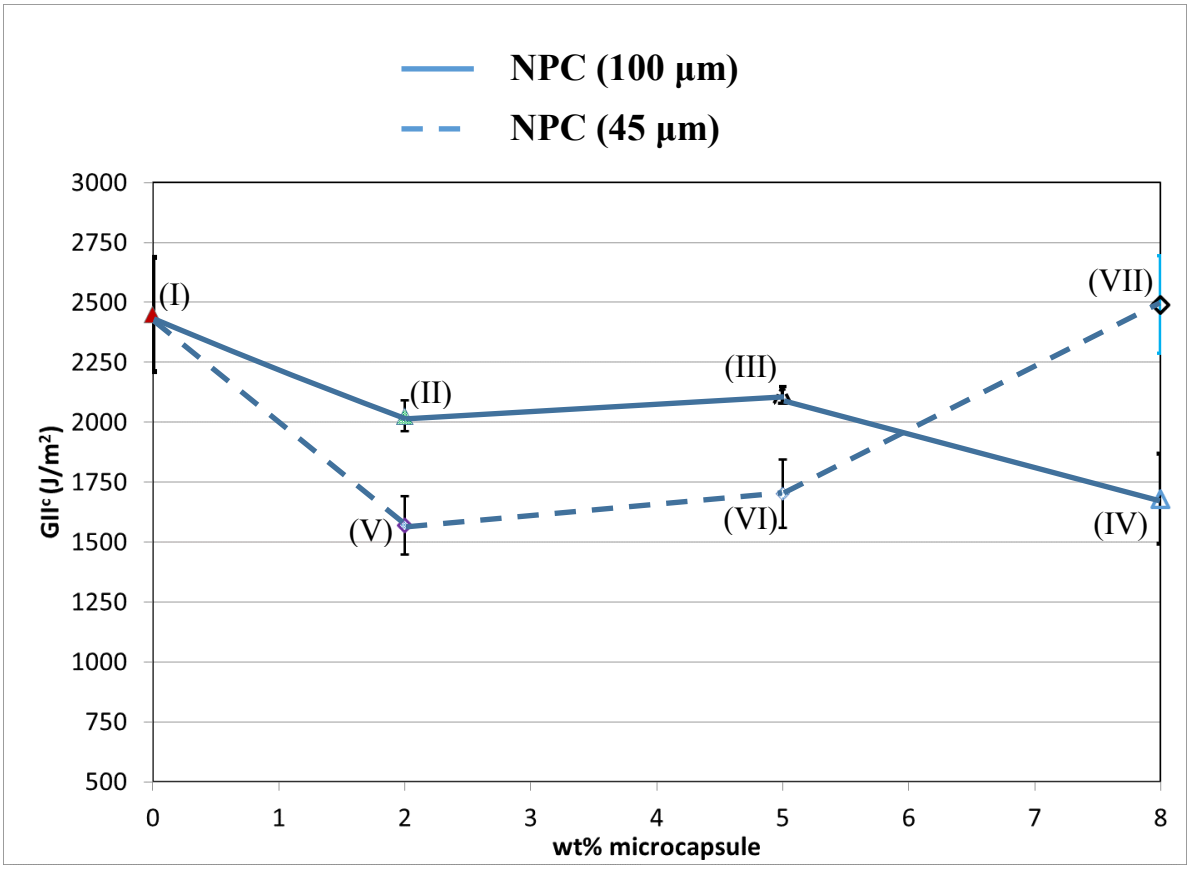

Figure 6.18 Effect of size of microcapsules on the NPC fracture toughness of modified composite samples (Type II-VII). Error bars represent one standard deviation of measured values.

Figure 6.18 shows that incorporation of larger microcapsules (average size 100 µm) reduces the NPC fracture toughness of modified composites (Type II-IV) compared with regular composites (Type I) and it worsens above the concentration of 5 wt% due to the debonding issues of larger microcapsules discussed before. On the other hand, compared with regular composite samples (Type I), significant reduction in NPC fracture toughness is observed with samples type V and VI incorporated with 2wt% and 5 wt% of small microcapsules (average size 45 µm), respectively, due to some manufacturing issues (like accumulation of extra resin incorporated with microcapsules at the NPC crack front of the modified sample during the hand lay-up) discussed before. Once the manufacturing issues are detected and resolved, incorporation of even higher concentration (8 wt%) of small microcapsules does not reduce its NPC fracture toughness. Thus, considering the deterioration of the original fracture toughness (i.e. $\boldsymbol{G^{C}_{II,NPC}}$),

small microcapsules are preferred for their good bonding properties with the matrix as evidenced earlier.

6.4.3 Effect of self-healing on PC fracture toughness of composite samples

Again, as a reminder, PC test is carried out after allowing the naturally occurred crack to be healed (for the modified composite samples) for 24 hours. The regular composite sample (Type I), however, does not have the self-healing ability. Thus, any difference in PC fracture toughness between the Type I and modified composite samples (Type II-VII) is due to the self-healing reaction between the monomer which oozed out from broken microcapsules and the catalyst particles at the natural crack plane of modified composites.

The effects of self-healing on the PC fracture toughness of modified composite samples (Type II-VII) measured at room temperature are discussed below.

Effect of concentration of larger microcapsules (average size 100 μm) on the PC fracture toughness

The values of the PC fracture toughness ($G_{II,PC}^{C}$) of the composite samples (Type I, II, III and IV) as a function of concentration of microcapsules of average size 100 μm are shown in figure 6.19.

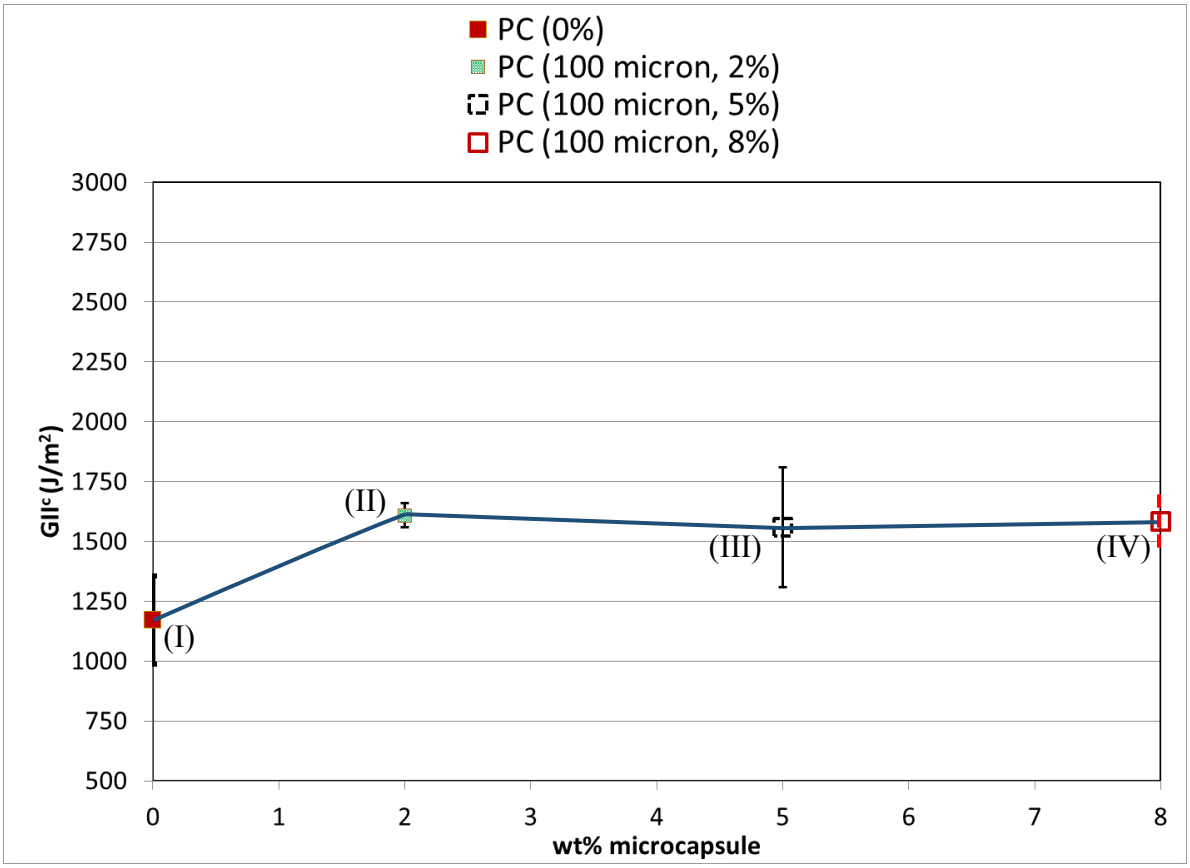

Figure 6.19 PC fracture toughness of composite samples as a function of concentration of microcapsules of average size of 100 µm. Error bars represent one standard deviation of measured values.

Figure 6.19 shows that the values of $G_{II,PC}^{C}$ of modified composite samples of type II, III and IV [containing certain wt% of larger microcapsules (average size 100 µm)] are always greater than the values of $G_{II,PC}^{C}$ of regular composite samples of type I (containing no microcapsules). This first implies that the natural precrack is healed in the modified composite samples incorporated with larger microcapsules. Compared with type I samples, PC fracture toughness is improved by 37% in type II sample, 33% in type III sample and about 35% in type IV sample. In other words, the values of $G_{II,PC}^{C}$ are improved by 37%, 33% and 35% when the composite samples are incorporated with 2wt%, 5 wt% and 8 wt% of larger microcapsules (average size 100 µm), respectively.

Percentage improvement in PC fracture toughness of modified composites due to the self-healing of the natural crack is calculated as

$$\%\ \boldsymbol{imp}._{(\boldsymbol{PC})} = \frac{((G^C_{II,PC})_{\boldsymbol{M}} - (G^C_{II,PC})_R)}{(G^C_{II,PC})_{\boldsymbol{R}}} \times \mathbf{100} \text{ ----------(6.11)}$$

where,

$(G^C_{II,PC})_{\boldsymbol{R}}$---------- PC fracture toughness of regular composite sample (Type I) not incorporated with microcapsules, and

$(G^C_{II,NPC})_{\boldsymbol{M}}$----------PC fracture toughness of modified composite sample (Type II-VII) incorporated with certain wt% of microcapsules.

This improvement of PC fracture toughness of modified composite samples (Type II-IV containing certain wt% of microcapsules of average size 100 μm) compared with regular sample (Type I containing no microcapsules) is the direct contribution of self-healing of the naturally occurred pre-crack. Comparison of SEM micrographs of the fracture surfaces of the regular and modified composites, as shown in figure 6.20 below, show the presence of the self-healed polymer layer which is believed to be formed by the reaction between the monomer oozed out from broken microcapsules and dispersed Gruubs catalyst in the delamination crack plane. Comparison of representative SEM micrographs (as shown in figure 6.20) of the fracture surfaces of the regular and modified composite samples shows the difference in features between the healed (modified) and unhealed (regular) samples.

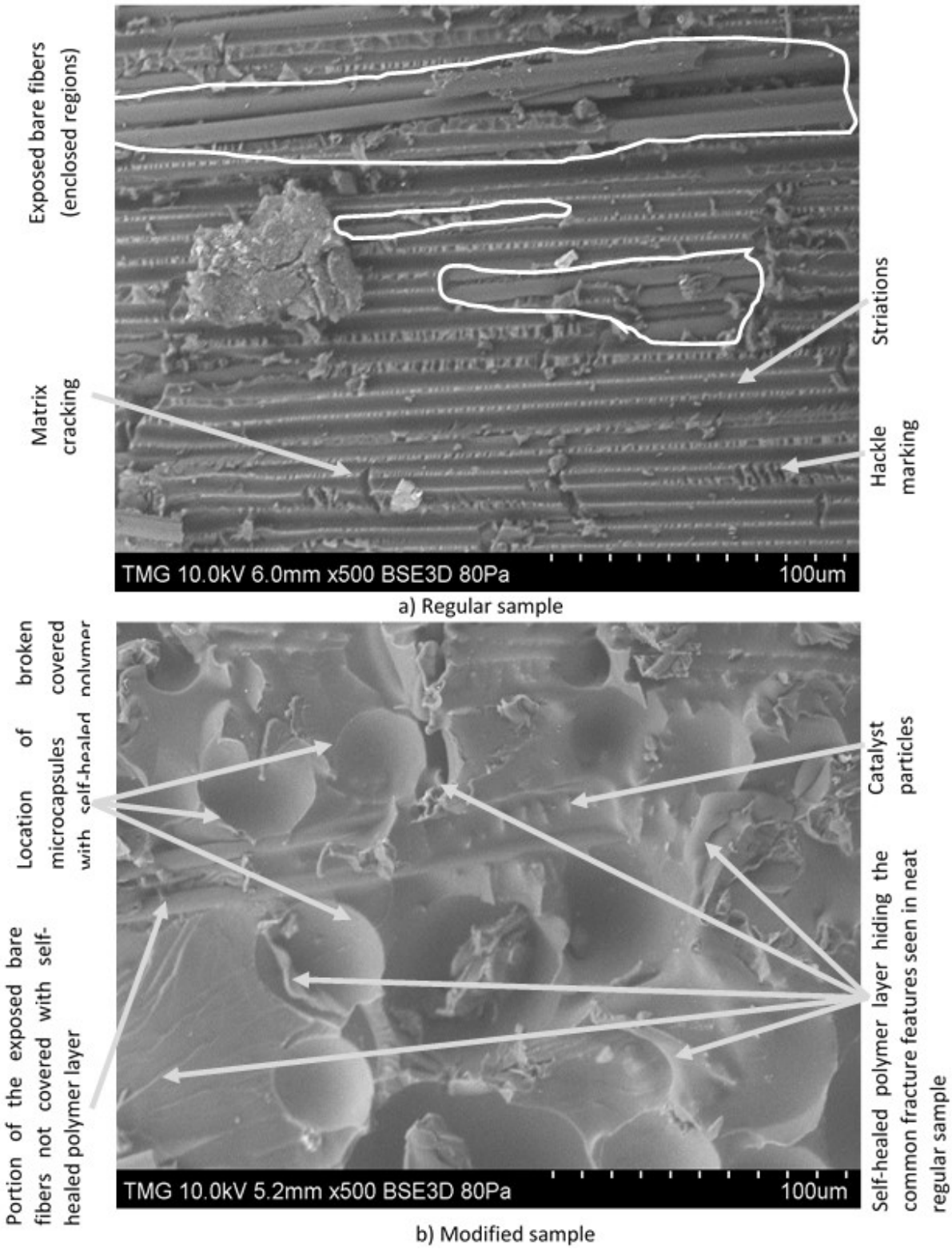

Figure 6.20 Comparison of representative fracture surfaces of (a) regular and b) modified composite samples showing the differences in morphology and appearance between unhealed and healed fracture surfaces.

The differences in morphology and appearance of fracture surfaces of regular and modified composite samples as shown in figure 6.20 indicate clearly the presence of self-healed polymer layers produced by self-healing reaction between the monomers released out of broken microcapsules and the dispersed Grubbs catalyst. Fracture surface of regular (without microcapsules and catalyst) composite sample, as shown in figure 6.20 a), is featured with exposed bare fibers, striations, hackle markings and marks of matrix cracking which are the common mode of fractures for mode II delamination. These markings indicate a combination of adhesive- cohesive failure of regular composite sample. On the other hand, an absence (or limited presence) of these common fracture features is observed on the fracture surface of modified (with microcapsules and catalyst) composite sample. This indicates that the fracture features of mode II delamination (which were observed in regular samples) are mostly covered and hidden by a newly created polymer layer which is the product of self-healing reaction between monomer oozed out of broken microcapsules and Grubbs catalyst. Fracture surface of modified composite sample, as shown in figure 6.20 b), is featured with relatively smooth surface made of self-healed polymer layer with marks of broken microcapsules, abrasion marks and other stress marks indicating mostly cohesive failure. Some portion of the same fibers can also be seen exposed bare while the remaining portion is covered under the self-healed polymer layer. The comparative observation of fracture surfaces of regular and modified composites thus confirms the self-healing of the mode II fracture cracks which effectively translates into superior PC fracture toughness of modified composites compared to regular composites as shown before in figure 6.19.

The improvement in PC fracture performance of modified composites containing larger microcapsules (Type II-IV), however, is not increased proportionally with increasing concentration of microcapsules (average size 100 μm) as can be seen in figure 6.19. Higher concentration of microcapsules means higher number of microcapsules available per unit fracture area which is expected to deliver higher amount of self-healing monomer upon their breaking to cover increased area of the fracture plane resulting in increased PC fracture toughness. However, in reality, the PC fracture toughness of the type II, III and IV samples containing increasing concentration of microcapsules (2wt%, 5wt% and 8 wt%, respectively) remains almost the same as shown in figure 6.19. Debonding of larger microcapsules (average size 100 μm) in modified composites (Type II-IV), as evidenced in figure 6.12 before, which

limits the breaking of sufficient number of microcapsules during crack propagation, again, explains the fact.

Effect of concentration of small microcapsules (average size 45 µm) on the PC fracture toughness

The values of the PC fracture toughness ($G^C_{II,PC}$) of the composite samples (Type I, V, VI and VII) as a function of concentration of microcapsules of average size 45 µm are shown in figure 6.21 below.

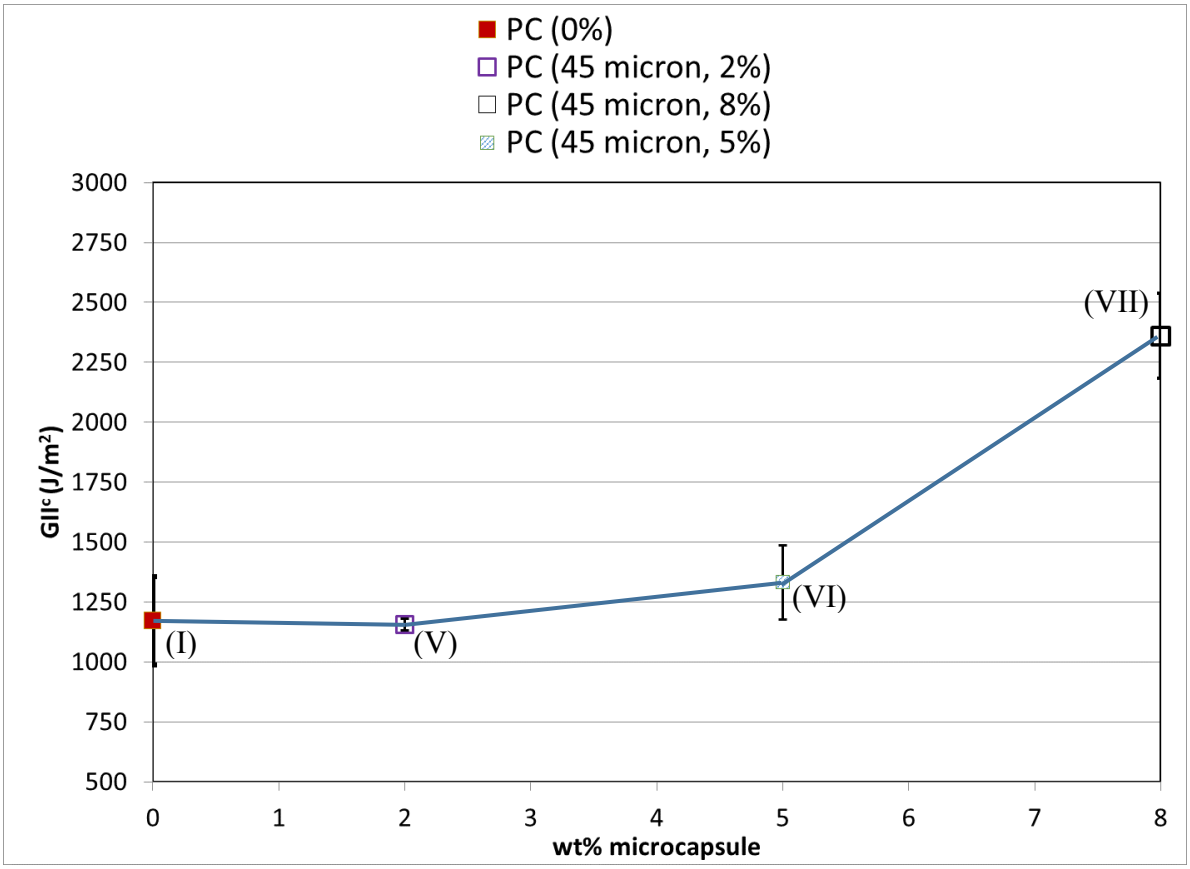

Figure 6.21 PC fracture toughness of composite samples as a function of concentration of microcapsules of average size of 45 µm. Error bars represent one standard deviation of measured values.

Figure 6.21 shows that the values of $G^C_{II,PC}$ of modified composite samples (Type V-VII) tend to be higher than the value of $G^C_{II,PC}$ of regular composite sample (Type I). This first implies that the natural precrack is healed in the modified composite samples. Figure 6.21 also indicates that the values of $G^C_{II,PC}$ of modified composite samples increases with increasing concentration of

small microcapsules. Compared with the value of $G_{II,PC}^{C}$ of regular composite samples of type I, the values of $G_{II,PC}^{C}$ of modified composite samples of type V [containing 2 wt% of microcapsules (average size 45 μm)] does not improve significantly (containing no microcapsules). $G_{II,PC}^{C}$ is, however, improved by 14% with type VI sample and by about 100% with type VII sample as calculated by equation.6.11. In other words, the values of $G_{II,PC}^{C}$ are improved by 0%, 14% and 100% when the composite samples are incorporated with 2wt%, 5 wt% and 8 wt% of small microcapsules (average size 45 μm), respectively. Rule et al. [47] observed that the healing performance of epoxy sample (without fibers) was maximized when sufficient volume of monomer was present to fill the cracks completely. For the fiber reinforced composite samples of type V and VI, in the current work, incorporation of small microcapsules of average size 45 μm does not improve the $G_{II,PC}^{C}$ significantly up to 5wt% because of insufficient coverage of the fracture surface with relatively less number of microcapsules, as shown in the SEM micrograph in figure 6.22 a). Figure 6.22 b), on the contrary, shows the SEM micrograph of the fracture surface of composite sample of type VII (containing 8wt% of small microcapsules of average size 45 μm) showing sufficient number of microcapsules covering the full fracture surface area resulting in 100% improvement in PC fracture toughness which is consistent with the observation of Rule et al. [52].

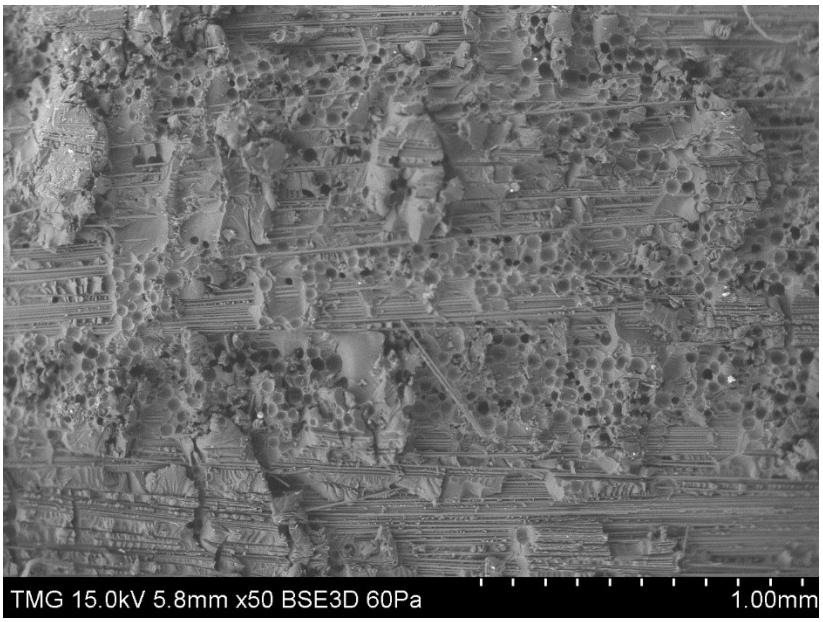

a) Fracture surface of sample type VI (5wt%, 45 µm)

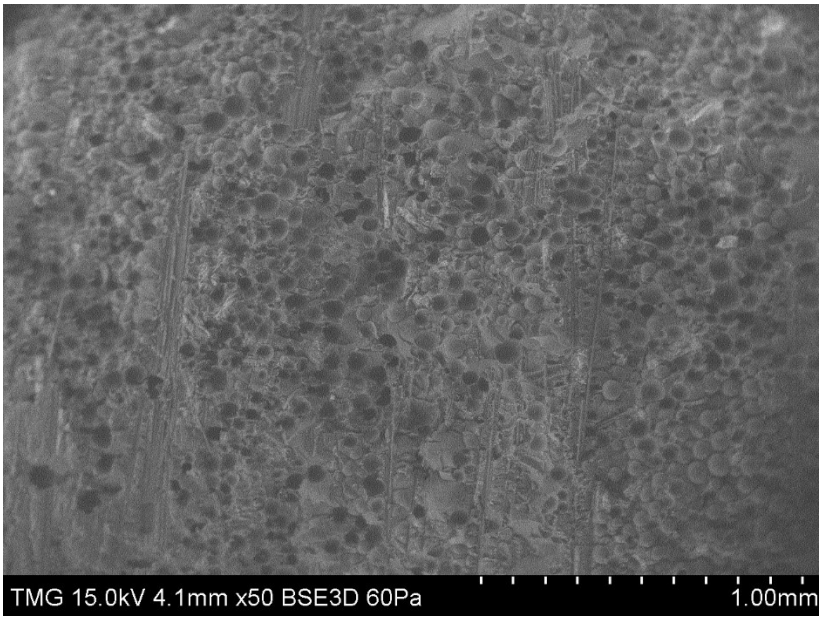

b) Fracture surface of sample type VII (8wt%, 45 µm)

Figure 6.22 SEM micrograph of the fracture surface of composite samples containing a) 5wt%, microcapsules (45 µm) showing insufficient number of microcapsules to cover the full fracture surface area and b) 8wt%, microcapsules (45 µm) showing sufficient number of microcapsules covering the full fracture surface area

Complete coverage of fracture surface with 8wt% small microcapsules (45 µm) together with good bonding with matrix as evidenced in figure 6.22, 6.14 and 6.15 results in excellent

improvement (100%) in $G_{II,PC}^{C}$ (PC fracture toughness) of type VII sample. Figure 6.29 b) further shows that microcapsules are well distributed in the matrix and attached well with it even after their breaking. A substantial number of microcapsules distributed over the fracture surface are also seen broken with the lower portion of their shells still attached to the matrix (black dots in figure 6.22 b). The good matrix-microcapsule bonding and its well distribution over the entire fracture surface enable the breaking of a large number of microcapsules releasing sufficient amount of monomer to cover the entire fracture surface area and subsequent self-healing reaction with dispersed catalyst. This translates into 100% increase in PC fracture toughness of type VII composite samples (containing 8wt% of small microcapsules) compared with regular type I composite samples where no self-healing takes place due to the absence of microcapsules and catalyst.

The self-healed polymer layer on the fracture surface of the modified composite samples can be clearly observed with higher magnification as shown in figure 6.23.

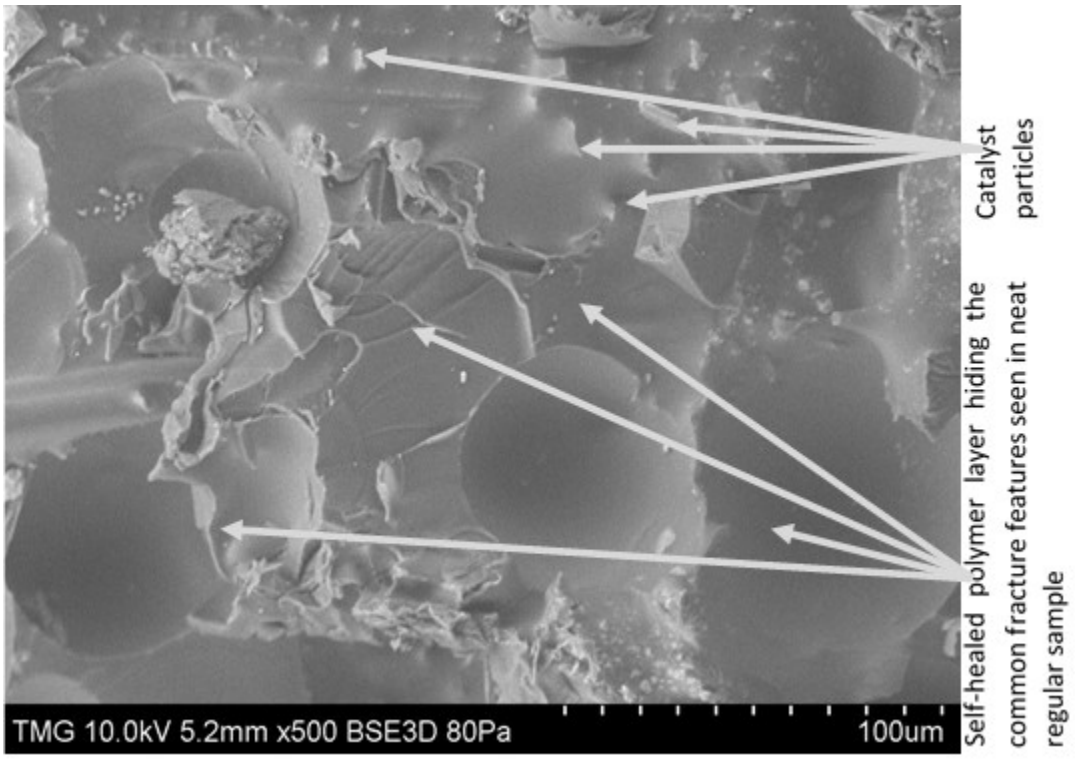

Figure 6.23 SEM micrograph of the fracture surfaces of modified composite sample containing microcapsules of average size 45 µm showing healed polymer layer.

Effect of average size of microcapsules on the PC fracture toughness

The effect of average size of microcapsules on the PC fracture toughness of modified composites can be extracted by simply comparing the figures 6.19 and 6.21 which is shown in figure 6.24.

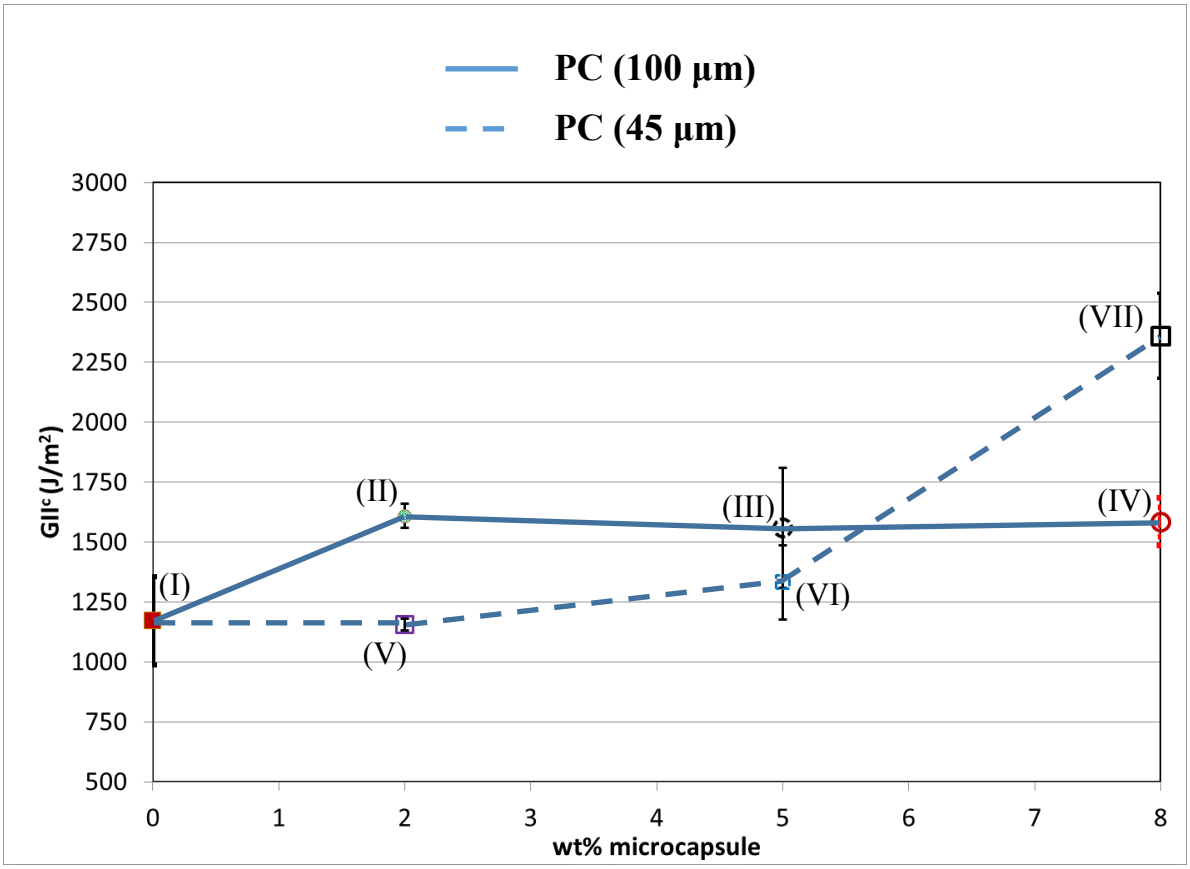

Figure 6.24 Effect of size of microcapsules on the PC fracture toughness of modified composite samples (Type II-VII). Error bars represent one standard deviation of measured values.

From figure 6.24, it can be observed that, up to the concentration of 5wt%, modified composite samples containing larger microcapsules (type II and e III) have better PC fracture toughness compared with samples containing small microcapsules (type V and VI). However, the highest PC fracture toughness is achieved by the samples containing higher concentration (8wt%) of small microcapsules (type VII). This phenomenon can be explained by the fact that larger microcapsules being able to release relatively higher volume of monomer upon their breaking can cover larger area of the crack surface than small microcapsules in the low concentration range (up to 5 wt%). However, because of the debonding nature of larger

microcapsules, increased concentration of larger microcapsules beyond 5wt% does not result in breaking of sufficient number of microcapsules to release proportionately increased amount of monomer to cover the entire crack surface area. On the other hand, small microcapsules up to 5wt% cannot deliver sufficient amount of monomer upon their breaking to cover the entire crack surface area. However, as they bond well with the matrix, increased concentration up to 8wt% of small microcapsules results in breaking of increased number of microcapsules during crack propagation releasing increased amount of monomer to cover the entire crack surface area. This results in much better PC fracture toughness of type VII sample than type IV sample as shown in figure 6.24.

In summary, it is observed through the investigation that drastic deterioration of NPC fracture toughness can be caused by issues related to manufacturing of modified composites. These are, however, more easily controllable once identified. The other key factor that mostly affect the NPC fracture toughness is the debonding of microcapsule during the crack propagation. On the other hand, PC fracture toughness is mainly dependent upon the availability of self-healing monomer over the entire fracture surface which, ultimately, depends on the distribution of microcapsules and their ability to break during crack propagation. The ability of breaking of microcapsules, in turn, depends on the matrix-microcapsule bonding. In addition to deteriorating the NPC fracture toughness, debonding of microcapsules also restricts the breaking of sufficient number of microcapsules during crack propagation. The microcapsules debond, in such case, rather than break, which in turn, limits the availability of sufficient monomer over the entire fracture surface area restricting self-healing.

It is further observed from the investigation that larger microcapsules (average size 100 μm) tend to debond from the matrix. Debonding of larger microcapsules during the mode II crack propagation deteriorates both the NPC fracture toughness and limits self-healing leading to reduced PC fracture toughness. Due to this debonding, again, increasing the concentration of larger microcapsules in the composites does not supply proportionately increased amount of monomer over the fracture surface to achieve higher PC fracture toughness. Smaller microcapsules (average size 45 μm), on the contrary, can be smeared into the matrix more efficiently possibly due to their smaller individual surface area and are observed to have good bonding with the matrix which results in excellent self-healing performance at high microcapsule concentration (8 wt%). There was no deterioration in NPC fracture toughness and excellent

improvement in PC fracture toughness was achieved at this high concentration (8 wt%) of small microcapsules. As stated earlier, the size, size distribution, morphology and shell thicknesses of the microcapsules, which are shown to be different for larger and smaller microcapsules. as investigated in the current work and discussed in chapter 3, might have significant effects on the matrix-microcapsule bonding and requires more research works to understand their behavior. The modified composites containing lower concentration (2wt% and 5 wt%) of small microcapsules, however, did not possess acceptable NPC fracture toughness due to some manufacturing issues discussed earlier as well as show unattractive PC fracture toughness due to the lack of sufficient coverage of the fracture surface by lower concentration of small microcapsules.

6.5 Comparison of fracture toughness and evaluation of healing performance of the composites

In this section, NPC and PC fracture toughness of each type of composite samples (I-VII) are compared. The conventional healing efficiency, $\eta_{h,c}$ and healing performance index PI as defined in equations 5.2-5.5 (in chapter 5) are also evaluated and compared. The comparison proves the rational for choosing PI instead of $\eta_{h,c}$ as the better indicator of actual healing performance. Using the, values of PI, the type of composite samples showing the best healing performance can be identified accurately. The findings from this investigation of self-healing of FRP composites at room temperature are utilized in investigating self-healing of FRP composites at low temperature which is discussed in chapter 7.

Figure 6.25 shows the comparison of NPC and PC fracture toughness of composite samples of type I-IV as a function of concentration of microcapsules of average size 100 μm.

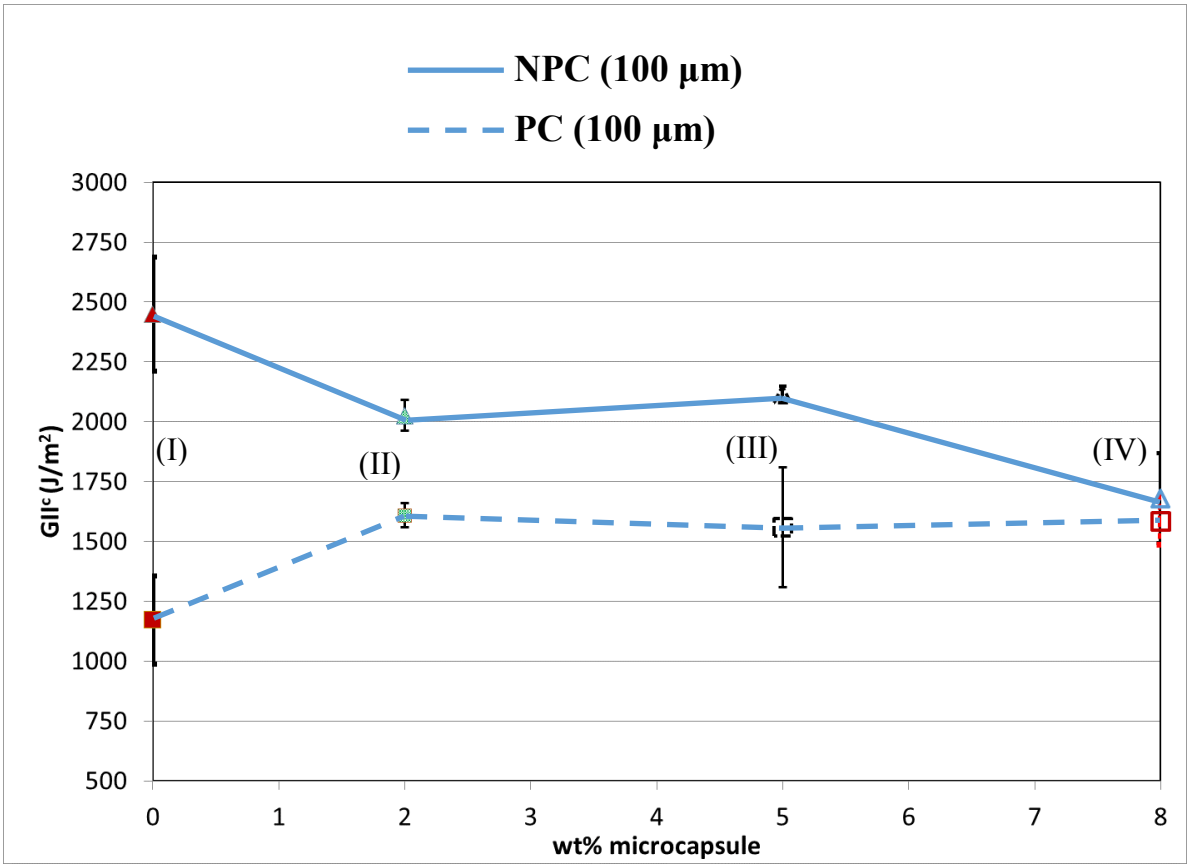

Figure 6.25 Comparison of NPC and PC fracture toughness of composite samples as a function of concentration of microcapsules of average size of 100 µm. Error bars represent one standard deviation of measured values.

The percentage changes (improvement or deterioration) in fracture toughness values in different modified composites (Type II, III and IV) compared to regular composites (Type I) as calculated by equations (6.10) and (6.11) are shown in table 6.3. The corresponding values of $\eta_{h,c}$ and *PI* are also indicated in the table.

Table 6-3. Comparison of changes in fracture toughness of modified composites (Type II, III and IV) compared with regular composites (Type I) containing no microcapsules

Changes in fracture toughness (%)	Type of modified composite samples			Causes of change
	II (2wt%, 100 μm)	III (5wt%, 100 μm)	IV (8wt%, 100 μm)	
% $\boldsymbol{red}_{.(NPC)}$	17	14	31	Debonding of microcapsules
% $\boldsymbol{imp}_{.(PC)}$	37	33	35	Self-healing reaction
$\eta_{h,c}$ (%)	79	74	94	-
PI (%)	17	17	1	-

Figure 6.26 compares the corresponding values of $\eta_{h,c}$ and PI for the three types of modified composite samples (Type II, III and IV) containing larger microcapsules of average size of 100 μm.

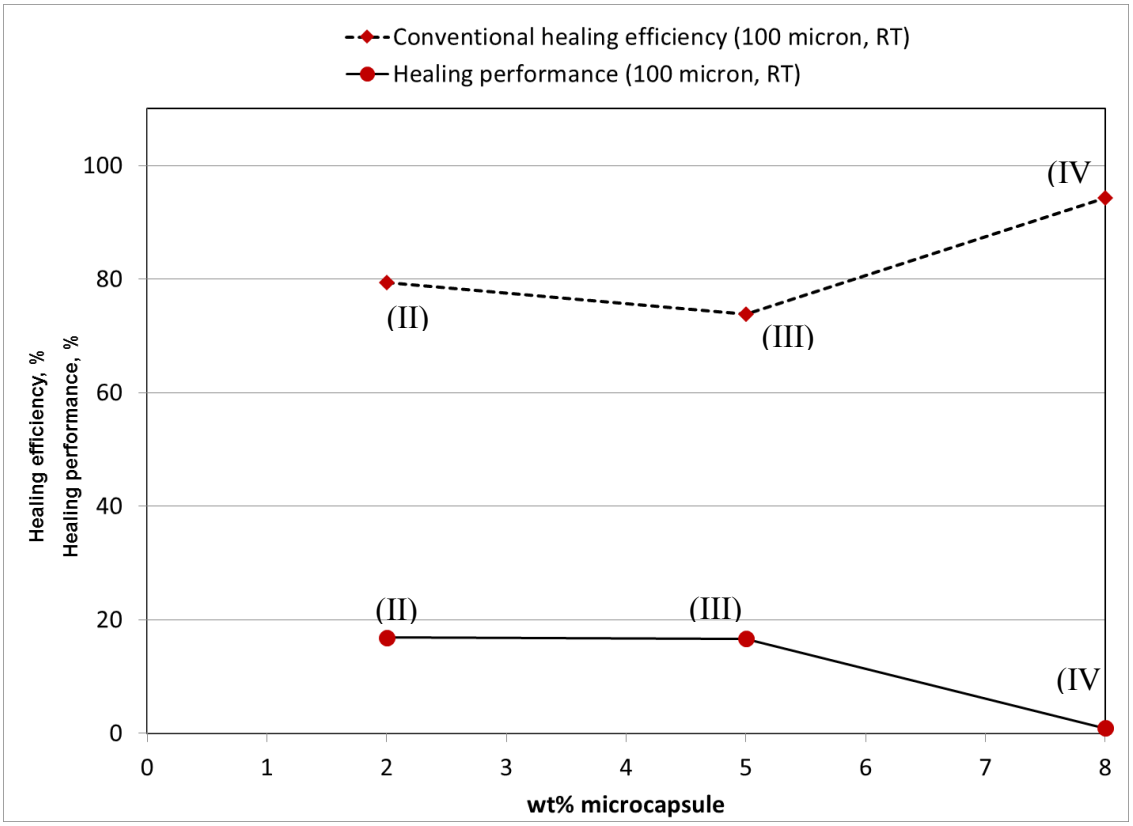

Figure 6.26 Comparison of conventional healing efficiency and healing performance index of modified composite samples as a function of concentration of microcapsules of average size of 100 μm.

Figure 6.26 shows that type II samples have high value of $\eta_{h,c}$ (about 80%) although incorporation of 2wt% larger microcapsules (100 μm) into the samples reduced the value of $G_{II,NPC}^{C}$ by 17% and improved the value of $G_{II,PC}^{C}$ by only 37% compared with regular type I sample as can be seen in table 6.3. PI, on the contrary, takes into account both information of the reduction of $G_{II,NPC}^{C}$ and the improvement of $G_{II,PC}^{C}$ of type II sample to give a realistic value of only about 17%. Type III samples show similar values of $\eta_{h,c}$ and PI as in the previous case. Interestingly, for the type IV composite sample for which the value of $G_{II,NPC}^{C}$ is further worsen by 31% while having the similar improvement in the value of $G_{II,PC}^{C}$ of only 35% compared to regular type I sample, as can be seen in table 6.3, the value of $\eta_{h,c}$ increases oppositely up to about 94% (see figure 6.26). This is, indeed, a wrong indication given by the value of conventional healing efficiency $\eta_{h,c}$. Healing performance index, PI, on the other hand, takes this reduction of the value of $G_{II,NPC}^{C}$ into account correctly, and correspondingly lowers its value near to 0% as can be seen in figure 6.26 for the type IV sample . PI thus gives realistic and reliable values of actual healing performance. The comparison in figure 6.26 thus proves the rational for choosing PI instead of $\eta_{h,c}$ as the better indicator of actual healing performance.

Similarly, figure 6.27 shows the comparison of NPC and PC fracture toughness of composite samples of type I, V, VI and VI as a function of concentration of microcapsules of average size 45 μm.

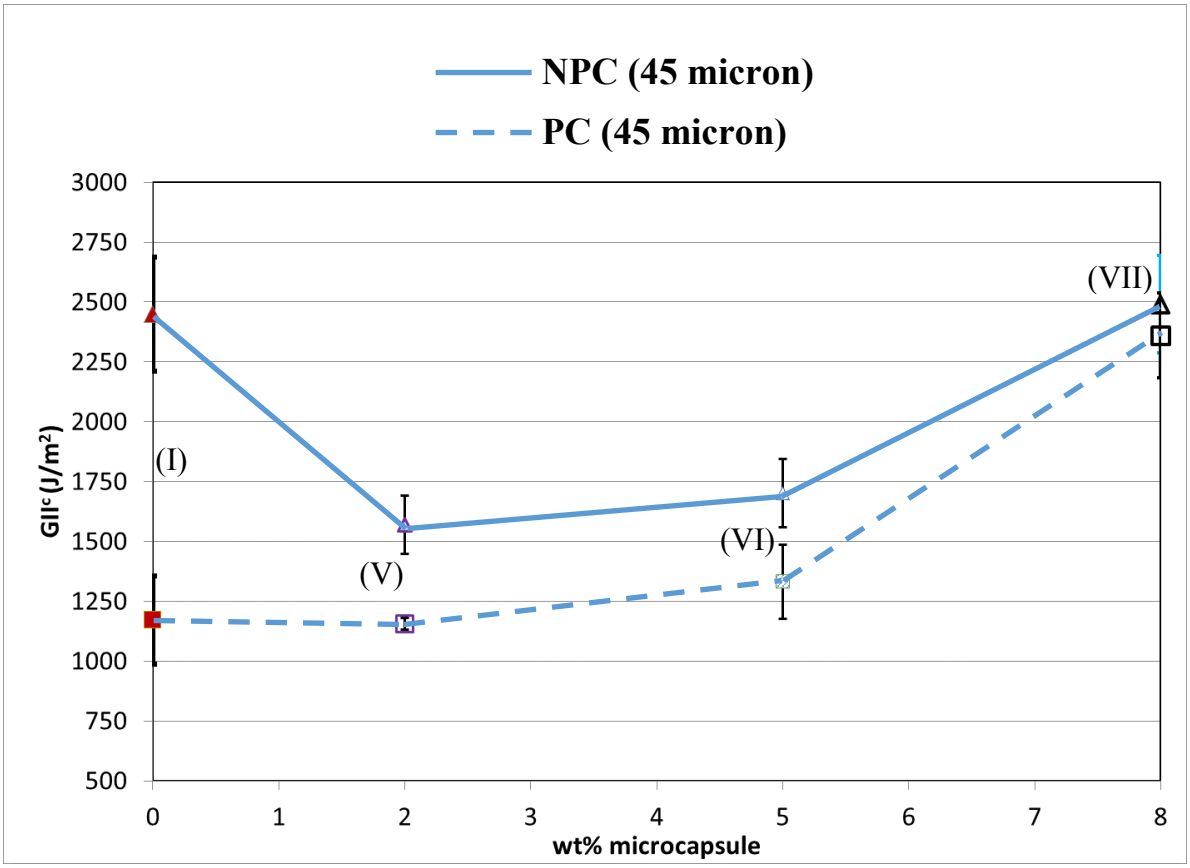

Figure 6.27 Comparison of NPC and PC fracture toughness of composite samples as a function of concentration of microcapsules of average size of 45 µm. Error bars represent one standard deviation of measured values.

The percentage changes (improvement or deterioration) in fracture toughness values in different modified composites (Type V, VI and VII) compared to regular composites (Type I) as calculated by equations (6.10) and (6.11) are shown in table 6.4. The corresponding values of $\eta_{h,c}$ and *PI* are also indicated in the table.

Table 6-4. Comparison of changes in fracture toughness of modified composites (Type V, VI and VII) compared with regular composites (Type I) containing no microcapsules

Changes in fracture toughness (%)	Types of composite samples			Causes of change
	V (2wt%, 45 μm)	VI (5wt%, 45 μm)	VII (8wt%, 45 μm)	
% $\boldsymbol{red.}_{(NPC)}$	35	30	0	Manufacturing issues
% $\boldsymbol{imp.}_{(PC)}$	0	14	100	Self-healing reaction
$\eta_{h,c}$ (%)	74	78	95	-
PI (%)	-37	-18	95	-

Figure 6.28 compares the corresponding values of $\eta_{h,c}$ and PI for the three types of modified composite sample (Type V, VI and VII) containing small microcapsules of average size of 45 μm.

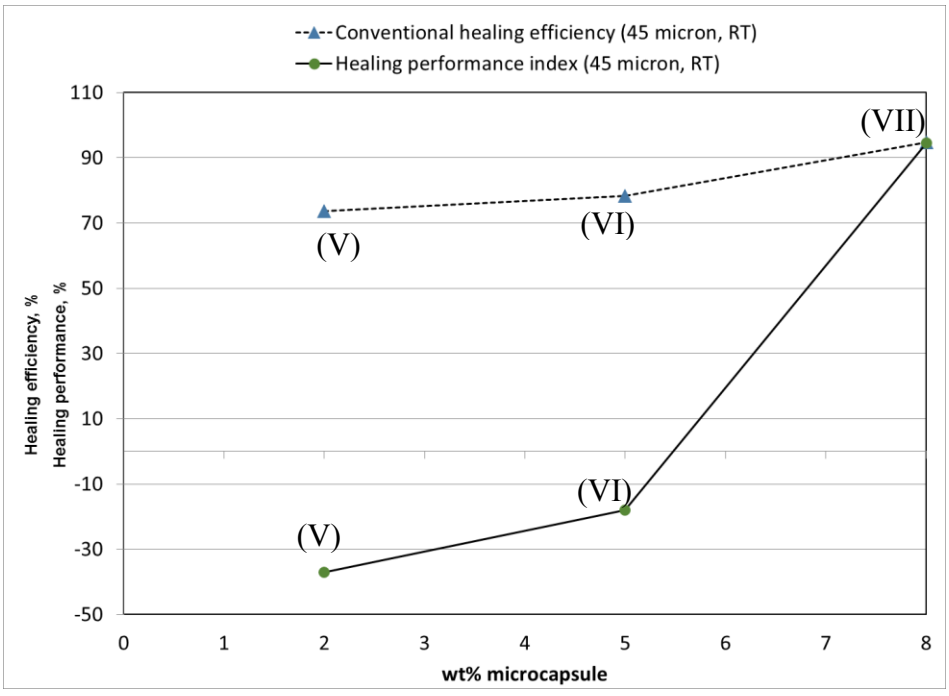

Figure 6.28 Comparison of conventional healing efficiency and healing performance index of composite samples as a function of concentration of microcapsules of average size of 45 μm.

Figure 6.28 shows that type V samples have high value of $\eta_{h,c}$ (about 73%) although incorporation of 2wt% smaller microcapsules (μm) reduced the values of $G_{II,NPC}^{C}$ by 35% and, even, there is no improvement in $G_{II,PC}^{C}$ compared with regular type I sample as can be seen in table 6.4. PI, on the contrary, takes both of this information into account and gives a negative value of about -37%. The negative value of PI gives a warning that there is more degradation of $G_{II,NPC}^{C}$ due to incorporating microcapsules than any improvement of $G_{II,PC}^{C}$ achieved due to self-healing. A negative value of PI, thus, tells us that there is no real advantage of incorporating microcapsules into composites in such case. $\eta_{h,c}$ does not give such warning and always gives a positive value indicating a good advantage of incorporating microcapsules even for the type V sample. Healing performance index,PI, thus again proves to be a better indicator of actual healing performance in such case. Type VI samples show similar values of $\eta_{h,c}$ and PI as in the previous case. For the type VII samples, the value of $G_{II,NPC}^{C}$ is not reduced compared with type I samples and the value of its $G_{II,PC}^{C}$ closely matches the value of $G_{II,PC}^{C}$ of type I sample as can be seen in table 6.4 and figure 6.27. In such case only, both $\eta_{h,c}$ and PI give close values of about 94% (see figure 6.28). In most other likely situations, $\eta_{h,c}$ gives exaggerated values as shown in the above examples and as discussed in more detail in chapter 5. Thus, in every likely situations, healing performance index, PI gives a reliable and better indication of actual healing performance of composite samples compared to conventional healing efficiency, $\eta_{h,c}$.

Among the types of composite samples tested that showed the best healing performance, thus, can easily be detected just by comparing the PI values of each type of modified composite samples. Figure 6.29 below shows the comparison of PI values (%) of all types of modified composite samples (Type II-VII) tested at room temperature.

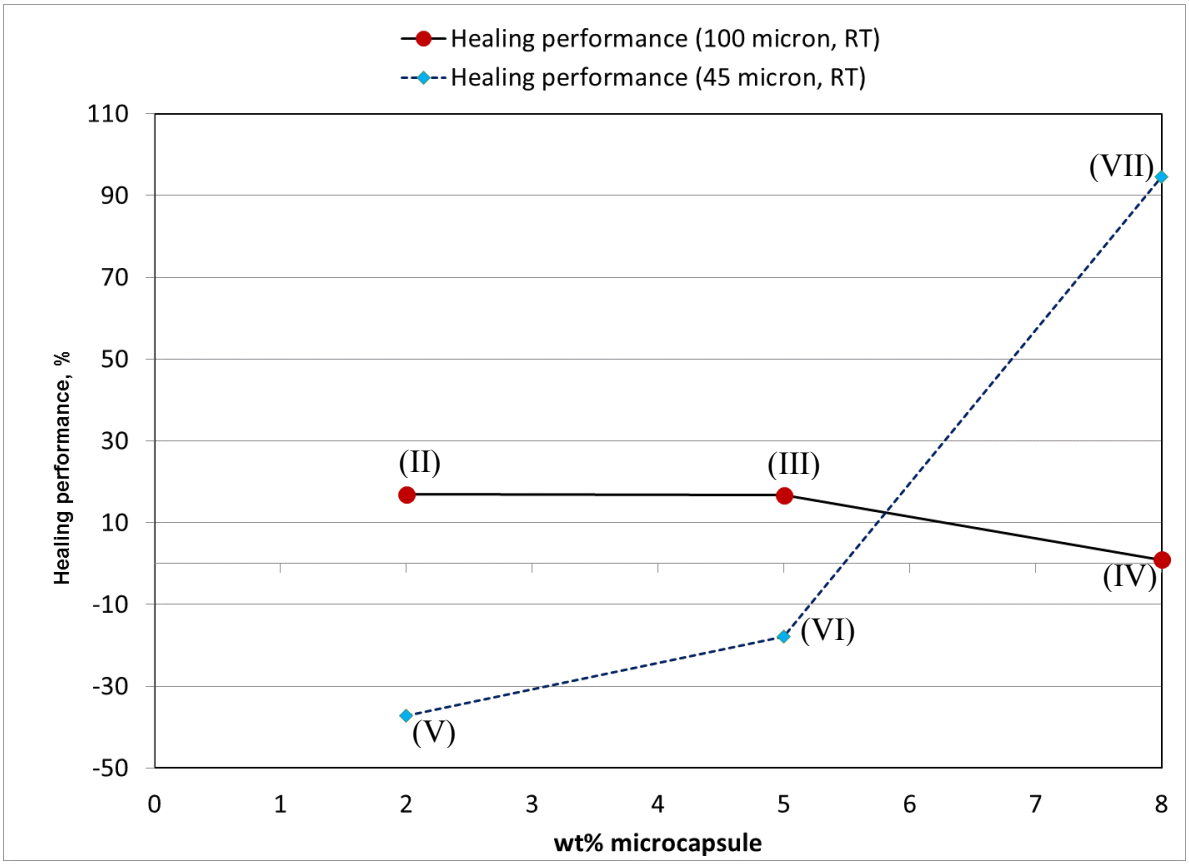

Figure 6.29 Comparison of healing performance index (%) of all modified composite samples (Type II-VII) tested at room temperature

Studying figure 6.29, it can be concluded that, among the modified composite samples tested at room temperature, type II and type III samples containing larger microcapsules (average size 100 μm) show better healing performance at room temperature with low concentration up to 5 wt%. However, the best healing performance at room temperature is achieved by type VII samples containing small microcapsules (average size 45 μm) with higher concentration of 8wt%. This phenomenon can be explained by the fact that larger microcapsules being able to release higher volume of monomer upon their breaking can cover larger area of the crack surface than small microcapsules. However, because of the debonding issues, increased concentration of larger microcapsules beyond 5wt% does not result in breaking of sufficient number of microcapsules to release proportionately increased amount of monomer to cover the entire crack surface area. Additionally, increased concentration of larger microcapsules degrades the original NPC fracture toughness of composites due to debonding nature reducing the healing performance. On the other hand, NPC fracture toughness of the composites containing 2wt% and

5wt% of small microcapsules of average size 45 μm (Type V and VI) was drastically reduced by some manufacturing issues which was resolved later for samples with higher concentration (8wt%). Further, small microcapsules up to 5wt% cannot deliver sufficient amount of monomer upon their breaking to cover the crack surface area. However, as they bond well with the matrix, increased concentration up to 8wt% of small microcapsules does not degrade the original NPC fracture toughness of composites while being capable of releasing increased amount of monomer to cover the crack surface area. This results in excellent healing performance at relatively higher concentration of small microcapsules. Thus, for best healing performance, composites should be incorporated with relatively high concentration (8wt%) of small microcapsules of average size of 45 μm.

6.6 Conclusions

Investigation of self-healing at room temperature is carried out with different types of FRP composite samples containing varying percentage of microcapsules with different average sizes. Two average sizes (100 μm and 45 μm) and three different concentrations (2wt%, 5wt% and 8wt%) of microcapsules are selected to investigate their effect on self-healing performance of FRP composite. Self-healing performance is evaluated by measuring the NPC and PC fracture toughness of the composite samples according to ASTM D7905/D7905M. The values of NPC fracture toughness are obtained by propagating a delamination from the pre-implanted insert in the composite sample. The values of PC fracture toughness, on the other hand, are determined by propagating the natural precrack (allowed to heal beforehand) that is created during the NPC test. Larger microcapsules (average size 100 μm) are found to debond from the matrix more easily during the mode II fracture. This limits the self-healing performance of composites containing larger microcapsules. Debonding of microcapsules affects both the NPC fracture toughness and the PC fracture toughness of modified composites. Increasing the concentration of larger microcapsules up to 8 wt% did not help in achieving high PC fracture toughness post healing at room temperature. Rather, increased concentration of larger microcapsules degrades the base NPC fracture toughness significantly due to the debonding of larger microcapsules as evidenced in SEM micrographs. On the contrary, smaller microcapsules (average size 45μm) are shown to form good bonding with the matrix leading to excellent improvement of PC fracture toughness post healing at room temperature while not deteriorating the NPC fracture toughness at high concentration (8 wt%) of microcapsules. Care should, however, be taken in manufacturing

modified composites so that the microcapsules does not preferentially accumulate at a preferred site which might weaken the crack-front to reduce the original NPC fracture toughness.

Self-healing performance is evaluated by calculating both conventional healing efficiency $\eta_{h,c}$ and healing performance index PI as defined in chapter 2. $\eta_{h,c}$ is found to give exaggerated values in many instances while PI is found to give reliable values better indicating the actual healing performance of modified composites taking into account the likely degradation and improvement of NPC and PC fracture toughness compared to regular composites containing no microcapsules. The best healing performance at room temperature is obtained with FRP composite sample containing 8wt% of microcapsules of average size 45 μm.

The investigation of self-healing of FRP composites is also carried out in a low temperature set up to understand the effect of low temperature on self-healing performance and the results are discussed in chapter 7.

CHAPTER 7

Investigation of Self-healing of FRP Composites at Low Temperature

7.1 Introduction

Structures and parts made of fiber reinforced polymer (FRP) composites are often subjected to low temperature in service. For example, external key structures and parts like the fuselage, wings and rotor blades of modern air planes and helicopters made of FRP composites are subjected to cold temperatures (-40^{o}C to -60^{o}C) at cruising altitudes during in-flight operations. These air vehicles also often stay in mild cold temperatures in runways and tarmacs for a considerable time in colder regions on earth where the environment temperature remains as low as -40^{o}C and less, especially, during the winter seasons. Further, after the inflight operations at high altitude, the air vehicles land in warmer environments thus might be subjected to thermal cycling. Modern satellites and their components made of FRP composites are also exposed to extreme cold (down to -150^{o}C) conditions and again return to extreme hot (up to +150^{o}C) conditions during their orbiting in space. It is thus interesting to investigate the effect of low temperatures as well as effect of thermal cycling on self-healing of composites. The current work explores the effect of thermal cycling on self-healing of unreinforced epoxy samples and investigates in detail the effect of mild low temperature (-40^{o}C) on the self-healing of FRP composites.

The reason for choosing the value of the low temperature at -40^{o}C for investigation of self-healing of FRP composites lies in making a balance between limitations imposed by the thermal properties of the healing agents (i.e., the monomers and catalyst used) used and the fact that it nearly represents the actual conditions in earth atmosphere. The thermal shock investigation of epoxy (without fiber), however, is done in wider temperature range (-196^{o}C to 120^{o}C) representing space conditions as it suits the requirement of self-healing.

7.2 Limitations of healing agents at low temperature and choice of suitable catalyst

The healing agents used for investigating self-healing at room temperature in this study are 5E2N and Grubbs catalyst first generation. 5E2N remains functional at a much wider temperature range compared to DCPD. However, it has a freezing point near -80ºC [93]. That means, around this temperature liquid 5E2N gets frozen and loses its ability to flow which is a key requirement for self-healing to take place. Thus, on principle, self-healing cannot take place with 5E2N if the working temperature remains fixed around -80ºC and below. This is the material limitation imposed by the monomer used in this study. Another material limitation, observed in this study, was imposed by the other healing agent, i.e. the first generation Grubbs catalyst, (G1) at low temperature. A simple experiment was carried out to reveal this limitation. In this experiment, some liquid 5E2N monomer was first taken into a scintillation vial (vial #1) and kept inside a covered chamber full of dry ice (the temperature inside the box was measured to be around -40ºC) for 2 hours. Similarly, a pinch amount of first generation Grubbs catalyst was taken into another scintillation vial (vial #2) and kept inside the dry ice chamber. After 2 hours, liquid 5E2N from vial #1 was poured into vial #2, hand shaken and immediately put back into the dry ice chamber. The 5E2N/G1 mixture was then kept in the dry ice chamber for 24 hours. Interestingly, the mixture was observed to be liquid even after 24 hours which implies that no self-healing reaction took place between 5E2N and G1 at a temperature of -40ºC in 24 hours. When the same experiment was carried out, but with second generation Hoveyda-Grubbs catalyst (HG2) this time, the mixture (of 5E2N and HG2) kept at -40ºC was found to be polymerized when observed after 24 hours. It is noteworthy to mention that when the liquid 5E2N was mixed with G1 or HG2 in a scintillation vial at room temperature, it started reaction, got polymerized and became solid within few seconds. In order to understand this behavior, the mechanism of self-healing reaction between the monomer and the Grubbs catalyst needs to be understood.

7.2.1 Understanding the mechanism of self-healing reaction between 5E2N and Grubbs catalyst

The self-healing reaction that takes place between the 5E2N monomer (similarly as DCPD) and Grubbs catalyst, is essentially a Ring Opening Metathesis Polymerization (ROMP) reaction.

ROMP is a chain growth polymerization process where a mixture of cyclic olefins is converted to a polymeric material as demonstrated in figure 7.1 [112].

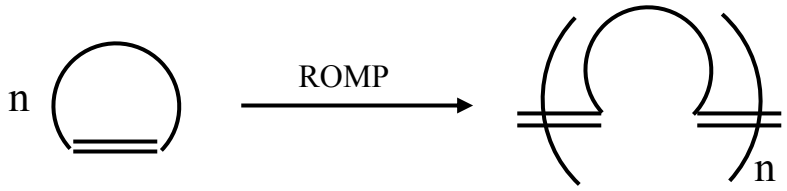

Figure 7.1 A generalized example of ROMP reaction [112]

The mechanism of the polymerization is based on olefin metathesis, a unique metal-mediated carbon-carbon double bond exchange process. As a result, any unsaturation associated with the monomer is conserved as it is converted to polymer. This is an important feature that distinguishes ROMP from typical olefin addition polymerization (e.g. ethylene-polyethylene). The reaction is driven from monomer to polymer by the release of strain associated with the cyclic olefin (ring strain) balanced by entropic penalties [112].

Similarly, cyclic olefins with high ring strain, such as 5-ethylidene-2-Norbornene (5E2N), is suitable for ROMP as shown in figure 7.2, even, at low temperature.

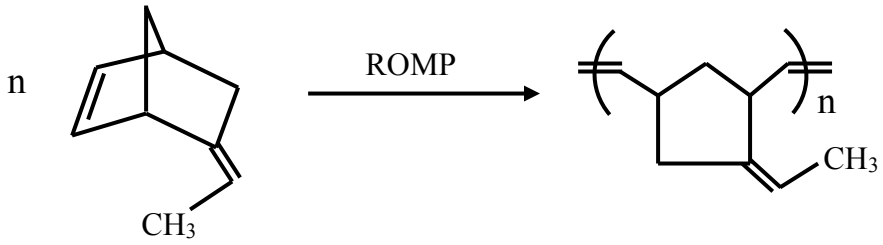

5-ethylidene-2norbornene (5E2N) Poly (5E2N)

Figure 7.2 Ring Opening Metathesis Polymerization of 5E2N

The temperature, however, has significant influence on the activity of catalyst that initiates the ROMP reaction by opening up the cyclic ring of the olefin releasing its ring strain. A number of transition metal alkylidene complexes based on tungsten and molybdenum metals are capable of catalyzing the metathesis of olefins. However, it is the ruthenium based alkylidene complexes which has found widespread applications in polymer and organic chemistry as a catalyst including for the ROMP of cyclic olefins. Ruthenium based Grubbs catalysts exhibits high

tolerance to most functional groups, relatively thermally stable and possess ease of handling characteristics due to its stability in air and moisture. [112]

In order to understand the effect of temperature on the reactivity of Grubbs catalyst in ROMP of cyclic olefins, it is necessary to understand the chemical structure of the catalyst and how it takes part in the ROMP reaction. Grubbs catalysts are based on a ruthenium atom surrounded by five ligands and can generally be written as (L) (L') X2 Ru=CHR, where L and L' are two neutral electron donating entities (e.g. tryalkylphosphines), X2 are the two mono-anionic groups (e.g halides) and one alkylidene moiety (e.g. substituted methylidenes, =CHR) [113]. Ligands play a key role in stabilizing and activating the central metal atom [114]. For example, phosphine ligands in the first generation Grubbs catalyst has profound impact on the reaction initiation [112]. Besides the neutral ligands, the nature of the halide and alkylidene ligands also has an impact on the catalyst initiation rate [113].

ROMP of cyclic olefins proceeds broadly in two stages. The first stage is the initiation or activation of reaction. The second stage is the propagation or chain growth reaction stage. The general accepted mechanism of metal-mediated ROMP is shown in figure 7.3.

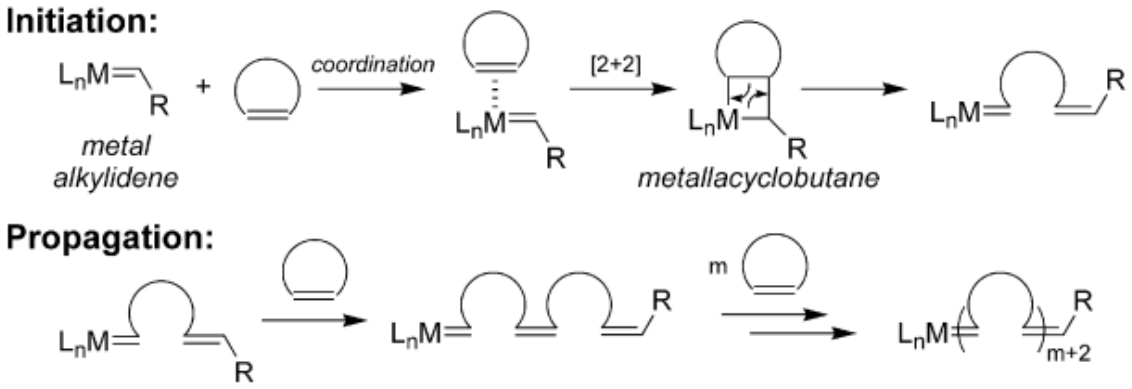

Figure 7.3 A general mechanism to a typical ROMP reaction [112]

At the beginning, the metal alkylidene remains inactive until it comes into contact with a cyclic olefin. In the presence of a cyclic olefin (with some ring strain such as 5E2N), a coordination reaction activates the catalyst by forming a coordination complex. The coordination metal complex then undergoes a [2+2] cycloaddition reaction to form an intermediate metallacyclobutane. This intermediate then undergoes a cycloreversion reaction which opens up the ring of the olefin and a new metal alkylidene forms as shown in the initiation step in 7.4. The

reactivity of this newly formed metal alkylidenes remains similar to that of the initiator and, thus, the analogous steps are repeated during the propagation stage until polymerization ceases (i.e. all monomer is consumed, a reaction equilibrium is reached or the reaction is terminated) [112]. As an example, the chemical structure of the first generation Grubbs catalyst is shown in figure 7.4. [115]

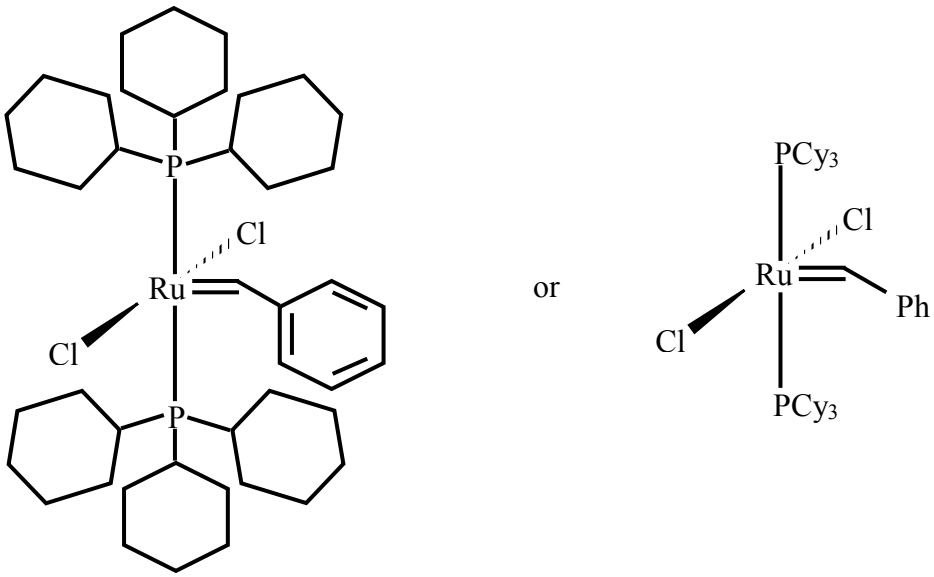

Figure 7.4 Chemical structure of first generation Grubbs catalyst containing two neutral phosphines, two chlorides and one benzylidene ligands [115]

First generation Grubbs catalyst is a five coordinated ruthenium alkylidene which contains two neutral phosphine ligands, two chloride ligands and one benzylidene ligand as shown in figure 7.4. This five coordinated form of the Grubbs catalyst remains inactive until it comes into contact with a cyclic olefin. It was determined that the mechanism to the olefin metathesis reaction with the catalyst was dissociative in nature. Thus, one of the phosphine ligands of the first generation Grubbs catalyst must separate from the inactive five coordinated form of the catalyst before olefin coordination (and subsequent reaction) may occur [115] as shown previously in the general mechanism to ROMP in figure 7.3. The scheme is also shown in figure 7.5 [116] below for the phosphine containing Grubbs catalyst systems.

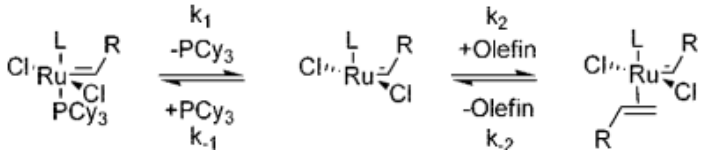

Figure 7.5 Scheme for ROMP with Grubbs catalyst showing phosphine dissociation and olefin binding steps during coordination and subsequent metathesis [116]

Thus the first step of the ROMP reaction of olefins (e.g. 5E2N) with first generation Grubbs catalyst involves dissociation of the bound PCy_3 in the inactive five coordinated form of the catalyst to form the active four coordinated intermediate. This intermediate can be trapped by free PCy_3 to generate the starting inactive alkylidene or bind an olefin substrate during the coordination reaction and undergo subsequent metathesis as shown in figure 7.5 [116]

The activity of first generation Grubbs catalyst therefore depends not only on phosphine dissociation but also on the ratio of the rate of phosphine reassociation (k-1) and the rate of olefin binding (k2). While phosphine dissociation occurs rapidly at room temperature in first generation Grubbs catalyst, it is the ratio k-1/k2 which determines whether the four coordinated intermediate returns to the inactive five coordinated form or binds to the olefin [116]. Phosphine dissociation, which is a requirement to provide active catalyst for ROMP, is slow at low temperatures and, therefore, first generation Grubbs catalyst (together with other phosphine containing catalysts) suffer from decreased reactivity at low temperatures [117]. This is the reason why the mixture of 5E2N and first generation Grubbs catalyst, in our experiment, remained liquid at -40°C even after 24 hours of healing time. Second generation Hoveyda-Grubbs catalyst, the chemical structure of which is given in figure 7.6 [118], on the other hand, is a phosphine free catalyst.

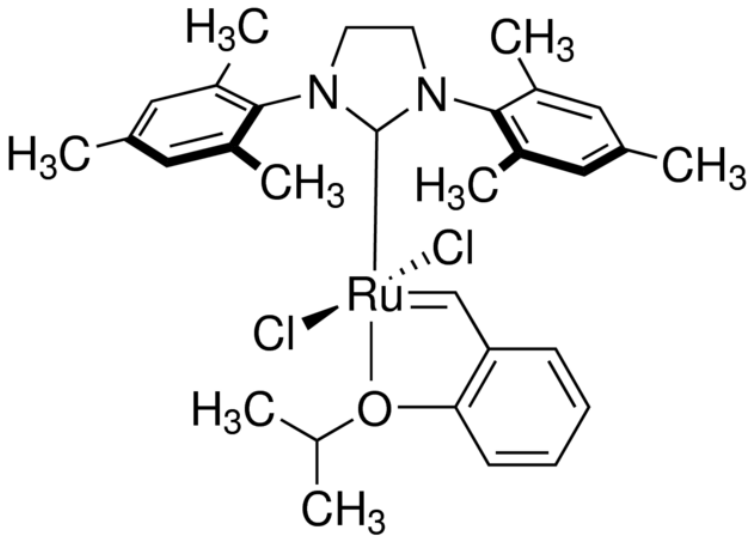

Figure 7.6 Chemical structure of phosphine free second generation Hoveyda-Grubbs catalyst [118]

Being phosphine free, HG2 does not require prior phosphine dissociation to activate the catalyst and the ROMP reaction with strained cyclic olefin (such as 5E2N) initiates more readily at lower temperatures [118]. This explains the observation made in our experiment at -40^{o}C. HG2 catalyst is thus chosen for fabricating carbon/epoxy composite samples and subsequent investigation of self-healing at low temperature (-40^{o}C).

7.3 Fabrication of composite samples

Epoxy samples (without reinforcement) and fiber reinforced carbon/epoxy samples were fabricated for self-healing experiments. Two types of epoxy samples were fabricated. One type is regular epoxy sample that does not contain healing agents (i.e. no microcapsules or catalyst). The other type is modified epoxy sample which contains healing agents (i.e. both microcapsules and catalyst). The epoxy samples were used for thermal shock experiments.

Similarly, two types of fiber reinforced carbon/epoxy composite samples were fabricated. Regular composite samples do not contain any healing agents. Modified, composite samples, on the other hand, contain healing agents. The fiber reinforced composite samples were used for mode II fracture tests. All composite samples manufactured contain a pre-implanted teflon insert as a crack initiator. All FRP composite samples manufactured are thus of NPC configuration.

The formulation of regular (without healing agents) and modified (with healing agents) epoxy matrix and the procedure of fabricating fiber reinforced composite samples were discussed in chapter 6. The procedure of fabricating epoxy (without reinforcement) samples for thermal shock experiment is discussed in the following section.

7.3.1 Fabrication of epoxy (without reinforcement) samples

Epoxy (without reinforcing fibers) samples with taper doubled cantilever beam (TDCB) geometry (extensively used by the research group of White and Sottos [6] for self-healing experiments) were fabricated for the thermal shock experiment. This geometry of the samples already contains some discontinuities (holes, grooves, tapered regions etc.) which are expected to facilitate cracking of the samples due to thermal stresses induced during the thermal shock experiment. In order to fabricate the epoxy samples, a silicone mold containing the cavity with TDCB geometry was first manufactured. Aluminum blocks which were machined to form the TDCB geometry with specified configuration were used as the tool (positive of the cavity) to make the cavity. The tools were attached to a flat aluminum plate with adhesives and enclosed

within boundary walls built by cardboards attached together by silicone tape adhesives. Mold making silicone rubber materials and hardener (V-340 mold making silicone rubber, Freeman Mfg. & supp. Co.) were mixed in appropriate ratio and poured inside the cardboard wall boundaries upon the aluminum tools attached to flat aluminum plate. The mixture was then cured at room temperature for few days, demolded and post cured in an oven.

Regular epoxy samples without self-healing capability were manufactured by pouring regular epoxy matrix (without healing agents) into the cavities of the mold kept on a flat surface. It was then cured at room temperature for 2 weeks followed by post curing at 100^{o}C for 2 hours. The regular epoxy samples were then demolded to be ready for thermal shock experiment. In a similar way, modified epoxy samples with self-healing capability were manufactured by pouring modified epoxy matrix (with healing agents) into the cavities of the mold kept on a flat surface. It was then cured, similarly, at room temperature for 2 weeks followed by post curing at 100^{o}C for 2 hours. The modified epoxy samples were then demolded to be ready for thermal shock experiment. The epoxy samples with TDCB geometry are shown in figure 7.7.

a) b)

Figure 7.7 a) Regular (without healing agents) and b) modified (with healing agents) epoxy samples

7.4 Testing

Unreinforced epoxy samples were subjected to thermal cycles (between -196^{o}C and +120^{o}C) which is representative of the actual thermal environment that a space shuttle can be exposed to

while orbiting the earth. Both regular and modified epoxy samples underwent the thermal shock experiment in order to investigate the effect of extreme thermal environment on the materials and any improvement that can be achieved through imparting self-healing capability to the materials. As the thermal shock experiment involves both cooling and heating cycles, the limitations imposed by healing agent materials are minimal. Thus, if the self-healing mechanism works at this extreme thermal shock environment, it will also work for other mild thermal cycling environment.

Mode II fracture test, on the other hand, was carried out for the FRP composite samples, under three-point bending loading conditions which represent realistic scenario that a composite structures are often exposed to in many applications at mild cold conditions (-40^{o}C), prevailing, mostly, in earth's environment. Extreme cold conditions prevailing in space was not intended to imitate, in this case, because of the limitations of the healing agent materials discussed in section 7.2.

7.4.1 Thermal shock testing of unreinforced epoxy sample

Unreinforced regular (without healing agent) and modified (with healing agent) epoxy samples with TDCB geometry were exposed to extreme cold temperature of liquid nitrogen (boiling point, -196^{o}C) and a high set temperature of 120^{o}C, cyclically. First, the regular epoxy sample was completely submerged into an open container filled with liquid nitrogen. The sample was kept submerged under liquid nitrogen for 2 minutes. The sample was then taken out of liquid nitrogen and quickly transferred to a convection oven preheated at 120^{o}C. The sample was kept in the oven for 2 minutes at 120^{o}C. The thermal cycles were continued a number of times. The same experiment was carried out for modified epoxy samples. The difference in appearance of the epoxy samples before and after the thermal shock test were observed visually and the result is discussed in section 7.5.

7.4.2 Fracture test of fiber reinforced composites at low temperature (-40^{o}C)

Mode II fracture toughness of FRP composites was directly measured according to ASTM D7905-7905M-14 standard using a compliance calibration method [3] in a low temperature set up consisting of an environmental chamber with liquid nitrogen supply which is shown in section

7.4.3. Two values of fracture toughness at low temperature were measured from each composite sample. The fracture toughness obtained with the propagation of delamination from the pre-implanted insert (acting as artificially introduced initial crack) is termed as NPC (Non-pre-cracked) fracture toughness. The fracture toughness obtained afterwards with the propagation of delamination from naturally occurred initial crack is termed as PC (Pre-cracked) fracture toughness. The samples are allowed to heal for 24 hours at low temperature (-40^{o}C) in-between the completion of the NPC test and beginning of PC test.

The configurations of composite samples and the procedure of determining the two values of fracture toughness are explained, separately, in chapter 6. The only difference is that before the NPC test, the composite samples are kept inside a zipped plastic bag which is kept inside a dry ice chamber for few hours. The composite samples are then removed from the dry ice chamber and loaded into the three point bending fixture of the MTS machine surrounded by environment chamber which is already maintained at target low temperature (-40^{o}C). The low temperature set up is shown later in section 7.4.3. Once the NPC test of the composite sample is completed, the samples are kept similarly inside a zipped plastic bag and kept inside a dry ice chamber for 24 hours to allow for healing of the natural crack before the PC test. Regular composite samples (without healing agents), however, do not require healing time. They are, however, also kept inside the zipped plastic bag and kept inside the dry ice chamber for 24 hours before the PC test. After 24 hours, the samples are removed from the dry ice chamber and similarly loaded into the three point bending fixture of the MTS machine surrounded by environment chamber which is already maintained at target low temperature (-40^{o}C). The low temperature set up is shown in section 7.4.3.

7.4.3 Set up for low temperature test

The composite samples are loaded into a three point bending fixture attached with the required extensions. The entire fixture with the extensions are inserted into an environmental chamber equipped with liquid nitrogen flow facility and temperature controller. The fixture is then attached to the MTS machine. Liquid nitrogen cylinder is attached to the environmental chamber. The test set up is shown in figure 7.8. When the temperature reaches to the desired level and becomes stable, loading of the composite samples starts. Instantaneous load and displacement data are recorded during the test for later analysis.

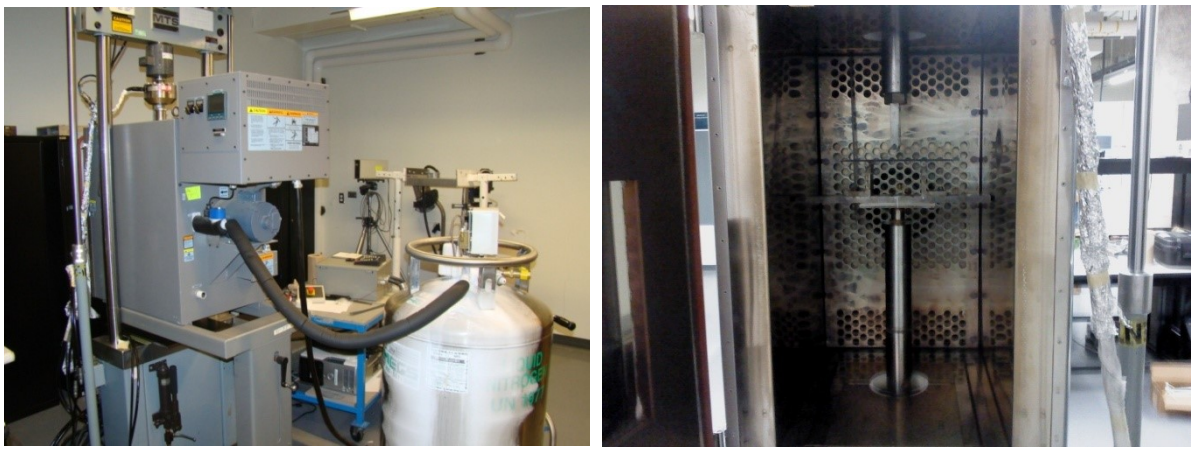

Figure 7.8 a) Environmental chamber enclosing the fixtures in the MTS machine, and attached to liquid nitrogen supply. b) 3-point bending fixtures holding the composite samples inside the environmental chamber and extensions attached to MTS machine and c) The controller of the environmental chamber showing that the set temperature of -40°C has been reached

The dry ice chamber where the composite samples are kept enclosed before and after the NPC test until the PC test is carried out is shown in figure 7.9.

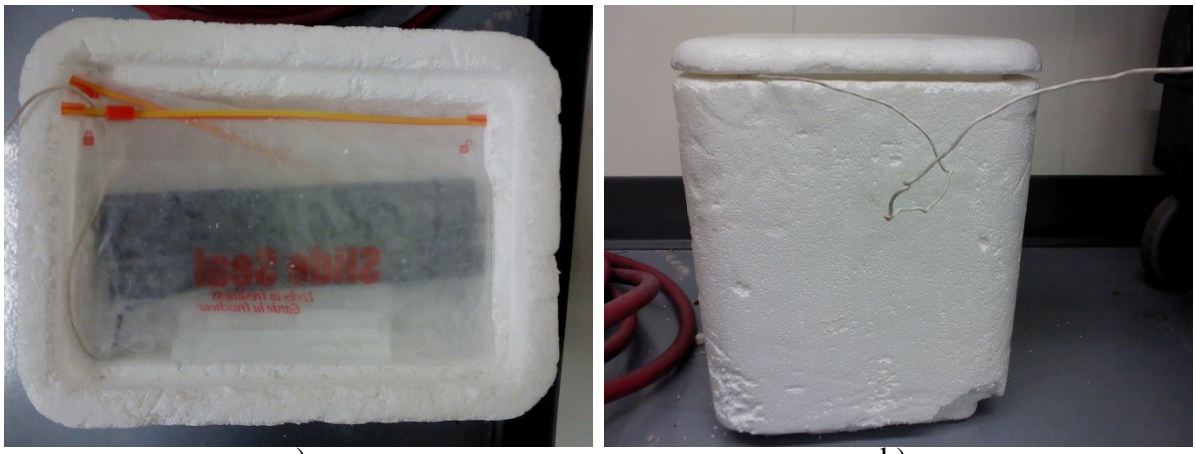

a) b)

c)

Figure 7.9 a) Composite samples are put inside the zipped plastic bag which is kept inside the chamber containing dry ice pellets. b) A thermocouple wire is placed inside the zipped plastic bag in the dry ice chamber and is connected to a digital display to monitor the temperature c) The digital display showing that the temperature inside the zipped plastic bag where the composite samples are kept is maintained at a stable temperature of (41 ± 3) °C.

7.4.4 Types of tests performed on different types of FRP samples at -40°C

FRP composite panels incorporated with no microcapsules (Type I), 2wt% (Type II), 5wt% (type III) and 8 wt% [type IV] microcapsules of average size 100 µm were fabricated. with mid-layer teflon insert (NPC configuration) as described in chapter 6. All modified composite panels are incorporated with 1wt% of HG2 catalyst also. Investigation of self-healing of composites at room temperature revealed that among the different types of modified composite samples investigated, the samples containing 8 wt% microcapsules of average size 45 µm (Type VII) showed the best healing performance. For this reason, an additional composite panel with 8 wt%

microcapsules of average size 45 μm (Type VII) was also fabricated and tested at low temperature to compare the best results between room temperature and low temperature.

A summary of the types of tests performed at low temperature (-40°C) with different types of FRP composite samples indicating the designation of the individual test result are listed in table 7.1. At least 3 replicates are tested for each type of samples to determine the mode II fracture toughness with NPC and PC configurations.

Table 7-1. Summary of the type of tests performed at CT (-40°C) with different types of composite samples (I-VII) indicating the designation of individual test results

wt.% of MC	Average size of MC (μm)	Categories of composite samples manufactured with pre-implanted teflon insert (NPC configuration)	Types of tests performed at low temperature (-40°C) and its designation	
			Non Pre-cracked $G^{C}_{II,NPC}$	Pre-cracked $G^{C}_{II,PC}$
0	-	I	NPC (0%)	PC (0%)
2	100	II	NPC(2%,100 μm)	PC(2%,100 μm)
5	100	III	NPC(5%,100 μm)	PC(5%,100 μm)
8	100	IV	NPC(8%,100 μm)	PC(8%,100 μm)
8	45	VII	NPC(8%,45 μm)	PC(8%, 45 μm)

MC: Microcapsules; **CT:** Cold Temperature

7.5 Results and Discussions

Results of the thermal shock experiment of the unreinforced epoxy sample is shown in section 7.5.1. Representative load-displacement curves for the NPC and PC fracture loading of the fiber reinforced composite samples and the corresponding NPC and PC fracture toughness values as measured at cold temperature (-40°C) according to the procedure described in section 7.4.2 are shown and discussed in section 7.5.2.

7.5.1 Result of the thermal shock experiment of unreinforced epoxy samples

The appearances of regular epoxy sample (without microcapsules and catalysts) before and after the thermal shock experiment as described in section 7. 4.1 is shown in figure 7.10.

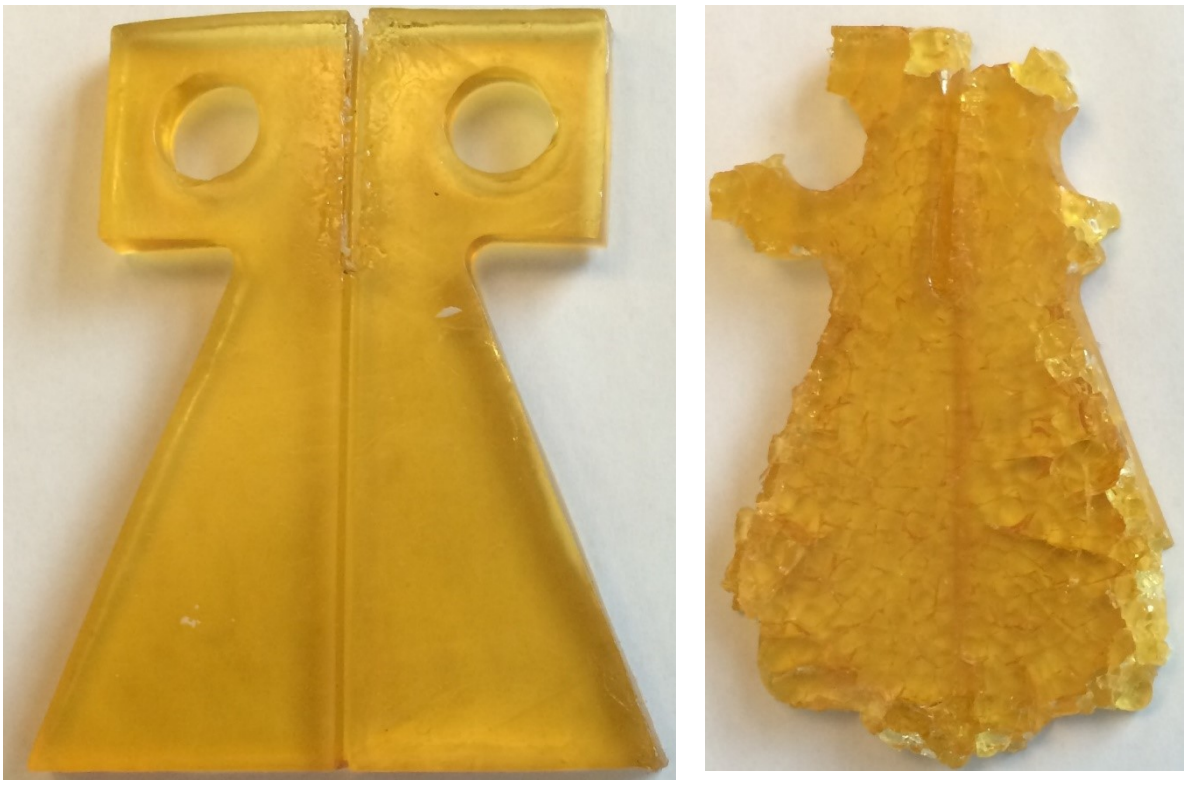

a) b)

Figure 7.10 Regular epoxy sample a) before the thermal shock cycles and b) after 5 thermal shock cycles between -196°C to +120°C

Regular epoxy sample (without microcapsules and catalysts) shattered rapidly during the initial cycles of the thermal shock experiment. A significant portion of the regular epoxy sample fell off (particularly at the corners and regions of holes) after only 5 thermal shock cycles between -196°C and 120°C. This result indicates that the regular epoxy sample without self-healing capability is vulnerable to failure at extreme thermal shock environment.

Similarly, the appearance of modified epoxy sample (incorporated with microcapsules and catalysts) before and after the thermal shock experiment is shown in figure 7.11 below.

a) b)

Figure 7.11 Modified epoxy sample a) before the thermal shock cycles and b) after 15 thermal shock cycles between -196°C to +120°C

Modified epoxy sample (with microcapsules and catalysts) remained intact up to 8 thermal shock cycles between -196°C and 120°C after which a little portion at the right corner of the sample fell off. The sample remained as it is even after 15 cycles of thermal shock. A fine network of cracks was seen on the samples which are believed to be self-healed at the crack surfaces restricting the shattering and subsequent falling apart at the weaker regions of the samples even after 15 thermal shock cycles. This result proves that self-healing with microencapsulated 5E2N monomer and Hoveyda-Grubbs catalyst (HG2) system works well even at the extreme thermal shock environment and can improve the lifetime of composite structures.

In the following section, the effects of inclusion of microcapsules on the NPC fracture toughness and the effect of self-healing reaction on the PC fracture toughness of fiber reinforced composites measured at -40°C are discussed.

7.5.2 Effect of inclusion of microcapsules on the low temperature NPC fracture toughness of FRP composite samples

The effect of inclusion of microcapsules on the NPC fracture toughness of modified composite samples (Type II, III, IV and VII) measured at -40°C temperature is discussed below.

Effect of concentration of larger microcapsules (average size 100 µm) on the low temperature NPC fracture toughness

The values of the low temperature NPC fracture toughness ($G^{C}_{II,NPC}$) of the composite samples (Type I, II, III and IV) as a function of concentration of microcapsules of average size 100 µm are compared in figure 7.12.

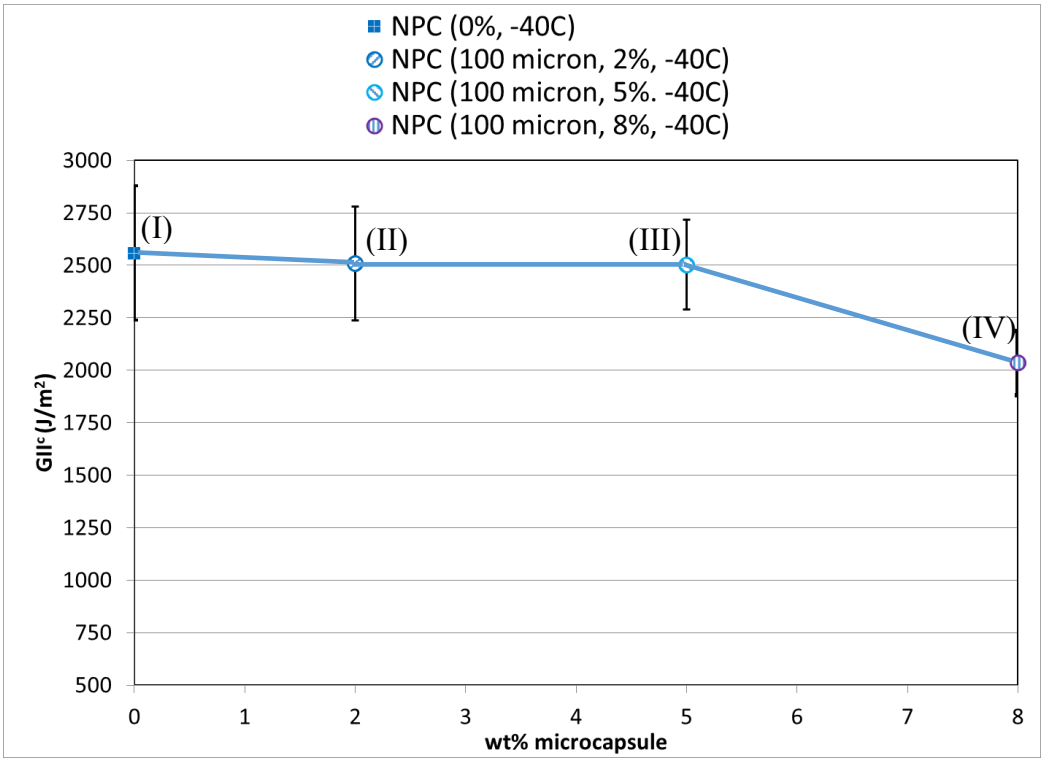

Figure 7.12 Low temperature NPC fracture toughness of composite samples containing varying concentration of microcapsules of average size 100 µm. Error bars represent one standard deviation of measured values.

Figure 7.12 shows that incorporation of microcapsules of average size 100 μm into composites reduces the low temperature NPC fracture toughness($G^C_{II,NPC}$) slightly up to 5 wt% beyond which the drop in $G^C_{II,NPC}$ is considerable. The values of low temperature $G^C_{II,NPC}$ is reduced by only 2% in type II sample, again only 2% in type III sample and about 20% in type IV sample compared with type I sample. In other words, the values of low temperature $G^C_{II,NPC}$ are reduced by 2%, 2% and 20% when incorporated with 2wt%, 5 wt% and 8 wt% of larger microcapsules (average size 100 μm), respectively, in the composites. Increasing the concentration of larger microcapsules into composites beyond 5 wt% considerably degrades its low temperature $G^C_{II,NPC}$ which is likely due to the debonding of the microcapsules to the matrix [[49]- [52]]. The debonding of larger microcapsules is also evidenced by the observation of debonding impressions on the crack surface as shown in figure 7.13 which shows a typical SEM micrograph of the fracture surface of the modified composites (with larger microcapsules) tested at low temperature.

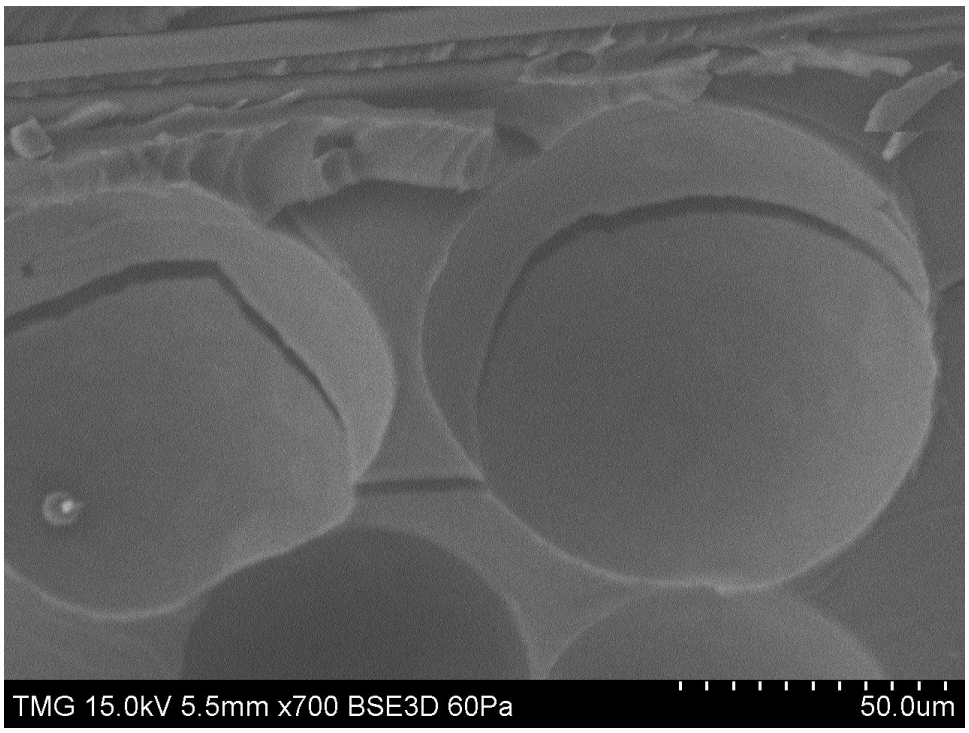

Figure 7.13 Evidence of debonding of larger microcapsules (average size 100 μm) leaving a smooth deep impression on the matrix surface during NPC crack propagation at low temperature

The micrograph in figure 7.13 shows the debonding of larger microcapsules leaving a smooth deep impression on the crack surface. This is similar to what was observed for the modified composite samples (with larger microcapsules) tested at room temperature.

Effect of concentration of small microcapsules (average size 45 µm) on the low temperature NPC fracture toughness

Figure 7.14 shows the low temperature $G^{C}_{II,NPC}$ of type VII sample (containing 8wt% of small microcapsules of average size 45 µm) compared with type I sample (containing no microcapsules) both fractured at -40°C.

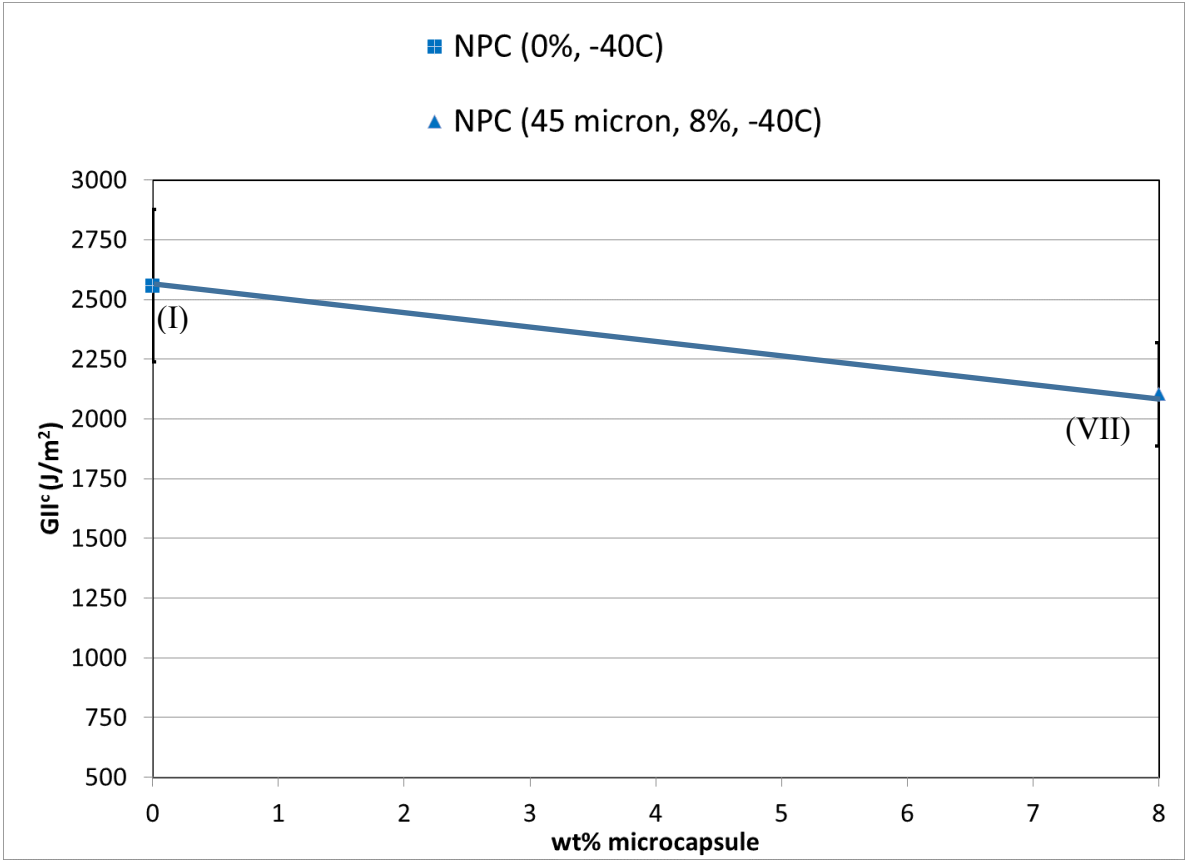

Figure 7.14 Low temperature NPC fracture toughness of composite samples containing 8 wt% microcapsules of average size 45 µm (Type VII) compared with regular sample (Type I). Error bars represent one standard deviation of measured values. The scale and spacing of the graph is kept the same as previous for later comparison.

Figure 7.14 shows that, similar as in the case of larger microcapsules, incorporation of 8wt% small microcapsules (average size 45 µm) also reduces the low temperature $G^{C}_{II,NPC}$ by about

18% in type VII modified samples compared with low temperature $G_{II,NPC}^{C}$ of type I regular sample. SEM observations of the fracture surface of the composites tested at low temperature, however, shows that the smaller microcapsules (average size 45 µm) forms good bonding with the matrix as shown in figure 7.15.

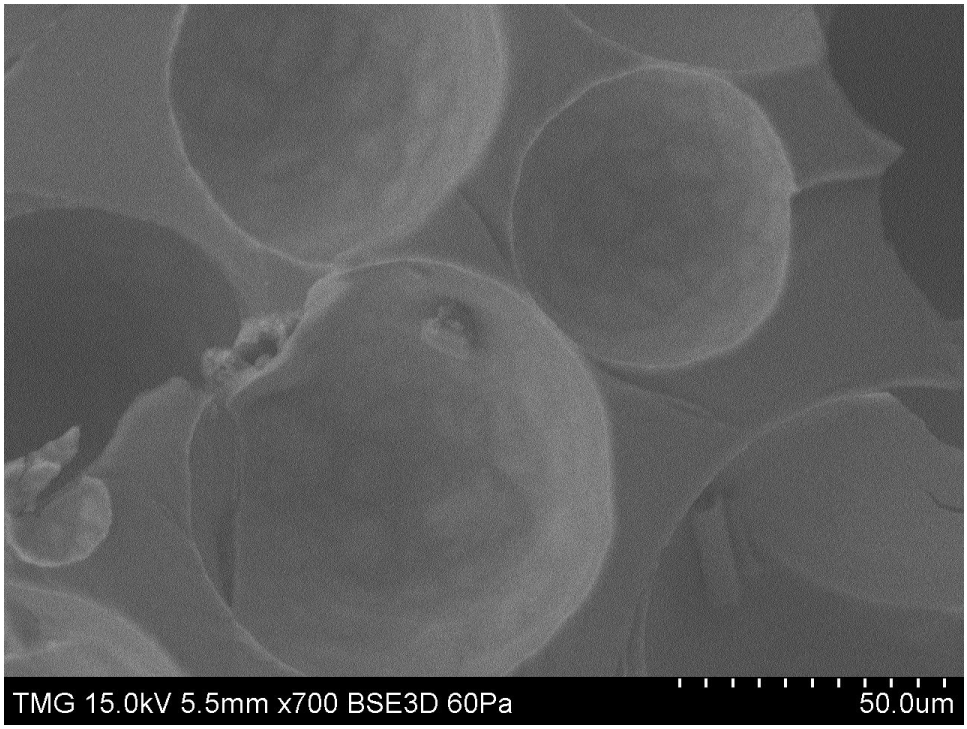

Figure 7.15 Evidence of good bonding of smaller microcapsules (average size 45 µm) showing the rough inner surfaces of the lower halves of microcapsules still attached to the matrix after the crack propagation at low temperature.

SEM micrograph in figure 7.15 demonstrates that the smaller microcapsules forms good bonding with the matrix showing the rough inner surface of the lower halves of the smaller microcapsules still attached to the matrix after the crack propagation at low temperature. The good bonding of small microcapsules, however, does not explain the observed reduction in low temperature $G_{II,NPC}^{C}$ in type VII sample as seen in figure 7.14. This reduction in $G_{II,NPC}^{C}$ is possibly associated with some manufacturing issues related to the hand lay-up process as found in room temperature cases discussed in the previous chapter.

7.5.3 Effect of self-healing on the low temperature PC fracture toughness of composite samples

The effect of self-healing on the PC fracture toughness of modified composite samples (Type II-VII) measured at low temperature are discussed below.

Effect of concentration of larger microcapsules (average size 100 µm) on the low temperature PC fracture toughness

The values of the low temperature PC fracture toughness ($G^C_{II,PC}$) of the composite samples (Type I, II, III and IV) as a function of concentration of microcapsules of average size 100 µm are shown in figure 7.16.

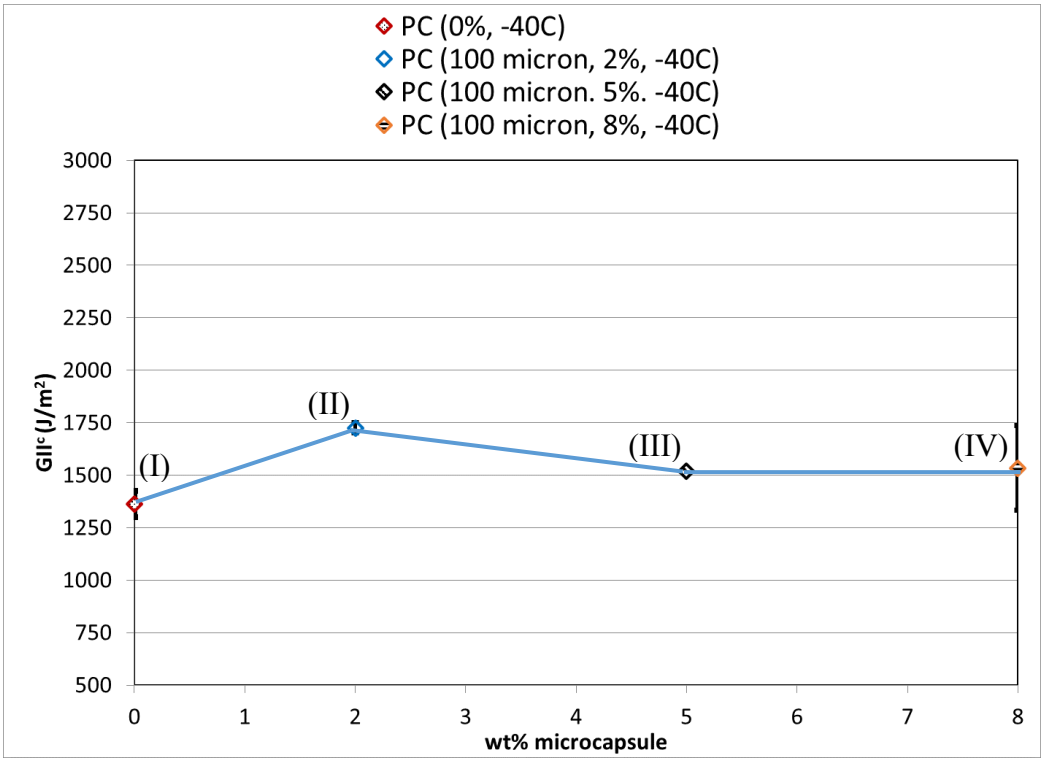

Figure 7.16 Low temperature PC fracture toughness of composite samples containing varying concentration of microcapsules of average size 100 µm. Error bars represent one standard deviation of measured values. The scale and spacing of the graph are kept the same as the previous graphs for later comparisons.

Figure 7.16 shows that the values of low temperature $G^C_{II,PC}$ of modified composite samples of type II, III and IV [containing certain wt% of larger microcapsules (average size 100 µm)] are always greater than the values of low temperature $G^C_{II,PC}$ of regular composite samples of type I

(containing no microcapsules). This implies that the natural precrack is healed in the modified composite samples at low temperature also. Compared with type I samples, low temperature PC fracture toughness is improved by 27% in type II sample, 11% in type III sample and about 13% in type IV sample. In other words, compared with regular sample (0wt% microcapsules), the values of low temperature $G_{II,PC}^{C}$ are improved by 27%, 11% and 13% when the samples are incorporated with 2wt%, 5 wt% and 8 wt% of larger microcapsules (average size 100 μm), respectively. The improvement in low temperature $G_{II,PC}^{C}$, however, diminishes with increasing concentration of larger microcapsules beyond 2 wt%. Debonding of larger microcapsules during the NPC crack propagation, as evidenced in figure 7.13 before, limits the number of microcapsules broken which restricts the release of sufficient amount of monomer into the crack plane. Thus, as in the case of room temperature, increasing the concentration of larger microcapsules (average size 100 μm) does not translate into proportionate increase in $G_{II,PC}^{C}$ at low temperature.

Effect of concentration of small microcapsules (average size 45 μm) on the low temperature PC fracture toughness

Finally, figure 7.17 shows the best results showing significantly improved low temperature $G_{II,PC}^{C}$ of modified composite samples of type VII [containing 8 wt% of smaller microcapsules (average size 45 μm)] compared to low temperature $G_{II,PC}^{C}$ of regular composite samples of type I (containing no microcapsules).

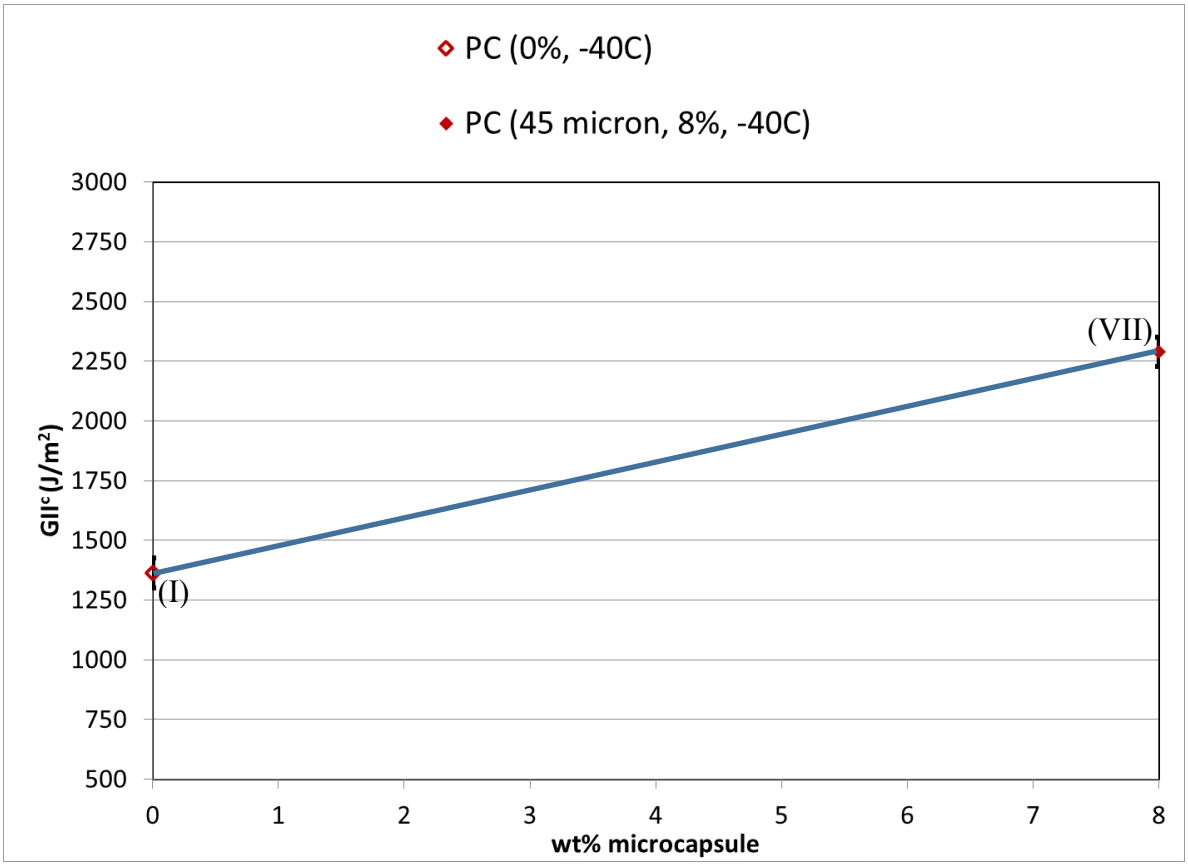

Figure 7.17 Low temperature PC fracture toughness of composite samples containing 8wt% microcapsules of average size 45 µm compared with regular sample [(PC (0%)]. Error bars represent one standard deviation of measured values.

About 68% improvement in low temperature $G^C_{II,PC}$ is observed in type VII sample compared with type I sample. This, again, first implies that self-healing of the natural precrack in the modified composite samples takes place, even at low temperature.

The improvement of low temperature $G^C_{II,PC}$ of modified composite samples containing certain wt% of microcapsules (Type II-VII) compared with low temperature $G^C_{II,PC}$ of regular composite sample containing no microcapsules (Type I), as shown in figure 7.17 and 7.16 before, is the direct contribution of self-healing of the naturally occurred precrack at low temperature. Comparison of representative SEM micrographs (as shown in figure 7.18) of the fracture surfaces of the regular and modified composite samples, both fractured at low temperature, shows the difference in features between the healed (modified) and unhealed (regular) samples.

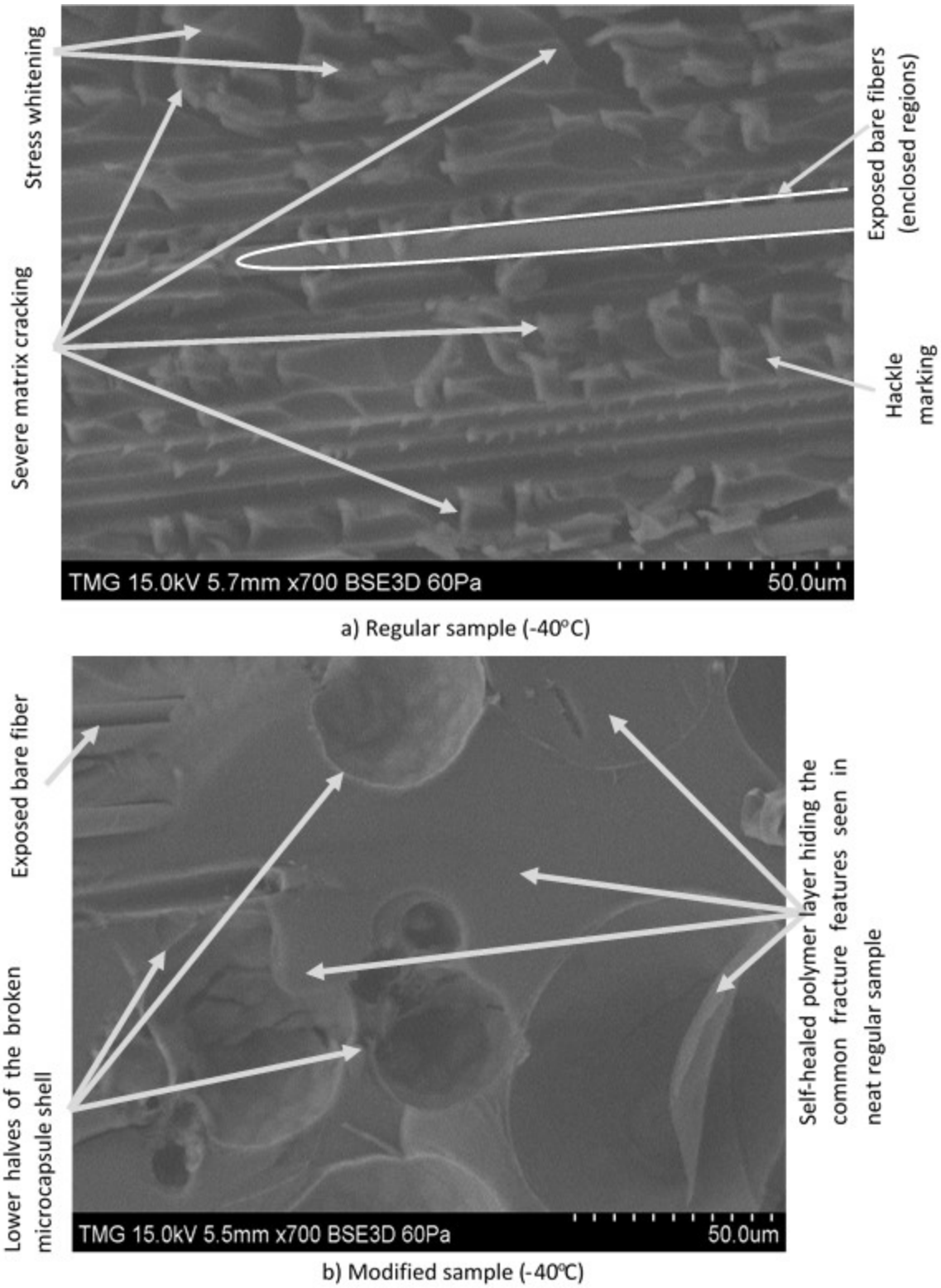

Figure 7.18 Comparison of fracture surfaces of (a) regular (no microcapsules) and b) modified (with microcapsules) composite samples both fractured at -40°C. Broken shells of microcapsules and layer of self-healed material [poly (5E2N)] is evident in the second micrograph.

The micrograph in figure 7.18 a) shows exposed bare fibers, striations, hackle markings, marks of stress whitening and severe matrix cracking which are the common features of low temperature mode II fracture of regular sample (no microcapsules). The fracture features indicates a combination of adhesive-cohesive failure. The micrograph in figure 7.18 b), on the other hand, shows the presence of relatively smooth self-healed polymer layer (more clearly seen at the bottom right corner of the micrograph 7.18 b) which is believed to be the product of the self-healing ROMP reaction (poly 5E2N) hiding the common fracture features seen in regular samples. The self-healed polymer layer is formed by the reaction between the monomer oozed out from broken microcapsules and dispersed HG2 catalyst in the delamination crack plane at low temperature.

The presence of lower halves of the microcapsules together with relatively smooth self-healed layer and some portion of the exposed bare fibers (at the top left corner of the micrograph 7.18b) implies that the failure of the modified sample is mostly cohesive in nature. The micrograph also confirms the fact that the self-healing mechanism still works at low temperature (-40^{o}C).

Comparing figures 7.16 and 7.17 it can be concluded that relatively high concentration in the vicinity of 8 wt% of smaller microcapsules (average size 45 μm) works better for self-healing of the natural precrack than high concentration of larger microcapsules (average size 100 μm), even at low temperature. This is due to the tendency of smaller microcapsules of forming better bonding with the matrix (as evidenced in figure 7.15 before) allowing the breaking of greater number microcapsules releasing sufficient amount of liquid monomer into the crack plane for effective self-healing.

7.5.4 Comparison of fracture toughness and evaluation of healing performance of the composites tested at low temperature

In this section, the low temperature NPC and PC fracture toughness of each type of composite samples (Type I-IV and VII) are compared. As the healing performance index, PI, as defined in equations 5.2-5.4 (in chapter 5) is found to be the reliable indicator of actual healing performance, the values of PI are evaluated for each type of samples tested at low temperature and compared. Using the, values of PI, the composite sample showing the best healing performance at low temperature can be correctly identified.

Figure 7.19 shows the comparison of low temperature NPC and PC fracture toughness of composite samples of type I-IV as a function of concentration of larger microcapsules of average size 100 µm.

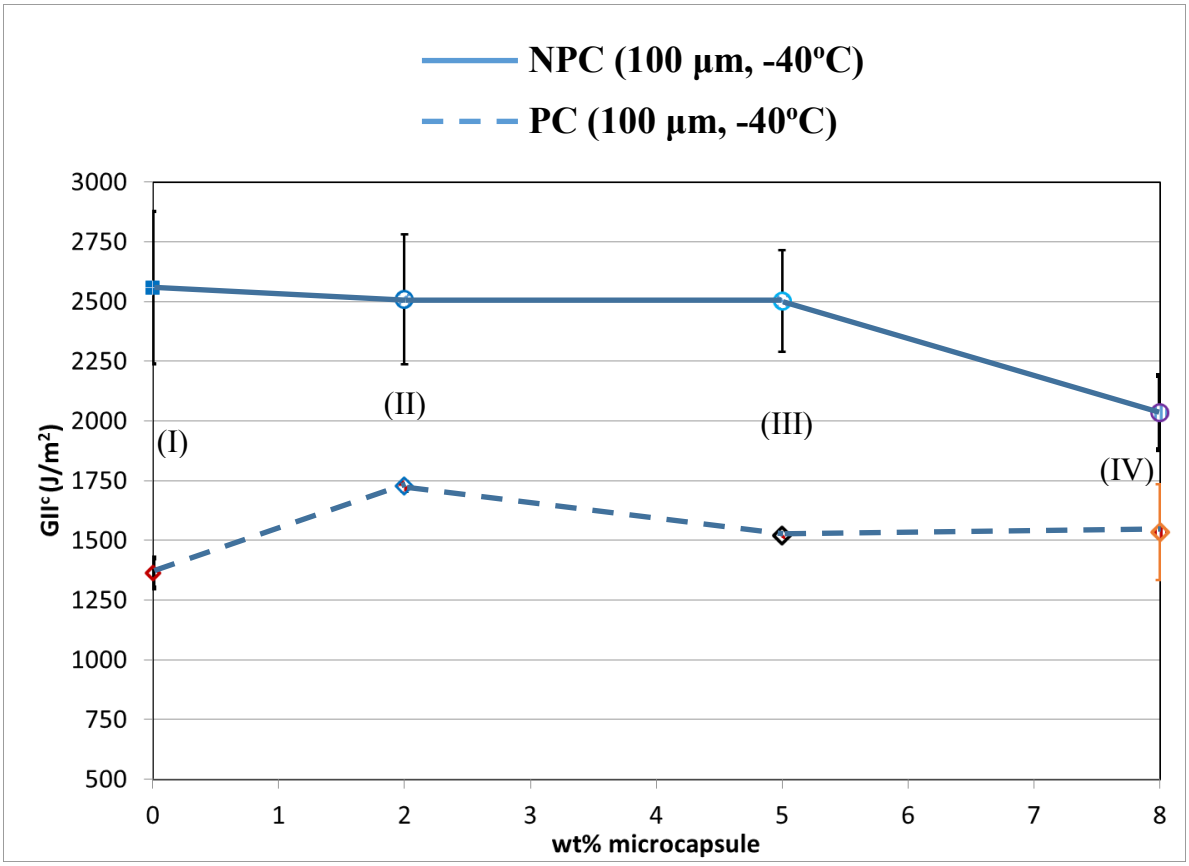

Figure 7.19 Comparison of low temperature NPC and PC fracture toughness of composite samples as a function of concentration of microcapsules of average size of 100 µm. Error bars represent one standard deviation of measured values.

Similarly, figure 7.20 below shows the comparison of low temperature NPC and PC fracture toughness of composite samples of type I containing no microcapsules and type VII containing 8wt% of small microcapsules of average size 45 µm.

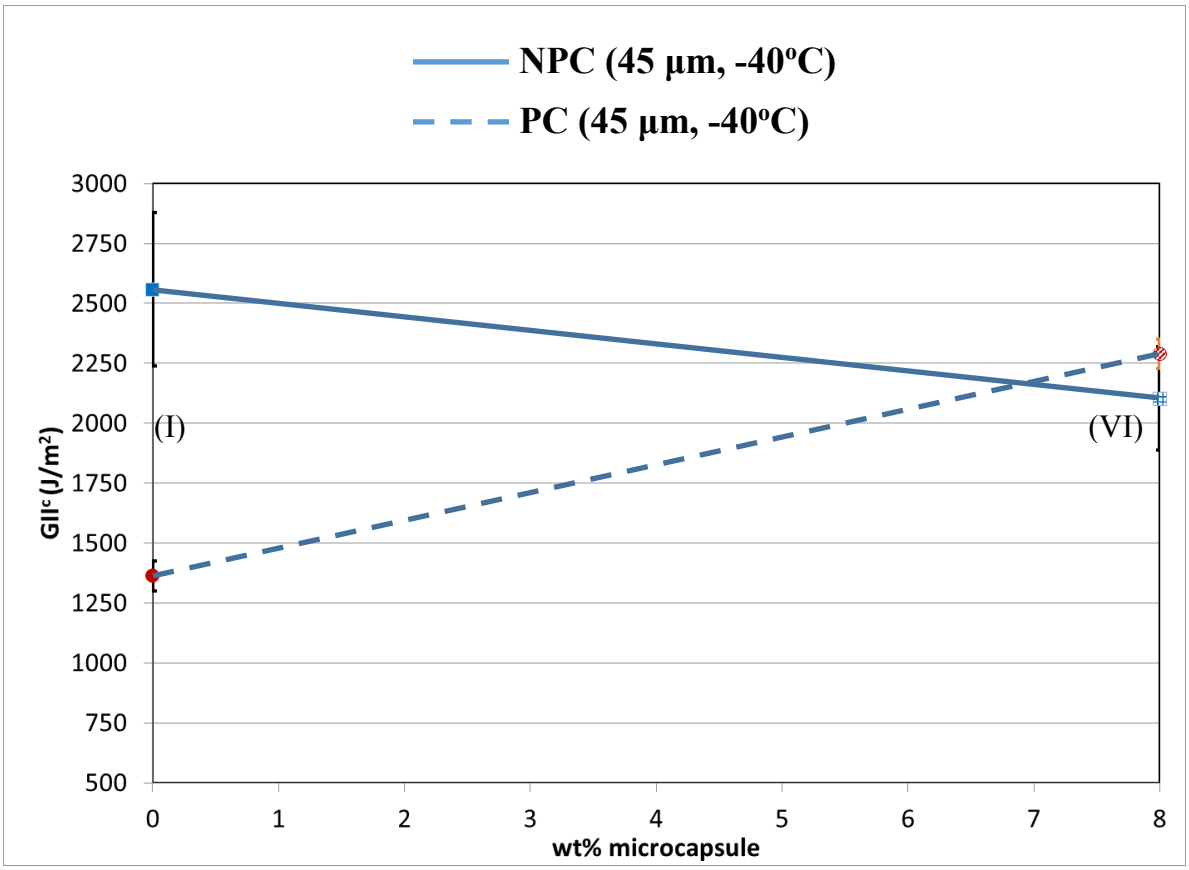

Figure 7.20 Comparison of low temperature NPC and PC fracture toughness of composite samples of type I containing no microcapsules and type VII containing 8wt% of microcapsules of average size of 45 µm. Error bars represent one standard deviation of measured values.

The percentage changes (improvement or deterioration) in low temperature fracture toughness values in the modified composites (Type II, III, IV and VII) compared with regular composites (Type I) as calculated by equations (6.10)-(6.11) are shown in table 7.2.

Table 7-2. Comparison of changes in low temperature fracture toughness of modified composites (Type II, III and IV) compared with regular composites (Type I) containing no microcapsules

Changes in Fracture toughness (%)	Types of composite samples tested at low temperature (-40oC)				Causes of change
	II (2wt%, 100 μm)	III (5wt%, 100 μm)	IV (8wt%, 100 μm)	VII (8wt%, 45 μm)	
% $\boldsymbol{red.}_{(NPC)}$	2	2	20	18	**Debonding of larger microcapsules and manufacturing issues**
% $\boldsymbol{imp.}_{(PC)}$	27	11	13	68	**Self-healing reaction**

Figure 7.21 compares the corresponding values of *PI* (%) for the three types of modified composite samples (Type II-IV) containing larger microcapsules of average size of 100 μm and composite samples (Type VII)) containing small microcapsules of average size of 45 μm.

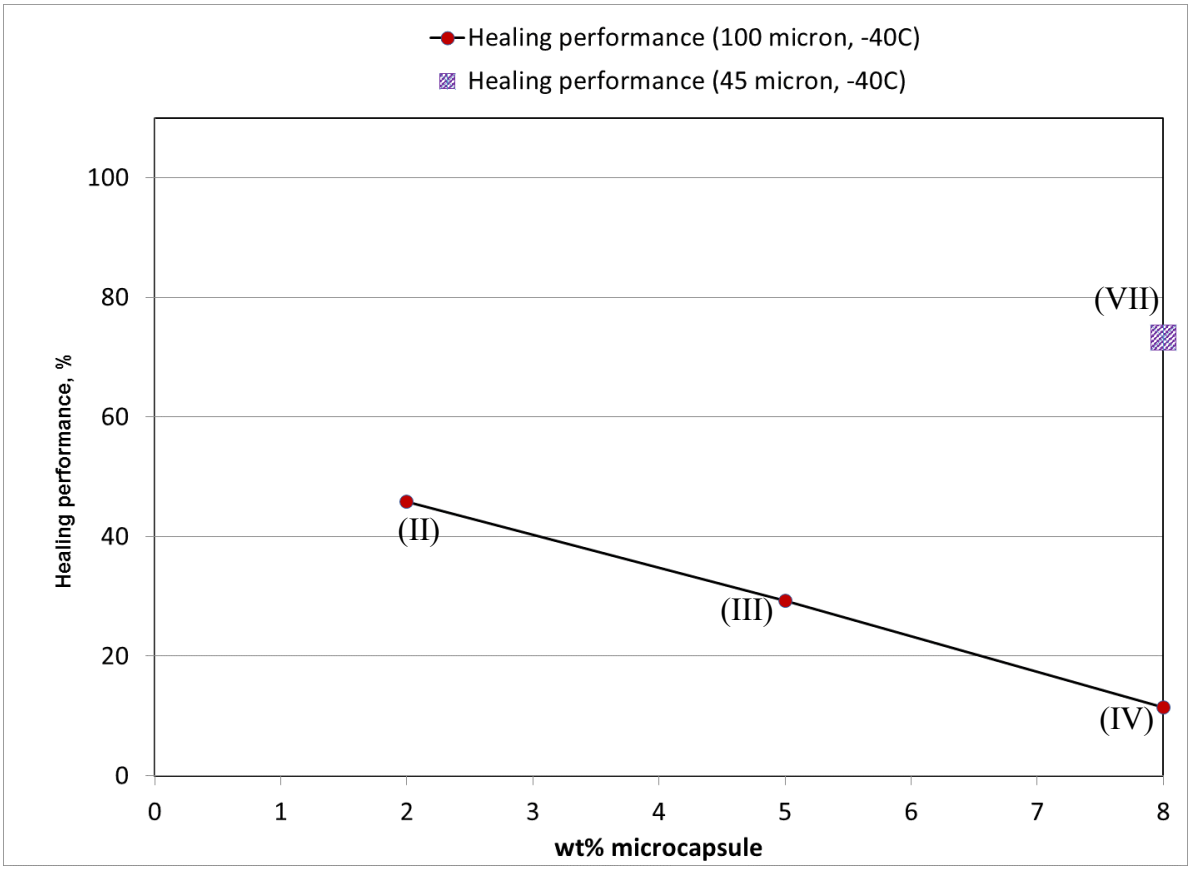

Figure 7.21 Comparison of healing performance index, PI (%) of modified composite samples (Type II, III, IV and VII) tested at low temperature.

PI values of about 45%, 30%, 12% and 73% are achieved in type II, III, IV and VII samples, respectively, tested at low temperature. A continuous reduction of *PI* values with increasing concentration of larger microcapsules (average size 100 μm) in the composite samples (Type II, III and IV) is also indicated in figure 7.21. The best PI value at low temperature is obtained with the modified composite samples of type VII containing 8wt% of small microcapsules of average size of 45 μm. The values of PI (%) corresponds appropriately with the percentage reduction in NPC fracture toughness due to the effect of inclusion of microcapsules into the composites and percentage improvement in PC fracture toughness due to the effect of self-healing as indicated in table 7.2. Thus, from the above investigation, it is concluded that for best healing performance at low temperature, composites should be incorporated with relatively high concentration (8wt%) of small microcapsules of average size of 45 μm.

7.5.5 Effect of low temperature on the self-healing performance of the composites

The effect of low temperature (-40°C) on the self-healing performance of the composites can be extracted by comparing the fracture toughness and *PI* values measured both at room temperature and low temperature.

As such, figure 7.22 shows the effect of low temperature on the NPC fracture toughness, of the composite samples of type II-IV containing larger microcapsules (average size 100 µm) compared with type I sample.

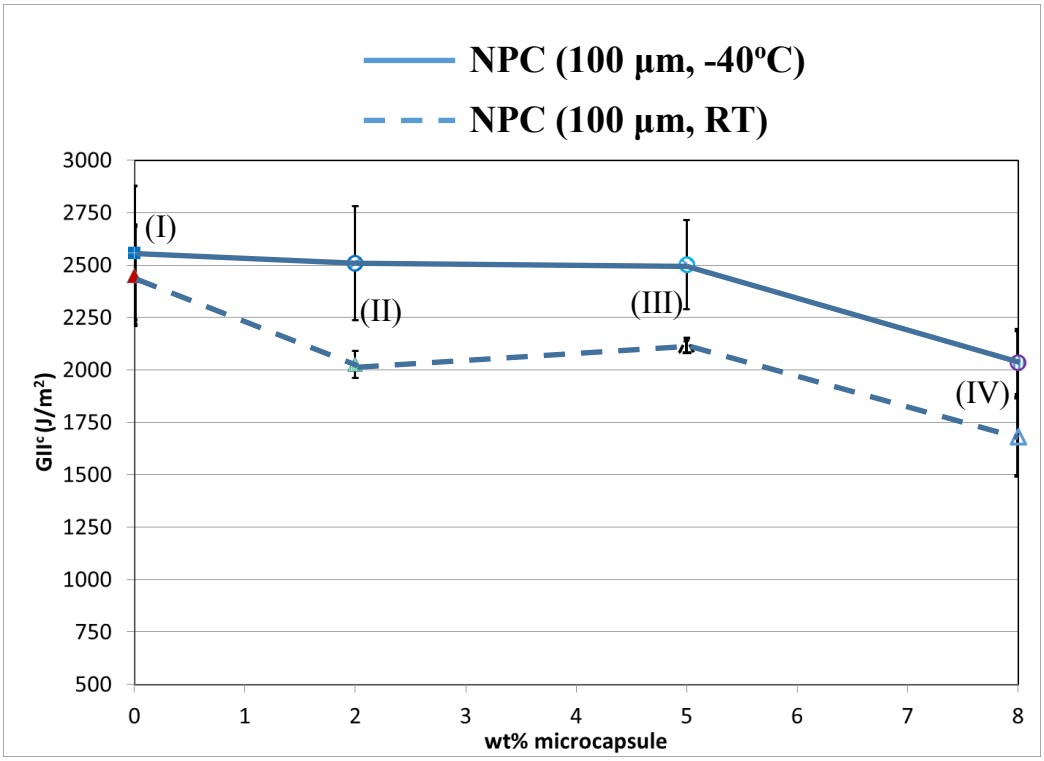

Figure 7.22 Comparison of NPC fracture toughness of composite samples (Type I-IV) measured at room temperature and low temperature.

The comparison in figure 7.22 indicates that the low temperature NPC fracture toughness is greater than room temperature fracture toughness in all composite samples (I-IV). This implies that exposure of the composite samples to low temperature tends to increase their NPC fracture toughness. Kichhannagari [119] studied the effect of low temperature on the FRP composites and observed a continuous increase in apparent interlaminar shear strength, as measured by short beam shear test, with decrease in temperature from room temperature down to -100°C. According to Isacc and Ishai [120], interlaminar shear strength is a measure of the in situ shear

strength of the matrix layer between plies. She [119] observed about 29%, 57% and 110% increase in shear strength of carbon/epoxy composites at -5^{o}C, -50^{o}C and -100^{o}C compared with shear strength at room temperature. This can explain the observed increase in NPC fracture toughness of composites at low temperature compared with room temperature as shown in figure 7.22. A comparison of the fracture surfaces of regular (Type I) composites fractured at room temperature and low temperature (-40^{o}C) is shown in figure 7.23 a) and b) below.

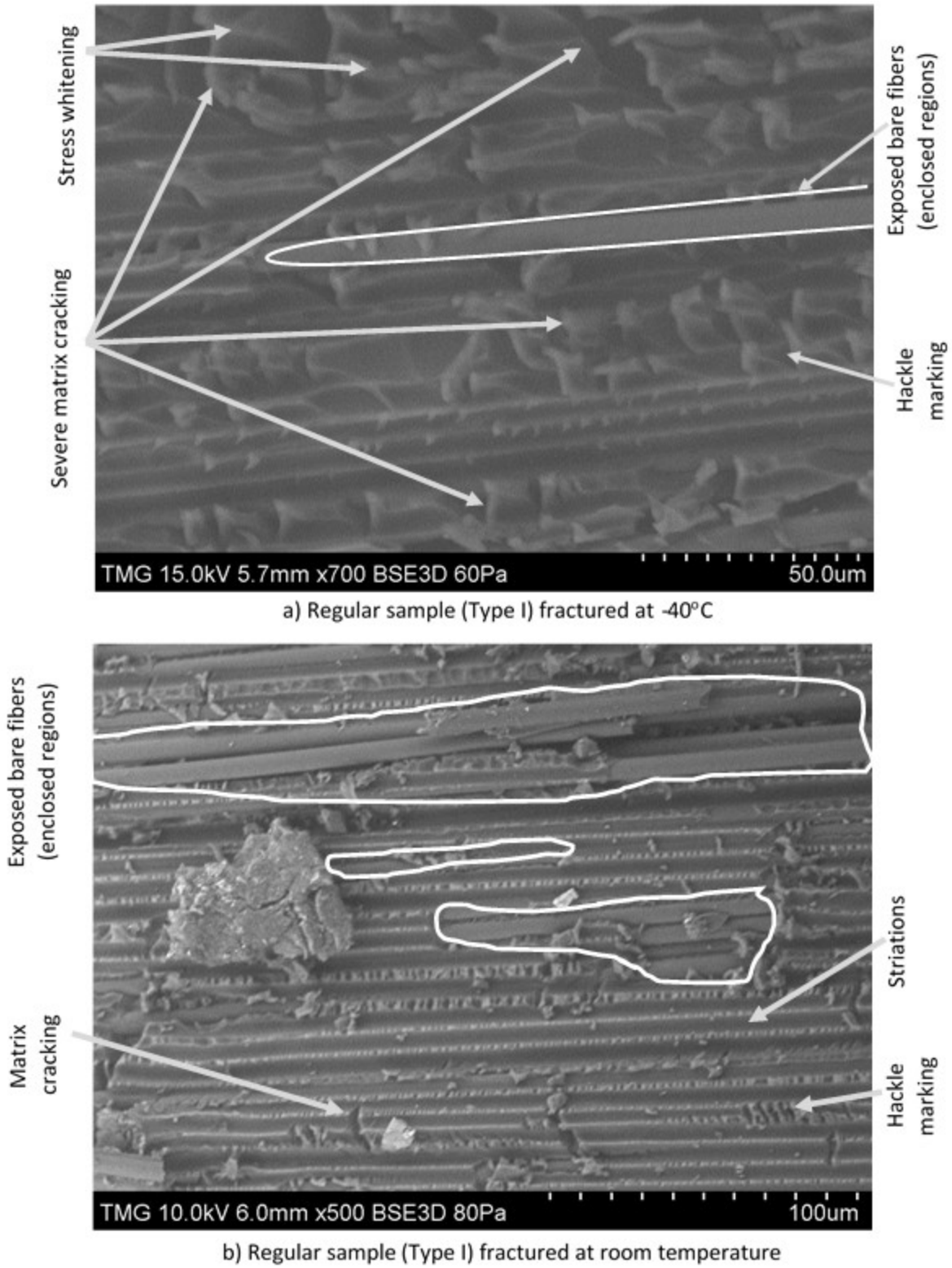

Figure 7.23 Comparison of fracture surfaces of regular composite samples (Type I) measured at a) -40°C and b) room temperature

Both fracture surfaces in figure 7.23 are associated with common features of mode II fracture which include striations, exposed bare fibers, hackle markings and matrix cracking. However, severe matrix cracks along with distinct marks of stress whitening observed in the composite samples fractured at low temperature differentiates it from the sample fractured at room temperature. The presence of severe matrix cracks and marks of stress whitening indicates that the composite samples at low temperature undergoes more severe shear stress before the propagation of cracks further indicating higher fracture toughness than composite samples fractured at room temperature.

Figure 7.24 below, on the other hand, indicates the effect of low temperature on self-healing of natural precracks translated into PC fracture toughness of composite samples of type II-IV containing larger microcapsules (average size 100 µm) compared with type I sample.

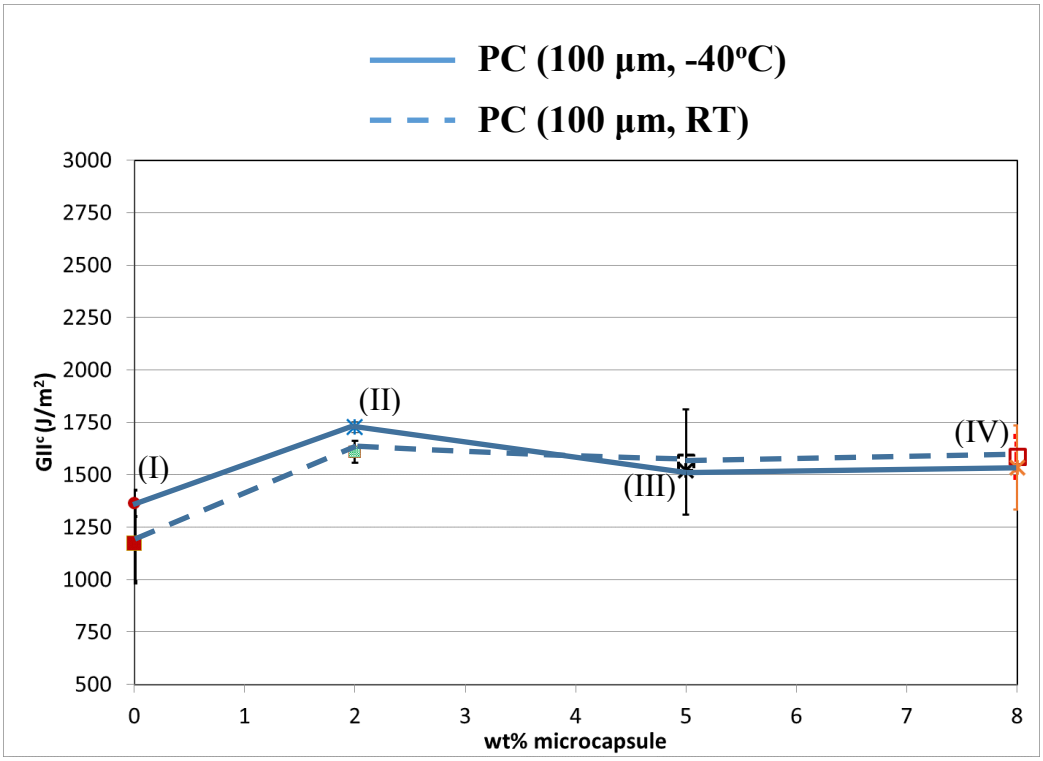

Figure 7.24 Comparison of PC fracture toughness of composite samples (Type I-IV) measured at room temperature and low temperature.

The values of low temperature PC fracture toughness of the composite samples of each type (II-IV) matches closely with the PC fracture toughness measured at room temperature. This indicates that, low temperature (-40°C) does not have significant effect on self-healing of composites.

Similarly, figure 7.25 a) and b) below show the effect of low temperature on the NPC and PC fracture toughness of the composite samples of type VII containing 8wt% of small microcapsules (average size 45 μm) compared with type I sample both tested at room temperature and low temperature.

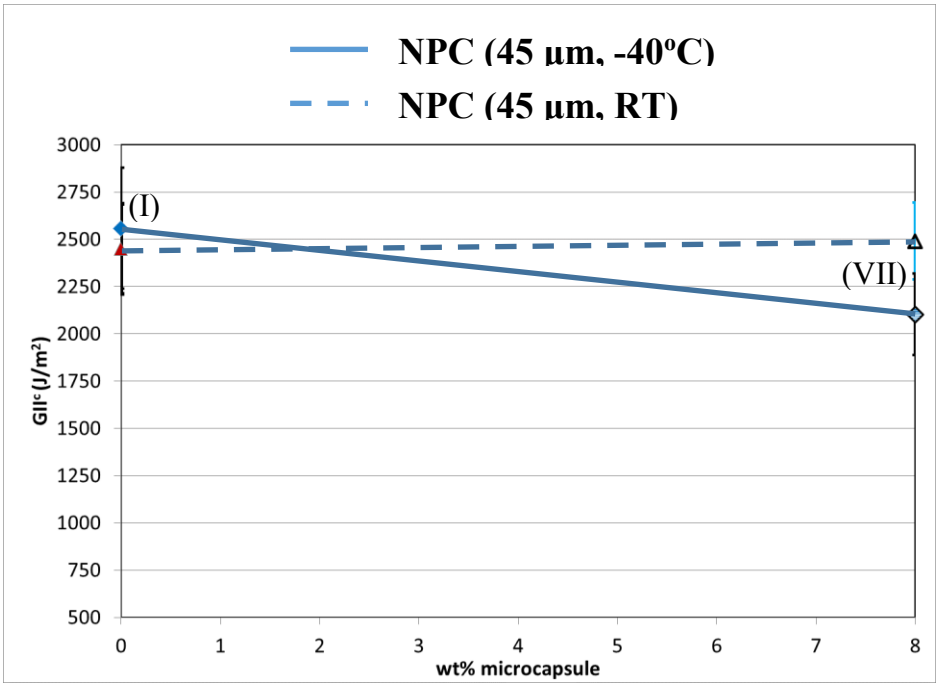

a)

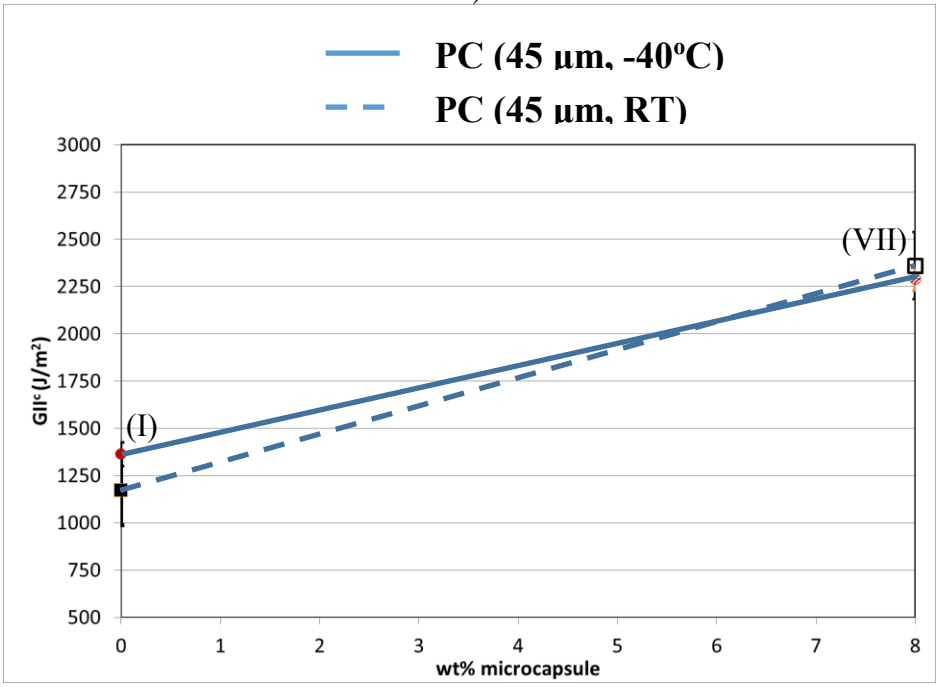

b)

Figure 7.25 Comparison of a) NPC and b) PC fracture toughness of composite samples of type VII measured at room temperature and low temperature in relation to type I sample.

Figure 7.25 a) shows some reduction of low temperature NPC fracture toughness of composite sample of type VII compared with room temperature NPC fracture toughness of the same type of sample. This reduction of low temperature NPC fracture toughness is possibly due to the variations in human control in the manufacturing of composites using the hand lay-up methods. The values of PC fracture toughness of the type VII sample (containing 8wt% of small microcapsules) measured at room temperature and low temperature, however, matches closely indicating, again, a little influence of low temperature (-40^{o}C) on the self-healing of composites.

7.6 Conclusions

In order to extract the effect of low temperature, investigation of self-healing at low temperature (-40^{o}C) is carried out with the same type of FRP composite samples (Type I-IV) containing larger microcapsules (average size 100 μm) which are tested at room temperature. Additionally, composite samples containing 8wt% of small microcapsules (average size 45 μm) (Type VII) which showed the best healing performance at room temperature are also tested at low temperature to verify the effectiveness of self-healing at low temperature. However, the modified composite samples, in this case, contained HG2 catalyst (instead of Grubbs 1st generation catalyst) suitable for self-healing ROMP reaction at low temperature. Self-healing performance is evaluated by measuring the NPC and PC fracture toughness of the composite samples at -40^{o}C according to ASTM D7905/D7905M. The values of NPC fracture toughness are obtained by propagating a delamination at low temperature from the pre-implanted insert in the composite sample. The values of PC fracture toughness, on the other hand, are determined by propagating the natural precrack (allowed to heal beforehand at low temperature) that is created during the NPC test at low temperature.

Generally, NPC fracture toughness of the composites are found to be increased at lower temperature. The PC fracture toughness, on the other hand, remained almost the same as of the room temperature. It is thus first concluded from the above investigation that self-healing of FRP composites takes place at low temperature (-40^{o}C). NPC fracture toughness of composites is increased at low temperature. However, low temperature (-40^{o}C) has no significant effect on the self-healing of FRP composites. The type of composite samples (Type VII) that shows the best healing performance at room temperature also shows very attractive healing performance at low temperature.

CHAPTER 8

Conclusions, Contributions and Recommendations for Future Work

8.1 Conclusions

The investigation is this work offers a complete package of procedures of manufacturing FRPC with optimal healing capability starting from the raw materials (fiber, matrix, monomer, catalyst, encapsulating reagents etc.) using 5E2N and Grubbs catalyst as healing agents.

Microcapsules containing liquid 5E2N in the core with PMUF shells have been synthesized using the established procedure in literature. The effect of agitation speed and SLS concentration is investigated and an optimum combination of speed-SLS concentration is established through numerous synthesis trials. The quality of produced microcapsules in terms of average size, size distribution, surface morphology and shell thickness are compared. Microcapsules produced with optimum process parameters (agitation speed and SLS concentration) meets the desired quality standard of microcapsules with good thermal stability and core monomer content. The procedure established can be utilized to produce microcapsules of required average size with desired quality characteristics.

In the preliminary investigations, feasibility of self-healing with the microencapsulated 5E2N and Grubbs catalyst system is demonstrated by visual observation of the self-healed cracks which are created on the resin sample (without fibers) with realistic loading (by high velocity projectile impacts). The self-healing of crack in the resin sample is demonstrated to be achieved without any requirement for assisting healing by manual intervention.

Strength based approach of evaluating self-healing performance of FRP composites based on the established testing standard (ASTM D7264) was found to be inadequate as the effect of self-healing on residual flexural properties of the composites cannot be extracted independently. It is due to the possible dependence of residual flexural properties of the FRP composites on the sample geometry and uncontrolled crack lengths.

Fracture based approach of evaluating self-healing performance of FRP composites based on recently approved ASTM standard (ASTM D7905.7905M-14) for measuring the mode II

interlaminar fracture, or delamination, toughness is found to be the better choice. The method is based on calibration of compliance of the composite sample with crack lengths under three point bending set up and provides values of mode II fracture toughness (G_{II}^{C}) which is independent of geometry of the samples. This method of determining G_{II}^{C} of the FRP composites, thus, matches well within the framework of the current work one of the global objectives of which is to propose a protocol of evaluating the healing performance of composites under realistic loading conditions and without any requirement for assisting healing by manual interventions.

The proposed protocol involves the measurement and comparison of mode II fracture toughness determined from NPC (non-pre-cracked) and PC (pre-cracked) configurations of both regular (without healing capability) and modified (with healing capability) FRP composite samples. Healing Performance Index (PI) is defined taking into account the possible improvement in PC fracture toughness due to healed crack in modified composites compared with PC fracture toughness with unhealed crack in regular composites. It also takes into account the possible effect of incorporating microcapsules into the NPC fracture toughness. Healing Performance Index (PI) is found to give reliable and much better indication of healing compared with conventional healing efficiency in every likely situations as found in different scenario analysis and in the real evaluations.

Investigation of self-healing at room temperature is first carried out with different types of FRP composite samples containing varying percentage of microcapsules with different average sizes. Two average sizes (100 μm and 45 μm) and three different concentrations (2wt%, 5wt% and 8wt%) of microcapsules are selected to investigate their effect on self-healing performance of FRP composite.

Larger microcapsules (average size 100 μm) are found to debond from the matrix more easily during the mode II fracture. This limits the self-healing performance of composites containing larger microcapsules. Debonding of microcapsules affects both the NPC fracture toughness and the PC fracture toughness of modified composites. Increasing the concentration of larger microcapsule up to 8 wt% did not help in achieving high PC fracture toughness post healing at room temperature. Rather, increased concentration of larger microcapsules degrades the base NPC fracture toughness significantly due to the debonding of larger microcapsules as evidenced in SEM micrographs. On the contrary, smaller microcapsules (average size 45μm) are shown to form good bonding with the matrix leading to excellent improvement of PC fracture

toughness post healing at room temperature while not deteriorating the NPC fracture toughness at relatively high concentration (8 wt%) of microcapsules. The best healing performance at room temperature is obtained with FRP composite samples containing 8wt% of microcapsules of average size 45 μm.

In order to extract the effect of low temperature, investigation of self-healing at low temperature (-40^{o}C) is carried out with the same type of FRP composite samples containing larger microcapsules (average size 100 μm) which are tested at room temperature. Additionally, composite samples containing 8wt% of small microcapsules (average size 45 μm) which showed the best healing performance at room temperature are also tested at low temperature to verify the effectiveness of self-healing at low temperature. However, the modified composite samples, tested at low temperature, contained HG2 catalyst (instead of Grubbs 1st generation catalyst) suitable for self-healing ROMP reaction at low temperature.

Generally, NPC fracture toughness of the composites are found to be increased at lower temperature. The PC fracture toughness post healing, on the other hand, remained almost the same as of the room temperature. It is thus concluded that low temperature (-40^{o}C) has no significant effect on the self-healing of FRP composites.

8.2 Contributions

The main contributions from this work are given below.

1) A complete package of procedures of producing FRPC with optimal healing capability (both at room temperature and low temperature) is offered in this work starting from the raw materials (i.e. fiber, resin, monomer, catalyst, encapsulating reagents etc.)
2) Self-healing of cracks in the resin sample created with realistic loading (impact of projectile) is demonstrated directly by visual observation.
3) A suitable protocol for evaluating self-healing performance of FRPC under realistic loading conditions and without any requirement for assisting healing by manual interventions is proposed and verified to provide reliable indication of realistic healing performance.
4) Effects of agitation speed and SLS concentration on the quality characteristics of microcapsules (containing 5E2N monomer) are investigated. The results of the investigation can be utilized to produce microcapsules of required average size with desired quality characteristics.

5) Effects of average size and concentration of microcapsules on the self-healing performance of FRP composites are investigated at room temperature with the current healing agent system (i.e. 5E2N/Grubbs catalyst system)
6) Effect of low temperature on the self-healing performance of FRP composites are also investigated in this work.

8.3 Recommendations for future work

Many technical challenges and issues were encountered during the investigations in this work. Recommendations for related future work based on the practical experience gained and the thorough literature studies are given below

1) Physical or chemical functionalization of microcapsule surfaces can improve their bonding with the matrix resulting in superior healing performance.
2) Self-healing of other forms of damages than the delamination in composites can be investigated
3) Self-healable composites can be made from prepregs incorporated with microcapsules and catalyst.
4) Efforts can be made to produce line-shaped microcapsules instead of current spherical microcapsules to have more encounter events with a propagating cracks.
5) Investigations can be made to find alternative catalyst systems which is less expensive or find a more efficient ways of utilizing current catalysts to reduce the cost of the components.
6) Investigations can be made to determine the effects of space conditions (e.g. thermal cycling between -150^{o}C to +150^{o}C, microgravity etc.) on self-healing of FRP composites.

References

[1] M. Wicklein, S. Ryan, D. White and R. Clegg, "Hypervelocity Impact on CFRP: testing, material modeling and numerical simulation," *International Journal of Impact Engineering,* vol. 35, pp. 1861-1869, 2008.

[2] M. Grujicic, B. Pandurangan, C. Zhao, S. Biggers and D. Morgan, "Hypervelocity Impact resistance of reinforced carbon-carbon-foam thermal protection systems," *Applied Surface Science,* vol. 252, pp. 5035-5050, 2006.

[3] S. White, N. Sottos, P. Geubelle, J. Moore, M. Kessler, S. Sriram, E. Brown and S. Viswanathan, "Autonomic healing of polymer composites," *Nature,* vol. 409, pp. 794-817, 2001.

[4] R. Talreja, "Damage developement in composites, mechanisms and modeling," *Journal of Strain analysis for Engineering Design,* vol. 24, pp. 215-222, 1989.

[5] H. Zamal, "Monitoring fatigue damage behavior of glass/epoxy composites using carbon nanotubes as sensors," 2011.

[6] S. White, B. Blaiszik, S. Kramer, S. Olugebefola, J. Moore and N. Sottos, "Self-healing polymers and composites," *American Scientist,* vol. 99, pp. 392-399, 2011.

[7] S. Van der Zwaag, Self healing materials: an alternative approach to 20 centuries of materials science, S. Van der Zwaag, Ed., Dordrecht, The Netherlands: Springer, 2007.

[8] T. Mauldin, J. Leonard, K. Earl, J. Lee and M. Kessler, "A rheokinetic technique designed to identify the properties of liquid self healing agents," in *Proceedings of the 3rd international conference on self healing materials*, Bath, UK, 2011.

[9] J. Lee, S. Hong, X. Liu and S. Yoon, "Characterization of dicyclopentadiene and 5-ethylidene-2-norbornene as self healing agents for polymer composites and its microcapsules," *Macromolecular Research,* vol. 12, no. 5, pp. 478-483, 2004.

[10] B. Burchell, "The future of composite repairs," *Overhaul and Maintenance,* July 2010.

[11] N. Hearn, "Self healing, autogenous healing and continued hydration: What is the difference?," *Materials and Structures,* vol. 31, pp. 563-567, 1998.

[12] V. Li and E. Yang, "Self healing in concrete material," in *An alternative approach to 20 centuries of materials science*, S. Van der Zwaag, Ed., New York, Springer, 2007, pp. 161-193.

[13] K. Breugel, "Is there a market for self healing cement based materials?," in *Proceedings of the first international conference on self healing materials*, Noordwijk aan Zee, The Netherlands,, 2007.

[14] N. Sottos and J. Moore, "Spot on Healing," *Nature,* vol. 472, pp. 299-300, 2011.

[15] C. Dry, "Smart building materials which prevent damage or repair themselves," *MRS Proceedings,* vol. 276, pp. 311-314, 1992.

[16] C. Dry, "Matrix cracking repair and filling using active and passive modes for smart timed release of chemicals from fibers into cement matrices," *Smart Materials and Structures,* vol. 3, pp. 118-123, 1994.

[17] C. Dry and W. McMillan, "Three part methylmethacrylate adhesive system as an internal delivery system for smart resposive concrete," *Smart Materials and Structures,* vol. 5, pp.

297-300, 1996.

[18] C. Dry, "Three designs for the internal release of sealants, adhesives and waterproofing chemicals into concrete to reduce permeability," *Cement and Concrete Research,* vol. 30, pp. 1969-1977, 2000.

[19] V. Li, Y. Lim and Y. Chan, "Feasibility study of a passive smart self healing cementitious composite," *Composites, part B,* vol. 29B, pp. 819-827, 1998.

[20] M. Wu, B. Johanneson and M. Geiker, "A review: Self healing of cementitous materials and engineered cementitous composites as a self healing material," *Construction and Building Materials,* vol. 28, pp. 571-583, 2012.

[21] S. Pareek and A. Oohira, "A fundamental study on regain of flexural strength of mortars by using a self-repair network system," in *3rd international conference on self healing materials*, Bath, UK, 2011.

[22] E. Tsangouri and D. Hemelrijck, "Development of a self healing skin for more durable concrete structures," in *3rd international conference on self healing materials*, Bath, UK, 2011.

[23] S. Sangadji and E. Schlangen, "Porous concrete: a new approach to make concrete structures self healing using prefabricated porous layer," in *3rd international conference on self healing materials*, Bath, Uk, 2011.

[24] T. Nishiwaki, O. A. and S. Pareek, "An experimental study on the application of self repairing system to RC structures using selective heating," in *3rd international conference on self healing materials*, Bath, UK, 2011.

[25] T. Nishiwaki, H. Mihashi, B. Jang and K. Miura, "Development of self healing system for concrete with selective heating around crack," *Journal of Advanced Concrete Technology,* vol. 4, no. 2, pp. 367-375, 2006.

[26] D. Pang, P. Thao, T. Diep and S. Ouek, "Self healing concrete structural elements," in *3rd international conference on self healing materials*, bath, UK, 2011.

[27] C. Dry, "Procedure developed for self repair of polymer matrix composite materials," *Composite Structures,* vol. 35, pp. 263-269, 1996.

[28] M. M., U. Vaidya and G. Janowski, "Parametric studies on self repairing approaches for resin infused composites subjected to low velocity impact," *Smart Materials and Structures,* vol. 8, pp. 623-638, 1999.

[29] S. Belay, C. Loader, V. Hawyes, L. Humberstone and P. Curtis, "A smart repair system for polymer matrix composites," *Composites: Part A,* vol. 32, pp. 1767-1776, 2001.

[30] A. Kousorakis and A. Mouritz, "The effect of self healing hollow fibers on the mechanical properties of polymer composites," *Smart Materials and Structures,* vol. 19, pp. 1-9, 2010.

[31] J. Pang and I. Bond, "Bleeding composites-damage detection and self repair using biomimetic approach," *Composites: part A,* vol. 36, pp. 183-188, 2005.

[32] R. Trask, G. Williams and I. Bond, "Bioinspired self healing of advanced composite structures using hollow glass fibers," *Journal of the Royal Society : Interface,* vol. 4, pp. 363-371, 2007.

[33] G. Williams, R. Trask and I. Bond, "A self healing carbon fiber reinforced polymer for aerospace applications," *Composites Part A: Applied Scienc and Manufacturing,* vol. 38, no. 6, pp. 1525-1532, 2007.

[34] D. Therriault, S. White and J. Lewis, "Chaotic mixing in three-dimensional microvascular networks fabricated by direct-write assembly," *Nature Materials,* vol. 2, no. 4, pp. 265-271, 2003.

[35] K. Toohey, N. Sottos, A. Jennifer, J. Lewis, J. Moore and S. White, "Self healing materials with microvascular networks," *Nature Materials,* vol. 6, pp. 581-585, 2007.

[36] K. Toohey, C. Hansen, J. Lewis, S. White and N. Sottos, "Delivery of two part self healing chemistry via microvascular networks," *Advanced Functional Materials,* vol. 19, pp. 1399-1405, 2009.

[37] C. Hansen, S. White, N. Sottos and J. Lewis, "Interpenetrating microvascular networks for thermal acceleration of self healing," in *Proceedings of the 3rd internetional conference on self healing materials*, Bath, UK, 2011.

[38] C. Hansen, W. Wu, K. Toohey, N. Sottos, S. White and L. Lewis, "Self healing materials with interpenetrating microvascular networks," *Advanced Materials,* vol. 21, pp. 4143-4147, 2009.

[39] C. Hansen, S. White, N. Sottos and J. Lewis, "Accelerated self healing via ternary interpenetrating microvascular networks," *Advanced Functional Materials,* vol. 21, pp. 4320-4326, 2011.

[40] C. Norris, I. Bond and R. Trask, "Fiber reinforced polymers with embedded microvascular networks-bioinspired in both design and function," in *Proceedings of the 3rd internetional conference on self healing materials*, Bath, UK, 2011.

[41] C. Norris, I. Bond and R. Trask, "The role of embedded bioinspired vasculature on damage formation of self healing carbon fiber composites," *Composites A,* vol. 42, pp. 639-648, 2011.

[42] C. Norris, I. Bond and R. Trask, "Interaction between damage events and bioinspired vasculatures embedded in fiber reinforced composites," in *Proceedings of the 3rd internetional conference on self healing materials*, Bath, UK, 2011.

[43] C. Norris, I. Bond and R. Trask, "Interactions between propagating cracks and bioinspired self healing vascules embedded in glass fiber reinforced composites," *Composite Science and Technology,* vol. 71, pp. 847-853, 2011.

[44] A. Hamilton, N. Sottos and S. White, "Pressurized vascular systems for healing crack damage and mitigating fatigue crack propagation," in *Proceedings of the 3rd internetional conference on self healing materials*, Bath, UK, 2011.

[45] P. Thakre, H. Dong, J. Patrick, K. Hart, A. Esser-Kahn, J. Moore, N. Sottos and S. White, "Thermal and mechanical response of three-dimensional microvascular composites," in *Proceedings of the 3rd internetional conference on self healing materials*, Bath, UK, 2011.

[46] A. Esser-Kahn, P. Thakre, H. Dong, J. Patrick, V. Vlasko-Vlasov, N. Sottos, J. Moore and S. White, "Three-dimensional microvascular fiber-reinforced composites," *Advanced Materials,* vol. 23, no. 2, pp. 3654-3658, 2011.

[47] H. Dong, Esser-Kahn, A., P. Thakre, J. Patrick, N. Sottos, S. White and J. Moore, "Microvascular composites fabricated from sacrificial fibers," in *Proceedings of the 3rd internetional conference on self healing materials*, Bath, UK, 2011.

[48] A. Esser-Kahn, H. Dong, P. Thakre, J. Patrick, N. Sottos, S. White and J. Moore, "Three dimensional microvascular composites fabricated from sacrificial fibers: manufacturing

and materials," in *Proceedings of the 3rd internetional conference on self healing materials*, Bath, UK, 2011.

[49] M. Keller and N. Sottos, "Effect of microcapsule properties on self healing composite performance," in *Proceedings of the 2004 SEM X international congress on experimental and applied mechanics*, 2004.

[50] E. Brown, S. White and N. Sottos, "Microcapsules induced toughening in a self healing polymer composite," *Journal of Materials Science,* vol. 39, pp. 1703-1710, 2004.

[51] E. Brown, S. White and N. Sottos, "Fracture testing of a self healing polymer composite," *Experimental Mechanics,* vol. 42, no. 4, pp. 373-379, 2002.

[52] J. Rule, N. Sottos and S. White, "Effect of microcapsule size on the performance of self healing polymers," *Polymer,* vol. 48, pp. 3520-3529, 2007.

[53] E. Brown, "Use of the tapered double-cantilever beam geometry for fracture toughness measurements and its application to the quantification of self healing," in *Proceedings of the 3rd internetional conference on self healing materials*, Bath, UK, 2011.

[54] E. Kirkby, J. Rule, V. Michaud, N. Sottos, S. White and J. Manson, "Embedded shape memory alloy wires for improved performance of self healing polymers," *Advanced Functional Materials,* vol. 18, pp. 2253-2260, 2008.

[55] S. Mostovoy, P. Crosley and E. Ripling, "Use of crack-line loaded specimens for measuring plain-strain fracture toughness," *Journal of Materials,* vol. 2, pp. 661-681, 1967.

[56] M. Kessler and S. White, "Self activated healing of delamination damage in woven composites," *Composites: Part A,* vol. 32, pp. 360-368, 2001.

[57] M. Kessler, N. Sottos and S. White, "Self healing structural composite materials," *Composites: Part A,* vol. 34, pp. 743-753, 2003.

[58] A. Patel, N. Sottos, E. Wetzel and S. White, "Autonomic healing of low velocity impact damage in fiber reinforced composites," *Composites: Part A,* vol. 41, pp. 360-368, 2010.

[59] T. OBrien and S. White, "Assessment of composite delamination self healing via microencapsulation," in *American society for composites 23rd international conference proceedings*, Memphis, USA, 2008.

[60] H. Jin, C. Mangun, D. Stradley, N. Sottos and S. White, "Epoxy-amine based self healing in high temperature cured epoxy," in *Proceedings of the 3rd internetional conference on self healing materials*, Bath, UK, 2011.

[61] T. Yin, M. Rong and G. Yang, "Self healing epoxy composites-preparation and effect of the healant consisting of microencapsulated epoxy and latent curing agent," *Composites Science and Technology,* vol. 67, pp. 201-212, 2007.

[62] D. Xiao, Y. Yuan, M. Rong and M. Zhang, "A facile strategy for preparing self healing polymer composites by incorporation of cationic catalyst-loaded vegetable fibers," *Advanced Functional Materials,* vol. 19, pp. 2289-2296, 2009.

[63] Y. Yuan, Y. Yueping, M. Zhirong, H. Chen, J. Wu, M. Zhang, S. Qin and G. Yang, "Self healing of low velocity impact damage in glass fabric epoxy composites using an epoxy-mercaptan healing agent," *Smart Materials and Structures,* vol. 20, pp. 1-11, 2011.

[64] L. Meng, Y. Yuan, M. Rong and M. Zhang, "A dual mechanism single-component self healing strategy for polymers," *Journal of Materials Chemistry,* vol. 20, pp. 6030-6038,

2010.

[65] M. Zhang, M. Rong and X. Jiang, "Self healing of cracks in epoxy via free radical polymerization," in *Proceedings of the 3rd internetional conference on self healing materials*, Bath, UK, 2011.

[66] M. Caruso, B. Blaiszik, S. White, N. Sottos and J. Moore, "Full recovery of fracture toughness using a non-toxic solvent-based self healing system," *Advanced Functional Materials,* vol. 18, pp. 1898-1904, 2008.

[67] M. Caruso, D. Delafuente, V. Ho, N. Sottos, S. White and J. Moore, "Solvent-based self healing epoxy materials," *Polymer Preprints,* vol. 49, no. 1, pp. 974-975, 2008.

[68] S. Neuser, V. Michaud, N. Sottos and S. White, "Solvent based self healing of thermosets with embedded SMA wires," in *Proceedings of the 3rd internetional conference on self healing materials*, Bath, UK, 2011.

[69] X. Chen, M. Dam, K. Ono, A. Mal, H. Shen, S. Nutt, K. Sheran and F. Wudl, "A thermally re-mendable crosslinked polymeric material," *Science,* vol. 295, pp. 1698-1702, 2002.

[70] X. Chen, F. Wudl, A. Mal, H. Shen and S. Nutt, "New thermally remendable highly crosslinked polymeric materials," *Macromolecules,* vol. 36, pp. 1802-1807, 2003.

[71] A. Peterson, R. Jensen and G. Palmese, "Thermoreversible and remendable glass-polymer interface for fiber-reinforced composites," *Composites Science and Technology,* vol. 71, pp. 586-592, 2011.

[72] Y. Liu, Hsieh and C., "Crosslinked epoxy materials exhibiting thermal remendability and removability from multifunctional maleimide and furan compounds," *Journal of Polymer Science,* vol. 44, pp. 905-913, 2006.

[73] G. Scheltjens, J. Brancart, I. De Graeve, B. Van Mele, H. Terryn and G. Van Assche, "Self healing property characterization of reversible thermoset coatings," *Journal of Thermal Analysis and Calorimetry,* vol. 105, pp. 805-809, 2011.

[74] M. Zako and N. Takano, "Intelligent materials system using epoxy particles to repair microcracks and delamination damage in GFRP," *Journal of Intelligent Materials System and Structure,* vol. 10, pp. 836-841, 1999.

[75] "Varley, R.; Parn, G.," *Thermally activated healing in a mendable resin using a non-woven EMMA fabric,* vol. 10, pp. 453-460, 2012.

[76] S. Meure, R. Varley, D. Wu, S. Mayo, K. Narin and S. Furman, "Confirmation of the healing mechanism in a mendable EMAA-epoxy resin," *European Polymer Journal,* vol. 48, no. 3, pp. 524-531, 2012.

[77] S. Cho, S. White and P. Braun, "Self healing polymer coatings," *Advanced Materials,* vol. 21, pp. 645-649, 2009.

[78] M. Wouters, E. Craenmehr, K. Tempelaars, H. Fischer, N. Stroeks and J. Van Zanten, "Preparation and properties of a novel remendable coating concept," *Progress in Organic Coatings,* vol. 64, pp. 156-162, 2009.

[79] Z. Yang, Z. Wei, L. Le-Ping, W. Si-jie and L. Wu-Jun, "Self healing coatings containing microcapsule," *Applied Surface Science,* vol. 258, pp. 1915-1918, 2012.

[80] X. Liu, H. Zhang, J. Wang and S. Wang, "Preparation of epoxy microcapsule-based self healing coatings and their behavior," *Surface and Coating Technology,* vol. 206, no. 23, pp. 4976-4980, 2012.

[81] V. Sauvant-Moyont, S. Gonzalez and J. Kittel, "Self healing coatings: An alternative route for anticorrosion protection," *Progress in Organic Coatings,* vol. 63, pp. 307-315, 2008.

[82] C. Suryanarayanaa, K. Raob and D. Kumara, "Preparation and characterization of microcapsules containing linseed oil and its use in self healing coatings," *Progress in Organic Coatings,* vol. 63, pp. 72-78, 2008.

[83] F. Micciche, H. Fischer, R. Varley and S. Van der Zwaag, "Moisture induced crack filling in barrier coatings containing montmorillonite as an expandable phase," *Surface and Coatings Technology,* vol. 202, pp. 3346-3353, 2008.

[84] A. Kumara, L. Stephenson and J. Murray, "Self healing coatings for steel," *Progress in Organic Coatings,* vol. 55, pp. 244-253, 2006.

[85] X. Liu, J. Lee, S. Yoon and M. Kessler, "Characterization of diene monomer as healing agents for autonomic damage repair," *Journal of Applied Polymer Science,* vol. 101, no. 3, pp. 1266-1272, 2006.

[86] M. Raimondo, P. Longo, A. Mariconda and L. Guadagno, "Healing agent for the activation of self-healing function at low temperature," *Advanced Composite Materials,* vol. 24, no. 6, pp. 519-529, 2015.

[87] E. Brown, M. Kessler, N. Sottos and S. White, "In situ poly (urea-formaldehyde) microencapsulation of dicyclopentadiene," *Journal of Microencapsulation,* vol. 20, no. 6, pp. 719-730, 2003.

[88] X. Liu, X. Sheng, J. Lee and M. Kessler, "Synthesis and characterization of melamine-urea-formaldehyde microcapsules containing ENB-based self healing agents," *Macromolecular Materials and Engineering,* vol. 294, pp. 389-395, 2009.

[89] M. Abramoff, P. Magalhaes and S. Ram, "Image processing with ImageJ," *Biophotonics International,* vol. 11, no. 7, pp. 36-42, 2004.

[90] B. Boh and B. Sumiga, "In situ polymerisation of microcapsules," *Bioencapsulation Innovation,* pp. 3-6, 2013.

[91] A. Rochmadi and W. Hasokawati, "Mechanism of microencapsulation with urea-formaldehyde polymer," *American Journal of Applied Science,* vol. 7, pp. 739-745, 2010.

[92] F. Salaun, E. Devaux, S. Bourbigot and P. Rumeau, "Influence of process parameters on microcapsules loaded with n-hexadecane prepared by in situ polymerization," *Chemical Engineering Journal,* vol. 155, no. 1, pp. 457-465, 2009.

[93] [Online]. Available: http://www.fishersci.ca/viewmsds.do?catNo=AC166015000.

[94] [Online].Available: http://www.sigmaaldrich.com/catalog/product/aldrich/151467?lang=en&region=CA.

[95] J. Li, S. Wang, N. Liu and L. You, "Preparation and application of poly (melamine-urea-formaldehyde) microcapsules filled with sulphur," *Polymer-Plastics Technology and Enginnering,* vol. 50, no. 7, pp. 689-697, 2011.

[96] [Online]. Available: http://www.chm.bris.ac.uk/motm/SLS/SLSh.htm.

[97] [Online]. Available: http://pharmlabs.unc.edu/labs/emulsions/agents.htm.

[98] S. Alexandridou and C. Kiparissides, "Production of oil-containing polyterephthalamide microcapsules by interfacial polymerization," *Journal of Microencapsulation,* vol. 11, no. 6, pp. 603-614, 1994.

[99] B. Ovez, B. Citak, D. Oztemel, A. Balbas, S. Peker and S. Cakir, "Variation of droplet sizes during the formation of microcapsules from emulsions," *Journal of Microencapsulation,* vol. 14, no. 4, pp. 489-499, 1997.

[100] H. Tan, T. Ng and H. Mahabadi, "Interfacial polymerization encapsulation of a viscous pigment mix: emulsification conditions and particle size distribution," *Journal of Microencapsulation,* vol. 8, no. 4, pp. 525-536, 1991.

[101] N. Yan, P. Ni and M. Zhang, "Preparation and properties of microcapsules with non-ionic surfactant as emulsifier," *Journal of Microencapsulation,* vol. 10, no. 3, pp. 375-383, 1993.

[102] X. Liu, J. Le and M. Kessler, "Microencapsulation of self healing agents with melamine-urea-formaldehyde by the Shirasu porous glass (SPG) emulsification technique," *Macromolecular Research,* vol. 19, no. 10, pp. 1056-1061, 2011.

[103] W. Li, X. Zhu, N. Zhao and Z. Jiang, "Preparation and properties of melamine-urea-formaldehhyde microcapsules for cementitious materials," *Materials,* vol. 9, no. 3, p. 152, 2016.

[104] E. Kirkby, V. Michaud, J. Manson, N. Sottos and S. White, "Performance of self healing epoxy with microencapsulated healing agent and shape memory alloy wires," *Polymer,* vol. 50, no. 23, pp. 5533-5538, 2009.

[105] A. Devito, S. Matthew and A. Higgins, "Operating manual of 'single stage gas launcher;," Personal Communications, Montreal, 2011.

[106] *ASTM D7264 / D7264M-15, Standard Test Method for Flexural Properties of Polymer Matrix Composite Materials,,* ASTM International, West Conshohocken, PA, 2015.

[107] B. Davidson, "Standardization of the end-notched flexure test for Mode II interlaminar fracture toughness determination of unidirectional laminated composites," *Journal of Testing and Evaluation,* vol. 43, no. 6, pp. 1540-1553, 2015.

[108] *ASTM D7905/D7905M-14, Standard test method for determination of the Mode II interlaminar fracture toughness of unidirectional fiber-reinforced polymer matrix composites,* ASTM International, West Conshohocken, PA, 2014.

[109] S. Lee, "Mode II delamination failure mechanisms of polymer matrix composites," *journal of Materials Science,* vol. 32, no. 5, pp. 1287-1295, 1997.

[110] A. Cook, "Characterization of interlaminar fracture in composite materials, a case study approach," Masters Thesis Dissertation, Montana State University, Bozeman, USA, 2001.

[111] B. Lauke, "On the effect of particle size on fracture toughness of polymer composites," *Composites Science and Technology,* vol. 68, no. 15, pp. 3365-3372, 2008.

[112] C. Bielawski and R. Grubbs, "Living ring-opening metathesis polymerization," *Progress in Polymer Science,* vol. 32, no. 1, pp. 1-29, 2007.

[113] Y. Schrodi and R. Pederson, "Evolution and Applications od second-generation Ruthenium olefin metathesis catalysts," *Aldrichimica Acta,* vol. 40, no. 2, pp. 45-52, 2007.

[114] J. Kamphaus, J. Rule, D. D., J. Moore, N. Sottos and S. White, "Development and evaluation of an alternative ROMP catalyst for self healing polymers," in *First international conference on self healing materials*, Noordwizk aan Zee, The Netherlands, 2007.

[115] R. Grubbs, "Olefin metathesis," *Tetrahedron,* vol. 60, no. 34, pp. 7117-7140, 2004.

[116] G. Wilson, M. Caruso, N. Reimer, S. White, N. Sottos and J. Moore, "Evaluation of

Ruthenium catalysts for ring-opening metathesis polymerization-based self healing applications," *Chemistry of Materials,* vol. 20, no. 10, pp. 3288-3297, 2008.

[117] J. Nakhla, 2010. [Online]. Available: http://www.sigmaaldrich.com/technical-documents/articles/chemfiles/ultra-fast-initiating.html.

[118] [Online].Available: http://www.sigmaaldrich.com/catalog/product/aldrich/569755?lang=en&region=CA.

[119] S. Kichhannagari, *Effects of extreme low temperature on composite materials,* 2004.

[120] D. Isaac M., O. Ishai, I. Daniel and D. Ishai, Engineering Mechanics of Composite Materials, vol. 3, New York: Oxford University Press, 1994.

PUBLICATIONS AND PRESENTATIONS

Journal Articles

M. Asgar-Khan and S. Hoa, Evaluation of self-healing performance of microcapsule incorporated fiber reinforced polymer composites with a protocol based on determining the mode II fracture toughness, Smart Materials and Structures, 2016 (In-preparation)

M. Asgar-Khan and S. Hoa, Investigation of self-healing of carbon/epoxy composites for low temperature applications, Composite Science and Technology, 2016 (In-preparation)

Conference and Workshop Proceedings

M. Asgar-Khan and S. Hoa, "Self-healing materials for low temperature applications", Canada-Japan-Vietnam Workshop on Composites, Ho-Chi-Minh city, Vietnam, August, 2016.

Dee, J., Papanagiotou, E., Asgar-Khan, M., Velenosi, N., Kandela, R., Nguyen, O. and Sabzalian, M., A study of self-healing composites in microgravity within a cubesat, 67th International Astronautical Congress, Guadalajara, Mexico, September, 2016

M. Asgar-Khan and S. Hoa, "Investigation on the structural self-healing of FRPC for space applications", Canadian International Conference on Composite Materials (CANCOM 2015), Edmonton, Canada, August, 2015.

M. Asgar-Khan and S. Hoa, "Effect of low temperature on self-healing performance of carbon/epoxy composites", 20th International Conference on Composite Materials (ICCM 20), Copenhagen, Denmark, July, 2015.

M. Asgar-Khan, S. Hoa, B. Aissa, E. Haddad and A. Higgins, "Experimental investigation of the self-healing performance of CFRP composites subjected to high velocity impact",*3rd International Conference on Self-Healing Materials*, Bath, UK, June, 2011

Impact

i) CBC Radio-Canada Television aired our work on self-healing materials in the program DA©couverte in January, 2011.

ii) Using our self-healing composite samples as the payload for the micro/nano-satellite, Space Concordia satellite division won 2nd prize in 2014 and 1st prize in 2016 at the Canadian Satellite Design Challenge (CSDC) competition.

iii) Our self-healing samples are kept at Musee de la Civilisation, Quebec, Canada for exhibition from April 2016 to April 2017.